Mammalian EAK-7 Activates Alternative mTOR Signaling

by

Joe T. Nguyen

A dissertation submitted in partial fulfillment
of the requirements for the degree of
Doctor of Philosophy
(Oral Health Sciences)
in the University of Michigan
2019

Doctoral Committee:

Professor Paul H. Krebsbach, Co-Chair
Professor Jacques E. Nör, Co-Chair
Professor Renny T. Franceschi,
Assistant Professor Isabelle M.A. Lombaert,
Professor Max S. Wicha,

Joe T. Nguyen

joetnguy@umich.edu

ORCID ID: 0000-0002-6647-0561

“When something is important enough, you do it even if the odds are not in your favor.”

Elon Musk

Acknowledgements

I would like to give my sincere gratitude to Dr. Paul H. Krebsbach for his guidance, kindness and friendship throughout my training. You are one of the most free-thinking individuals that I know of and I aspire to become a wonderful mentor and rigorous scientist like you. If it wasn't for your patience and insight, I would not have been able to express myself as a scientist and think independently. I believe that most of the success that I've achieved has been in large part due to your guidance and flexibility in thought. I also want to thank you for taking me in during the holidays when I wasn't able to go home to see my family. I could not have asked for a better mentor and look forward to a lifetime of friendship.

To Patrick Hu, thank you for teaching one of the first graduate courses I've taken at the University of Michigan where you eagerly shared your novel findings on the EAK-7 gene. Your approach to science allowed me to think about the process of studying an entirely new gene and your insights into the EAK-7 gene in nematodes helped us elucidate the role of mammalian EAK-7 in humans.

To members of the Krebsbach Lab, I learned how to conduct science within this group of intellects from all over the world. My labmate, Dr. Tugba Topal, is one of my most cherished friends and I don't think I could retain my sanity throughout my time here. As the last graduate students in the Krebsbach Lab, we formed a special comradery that have enabled us to discuss ideas and science freely—also cats. To Dr.

Jin Koo Kim, thank you for being a scientific mentor to me and help push my ideas to make them stronger. To the students that I've personally mentored, Lauren Azzopardi, Connor Ray, Halimah Amatullah, Fatima Haidar, Aimee Cho, and Minjun Kim, I wish you all the best in your future careers and thank you for all of your hard work over the years.

To members of my dissertation committee, I am forever grateful for your time and feedback into my project. To Dr. Jacques Nör, thank you for helping Paul and I through the transition period and helping us maintain our F30 grant from the NIDCR. To Dr. Isabelle Lombaert, I cannot thank you enough for taking us into your lab when Paul left for his new position at UCLA. It's been an absolute blast to work with you on our collaborative projects and be able to finish up my projects. To Dr. Max Wicha, thank you for helping us troubleshoot challenging experiments and lending your expertise in our successfully funded Cancer Center Grant. To Dr. Renny Franceschi, thank you for your thoughtful insights into the mechanics of the signaling studies and time spent on my committee.

To OHS faculty, clinical faculty, and staff, I will constantly push myself to learn new things and become a better scientist and clinician due to your support. To my PhD program director, Dr. Jan Hu, you believed in me from the very beginning and your encouragement continues to enlighten my thought process for the sciences and academia. To Dr. David Kohn, I sincerely appreciate your honest and blunt advice during our "consultation sessions" and cannot ask for a better colleague. 3 Blue was my clinic home and I was lucky to work with the best clinic director at Michigan, Dr. Mark Snyder, who allowed me to attend more than a dozen conferences that were essential

to my scientific training and allowed me to tackle challenging cases to better my clinical training. I am also thankful for the wonderful staff that helped me throughout my clinical training, specifically, Ann Somppi and Kimberly Williams, who were essential in dealing with all of my issues in the clinic. Thanks to all of the auxiliary staff as well for your help during patient care.

To the BMS department, thank you for taking care of me before and after Paul's departure. Especially to Joel Clendenin, Kerry Boyd, Deb Keedy, and Erin Semmens. Your support has helped me complete my research projects and allowed me to become a successful scientist and dentist. I can't thank you enough!

To my fellow graduate students, it's been a blast to be part of this experience with each and every one of you. As a Rackham Merit Fellow, I was privileged to take part in the Summer Institute, where I made lifelong friendships. To my future business partner and free thinker, Uriah Israel, if anything at all, the best part of my education, that was not related to my clinician-scientist training program, was being able to pursue entrepreneurial ideas with you and our colleagues, like Jack Miner or Vince Groppi. To Dr. Chris Donnelly, thank you for your friendship and comradery as we discussed topics ranging from science, business, and the future. Thank you to Dr. Susana Chan for helping me format and edit my thesis. A special shout out to my core group of friends, Drs. Chris Miles, Irene Park, Susana Chan, Tom Hsieh, and Victor Wu.

To my fiancée, Linda Au, I love you with all of my heart and am forever grateful for your patience and love. From the moment I left California, you have been my rock and support throughout my training. You are my closest friend and confidante. We have our entire lives ahead of us and I'm excited for that journey. To my family, I'm so happy

for your support and guidance throughout my training. My mom, Yvonne Troung, and dad, Muc Nguyen, have worked their entire lives for their children to pursue the careers that suited their personalities best. Without your love and support, I would not be able to pursue my passions and be work on the most fascinating topics in science. Also, thank you to my siblings, especially my big sister, Linda Nguyen, that helped me apply for college, dental school, and prepare me for interviews. I also want to thank my younger brothers, Jason and Jacob, for their patience with me, even as intolerable as I was growing up. To my sister Lisa, I hope that we can become closer in the years to come. In the seven years that I will spend to obtain my DDS and PhD, I am reminded that through the bleakest moments in our lives, there is always light at the end of the tunnel. My dad spent 7 years in a concentration camp after the fall of South Vietnam and his only hope was the path for a better future for himself and his family. My mom met my dad at a refugee camp in Thailand where they would eventually make the dangerous trek to the US. I am truly fortunate to be living the dream—The American Dream. These stories remind me that, above all us, we must keep our hopes and spirits up, no matter the hardship.

To my funding sources, thank you so much for supporting myself and my ideas. We thank our funding sources: National Institute of Dental and Craniofacial Research (1F30DE026048-01, R01-DE016530, and T32-DE007057) and Stuart & Barbara Padnos Research Award from the Rogel Cancer Center at the University of Michigan. I would also like to thank the AADR and IADR for supporting my many conferences.

Table of Contents

List of Figures

Abstract

Strong evidence supports the concept that mammalian target of rapamycin (mTOR) regulates essential cell processes and that dysregulation of mTOR signaling leads to the pathogenesis of several debilitating human conditions. Aberrant activation of mTORC1 signaling contributes to the malignant behavior of cancer cells by controlling proliferation, invasion, and metastasis. We identified a novel effector of the mTORC1 pathway and provisionally named the human ortholog, mammalian enhancer of akt1-7 (EAK-7) or (mEAK-7), due to its original identification in *Caenorhabditis elegans*. In nematodes, EAK-7 negatively affects longevity through regulation of FoxO transcription factors. While there is no functional characterization of mEAK-7 (also known as expressed sequence tag KIAA109 or TDLC1), there are examples in the literature that demonstrate upregulated mEAK-7 gene expression and copy number amplification in diverse cancer types. We discovered that some cancer cell lines derived from head and neck squamous cell carcinomas, non-small lung carcinomas, and breast carcinomas express mEAK-7 protein, while somatic cells we screened do not. Moreover, more than half of the cancer cell lines screened were mEAK-7 positive (mEAK-7+) cancers, but why these cells express mEAK-7 is unknown. When this is coupled with the fact that mTORC1 signaling is amplified in distinct human cancers, it suggests that mEAK-7 may, in part, be responsible for the pathogenesis of certain human cancers. With increasing interest in developing mTOR signaling inhibitors to

treat cancer patients, this thesis explores the mechanisms by which mEAK-7 regulates mTOR signaling and functions to support the progression of human cancer. As an aspiring dentist-scientist, I am primarily interested in tumorigenesis in relation to mEAK-7 function under abnormal metabolism and DNA damage (X-ray irradiation). To this end, our central hypothesis is that mEAK-7 functions as a positive regulator of mTORC1 signaling in human cancers.

Canonical mTORC1 signaling utilizes nutrient rich conditions (insulin, amino acids, high energy levels) for activation of this evolutionarily conserved pathway. While stress conditions have been widely reported to inhibit mTOR signaling in non-cancerous cells, it has been shown that mTOR signaling can be sustained after DNA or oxidative stressors. We discovered that mTOR signaling increased after X-ray irradiation, and we provided evidence that mEAK-7 is required for sustained mTOR signaling after under DNA damage. Treatment options for cancer patients include 1) surgery and/or 2) chemo- or radio-therapy. However, patients who experience chemo- or radio- resistant cancers typically have poor clinical prognoses and there is a lack of well-defined biological markers indicative of this malignant process. Thus, the overarching goal of this thesis will be to elucidate the role of mEAK-7 in cancer, and to determine the extent to which mEAK-7 plays a role in tumorigenesis, and whether or not mEAK-7 is a cancer biomarker.

In chapter 1, we outline key facets of knowledge gathered during the last 20 years of mTOR signaling research, beginning with rapamycin's illustrious discovery on Easter Island and leading to the identification of the molecular kinase, mTOR. We also explore ideas of development and disease in craniofacial biology and cancer. In chapter

2, we rigorously outline the molecular mechanisms regarding mEAK-7 function. In chapter 3, we determined the role of mEAK-7 in human disease, specifically radioresistant cancers and metastatic cancers. Chapter 4, the final chapter, outlines the future goals of the mEAK-7 project and its potential to impact human medicine.

Chapter 1 – Introduction

Discovery of Rapamycin and mTOR signaling

Rapamycin was identified during a Canadian expeditionary search for novel antibiotic compounds on Rapa Nui (Easter Island), and it was subsequently demonstrated to block yeast growth and to have strong immunosuppressive effects in mammals (*1*). Rapamycin is a macrolide that is a secondary metabolite of the bacterium, *Streptomyces hygroscopicus (2)*. Several groups discovered that rapamycin forms a complex with FKBP12 resulting in a gain of function that inhibits signal transduction pathways required for cell growth and proliferation (*3*). It would take more than another decade before TOR/mTOR was identified as the target of the rapamycin-FKBP12 inhibitory complex in yeast (*4*) and eukaryotes (*5, 6*). Subsequently, laboratories across the world have demonstrated the essential role of mTOR signaling in eukaryotic development and disease in response to nutrient sensing and metabolic regulation (*1*).

TOR/mTOR is a member of the phosphatidylinositol-3 kinase-related kinase (PIKK) family (*7*). PIKKs are atypical Serine/Threonine protein kinases that also include ataxia-telangiectasia mutated (ATM), ataxia- and Rad3-related (ATR), DNA-dependent protein kinase catalytic subunit (DNA-PKcs), transformation/transcription domain-associated protein (TRRAP), and suppressor of morphogenesis in genitalia (SMG-1) (*8*). While these kinases share similar functional domains, they are responsible for

diverse actions, such as, regulating cell metabolism, DNA repair pathways, and genome surveillance. mTOR signaling is defined by its two best studied complexes: mTOR complex 1 (mTORC1) and mTOR complex 2 (mTORC2) in mammals (*1*), and TOR1 and TOR2 in yeast (*9*). mTORC1 is comprised of regulatory-associated protein of mTOR (raptor), mammalian lethal with SEC13 protein 8 (mLST8) or GβL, Proline-rich AKT1 substrate 1 (PRAS40), and DEPTOR (*1*). mTORC2 is comprised of mLST8, rapamycin-insensitive companion of mTOR (rictor), mammalian stress-activated protein kinase interacting protein 1 (mSIN1), Protor, DEPTOR, and Tti1 & Tel2 (*1*). Both complexes act at the lysosome, an essential cellular compartment for mTOR signaling, but govern different cellular processes (*10, 11*). The best known targets of mTORC1 are S6K1 and 4E-BP1, while the best known target of mTORC2 is Akt. Recently, we identified mammalian EAK-7 or mTOR associated, eak-7 homolog (mEAK-7) as a positive regulator of mTOR signaling through an S6K2/4E-BP1 axis, but not the canonical S6K1/4E-BP1 axis (*12*). This finding is striking, as we demonstrate that mEAK-7 possibly contributes to a novel, third mTOR complex (mTORC3) (Figure 1.1).

Although many molecular and biochemical analyses have demonstrated that these mTOR and associated proteins are capable for forming complexes, little was known with regard to the actual binding and mechanics of mTOR complex formation. Advances in cryo-EM technology, electron detectors, super-computers, and advanced algorithms have paved the way for previously un-identifiable protein structures at the atomic level (*13*). Previously, the structure of mTOR was elusive to the scientific community due to nuanced issues related to crystallizing such a large multimeric complex. In a seminal paper, the structure of mTORC1 was resolved revealing that

mTOR formed a homodimer and that the FKBP-rapamycin complex limited access to architectural elements of mTORC1 at the recessed active site (*14*). Further work demonstrated rictor was insensitive to rapamycin treatment because crucial mTORC2 protein partners blocked the structural site of rapamycin-FKBP12 binding (*15, 16*). While short-term rapamycin treatment does not disrupt rictor-mTOR binding (*17*), long-term rapamycin treatment is sufficient to block rictor-mTOR binding *in vivo*, though some animals still exhibit activated (Ser^{473}) p-Akt levels (*18*). Much work has been completed to provide a viable structural model for mTORC1 and mTORC2. Since our evidence suggests the existence of a novel mTOR complex, it will be essential to understand how novel mTOR complexes form at the structural level. This will be especially important for proving that mEAK-7 can interact with mTOR and form a legitimate multimeric complex, as a central component of mTORC3.

Upstream of mTOR signaling

mTOR signaling is an essential metabolic pathway in eukaryotes. Many nutrient sensing networks function upstream of mTOR to coordinate this complex process. Upstream of mTORC1, the tuberous sclerosis complex (TSC) integrates diverse biologic inputs ranging from low energy levels to growth factor and hormonal activation (*19*). For instance, activation of the insulin receptor results in a cascade of events that activate Akt signaling which, in turn, phosphorylates TSC (comprised of TSC1, TSC2, and TBC1D7) proteins to allow mTOR activation (*20*). The TSC functions as a sensor for specific nutrient conditions and possesses Rheb-GAP activity (*21*). In response to

nutrients, the TSC is recruited away from the lysosome, allowing Rheb-GTPase to bind and activate mTOR signaling (*22*).

In turn, multiple signaling modalities work in concert to ensure the activation of mTOR signaling. The lysosome is an essential hub for mTOR signaling and amino acids recruit mTOR to the lysosome through amino acid signaling via the Rag guanosine triphosphatase (GTPase) Rag A or B, which dimerizes with either Rag C or D (*23*). In the amino acid starved state, mTOR is diffuse within the cell, but amino acid stimulation allows the Ragulator-Rag complex to recruit mTOR directly to the lysosome (*24*). Thus, the culmination of these nutrient signals allows for Rheb GTPase to activate mTOR at the lysosome (*11*).

Despite intensive research in this area, it is unclear how Rheb interacts with mTOR at the lysosome to activate mTOR signaling. Rheb is identified in the early and late forming endosomes, but not necessarily at the lysosome. Curiously, TOR signaling is essential for the formation of the endosome and the inhibition of endosomal degradation in *Drosophila melanogaster (25).* The endosome is a crucial compartment for cell growth and activation of mTOR signaling via amino acids and insulin (*26*). TOR also localizes to the endosome in yeast (*27, 28*) and human cells (*23*). However, with mTOR recruitment to the lysosome and Rheb existing at the late endosome, it is unclear how Rheb interacts with mTOR and how that activation occurs. It was recently determined that a substantial percentage of Rheb interacts with mTOR at the Golgi-lysosome contact sites to activate mTORC1 signaling (*29*). This crucial evidence places mTOR at the lysosome, the cellular compartment for full activation by upstream signaling partners, though it is still unknown how Rheb activates mTOR. Ultimately,

there is much that is unknown, with regard to the specific players in the full activation of mTOR signaling. The molecular landscape of different types of tissues and cells allows for diverse combinations of mTOR complexes to form and upstream regulators to form and affect mTOR.

Downstream of mTOR signaling

As research groups gained interest on the role of mTOR signaling, it became apparent that mTOR was essential for many downstream events in metabolism, development, and disease. mTOR signaling exerts exquisite control over the production of organismal building blocks, namely, proteins, lipids, and nucleotides. In addition, mTOR signaling is essential for regulation of autophagy and whether or not cells undergo anabolism or catabolism. mTOR is a promiscuous protein that is capable of binding to diverse protein targets which result in a cascading effect to signal the cell to begin a specific and regimented program. There is still much that is unknown about the downstream targets of mTOR signaling. The comprehensive analysis of these pathways will unravel how dysregulation of mTOR signaling results in disease processes.

The central dogma of molecular biology is the flow and preservation of genetic information within a biological system. As Francis Crick once stated, “DNA makes RNA and RNA makes protein”. With few exceptions, this fundamental truth has stood the test of time and accentuates the simplicity of nature at its core. As technology advances, there are likely many more discoveries to solve. mTOR signaling is best known for regulation of protein synthesis through downstream effectors S6 (cap-independent protein translation) and 4E-BP1 (cap-dependent protein translation). By regulating two

different processes for protein synthesis, mTOR and its affiliated complexes are crucial players in protein production. As a direct effect, mTORC1 targets S6K1/S6K2 and 4E-BP1 to regulate cell size through its regulation of protein synthesis (*30*). Many of these findings were based upon the observation that rapamycin plays a crucial role in regulating cell growth and proliferation. Although it would be many years before mTOR would be identified as the protein kinase responsible for the effects of rapamycin, it is now clear that mTOR is an essential protein. Rapamycin is a potent inhibitor of cell growth processes (*3, 31*) and mTOR was shown to be the kinase targeted by rapamycin and responsible for S6K activity (*32*). mTORC1 directly phosphorylates S6K1/S6K2, at the hydrophobic motif at Thr389/Thr388 to allow for full activation and downstream targeting of S6 (*33, 34*). This coordinated effort to regulate downstream targets allows for specific control of cap independent protein translation. Additionally, it has only recently been appreciated that the regulation of S6K1 and S6K2 could have different target proteins. Much of the body of knowledge of mTOR signaling has been identified with S6K1, and much more work needs to be carried out to understand how S6K2 regulates protein translation. The most immediate downstream target of the S6Ks is 40S ribosomal protein S6, an essential regulator of a subclass of mRNA translation which contain a short oligopyrimidine sequence immediately after the transcriptional start site (*35*). Our work has demonstrated that there are certain cell specific scenarios where S6K2 plays a more important role than S6K1 in regulating S6 suggesting that there are specific adaptor proteins that are upregulated or downregulated, depending on the context.

mTOR signaling further regulates protein synthesis by modulating cap-dependent protein translation by phosphorylating the eukaryotic translation initiation factor 4E-binding protein 1 (4E-BP1). mTOR binds 4E-BP1 via raptor (mTORC1) at Thr37/46 (*36*), which primes the 4E-BP1 phosphorylation site at Ser65 and Thr70, and allows 4E-BP1 detachment from eukaryotic translation initiation factor 4E (eIF4E) (*37*). This elaborate sequence of events must occur for the full inhibition of 4E-BP1 by mTORC1. From an evolutionary perspective, intricate regulation of protein synthesis is required so that the organism can develop properly and respond quickly to beneficial or harmful stimuli. While mTOR inhibition modestly downregulates mRNA translation, it has been demonstrated that it significantly regulates mRNAs containing pyrimidine-rich 5′ TOP, mainly genes involved in protein synthesis (*38*). Thus, S6K and 4E-BP1 regulation by mTOR signaling is essential for proper production of proteins.

As mTOR signaling is the master regulator of cellular metabolism, it also plays an essential role in blocking autophagy and protein catabolism. mTORC1 targets ULK1/2, which forms a complex with ATG13, FIP2000, and ATG101 to suppress the formation of the autophagosome (*39*). Suppression of mTOR signaling prevents the phosphorylation of ULK1/2, thereby allowing AMPK to activate the ULK and allow the autophagosome to proceed forward. Thus, when the cell is ready to divide, it must decrease the propensity of the cell to undergo energy saving regimens, where autophagy is activated. When the cell senses the reduction of nutrients, thereby inhibiting mTOR signaling, the cell will be able to recycle non-essential proteins to conserve energy and wait for its next energy bolus. Though we have a preliminary idea of how mTOR regulates autophagy under normal metabolic programs, understanding how this process is controlled in diseased

states will be important since autophagy is dysregulated in cancer. Primarily, cancer cells are capable of utilizing autophagy to survive microenvironmental stresses and to increase cell growth and aggressiveness (*40*).

A third mTOR complex

It has been theorized that additional mTOR complexes may complement mTORC1 and mTORC2 in mammals. Through ATP-competitive studies, Torin 1, a potent mTOR inhibitor, was shown to inhibit mTOR to a greater extent than rapamycin treatment alone. These results were similar to raptor knock-down, but there was no difference when rictor$^{-/-}$ cells were treated with Torin1 (*41*). These findings suggest that completely targeting mTOR kinase can strongly reduce downstream signaling, but blocking mTORC1 or mTORC2 specifically is not sufficient to yield potent effects. Additionally, though mTOR regulates TOP mRNA translational machinery through mTORC1 (raptor), cells lacking raptor or rictor can regulate TOP mRNA through an alternative mechanism, suggesting that there are other complexes that exist to regulate downstream mTOR targets (*42*). More recently, astrocytes provide one such example of how mTOR may function in a cell-type or tissue-type specific manner. GIT1 is an interacting partner of mTOR that does not associate with either raptor or rictor, though the molecular mechanism is unknown, is crucial for cell apoptosis (*43*). Thus, there may be cell-type specific mTOR complexes that remain to be discovered. In B cell cancers, ETV7 was identified as an interacting molecule of mTOR and was also resistant to rapamycin treatment, suggesting that other complex molecules are capable of sustaining mTORC1 activity, even in the presence of the potent mTORC1 inhibitor,

rapamycin (*44*). We provide evidence that mEAK-7 forms an alternative mTOR complex to regulate S6K2/4E-BP1 signaling in human cells, where mEAK-7 does not interact with canonical mTORC1 nor mTORC2 partners (*12*). Thus, though sparse, these findings demonstrate that cell-type specificity may dictate the molecular landscape that supports mTOR regulation and activation (Figure 1.2).

mEAK-7 and the TLDc domain family of proteins

EAK-7 (enhancer-of-akt1-7) integrates nematode insulin receptor signaling (IRS)to regulate DAF-16/FoxO (*45*), and through this network, functions in parallel with Akt to affect nematode dauer formation and lifespan. In humans, IRS also controls diverse signaling cascades related to cell growth, proliferation, and survival (*46, 47*). Downstream of IRS, PI3K signaling supports mTORC1 signaling through regulation of Akt signaling to regulate the tuberous sclerosis complex (Figure 1.1). Since nematode EAK-7 works in parallel to insulin receptor/Akt signaling, we hypothesized that mEAK-7 is capable of regulating either Akt signaling or mTORC1 signaling, as both pathways are downstream of insulin receptor signaling. We demonstrate that mEAK-7 activates mTOR signaling through a novel S6K2/4E-BP1 axis (*12*). Though these findings were pivotal for describing the possibility of novel mTOR complexes in humans, the exact mechanism by which mEAK-7 regulates mTOR remains unclear.

To describe mEAK-7 molecular function, we looked for clues that could potentially point us in the direction of how mEAK-7 works. To engage in that first step, we sought the molecular compartment where mEAK-7 resides. We discovered that mEAK-7 is an evolutionarily conserved, lysosomal protein that activates mTOR

signaling in human cells. mEAK-7 was determined to be a lysosomal protein due to its co-localization at the lysosome to a significant degree, in comparison to other cellular compartments. Another way to determine protein function is to understand which domains are conserved within the mEAK-7 protein. mEAK-7 contains an *N*-myristoylation motif, a conserved TLDc domain, and a newly identified mTOR binding domain (MTB) (*12*). Unfortunately, little is known with regard to the role of these domains. The *N*-myristoylation motif is required for lipid-membrane tethering of proteins within the cell. We demonstrated that a glycine to alanine mutation was sufficient to untether mEAK-7 from the lysosome and the plasma membrane, suggesting that it played a crucial role in those cellular compartments (*12*). The TLDc domain is conserved in eukaryotes, but it is unclear what the role of this protein is. There are some instances which suggest that TLDc domain containing proteins confer neuroprotection against oxidative stress, but this appears to be dependent on the organism and cell type (*48*). Though evolutionarily conserved, the role of EAK-7 in nematodes versus mammalian cells are opposite of one another under stress conditions. *eak-7* null nematodes treated with H_2O_2 demonstrate enhanced survivability (*45*), meaning that the loss of EAK-7 enables the organism to improve their ability to respond to noxious stimuli. Overexpression of mEAK-7 in mammalian neurons results in protection against oxidative stress and silencing mEAK-7 in combination with arsenite (oxidative stressor) results in enhanced apoptosis (*49*), demonstrating that mEAK-7 evolved to combat toxic stimuli. Thus, understanding the context by which EAK-7 functions across different eukaryotes will be essential to understand the mechanistic differences in species.

Finally, we demonstrate that mEAK-7 directly binds to mTOR, and that binding is dependent on a newly discovered domain on mEAK-7, known as the MTB domain. The finding that mEAK-7 directly binds to mTOR suggests that it either acts as an adapter protein or an essential protein resulting in post-translational modification of mTOR. mEAK-7 recruits mTOR to the lysosome and is crucial for the function of mTOR signaling. mEAK-7 is an essential interacting protein of mTOR and mLST8, but not of other mTORC1 or mTORC2 components, suggesting that a third mTOR complex exists. From here onwards, we will use the term mTORC3 to describe this mEAK-7/mTOR complex because of its specificity in regulating S6K2/4E-BP1. In our second chapter, we demonstrated the molecular mechanism governing mTORC3 regulation in response to serum-, amino acid-, and insulin-mediated mTOR signaling. mEAK-7 is necessary for S6K2-mTOR interaction, S6K2 activity, and 4E-BP1-eIF4E interaction, it supports cell proliferation and cell migration. In the third chapter, we demonstrate a novel binding partner of mTORC3, namely, DNA-PK—which has a well-known role in non-homologous end joining after DNA damage. Thus, the culmination of these interacting molecules suggest that a third mTOR complex exists.

Prior to the discovery that mEAK-7 was a crucial regulator of mTOR signaling through S6K2/4E-BP1 axis, many reports demonstrated *MEAK7* overexpression in human cancer patients. *MEAK7* is 50-fold higher in metastatic hepatocellular carcinoma cell lines compared to normal hepatocellular cell lines and about 3-fold higher in liver cancer patients compared to healthy individuals (*50*). Microarray analysis of 76 primary tumors revealed that lymph node-positive breast cancers have a 1.66-fold increase in *MEAK7* expression over healthy controls (*51*). *MEAK7* expression is upregulated in

patients with metastatic renal clear-cell carcinoma and they are identified as a potential cancer immunotherapy targets (*52*). *MEAK7* is also the third most overexpressed target in non-tumor infiltrating lymphocytes in human ovarian cancers, suggesting that it could be a target for immunotherapy as well (*53*). These independent reports on the overexpression of *MEAK7* demonstrate the many different patient scenarios where mEAK-7 could be playing a role in tumorigenesis, since mEAK-7 activates mTOR signaling and mTOR signaling is implicated in cancer (*54*).

The mTOR signaling community may be on the verge of discovering new mTOR complexes in human cells. mEAK-7 supports the interaction of S6K2 and mTOR, but does not bind to raptor or rictor endogenously or exogenously (*12*). These findings were quite surprising because of the evolutionary differences that arose between mammalian EAK-7 and nematode EAK-7. Nematode EAK-7 functions in parallel to Akt signaling to control DAF-16 nuclear localization (human FoxO) during development and lifespan (*45*). mEAK-7 is essential for alternative mTOR signaling to regulate S6K2 and 4E-BP1, but nematodes only possess one S6 kinase, RSKS-1, making it unclear how or if, EAK-7 regulates TOR signaling in nematodes. Thus, understanding mEAK-7/mTORC3 in humans will further our understanding of this growth complex and human development and disease.

In concert with these findings, DNA-PK has been identified to interact with mEAK-7 to regulate mTOR and S6K2 signaling (Figure 3.5). DNA-PK is an essential conductor of non-homologous end joining DNA repair (*8*), but also has unexplored roles in regulation of cell metabolism (*55*). In human cancer, mEAK-7 protein is detectable at higher levels, compared to normal lung tissue and lymph nodes, suggesting a role in the

disease progression of human cancer patients with mEAK-7 (Figure 3.2). Thus, understanding how DNA damage responses and metabolism intersect will be essential to understanding the role of disease processes where cancer cells can hijack DNA damage responses to improve survival after DNA damage, resulting in chemoresistant or radioresistant cancers.

For the future, it will be important to elucidate the structure of mTORC3, to shed insight on how mEAK-7 interacts with other components to bind mTOR to affect downstream signaling. Understanding the structure of mTORC3 will allow for the development of mEAK-7-specific inhibitors for the treatment of human cancer and other aberrant mTOR activation and related diseases.

mTOR signaling through S6K1 versus S6K2

Studying mTOR in mammalian systems is challenging because gene knockout strategies pertaining to mTORC1 or mTORC2 components often result in embryonic lethality (*56*). This makes sense since the developing eukaryote requires a precise metabolic sensor that is capable of signaling to other cells when to grow and when to divide. Because S6K1 was the isoform first identified as the primary mTOR target in eukaryotes, it is the best-studied molecular target. S6K1 is an essential regulator of eukaryotic cell size and a common mTOR signaling marker (*30*). In transgenic S6K1 knockout mice with high-fat diets (HFD), loss of S6K1 leads to weight loss and increases insulin sensitivity (*57*) while mice with standard diets (SD) are glucose-intolerant, hypoinsulinaemic, and have reduced β cell size (*58*). This evidence suggests that loss of mTORC1 signaling via S6K1 alone may be detrimental to organismal

metabolism. Intriguingly, loss of both S6K1 and S6K2 reverses the deleterious effects of S6K1 knockout in mice, restores glucose tolerance under a SD, and enhances glucose tolerance with a HFD, suggesting that S6K2 plays a crucial role in the metabolism of mammals (*59*). Because mEAK-7 is the key regulator of an mTORC3/S6K2/4E-BP1 axis, mEAK-7 knockout mice may result in improved metabolic function and reduction of a type II diabetic state.

Much less is known about S6K2 in development, metabolism, and disease, but there has been a steadily growing interest in understanding the specific molecular role of S6K2 (*12*). For instance, S6K1 is a potent regulator of cell size, and postnatal delivery of S6K1 null mice are smaller than wild-type mice and S6K2 null mice are slightly larger, which suggests that S6K2 null mice may regulate another metabolic phenomenon unrelated to cell size. However, it is clear that S6K1 and S6K2 have some redundant targets because double knockout mice results in perinatal lethality (*60*). Intriguingly, S6K1 knockout mice express higher levels of S6K2 in the liver, muscles, thymus, and brain, and S6K2 remains responsive to rapamycin-mediated inhibition of S6 phosphorylation (*61*). Thus, S6K2 is not simply redundant to S6K1 and tissue-specific functions of S6K2 are increasingly being identified. Linking mEAK-7 to S6K2 activity demonstrates that there is specificity in the ability of mTOR to choose its complex, pending the cell context.

Adult S6K2 null mice tend to have higher basal levels of insulin in plasma, 2.5x more β cell mass with a SD, and improved glucose tolerance, as well as enhanced insulin sensitivity with a HFD (*62*). Additionally, single S6K2 knockout enhances ketone body production and increases peroxisome proliferator-activated receptor alpha activity

in the liver, and S6K1 knockout mice are capable of maintaining ($Ser^{240/244}$) p-S6 levels, while S6K2 knockout mice are not (*63*). Hence, elucidating the role of mEAK-7/mTORC3 signaling in mammals will further our understanding of diseases activated by mTOR signaling through aberrant S6K2 activity.

Therefore, ongoing research challenges the canon that S6K1 phosphorylation is a bona fide readout of mTORC1 activity. Because mTOR is capable of targeting S6K2, it has proven to be a crucial kinase that regulates diverse metabolic targets (*64*). Further study of mTORC3 will yield novel insights to human metabolism and disease, and will perhaps allow this pathway to be a specific therapeutic target. In these next sections, we will focus on development and disease states of the craniofacial region due to our interest as dentist-scientists.

mTOR signaling in head and neck squamous cell carcinoma

Aberrant or hyperactive mTORC1 and mTORC2 signaling has been implicated in human cancer progression and pathogenesis (*1*). Recently, a prostate cancer transgenic mouse model of mTOR-mediated tumor formation demonstrated that the 4E-BP1 axis controlled cancer initiation and genes associated with metastasis (*38*). In 2018, there was an estimated 51,540 new cases of head and neck squamous cell carcinoma, comprising 3% of all new cancers (*65*). Of those new cases of head and neck cancers, 10,030 patient deaths were recorded, comprising 1.6% of all cancer-related deaths in the United States (*65*). The Gutkind group demonstrated that 5 day treatment with rapamycin in HNSCC xenografts resulted in a regression of tumor size (*66*). Due to extensive interest in HNSCC, much work has been accomplished to

demonstrate that mTOR signaling is a viable molecular target against HNSCC (*66*) (Figure 1.3). However, the standard therapy for aggressive HNSCC patients includes tumor resection and several courses of chemotherapy and/or radiotherapy. Unfortunately, this treatment regimen results in populations of patients who still exhibit residual cancerous lesions. In a mouse model of minimal residual disease of HNSCC, rapamycin treatment could prevented HNSCC recurrence, and the cancers that did regrow were significantly smaller than their control counterparts. These data suggest that rapamycin could serve as adjuvant therapy given concurrently with standard surgery and chemo/radiotherapy (*67*). mTOR inhibition by rapamycin treatment is capable of preventing oral-tumor progression in a chemical carcinogenesis model (*68*). Though many clinicians and scientists had high hopes for rapalogs to help treat cancers with high mTOR activity, blocking mTOR signaling in a non-specific manner results in toxicities and ultimately requires a higher precision target within the mTOR signaling pathway (*1*). Decades of clinical trials using previous and current mTOR inhibitors demonstrate that a cancer specific target of mTOR signaling is required to reduce widespread toxicities in humans.

mTOR signaling in epithelial stem cell biology and mucositis

While the mTOR signaling community touts the benefits of mTOR inhibition for the treatment of hyperactivated mTOR cancers, there are still many challenges and side effects that occur with inhibition of this important metabolic sensor. mTOR inhibitors in the clinic have resulted in many different types of toxicities in humans. Up to 31% of patients taking mTORC1 inhibitors (temsirolimus) for the treatment of advanced renal

cell carcinoma reported mucositis (*69, 70*). Mucositis is defined as the painful inflammation and ulceration of the mucous membranes and is one of the most widely reported toxicities with mTOR signaling inhibitors. These findings in humans are intriguing because they are counter to the results described in mouse models treated with radiation. Mice treated with rapamycin after radiation damage improves the survivability of the salivary gland, suppresses epithelial stem cell senescence, and mucositis (*71*). Thus, while mice may benefit from rapamycin treatment with limited toxicities, humans with prolonged rapamycin treatment or mTOR inhibitors result in unintended mucositis. Interestingly, patients who undergo mTOR inhibitor treatment, such as rapalogs, experience a high incidence of painful mTOR inhibitor associated stomatitis (*72, 73*). Thus, evolutionary differences between mice and humans may confound the pronounced benefit of rapamycin treatment to reduce radiation-mediated toxicities. These findings suggest that a more specific mTOR inhibitor, perhaps targeting mTORC3 would be beneficial to patients who take rapalogs for the treatment of cancer. Creating mEAK-7 specific inhibitors would potentially reduce the toxicities that accompany rapalog treatment, prove more effective in targeting cancers versus normal tissue, and improve the quality-of-life for patients.

mTOR signaling in cranial neural crest cells and craniofacial development

Since mTOR is expressed in nearly every tissue during development and adulthood, it is likely that mTOR plays an important role in craniofacial development, an area of oral biology of immense interest to dentist-scientists. mTORC1 activity is high in prehypertrophic and early hypertrophic chondrocytes, indicative of a role in mammalian

endochondral bone formation. Further, p-S6, which serves as a readout of mTORC1 signaling, is highly expressed in prehypertrophic and early hypertrophic chondrocytes. While the deletion of raptor resulted in impaired chondrogenesis, ablation of raptor had minor effects on later chondrocyte proliferation and survival. These studies suggests that mTORC1 has an important role in early mammalian endochondral bone formation. Compared to mTORC1, mTORC2 plays a secondary role in endochondral skeletal development. Ablation of rictor does not significantly affect bone formation.

During development, the craniofacial skull is formed by migrating cranial neural crest cells (NCCs) and the reorganization of facial prominences and pharyngeal arches, thus making it highly susceptible to a large number of birth defects, known as neurocristopathies (*74*). Understanding the molecular pathways that regulate NCCs during development is essential to understand the development of craniofacial bones since NCCs form the bulk of the frontal, nasal, and zygomatic bone (*75*). Hyperactivation of mTORC1 via TSC1 deletion results in sclerotic craniofacial bone lesions where neural crest-derived (NCD) cells resulted in overpopulation of the NCD bone and thicker frontal bone due to an increase in NCD osteoblasts and osteoprogenitor cells (*76*). Additionally, it was demonstrated that Akt signaling, a prominent mTORC2 target, was required for NCC migration *in vivo* in *Xenopus laevis* (*77*). Still, very few studies on mTOR signaling have been conducted on craniofacial development. It would be interesting to determine the role of mTORC3 in craniofacial biology.

mTOR signaling in the tongue, taste buds, and salivary glands

In line with notion that mTOR inhibitors cause nonspecific toxicities, there are instances where mTOR inhibitors could benefit patients treated for different diseases. Mammals that receive irradiation treatment demonstrate a protective benefit from rapamycin treatment (*71*). The tongue is an important organ responsible for essential human behaviors, such as speech and eating. mTOR signaling is essential for a properly stratified epithelium and mTOR knockout or rictor knockout mice resulted in a hypoplastic epithelium of the tongue (*78*). mTOR inhibition has also been shown to reduce the malignancy of chemically-induced tongue cancer formation (*79*). While limited, many studies are now focusing on the role of mTOR signaling during tongue development or squamous cell carcinoma in the tongue. mTORC3 may also play a vital role in the development of the tongue, taste buds, and the malignancies associated with the tongue.

mTOR signaling plays a crucial role in salivary gland development. For humans, saliva production occurs so food can be digested in the gastrointestinal tracts. Thus, salivary glands play an important role in the digestion of food. Furthermore, rapamycin treatment prior to X-ray irradiation resulted in a protective effect in salivary glands (*80*). Intriguingly, radiation-induced salivary gland dysfunction was rescued after the administration of IGF-1, a potent activator of Akt signaling, suggesting that upregulation of mTORC2 signaling is beneficial for cell survival in salivary glands (*81*). IGF-1 treatment of salivary gland spheroids resulted in an enhanced ability for self-renewal after radiation treatment (*81*).

mTOR signaling in the dental pulp development and disease

mTORC1 and mTORC2 were identified as crucial regulators of self-renewal, pluripotency, and fate determination in human embryonic stem cells (*82*). Our initial interest to study mEAK-7 was to study its potential role in stem cell self-renewal. In lieu with our interests and due to growing interest, many groups are starting to study the role of mTOR in teeth, which house multipotent cells capable of giving rise to this important mammalian organ for food consumption. Most recently, groups have demonstrated, using a mouse-incisor model, that an FAK-YAP-mTOR axis regulates stem cell self-renewal and proliferation (*83*). For instance, it was demonstrated that mTOR signaling plays a crucial role in odontoblast differentiation and function (*84*). IGF-1 stimulation in dental pulp stem cells promote proliferation and osteogenic differentiation due to activated mTOR signaling and the subsequent upregulation of RUNX2, OSX, and OCN. During mTOR signaling inhibition, this inductive effect of IGF-1 is reversed suggesting IGF-1 plays an important role during osteogenic differentiation and may have clinical implications for osteoporosis (*85*).

mTOR signaling in osteoarthritis of the temporomandibular joint

Osteoarthritis (OA) is a chronic degenerative disease defined by gradual cartilage loss, synovial inflammation, and subchondral bone restructuring which results in debilitating severe pain and dysfunction. OA of the temporomandibular joint (TMJ) or TMJOA is an important subset classification of temporomandibular disorders, but the exact pathogenesis and process of TMJOA remain to be understood (*86*). In an injury-induced human and chondrocyte-specific mTOR KO mouse model of OA, mTOR gene

and protein were demonstrated to be upregulated in OA and suppression of mTOR via rapamycin or genetic knockout rescued the disease state of OA (*87*). mTOR signaling is up-regulated in the mechanically induced OA articular knee joints and rapamycin treatment was demonstrated to reduce the severity of OA and maintain cartilage cellularity (*88*). However, in a rat model of biomechanical stimulated chondrocyte autophagy, mTOR signaling is suppressed during the early response in the degenerative cartilage (*89*). This provides a striking contrast to evidence found in skeletal articular joints versus temporomandibular joints, possibly due to their embryological origins and differing mechanisms of action. Thus, understanding the molecular mechanisms governing the pathogenesis and pathobiology of TMJOA will spearhead novel therapeutics that specifically modulate mTOR signaling in diseased tissues, but not normal tissues. It is also possible that an mTORC3 axis governs the pathobiology of TMJOA.

Summary

The mammalian/mechanistic target of rapamycin (mTOR) is an essential nutrient sensor that regulates diverse biologic processes, such as lifespan, metabolism, protein synthesis, and autophagy. Since the discovery of mTOR more than two decades ago, scientific groups from around the world have demonstrated the importance of mTOR signaling in diverse cell and tissue types and that dysregulation of mTOR results in diseases or conditions as diverse as cancer, diabetes, neurological diseases, and craniofacial developmental anomalies. mTOR signaling is an essential metabolic regulator of pluripotency, self-renewal, and differentiation. Many diseases, such as

osteoarthritis of the temporomandibular joint, oral mucositis, head and neck squamous cell carcinoma, and irradiation-induced salivary gland dysfunction are, in part, caused by hyperactivated mTOR signaling. Suppression via rapamycin analogs, or rapalogs, or mTOR kinase specific ATP-catalytic site inhibitors has been demonstrated to reduce these detrimental effects. The characterization of the mTOR complexes, mTORC1 and mTORC2, have added tremendous insight to the nuances of mTOR signaling, but the notion of novel mTOR complexes is enticing. However, furthering our understanding of mEAK-7/mTORC3 from a developmental biology perspective and a disease processes standpoint will inform the approach for drug discovery and treatment of mTOR related diseases.

The focus of my thesis is to investigate the role of a novel protein, mammalian EAK-7, in the context of metabolism and disease. We have tested the hypothesis that mEAK-7 is essential for mTOR signaling through an alternative mTOR complex. Additionally, we demonstrate a role for mEAK-7 in human cancer cells and describe a working molecular model for mEAK-7 within mTORC3 signaling. All of the work done in this thesis has been done in the context of non-cancerous and cancer cell lines, as well as analysis of human cancer patient samples. The following chapter will elucidate the molecular underpinnings of mEAK-7 with relation to mTOR signaling in human cells.

Figures

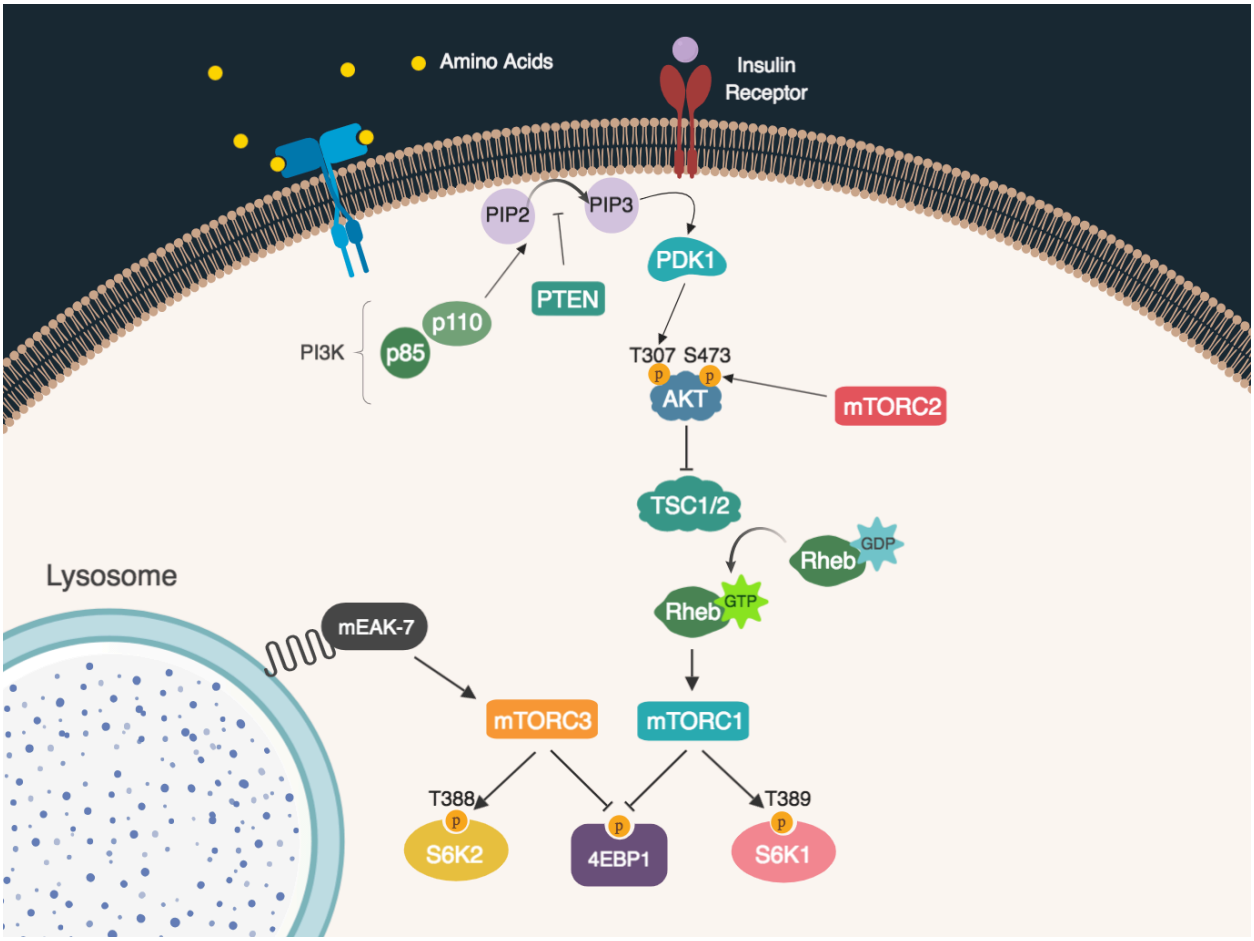

Figure 1.1. Summary of mTOR signaling and mTOR complexes. Insulin, amino acids, and nutrient signals are capable of activating mTOR signaling. Insulin binds to the insulin receptor, a receptor tyrosine kinase that ultimately activates PI3K to activate Akt signaling. PI3K activates PDK1 by inducing PIP3 from PIP2, where PDK1 phosphorylates T308. Activated Akt will phosphorylate and inhibit the Tuberous Sclerosis complex (TSC1/2), which inhibits Rheb GTPase in the absence of nutrients. Inhibition of TSC through nutrient stimulation allows for Rheb GTPase to activate mTORC1, and allows mTOR to phosphorylate and activate S6K1 and phosphorylate and inhibit 4E-BP1. mTORC2 also regulates Akt signaling, by phosphorylating S473, in response to nutrients. mTORC3 is formed by mEAK-7 and is necessary for S6K2 activation in human cells.

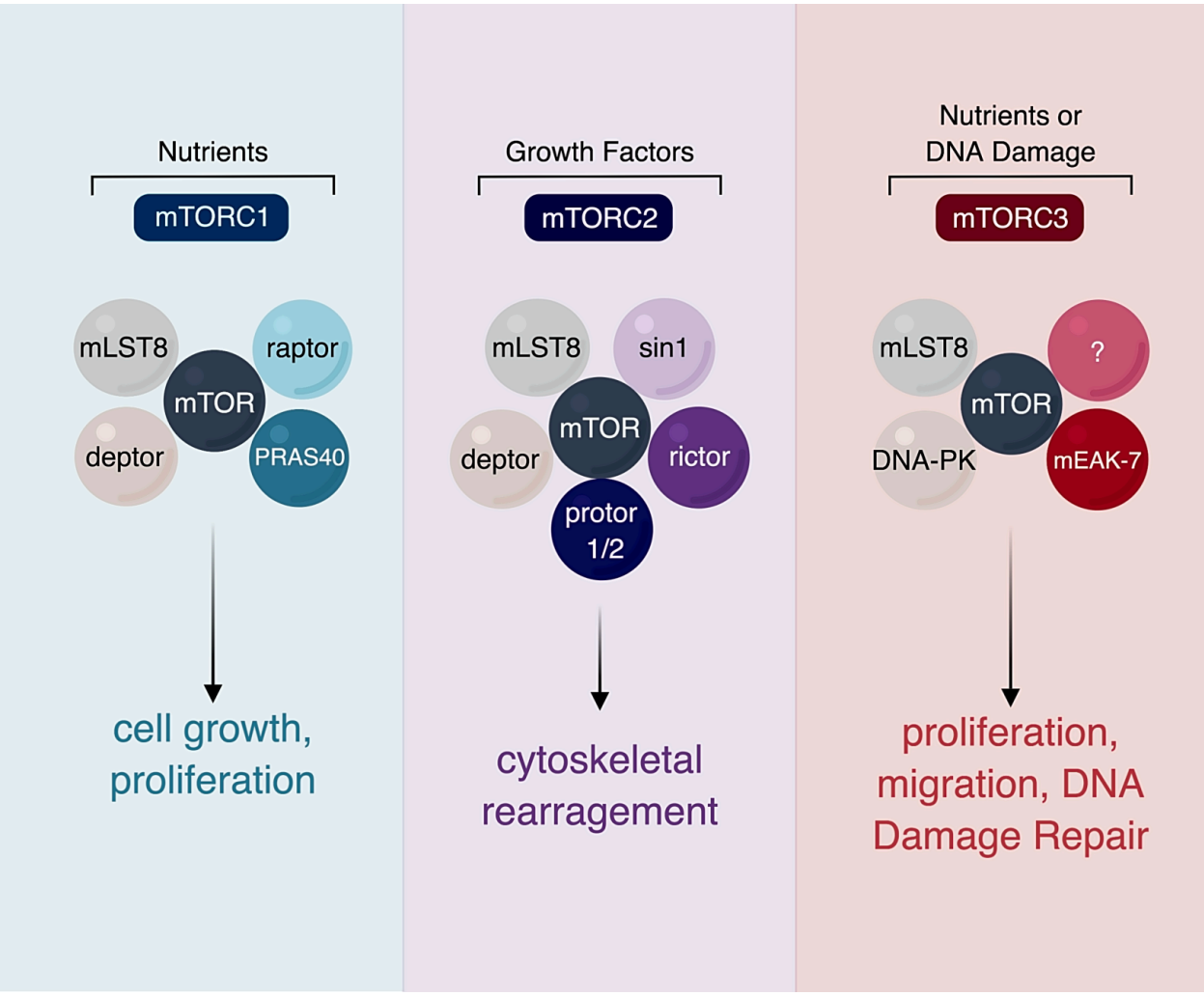

Figure 1.2. mTOR complex 1, 2, and 3. mTORC1 is comprised of regulatory-associated protein of mTOR (raptor), mammalian lethal with SEC13 protein 8 (mLST8) or GβL, Proline-rich AKT1 substrate 1 (PRAS40), and DEPTOR and is essential for cell growth and cell proliferation. mTORC2 is comprised of mLST8, rapamycin-insensitive companion of mTOR (rictor), mammalian stress-activated protein kinase interacting protein 1 (mSIN1), Protor, DEPTOR, and Tti1 & Tel2 to regulate cytoskeletal rearrangement. mTORC3 is comprised of mTOR, mEAK-7, mLST8, DNA-PK, and unknown proteins to regulate cell proliferation and migration in mEAK-7 positive cells like malignant cancer cells. All complexes act at the lysosome, an essential cellular compartment for mTOR signaling, but govern different cellular processes.

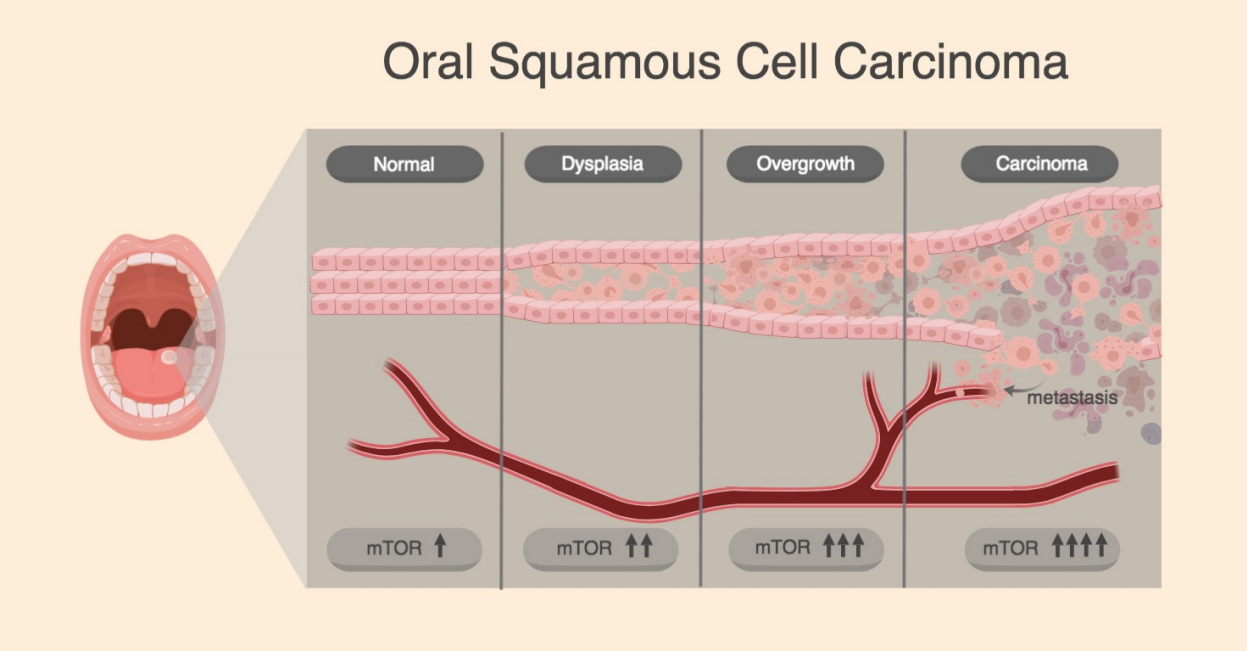

Figure 1.3. mTOR signaling is significantly enhanced in later stages of mTOR signaling. In 2018, 51,540 new cases of head and neck squamous cell carcinoma were discovered, comprising 3% of all new cancers. An estimated 10,030 new patient deaths are a direct result of patients with head and neck cancer, comprising of 1.6% of all cancer-related deaths in the US. As tissues of the oral cavity go from dysplasia to overgrowth to carcinoma stages, it's been demonstrated that mTOR signaling is upregulated. mTOR signaling is a viable molecular target against HNSCC. However, the standard therapy for cancer patients is to have tumor resection and undergo several courses of chemotherapy and/or radiotherapy. It was demonstrated that even with this treatment regimen, there are still populations of patients who exhibit residual cancer disease, even with pathology-graded clean tumor margins and that rapamycin was suitable for treatment of these patient populations. mTOR inhibition by rapamycin treatment is capable of preventing oral-tumor progression by chemical carcinogenesis model. Though many clinicians and scientists had high hopes for rapalogs to help treat cancers with high mTOR activity, blocking mTOR signaling in a non-specific manner results in toxicities and ultimately requires a higher precision target within the mTOR signaling pathway.

References

1. R. A. Saxton, D. M. Sabatini, mTOR Signaling in Growth, Metabolism, and Disease. *Cell* **168**, 960-976 (2017).
2. D. Benjamin, M. Colombi, C. Moroni, M. N. Hall, Rapamycin passes the torch: a new generation of mTOR inhibitors. *Nature Reviews Drug Discovery* **10**, 868-880 (2011).
3. J. Chung, C. J. Kuo, G. R. Crabtree, J. Blenis, Rapamycin-FKBP Specifically Blocks Growth-Dependent Activation of and Signaling by the 70 kd S6 Protein Kinases. *Cell* **69**, 1227-1236 (1992).
4. J. Heitman, N. R. Movva, M. N. Hall, Targets for Cell Cycle Arrest by the Immunosuppressant Rapamycin in Yeast. *Science* **253**, 905-909 (1991).
5. D. M. Sabatini, H. Erdjument-Bromage, M. Lui, P. Tempst, S. H. Snyder, RAFT1: a mammalian protein that binds to FKBP12 in a rapamycin-dependent fashion and is homologous to yeast TORs. *Cell* **78**, 35-43 (1992).
6. E. J. Brown, M. W. Albers, T. B. Shin, K. ichikawa, C. T. Keith, W. S. Lane, S. L. Schreiber, A mammalian protein targeted by G1-arresting rapamycin–receptor complex. *Nature* **369**, 756-758 (1994).
7. J. Kunz, R. Henriquez, U. Schneider, M. Deuter-Reinhard, N. R. Movva, M. N. Hall, Target of Rapamycin in Yeast, TOR2, Is an Essential Phosphatidylinositol Kinase Homolog Required for G1 Progression. *Cell* **73**, 585-596 (1993).

8. A. N. Blackford, S. P. Jackson, ATM, ATR, and DNA-PK: The Trinity at the Heart of the DNA Damage Response. *Mol Cell* **66**, 801-817 (2017).

9. S. B. Helliwell, P. Wagner, J. Kunz, M. Deuter-Reinhard, R. Henriquez, M. N. Hall, TOR1 and TOR2 Are Structurally and Functionally Similar but not Identical Phosphatidylinositol Kinase Homologues in Yeast. *Molecular Biology of the Cell* **5**, 105-118 (1994).

10. E. Arias, H. Koga, A. Diaz, E. Mocholi, B. Patel, A. M. Cuervo, Lysosomal mTORC2/PHLPP1/Akt Regulate Chaperone-Mediated Autophagy. *Mol Cell* **59**, 270-284 (2015).

11. C. Betz, M. N. Hall, Where is mTOR and what is it doing there? *J Cell Biol* **203**, 563-574 (2013).

12. J. T. Nguyen, C. Ray, A. L. Fox, D. B. Mendonça, J. K. Kim, P. H. Krebsbach, Mammalian EAK-7 activates alternative mTOR signaling to regulate cell proliferation and migration. *Science Advances* **4**, 1-15 (2018).

13. X. C. Bai, G. McMullan, S. H. Scheres, How cryo-EM is revolutionizing structural biology. *Trends Biochem Sci* **40**, 49-57 (2015).

14. C. H. S. Aylett, E. Sauer, S. Imseng, D. Boehringer, M. N. Hall, N. Ban, T. Maier, Architecture of human mTOR complex 1. *Science* **351**, 48-52 (2016).

15. M. Karuppasamy, B. Kusmider, T. M. Oliveira, C. Gaubitz, M. Prouteau, R. Loewith, C. Schaffitzel, Cryo-EM structure of Saccharomyces cerevisiae target of rapamycin complex 2. *Nat Commun* **8**, 1729 (2017).

16. E. Stuttfeld, C. H. Aylett, S. Imseng, D. Boehringer, A. Scaiola, E. Sauer, M. N. Hall, T. Maier, N. Ban, Architecture of the human mTORC2 core complex. *Elife* **7**, (2018).

17. D. D. Sarbassov, S. M. Ali, D. H. Kim, D. A. Guertin, R. R. Latek, H. Erdjument-Bromage, P. Tempst, D. M. Sabatini, Rictor, a novel binding partner of mTOR, defines a rapamycin-insensitive and raptor-independent pathway that regulates the cytoskeleton. *Curr Biol* **14**, 1296-1302 (2004).

18. D. W. Lamming, L. Ye, P. Katajisto, M. D. Goncalves, M. Saitoh, D. M. Stevens, J. G. Davis, A. B. Salmon, A. Richardson, R. S. Ahima, D. A. Guertin, D. M. Sabatini, J. A. Baur, Rapamycin-Induced Insulin Resistance Is Mediated by mTORC2 Loss and Uncoupled from Longevity. *Science* **335**, 1638-1643 (2012).

19. J. Huang, B. D. Manning, The TSC1-TSC2 complex: a molecular switchboard controlling cell growth. *Biochem J* **412**, 179-190 (2008).

20. K. Inoki, Y. Li, T. Zhu, J. Wu, K. L. Guan, TSC2 is phosphorylated and inhibited by Akt and suppresses mTOR signalling. *Nat Cell Biol* **4**, 648-657 (2002).

21. C. C. Dibble, W. Elis, S. Menon, W. Qin, J. Klekota, J. M. Asara, P. M. Finan, D. J. Kwiatkowski, L. O. Murphy, B. D. Manning, TBC1D7 is a third subunit of the TSC1-TSC2 complex upstream of mTORC1. *Mol Cell* **47**, 535-546 (2012).

22. S. Menon, C. C. Dibble, G. Talbott, G. Hoxhaj, A. J. Valvezan, H. Takahashi, L. C. Cantley, B. D. Manning, Spatial control of the TSC complex integrates insulin and nutrient regulation of mTORC1 at the lysosome. *Cell* **156**, 771-785 (2014).

23. Y. Sancak, T. R. Peterson, Y. D. Shaul, R. A. Lindquist, C. C. Thoreen, L. Bar-Peled, D. M. Sabatini, The Rag GTPases bind raptor and mediate amino acid signaling to mTORC1. *Science* **320**, 1496-1501 (2008).

24. Y. Sancak, L. Bar-Peled, R. Zoncu, A. L. Markhard, S. Nada, D. M. Sabatini, Ragulator-Rag complex targets mTORC1 to the lysosomal surface and is necessary for its activation by amino acids. *Cell* **141**, 290-303 (2010).

25. K. M. Hennig, J. Colombani, T. P. Neufeld, TOR coordinates bulk and targeted endocytosis in the Drosophila melanogaster fat body to regulate cell growth. *J Cell Biol* **173**, 963-974 (2006).

26. R. J. Flinn, Y. Yan, S. Goswami, P. J. Parker, J. M. Backer, The Late Endosome is Essential for mTORC1 Signaling. *Molecular Biology of the Cell* **21**, 833–841 (2009).

27. J. Kunz, U. Schneider, I. Howald, A. Schmidt, M. N. Hall, HEAT repeats mediate plasma membrane localization of Tor2p in yeast. *J Biol Chem* **275**, 37011-37020 (2000).

28. K. P. Wedaman, A. Reinke, S. Anderson, J. Yates III, J. M. McCaffery, T. Powers, Tor Kinases Are in Distinct Membrane-associated Protein Complexes in Saccharomyces cerevisiae. *J Biol Chem* **275**, 37011-37020 (2000).

29. F. Hao, K. Kondo, T. Itoh, S. Ikari, S. Nada, M. Okada, T. Noda, Rheb localized on the Golgi membrane activates lysosome-localized mTORC1 at the Golgi-lysosome contact site. *J Cell Sci* **131**, (2018).

30. D. C. Fingar, S. Salama, C. Tsou, E. Harlow, J. Blenis, Mammalian cell size is controlled by mTOR and its downstream targets S6K1 and 4EBP1/eIF4E. *Genes Dev* **16**, 1472-1487 (2002).

31. D. J. Price, J. R. Grove, V. Calvo, J. Avruch, B. E. Bierer, Rapamycin-induced inhibition of the 70-kilodalton S6 protein kinase. *Science* **257**, 973-977 (1992).

32. S. Isotani, K. Hara, C. Tokunaga, H. Inoue, J. Avruch, K. Yonezawa, Immunopurified Mammalian Target of Rapamycin Phosphorylates and Activates p70 S6 Kinase Alpha In Vitro. *J Biol Chem* **274**, 34493-34498 (1999).

33. M. Saitoh, N. Pullen, P. Brennan, D. Cantrell, P. B. Dennis, G. Thomas, Regulation of an activated S6 kinase 1 variant reveals a novel mammalian target of rapamycin phosphorylation site. *J Biol Chem* **277**, 20104-20112 (2002).

34. R. B. Pearson, P. B. Dennis, J. W. Han, N. A. Williamson, S. C. Kozma, R. E. Wettenhall, G. Thomas, The principal target of rapamycin-induced p70s6k inactivation is a novel phosphorylation site within a conserved hydrophobic domain. *EMBO J* **14**, 5279-5287 (1995).

35. O. Meyuhas, D. Avni, S. Shama, Translational control of ribosomal protein mRNAs in eukaryotes. *Cold Spring Harbor Laboratory Press*, 363-364 (1996).

36. A.-C. Gingras, S. P. Gygi, B. Raught, R. D. Polakiewicz, R. T. Abraham, M. F. Hoekstra, R. Aebersold, N. Sonenberg, Regulation of 4E-BP1 phosphorylation- a novel two-step mechanism. *Genes Dev.* **13**, 1422-1437 (1999).

37. A.-C. Gingras, B. Raught, S. P. Gygi, A. Niedzwiecka, M. Miron, S. K. Burley, R. D. Polakiewicz, A. Wyslouch-Cieszynska, R. Aebersold, N. Sonenberg,

Hierarchical phosphorylation of the translation inhibitor 4E-BP1. *Genes Dev.* **15**, 2852-2864 (2001).

38. A. C. Hsieh, Y. Liu, M. P. Edlind, N. T. Ingolia, M. R. Janes, A. Sher, E. Y. Shi, C. R. Stumpf, C. Christensen, M. J. Bonham, S. Wang, P. Ren, M. Martin, K. Jessen, M. E. Feldman, J. S. Weissman, K. M. Shokat, C. Rommel, D. Ruggero, The translational landscape of mTOR signalling steers cancer initiation and metastasis. *Nature* **485**, 55-61 (2012).

39. C. H. Jung, S. H. Ro, J. Cao, N. M. Otto, D. H. Kim, mTOR regulation of autophagy. *FEBS Lett* **584**, 1287-1295 (2010).

40. E. White, The role for autophagy in cancer. *Journal of Clinical Investigation* **125**, 42-46 (2015).

41. C. C. Thoreen, S. A. Kang, J. W. Chang, Q. Liu, J. Zhang, Y. Gao, L. J. Reichling, T. Sim, D. M. Sabatini, N. S. Gray, An ATP-competitive mammalian target of rapamycin inhibitor reveals rapamycin-resistant functions of mTORC1. *J Biol Chem* **284**, 8023-8032 (2009).

42. I. Patursky-Polischuk, M. Stolovich-Rain, M. Hausner-Hanochi, J. Kasir, N. Cybulski, J. Avruch, M. A. Ruegg, M. N. Hall, O. Meyuhas, The TSC-mTOR pathway mediates translational activation of TOP mRNAs by insulin largely in a raptor- or rictor-independent manner. *Mol Cell Biol* **29**, 640-649 (2009).

43. L. J. Smithson, D. H. Gutmann, Proteomic analysis reveals GIT1 as a novel mTOR complex component critical for mediating astrocyte survival. *Genes Dev.* **30**, 1383-1388 (2016).

44. F. C. Harwood, R. I. K. Geltink, B. P. O'Hara, M. Cardone, L. Janke, D. Finkelstein, I. Entin, L. Paul, P. J. Houghton, G. C. Grosveld, ETV7 is an essential component of a rapamycin-insensitive mTOR complex in cancer. *Science Advances* **4**, 1-18 (2018).

45. H. Alam, T. W. Williams, K. J. Dumas, C. Guo, S. Yoshina, S. Mitani, P. J. Hu, EAK-7 controls development and life span by regulating nuclear DAF-16/FoxO activity. *Cell Metab* **12**, 30-41 (2010).

46. S. Wullschleger, R. Loewith, M. N. Hall, TOR signaling in growth and metabolism. *Cell* **124**, 471-484 (2006).

47. M. Shimobayashi, M. N. Hall, Making new contacts: the mTOR network in metabolism and signalling crosstalk. *Nat Rev Mol Cell Biol* **15**, 155-162 (2014).

48. M. J. Finelli, P. L. Oliver, TLDc proteins: new players in the oxidative stress response and neurological disease. *Mamm Genome* **28**, 395-406 (2017).

49. M. J. Finelli, L. Sanchez-Pulido, K. X. Liu, K. E. Davies, P. L. Oliver, The Evolutionarily Conserved Tre2/Bub2/Cdc16 (TBC), Lysin Motif (LysM), Domain Catalytic (TLDc) Domain Is Neuroprotective against Oxidative Stress. *J Biol Chem* **291**, 2751-2763 (2016).

50. P. Riou, R. Saffroy, J. Comoy, M. Gross-Goupil, J.-P. Thiery, J.-F. Emile, D. Azoulay, D. Piatier-Tonneau, A. Lemoine, B. Debuire, Investigation in Liver Tissues and Cell Lines of the Transcription of 13 Genes Mapping to the 16q24 Region That Are Frequently Deleted in Hepatocellular Carcinoma. *Clinical Cancer Research* **8**, 3178-3186 (2002).

51. R. E. Ellsworth, L. A. Field, B. Love, J. L. Kane, J. A. Hooke, C. D. Shriver, Differential gene expression in primary breast tumors associated with lymph node metastasis. *Int J Breast Cancer* **2011**, 142763 (2011).

52. H. Kawashima, A. Obayashi, M. Kawamura, S. Masaki, S. Tamada, T. Iguchi, J. Uchida, K. Kuratsukuri, T. Tanaka, T. Nakatani, Galectin 9 and PINCH, novel immunotherapytargets of renal cell carcinoma-a rationale tofind potential tumour antigens and the resultingcytotoxic T lymphocytes induced by thederived peptides. *BJU International* **113**, 320–332 (2013).

53. R. J. Buckanovich, A. Facciabene, S. Kim, F. Benencia, D. Sasaroli, K. Balint, D. Katsaros, A. O'Brien-Jenkins, P. A. Gimotty, G. Coukos, Endothelin B receptor mediates the endothelial barrier to T cell homing to tumors and disables immune therapy. *Nat Med* **14**, 28-36 (2008).

54. M. Laplante, D. M. Sabatini, mTOR signaling in growth control and disease. *Cell* **149**, 274-293 (2012).

55. R. H. Wong, I. Chang, C. S. Hudak, S. Hyun, H. Y. Kwan, H. S. Sul, A role of DNA-PK for the metabolic gene regulation in response to insulin. *Cell* **136**, 1056-1072 (2009).

56. D. A. Guertin, D. M. Stevens, C. C. Thoreen, A. A. Burds, N. Y. Kalaany, J. Moffat, M. Brown, K. J. Fitzgerald, D. M. Sabatini, Ablation in mice of the mTORC components raptor, rictor, or mLST8 reveals that mTORC2 is required for signaling to Akt-FOXO and PKCalpha, but not S6K1. *Dev Cell* **11**, 859-871 (2006).

57. S. H. Um, F. Frigerio, M. Watanabe, F. Picard, M. Joaquin, M. Sticker, S. Fumagalli, P. R. Allegrini, S. C. Kozma, J. Auwerx, G. Thomas, Absence of S6K1 protects against age- and diet-induced obesity while enhancing insulin sensitivity. *Nature* **431**, (2004).

58. M. Pende, S. C. Kozma, M. Jaquet, V. Oorschot, R. Burcelin, Y. K. Le Marchand-Brustel, Judith, B. Thorens, G. Thomas, Hypoinsulinaemia, glucose intolerance and diminished β-cell size in S6K1-deficient mice. *Nature* **408**, 994-997 (2000).

59. T. R. Castaneda, W. Abplanalp, S. H. Um, P. T. Pfluger, B. Schrott, K. Brown, E. Grant, L. Carnevalli, S. C. Benoit, D. A. Morgan, D. Gilham, D. Y. Hui, K. Rahmouni, G. Thomas, S. C. Kozma, D. J. Clegg, M. H. Tschop, Metabolic control by S6 kinases depends on dietary lipids. *PLoS One* **7**, e32631 (2012).

60. M. Pende, S. H. Um, V. Mieulet, M. Sticker, V. L. Goss, J. Mestan, M. Mueller, S. Fumagalli, S. C. Kozma, G. Thomas, S6K1-/-/S6K2-/- Mice Exhibit Perinatal Lethality and Rapamycin-Sensitive 5'-Terminal Oligopyrimidine mRNA Translation and Reveal a Mitogen-Activated Protein Kinase-Dependent S6 Kinase Pathway. *Molecular and Cellular Biology* **24**, 3112-3124 (2004).

61. H. Shima, M. Pende, Y. Chen, S. Fumagalli, G. Thomas, S. C. Kozma, Disruption of the p70s6k:p85s6k gene reveals a small mouse phenotype and a new functional S6 kinase. *EMBO J* **17**, 6649-6659 (1998).

62. K. M. Taylor, J. Bajko, M. S. Cabrera, C. Kremer, B. Meyer-Puttlitz, A. M. Schulte, S. H. Cheng, R. K. Scheule, R. J. Moreland, S6 Kinase 2 Deficiency Improves Glucose Disposal in Mice Fed a High Fat Diet. *Journal of Diabetes & Metabolism* **05**, 1-7 (2014).

63. K. Kim, S. Pyo, S. H. Um, S6 kinase 2 deficiency enhances ketone body production and increases peroxisome proliferator-activated receptor alpha activity in the liver. *Hepatology* **55**, 1727-1737 (2012).

64. O. E. Pardo, M. J. Seckl, S6K2: The Neglected S6 Kinase Family Member. *Front Oncol* **3**, 191 (2013).

65. N. C. Institute, Cancer Stat Facts: Oral Cavity and Pharynx Cancer. 1 (2018).

66. P. Amornphimoltham, V. Patel, A. Sodhi, N. G. Nikitakis, J. J. Sauk, E. A. Sausville, A. A. Molinolo, J. S. Gutkind, Mammalian target of rapamycin, a molecular target in squamous cell carcinomas of the head and neck. *Cancer Res* **65**, 9953-9961 (2005).

67. C. O. Nathan, N. Amirghahari, X. Rong, T. Giordano, D. Sibley, M. Nordberg, J. Glass, A. Agarwal, G. Caldito, Mammalian target of rapamycin inhibitors as possible adjuvant therapy for microscopic residual disease in head and neck squamous cell cancer. *Cancer Res* **67**, 2160-2168 (2007).

68. R. Czerninski, P. Amornphimoltham, V. Patel, A. A. Molinolo, J. S. Gutkind, Targeting mammalian target of rapamycin by rapamycin prevents tumor progression in an oral-specific chemical carcinogenesis model. *Cancer Prev Res (Phila)* **2**, 27-36 (2009).

69. S. T. Sonis, Mucositis: The impact, biology and therapeutic opportunities of oral mucositis. *Oral Oncol* **45**, 1015-1020 (2009).

70. H. Gerullis, L. Bergmann, L. Maute, C. Eimer, T. Otto, Experiences and practical conclusions concerning temsirolimus use and adverse event management in

advanced renal cell carcinoma within a compassionate use program in Germany. *Cancer Chemother Pharmacol* **63**, 1097-1102 (2009).

71. R. Iglesias-Bartolome, V. Patel, A. Cotrim, K. Leelahavanichkul, A. A. Molinolo, J. B. Mitchell, J. S. Gutkind, mTOR inhibition prevents epithelial stem cell senescence and protects from radiation-induced mucositis. *Cell Stem Cell* **11**, 401-414 (2012).

72. D. E. Peterson, J. A. O'Shaughnessy, H. S. Rugo, S. Elad, M. M. Schubert, C. T. Viet, C. Campbell-Baird, J. Hronek, V. Seery, J. Divers, J. Glaspy, B. L. Schmidt, T. F. Meiller, Oral mucosal injury caused by mammalian target of rapamycin inhibitors: emerging perspectives on pathobiology and impact on clinical practice. *Cancer Med* **5**, 1897-1907 (2016).

73. C. B. Boers-Doest, J. B. Epstein, J. E. Raber-Durlacher, J. Ouwerkerk, R. M. Logan, J. A. Brakenhoff, M. E. Lacouture, H. Gelderblom, Oral Adverse Events Associated with Tyrosine Kinase and Mammalian Target of Rapamycin Inhibitors in Renal Cell Carcinoma- A Structured Literature Review. *The Oncologist* **17**, 135–144 (2012).

74. D. R. Cordero, S. Brugmann, Y. Chu, R. Bajpai, M. Jame, J. A. Helms, Cranial neural crest cells on the move: their roles in craniofacial development. *Am J Med Genet A* **155A**, 270-279 (2011).

75. X. Jiang, S. Iseki, R. E. Maxson, H. M. Sucov, G. M. Morriss-Kay, Tissue origins and interactions in the mammalian skull vault. *Dev Biol* **241**, 106-116 (2002).

76. F. Fang, S. Sun, L. Wang, J. L. Guan, M. Giovannini, Y. Zhu, F. Liu, Neural Crest-Specific TSC1 Deletion in Mice Leads to Sclerotic Craniofacial Bone Lesion. *J Bone Miner Res* **30**, 1195-1205 (2015).

77. K. Mathavan, V. Khedgikar, V. Bartolo, D. Alfandari, The ectodomain of cadherin-11 binds to erbB2 and stimulates Akt phosphorylation to promote cranial neural crest cell migration. *PLoS One* **12**, e0188963 (2017).

78. X. Ding, W. Bloch, S. Iden, M. A. Ruegg, M. N. Hall, M. Leptin, L. Partridge, S. A. Eming, mTORC1 and mTORC2 regulate skin morphogenesis and epidermal barrier formation. *Nat Commun* **7**, 13226 (2016).

79. S. H. Li, C. Y. Chien, W. T. Huang, S. D. Luo, Y. Y. Su, W. Y. Tien, Y. C. Lan, C. H. Chen, Prognostic significance and function of mammalian target of rapamycin in tongue squamous cell carcinoma. *Sci Rep* **7**, 8178 (2017).

80. Z. Zhu, B. Pang, R. Iglesias-Bartolome, X. Wu, L. Hu, C. Zhang, J. Wang, J. S. Gutkind, S. Wang, Prevention of irradiation-induced salivary hypofunction by rapamycin in swine parotid glands. *Oncotarget* **7**, 20271-20281 (2016).

81. O. Grundmann, J. L. Fillinger, K. R. Victory, R. Burd, K. H. Limesand, Restoration of radiation therapy-induced salivary gland dysfunction in mice by post therapy IGF-1 administration. *BMC Cancer* **10**, 1-9 (2010).

82. J. S. Yu, W. Cui, Proliferation, survival and metabolism: the role of PI3K/AKT/mTOR signalling in pluripotency and cell fate determination. *Development* **143**, 3050-3060 (2016).

83. J. K. Hu, W. Du, S. J. Shelton, M. C. Oldham, C. M. DiPersio, O. D. Klein, An FAK-YAP-mTOR Signaling Axis Regulates Stem Cell-Based Tissue Renewal in Mice. *Cell Stem Cell* **21**, 91-106 e106 (2017).

84. J. K. Kim, J. Baker, J. E. Nor, E. E. Hill, mTor plays an important role in odontoblast differentiation. *J Endod* **37**, 1081-1085 (2011).

85. X. Feng, D. Huang, X. Lu, G. Feng, J. Xing, J. Lu, K. Xu, W. Xia, Y. Meng, T. Tao, L. Li, Z. Gu, Insulin-like growth factor 1 can promote proliferation and osteogenic differentiation of human dental pulp stem cells via mTOR pathway. *Dev Growth Differ* **56**, 615-624 (2014).

86. X. D. Wang, J. N. Zhang, Y. H. Gan, Y. H. Zhou, Current understanding of pathogenesis and treatment of TMJ osteoarthritis. *J Dent Res* **94**, 666-673 (2015).

87. Y. Zhang, F. Vasheghani, Y. H. Li, M. Blati, K. Simeone, H. Fahmi, B. Lussier, P. Roughley, D. Lagares, J. P. Pelletier, J. Martel-Pelletier, M. Kapoor, Cartilage-specific deletion of mTOR upregulates autophagy and protects mice from osteoarthritis. *Ann Rheum Dis* **74**, 1432-1440 (2015).

88. B. Carames, A. Hasegawa, N. Taniguchi, S. Miyaki, F. J. Blanco, M. Lotz, Autophagy activation by rapamycin reduces severity of experimental osteoarthritis. *Ann Rheum Dis* **71**, 575-581 (2012).

89. M. Zhang, J. Zhang, L. Lu, Z. Y. Qiu, X. Zhang, S. B. Yu, Y. P. Wu, M. Q. Wang, Enhancement of chondrocyte autophagy is an early response in the degenerative cartilage of the temporomandibular joint to biomechanical dental stimulation. *Apoptosis* **18**, 423-434 (2013).

Chapter 2 – Mammalian EAK-7 activates alternative mTOR signaling to regulate cell proliferation and migration

Summary

Nematode EAK-7 regulates dauer formation and controls lifespan, but the function of the human ortholog, mammalian EAK-7 (mEAK-7), is unknown. We report that mEAK-7 activates an alternative mTOR signaling pathway in human cells, in which mEAK-7 interacts with mTOR at the lysosome to facilitate S6K2 activation and 4E-BP1 repression. Despite interacting with mTOR and mLST8, mEAK-7 does not interact with other mTORC1 or mTORC2 components, yet is essential for mTOR signaling at the lysosome. This phenomenon is distinguished by S6 and 4E-BP1 activity in response to nutrient stimulation. Conventional S6K1 phosphorylation is uncoupled from S6 activity in response to mEAK-7 knockdown. mEAK-7 recruits mTOR to the lysosome, a crucial compartment for mTOR activation. Loss of mEAK-7 results in a marked decrease in lysosomal localization of mTOR, while overexpression of mEAK-7 results in enhanced lysosomal localization of mTOR. Deletion of the C-terminus of mEAK-7 significantly decreases mTOR interaction. mEAK-7 knockdown decreases cell proliferation and migration, while overexpression of mEAK-7 enhances these cellular effects. Constitutively activated S6K rescues mTOR signaling in mEAK-7 knocked-down cells. Thus, mEAK-7 activates an alternative mTOR signaling pathway through S6K2 and 4E-BP1 to regulate cell proliferation and migration.

Introduction

In the first chapter, we focus on a broad overview of mTOR signaling in development and disease. In the second chapter, we focus on the role of a novel protein that we discovered in the lab. Evolution demonstrates that fundamental signaling pathways in eukaryotes are conserved through orthologous and paralogous genes. In *C. elegans*, EAK-7 (enhancer-of-akt1-7) integrates insulin receptor signaling (IRS) to regulate DAF-16/FoxO, and through this network, functions in parallel with Akt to affect nematode dauer formation and lifespan (*43*). However, how EAK-7 imparts these effects in mammals is unknown. In humans, IRS also controls diverse signaling cascades related to cell growth, proliferation, and survival (*45*). One of these crucial metabolic signaling cascades is the mechanistic or mammalian target of rapamycin (mTOR) signaling pathway. On an expeditionary search for novel antibiotic compounds in the South Pacific, rapamycin was discovered on Rapa Nui and was found to block yeast growth and to have strong immunosuppressive effects in mammals (*1*). Rapamycin was subsequently shown to form a complex with FKBP12, which resulted in a gain of function that inhibited signal transduction pathways required for cell growth and proliferation (*3*). mTOR was identified as the target of the rapamycin-FKBP12 inhibitory complex responsible for repressing protein production and cell metabolism in eukaryotes (*5*). Decades later, laboratories across the world have demonstrated the essential role of mTOR signaling in eukaryotic development and disease in response to nutrient sensing (*1*).

mTOR is a member of the phosphatidylinositol-3 kinase-related kinases family. mTOR signaling diverges into two known complexes: mTOR complex 1 (mTORC1) and mTOR complex 2 (mTORC2) (*1*). Both complexes act at the lysosome, an essential cellular compartment for mTOR signaling, but govern different cellular processes. Upstream of mTORC1, the tuberous sclerosis complex (TSC) integrates biologic inputs such as low energy levels and growth factor activation (*19*). However, for mTORC1 to be fully activated, it must be recruited to the lysosome through amino acid signaling via the Rag GTPases Rag A or B, which dimerizes with either Rag C or D (*23*). In the amino acid starved state, mTOR is diffuse within the cell, but amino acid stimulation is sufficient to allow the Ragulator-Rag complex to recruit mTOR to the lysosome (*24*). Thus, the culmination of these nutrient signals allows for Rheb GTPase to activate mTOR at the lysosome (*11*).

We focused on mTORC1 signaling because it integrates metabolic processes to affect macromolecular biosynthesis, growth, and protein synthesis (*1*). Dysregulation of the aforementioned mechanisms promotes cancer formation and progression, and aberrant mTORC1 signaling is implicated in the pathogenesis of human disease (*1*). Independent reports also reveal human EAK-7 mRNA is overexpressed in diseases such as hepatocellular carcinoma (*48*) and lymph-node positive breast cancers (*49*), suggesting that it may play a role in human disease. Because mTOR is an essential effector for many of these important cellular contexts and functions within the IRS pathway, we hypothesized the human ortholog of EAK-7, termed mammalian EAK-7 (mEAK-7), would potentially affect mTOR signaling in human cells.

Results

mEAK-7 is an evolutionarily conserved protein

Bioinformatics databases were analyzed to gain insight to the molecular functions of mEAK-7, also known through genomic and proteomic studies as KIAA1609 (*87*), LOC57707 (*88*), or TLDC1 (TBC/LysM-Associated Domain Containing 1) (*89*). Algorithmic analysis demonstrated that the amino acid identity of mEAK-7 and EAK-7 is 89% similar across eukaryotes (Figure 2.1.A and Figure 2.7.A) (*90*), suggesting mEAK-7 may be important to mammalian evolution.

mEAK-7 contains two known domains: the TLD (TBC-containing and LysM associated Domain) and the *N*-myristoylation motif (Figure 2.1.B). TLD domain-containing proteins confer neuroprotection against oxidative stress through unknown mechanisms (*47*). Computational analysis predicts mEAK-7 is an enzyme that folds into α/β+β sheets (*91*). The crystal structure of the TLDc domain of oxidation resistance protein 2 from zebrafish reveals that two antiparallel ß-sheets form a central ß-sandwich surrounded by two helices and two one-turn helices (*92*). The *N*-myristoylation motif irreversibly attaches myristate to anchor proteins to lipid bilayers or endomembrane compartments. Despite this information, the functional relevance of these domains is not known for mEAK-7.

To investigate the molecular function of mEAK-7, we verified an antibody that detects endogenous mEAK-7 in human cells (Figure 2.7.B) and identified cells that express endogenous mEAK-7 protein (Figure 2.1.C and Figure 2.7.C). mEAK-7 protein was detected in UM-SCC-1, H1975, MDA-MB-231, H1299, HCC1937, MDA-MB-436,

SUM149, MDA-MB-468, UM-SCC-10A, -11A, -17B, and -81B (Figure 2.1.C and Figure 2.7.C). Through this limited human cell screen, we detected mEAK-7 in many human cell lines.

mEAK-7 is anchored at the lysosomal membrane

mEAK-7 has been identified in membrane-bound/organelle fractions (*93*) and lysosomal fractions (*88*), but definitive evidence of the precise cellular compartment where mEAK-7 resides has not yet been demonstrated. By generating H1299 cell lines with stably expressed C-terminal HA-tagged mEAK-7 (HA-mEAK-7^{WT}) and co-staining with compartment-specific proteins, we determined HA-mEAK-7^{WT} strongly co-localizes with lysosomal-associated membrane protein-2 (LAMP2, lysosome; Figure 2.1.D), LAMP1 (lysosome; Figure 2.1.E), and, to a lesser extent, the plasma membrane. GFP-tagged EAK-7 in nematodes exhibited fluorescence in the plasma membrane of the pharynx, nervous system, intestine, body wall muscle, hypodermis, vulva, and a group of cells near the anus (*43*). However, subcellular localization at the lysosome has not been demonstrated in nematodes.

We observed little-to-no co-localization of HA-mEAK-7^{WT} in the endosome (Figure 2.7.A), mitochondria (Figure 2.7.B), endoplasmic reticulum (Figure 2.7.C), and Golgi complex (Figure 2.7.D). However, overexpression of exogenous protein can sometimes result in non-specific targeting to random cell compartments. Thus, we validated an antibody that targets endogenous mEAK-7 to determine the physiological localization within cells (Figure 2.8, A and B). We demonstrated that endogenous mEAK-7 strongly co-localizes with endogenous LAMP1 and LAMP2 (Figure 2.8.C).

These data illustrate that mEAK-7 is principally a lysosomal protein, an essential cellular compartment for mTORC1 signaling (*94*).

mEAK-7 supports mTORC1 signaling in response to nutrients

mTORC1 localizes to the lysosome in response to nutrient stimulation and this process is required for mTOR function (*11*). Further insights guiding our hypothesis that mEAK-7 may be an effector of mTORC1 signaling include the observations that nematode EAK-7 functions within the IRS pathway (*43*), mEAK-7 is primarily a lysosomal protein (Figure 2.1, D and E, and Figure 2.8), and mTORC1 is the core complex for this signaling pathway at the lysosome (*94*).

To test the extent to which mEAK-7 functions in mTORC1 signaling, H1975 cells were treated with three unique mEAK-7 siRNAs for 48 hours in 10% serum-containing medium ($DMEM^{+serum}$). mEAK-7 knockdown substantially decreased ($Ser^{240/244}$) p-S6 levels, an indicator of activated mTORC1 signaling (*95*), revealing mEAK-7 functions in mTORC1 signaling under $DMEM^{+serum}$ conditions (Figure 2.1.F). To determine if this was a universal phenomenon, H1975, MDA-MB-231, and H1299 cells treated with two unique mEAK-7 siRNAs which resulted in acutely diminished ($Ser^{240/244}$) p-S6 levels (Figure 2.1.G). Finally, H1299 cells were treated with mEAK-7 siRNA, starved of serum for 2 hours in $DMEM^{+AAs}$, and reintroduced to serum for 24 hours. mEAK-7 knocked-down H1299 cells failed to activate and sustain ($Ser^{240/244}$) p-S6 levels in response to serum stimulation (Figure 2.9.A). Together, these data indicate that mEAK-7 is important for basal-level and serum-mediated mTORC1 signaling in mEAK-7^{+} cells.

mTORC1 regulates cap-dependent protein translation by phosphorylating eukaryotic translation initiation factor 4E-binding protein 1 (4E-BP1) at $Thr^{37/46}$, which primes the 4E-BP1 phosphorylation site at Ser^{65} and Thr^{70}, and allows 4E-BP1 detachment from eukaryotic translation initiation factor 4E (eIF4E) (*96*). Because mEAK-7 supports S6 phosphorylation through mTOR, we sought to assess the functional status of 4E-BP1, a major target of mTOR. To test the effects of mEAK-7 on 4E-BP1 phosphorylation, H1975, MDA-MB-231, H1299, and HEK-293T cells were treated with control or mEAK-7 siRNA for 48 hours in $DMEM^{+serum}$. mEAK-7 knockdown appreciably decreased (Ser^{65}) p-4E-BP1, ($Thr^{37/46}$) p-4E-BP1, and (Thr^{70}) p-4E-BP1 levels (Figure 2.1.H). mEAK-7 knocked-down H1299 cells also failed to activate and sustain (Ser^{65}) p-4E-BP1 levels in response to serum stimulation (Figure 2.9.A). Thus, data suggest mEAK-7 is capable of regulating both S6 and 4E-BP1, two primary markers for mTORC1 signaling.

mTORC1 signaling is activated through amino acids and/or insulin stimulation at the lysosome (*11*). To address the possibility that mEAK-7 regulates mTORC1 signaling in response to specific nutrients, cells were starved for 2 hours in custom manufactured DMEM lacking amino acids (AAs) ($DMEM^{-AAs}$). Subsequently, cells were collected as a starved control or collected after reintroduction of AAs, insulin, or both. Control siRNA-treated H1975, MDA-MB-231, H1299, and HEK-293T cells increased mEAK-7 protein levels that correlated with increased ($Ser^{240/244}$) p-S6 levels in response to all nutrient conditions (Figure 2.1.I and Figure 2.11). mEAK-7 protein levels also increased after serum reintroduction at different time points following serum starvation in H1299 cells

(Figure 2.10.A). Thus, serum, AAs, and insulin facilitate the regulation of mEAK-7 protein levels.

H1975, MDA-MB-231, H1299, and HEK-293T cells treated with mEAK-7 siRNA demonstrated reduced ($Ser^{240/244}$) p-S6 levels under all conditions (Figure 2.1.I and Figure 2.11). In addition, mEAK-7 knocked-down H1299 cells displayed an impaired ability to activate and sustain (Ser^{65}) p-4E-BP1 levels in response to amino acid and insulin stimulation over time (Figure 2.10.B). Taken together, these data suggest that mEAK-7 can regulate mTORC1 signaling in response to serum, AAs, and insulin, and that mEAK-7 protein is influenced by nutrient stimulation. While HEK-293T cells, a widely used cell line to study mTOR signaling, exhibits comparatively low mEAK-7 protein levels (Figure 2.10.C), mEAK-7 knockdown still led to a significant reduction in mTOR signaling, as demonstrated by S6 and 4E-BP1 phosphorylation.

mEAK-7 functions through S6K2 rather than S6K1

Upon further examination of mEAK-7 function in mTORC1 signaling, we obtained evidence that was unexpectedly contrary to our initial hypothesis. After knocking down mEAK-7, we discovered that while ($Ser^{240/244}$) p-S6 levels were decreased, (Thr^{389}) p-S6K1 levels were increased (Figure 2.1.I, Figure 2.10, A and D, and Figure 2.11). Since (Thr^{389}) p-S6K1 is a reliable indicator of mTORC1 signaling, these findings appear to uncouple S6K1 activity from ($Ser^{240/244}$) p-S6 levels in certain contexts. HEK-293T cells demonstrated typical (Thr^{389}) p-S6K1 regulation in response to amino acid and/or insulin stimulation, while H1975, MDA-MB-231, and H1299 cells exhibited aberrantly

functioning S6K1 (Figure 2.1.I and Figure 2.11). Thus, an alternative kinase may exist to compensate for dysregulated S6K1 activity in H1975, MDA-MB-231, and H1299 cells.

To investigate this perceived molecular anomaly, we examined S6K2, an understudied target of mTORC1. S6K1 is a prominent target of mTOR, but mTOR also targets S6K2, a closely related homolog of S6K1 (*97*). It is believed that the role of S6K2 is redundant to S6K1, but emerging evidence suggests these kinases also have distinct functions. $S6K1^{-/-}$ cells are capable of regulating ($Ser^{240/244}$) p-S6 levels, while $S6K2^{-/-}$ cells fail to regulate ($Ser^{240/244}$) p-S6 levels, demonstrating that S6K1 may not always be the primary kinase linked to ($Ser^{240/244}$) p-S6 levels (*57*). Furthermore, S6K2 knockout mice and S6K2 siRNA-treated cells exhibit increased S6K1 function, demonstrated by a stark increase in (Thr^{389}) p-S6K1 levels (*61*). These data suggest S6K2 may play a vital role in mTOR signaling. Therefore, we investigated the extent to which S6K1 and S6K2 may be linked to ($Ser^{240/244}$) p-S6 levels in mEAK-7^{+} cells.

To elucidate the roles of S6K1 and S6K2, we analyzed ($Ser^{240/244}$) p-S6 levels in response to insulin stimulation after knockdown of mEAK-7, S6K1, or S6K2. Cells were starved for 2 hours in $DMEM^{+AAs}$ without serum and subsequently introduced to insulin at 1 μM or 10 μM for 30 minutes. In H1975 and MDA-MB-231 cells, mEAK-7 or S6K2 knockdown markedly reduced ($Ser^{240/244}$) p-S6 levels, but S6K1 knockdown had a lesser effect (Figure 2.1.J and Figure 2.12, A and B). We observed mEAK-7 or S6K2 knockdown dramatically increased (Thr^{389}) p-S6K1 levels, which suggests the uncoupling of S6K1 on ($Ser^{240/244}$) p-S6 levels in some cell contexts (Figure. 2.1.J and Figure 2.12, A and B).

In contrast, S6K1 affects ($Ser^{240/244}$) p-S6 levels to a greater degree in H1299 and HEK-293T cells, although mEAK-7 or S6K2 knockdown substantially abrogated ($Ser^{240/244}$) p-S6 levels (Figure 2.1.J and Figure 2.12, C and D). These findings suggest that most mEAK-7^{+} cell lines function primarily through S6K2, rather than S6K1, to activate mTOR signaling. Additionally, differential levels of mEAK-7 protein (Figure 2.10.C) were not predictive of whether cell lines will favor S6K2 over S6K1 in mTORC1-mediated signaling. These findings are consistent with reports that S6K1 and S6 phosphorylation are not exclusively linked, and that S6K2 has additional biological roles in eukaryotes (*61*).

Molecular analysis of mEAK-7 protein

To rule out the possibility that siRNA-mediated knockdown of mEAK-7 non-specifically influences mTORC1 signaling, we transduced H1975, MDA-MB-231, H1299, and HEK-293T cells with pLenti-III-HA-Control or pLenti-III-HA(C-terminus)-mEAK-7^{WT} lentivirus and selected these cells with 1μg/mL puromycin for 2 weeks. We demonstrate that overexpression of HA-mEAK-7 activated mTORC1 signaling in H1975, MDA-MB-231, H1299, and HEK-293T cells (Figure 2.2.A). Thus, both knockdown and overexpression studies demonstrated that mEAK-7 is an essential component of mTORC1 signaling in mEAK-7^{+} cells.

Next, we investigated the molecular domains necessary for mEAK-7 function. To assess the mEAK-7 domains essential for mTOR signaling, several mutants were generated and transduced with lentivirus into cells that expressed endogenous mEAK-7 (Figure 2.2.B). We compared HA-mEAK-7^{WT} with HA-mEAK-7 mutants for LAMP2 co-

localization at the lysosome (Figure 2.2, C-H). We also investigated differential overexpression effects of wild type (WT) and mutants on mTOR signaling under AAs and insulin stimulation (Figure 2.2, I and J). HA-mEAK-7^{WT} co-localized with LAMP2 (Figure 2.2.C) and AAs and insulin stimulation successfully induced (Ser$^{240/244}$) p-S6 in WT overexpressing H1299 cells (Figure 2.2.I).

HA-mEAK-7^{G2A}, a mutant with a point mutation that replaces the first glycine residue with alanine within the *N*-myristoylation motif, failed to anchor to the lysosome (Figure 2.2.D). However, AAs and insulin stimulation induced (Ser$^{240/244}$) p-S6, possibly due to endogenous mEAK-7 function (Figure 2.2.I). Deletion of amino acids 1-139 (HA-mEAK-7$^{\Delta NDEL1}$) also led to a lysosomal anchorage (Figure 2.2.E), due to the loss of the *N*-myristoylation motif, but did not significantly alter endogenous mTORC1 signaling (Figure 2.2.I). HA-mEAK-7$^{\Delta NDEL2}$ co-localized with LAMP2 (Figure 2.2.F) and also did not significantly alter endogenous mTORC1 signaling (Figure 2.2.I).

While both HA-mEAK-7$^{\Delta TLD}$ and HA-mEAK-7$^{\Delta CDEL}$ localize at the lysosome (Figure 2.2, G and H), stable expression of either HA-mEAK-7$^{\Delta TLD}$ or HA-mEAK-7$^{\Delta CDEL}$ inhibited the induction of (Ser$^{240/244}$) p-S6 levels by AAs and insulin (Figure 2.2, I and J), and resulted in increased (Thr^{389}) p-S6K1 levels (Figure 2.2.J). Although it is unclear how these mutants affect endogenous mEAK-7 function to impair mTOR signaling, these results demonstrate that the TLD domain and C-terminus are necessary for mEAK-7-mediated mTOR function.

mEAK-7 recruits mTOR to the lysosome in nutrient-deprived and nutrient-rich conditions

mTOR signaling components are translocated to the lysosome in response to nutrient stimulation and this shuttling is necessary to activate mTORC1 signaling (*1*). Because mEAK-7 is predominantly lysosomal, we posited a role for mEAK-7 in targeting mTOR to the lysosome. To determine the role of mEAK-7 in lysosomal localization of mTOR, H1299 cells were treated with control or mEAK-7 siRNA for 48 hours. Subsequently, cells were starved in DMEM^{-AAs} for 1 hour and AAs and insulin were reintroduced for 30 min. We found that mEAK-7 knockdown impaired mTOR localization to the lysosome (Figure 2.3.A), confirming that mEAK-7 is important for mTOR localization. While low levels of mTOR remained capable of migrating to the lysosome after mEAK-7 knockdown, this may be due to residual mEAK-7 still expressed since siRNA treatment is not 100% effective and because other major regulators of mTOR, such as the Rag GTPases, have been shown to recruit mTOR to the lysosome (*24*).

Further analysis demonstrated that the expression of mTORC1/2 components was not altered after mEAK-7 siRNA treatment (Figure 2.3.B). H1299 cells treated with mEAK-7 siRNA demonstrated a statistically significant decrease in mTOR/LAMP2 co-localization in the starved condition (Figure 2.3.C). In the nutrient replenished condition, H1299 cells treated with mEAK-7 siRNA also exhibited a statistically significant decrease in mTOR/LAMP2 co-localization (Figure 2.3.C). To substantiate this finding, we performed the reciprocal experiment by overexpressing HA-mEAK-7. HA-mEAK-7 overexpression in H1299 cells resulted in a statistically significant increase in mTOR/LAMP2 co-localization in the absence of nutrients (Figure 2.3, D and E).

Additionally, reintroduction of nutrients in control cells resulted in a significant enhancement of the co-localization of mTOR/LAMP2, and HA-mEAK-7 overexpression increased mTOR/LAMP2 co-localization in the presence of nutrients (Figure 2.3, D and E). Further analysis demonstrated nutrient reintroduction did not result in a statistically significant change of HA-mEAK-7/LAMP2 co-localization (Figure 2.3.F). We then hypothesized that endogenous mEAK-7 would co-localize with endogenous mTOR in response to nutrient stimulation because amino acids recruit mTOR to the lysosome. H1299 cells were nutrient starved for 1 hour and stimulated with AAs, insulin, or both for 1 hour. Endogenous mEAK-7 and endogenous mTOR strongly co-localized in response to nutrient stimulation (Figure 2.13, A-E).

We hypothesized that mEAK-7 could directly affect mTOR kinase function, possibly as an adaptor protein. mTOR interaction with its complex components is known to be sensitive under different buffer conditions (*98*). To rule out the possibility of non-specific or artificial interactions due to an abundance of exogenously produced protein and buffer-dependent conditions, we harvested either H1299, or HA-mEAK-7 expressing H1299 cells, in either NP40 or CHAPs buffer. Thus, we assessed the potential for interaction between these two proteins using a co-immunoprecipitation assay. Co-immunoprecipitation of exogenous HA-mEAK-7^{WT} confirmed significant interaction with endogenous mTOR, compared to an IgG control under serum-containing conditions (Figure 2.4.A). In addition, endogenous mEAK-7 interacted with endogenous mTOR (Figure 2.4.B). Finally, knockdown of mEAK-7 diminished the interaction of endogenous mEAK-7 with endogenous mTOR and mLST8 (Figure 2.4.C and Figure 2.14.A). However, mEAK-7 failed to interact with raptor or rictor, key

components of mTORC1 and mTORC2, respectively. Intriguingly, exogenous HA-mEAK-7^{WT} also interacted with mTOR and mLST8, but did not interact with rictor, Sin1, raptor, PRAS40, or DEPTOR (Figure 2.4.D). These findings suggest the possibility of an alternative mTOR complex that is yet to be identified in mammalian cells.

To assess the nutrient dependency of this interaction, HA-mEAK-7^{WT} cells were starved for 2 hours and AAs, insulin, or both were reintroduced for 30 min. All lysates for immunoprecipitation were collected in NP40 lysis buffer, unless noted otherwise. Under these conditions, exogenous HA-mEAK-7^{WT} and endogenous mTOR interacted in the starved condition and this interaction was increased by nutrient stimulation (Figure 2.4.E and Figure 2.14.B). To further demonstrate the validity of these nutrient-dependent interactions, data support that endogenous mEAK-7 also strongly interacts with endogenous mTOR under the AAs and insulin or AAs and serum conditions (Figure 2.4.F and Figure 2.14.C). Additionally, co-immunoprecipitation of endogenous mTOR to detect exogenous HA-mEAK-7^{WT} also confirmed this interaction increased under nutrient stimulation (Figure 2.4.G and Figure 2.14.D). Therefore, data suggest that both exogenous and endogenous mEAK-7 are capable of interacting with mTOR.

To determine the molecular domain necessary for mEAK-7 interaction with mTOR, co-immunoprecipitation was performed in cells stably expressing HA-mEAK-7^{WT}, HA-mEAK-$7^{\Delta TLD}$, and HA-mEAK-$7^{\Delta CDEL}$, because these domains are necessary for the activation of mTORC1 signaling in mEAK-7^{+} cells (Figure 2.2, I and J). We found that the C-terminus protein region is necessary for the interaction of exogenous HA-mEAK-7^{WT} and endogenous mTOR (Figure 2.4.H and Figure 2.14.E), so this region of the C-terminus was termed the mTOR-binding (MTB) domain. Other mEAK-7 mutants

were also capable of interacting with endogenous mTOR, suggesting that maintaining an intact MTB domain is sufficient for mTOR binding (Figure 2.13, F and G). Additionally, overexpression of HA-mEAK-7$^{\Delta TLD}$ and HA-mEAK-7$^{\Delta CDEL}$ increased (Thr^{389}) p-S6K1 levels (Figure 2.4.H). These findings suggest that the interaction of mEAK-7 and mTOR diverts mTOR targeting from S6K1 to S6K2, while loss of mEAK-7 diverts mTOR targeting from S6K2 to S6K1, resulting in increased (Thr^{389}) p-S6K1 levels.

We hypothesized that mEAK-7 regulates mTORC1 signaling through S6K2 because (Thr^{389}) p-S6K1 levels were not linked to its downstream target, (Ser$^{240/244}$) p-S6 (Figure 2.1, I and J, Figure 2.2.J, and Figure 2.10, A and D). To assess this possibility, H1299 cells were transiently transfected with pcDNA3-HA-S6K2-WT and either control or mEAK-7 siRNA, and HA-S6K2 was immunoprecipitated. mEAK-7 knockdown considerably decreased the interaction between endogenous mTOR and HA-S6K2 (Figure 2.4.I and Figure 2.14.F). To ensure mEAK-7 specificity in this interaction, two mEAK-7 siRNAs were employed and both demonstrated a substantial decrease in HA-S6K2 interaction with mTOR (Figure 2.4.J and Figure 2.14.G). These outcomes suggest that mEAK-7 supports the interaction of S6K2 and mTOR.

Next, we hypothesized mEAK-7 may also influence S6K1 and mTOR interaction. To test this, H1299 cells were transiently transfected with pRK7-HA-S6K1-WT and control or mEAK-7 siRNA, and HA-S6K1 was immunoprecipitated. mEAK-7 knockdown increased the interaction of exogenous HA-S6K1 with endogenous mTOR (Figure 2.4.K and Figure 2.14.H). Subsequently, two different mEAK-7 siRNAs confirmed these enhanced interactions were the result of mEAK-7 knockdown (Figure 2.4.L and Figure

2.14.I). Thus, we demonstrate that mEAK-7 intricately controls mTOR interaction with both S6K2 and S6K1.

While these data support the necessity of mEAK-7 for the interaction of mTOR with S6K2, they do not provide direct evidence of S6K2 function. To our knowledge, an antibody specific to (Thr^{388}) p-S6K2 does not exist. However, the amino acid sequences of the hydrophobic motifs of the S6Ks (Figure 2.4.M) are nearly identical. Given this similarity, we predicted the monoclonal antibody against (Thr^{389}) p-S6K1 (Cell Signaling Technology: clone 108D2) would reveal the relative phosphorylation status of S6K2, since it was designed to target the mTOR-targeting hydrophobic motif, and this is a strategy utilized by other groups (*60*). Because (Thr^{389}) p-S6K1 levels are a common readout of S6K1 kinase activity and mTORC1 functionality, we expected that (Thr^{388}) p-S6K2 levels would also indicate S6K2 kinase activity in this context. Additionally, the molecular weights of S6K1 and S6K2 are different in that S6K1 is 65-70 kDa and S6K2 is 60 kDa; therefore, immunoprecipitation would yield detectable phosphorylation differences of the concentrated kinase. To determine the phosphorylation status of S6K2 by mEAK-7, H1299 cells were transiently transfected with pcDNA3-HA-S6K2-WT and either control or mEAK-7 siRNA, starved of nutrients, and DMEM^{+serum} was reintroduced for 30 min. HA-S6K2 was then immunoprecipitated and probed with the 108D2 antibody. Data suggest that mEAK-7 is required for the interaction of mTOR with S6K2 in response to serum and regulates (Thr^{388}) p-S6K2 levels, as demonstrated by a loss of S6K2 phosphorylation in response to mEAK-7 knockdown (Figure 2.4.M). Furthermore, loss of mEAK-7 diminished S6K2-mediated phosphorylation of S6 in

response to serum stimulation (Figure 2.4.M). Therefore, mEAK-7 is required for S6K2 activity in these cells.

Finally, to demonstrate the extent to which mEAK-7 regulates 4E-BP1 and eIF4E interaction, we treated H1299 cells with either control or mEAK-7 siRNA and immunoprecipitated eIF4E. We discovered that mEAK-7 knockdown enhanced binding of 4E-BP1 to eIF4E (Figure 2.4.N and Figure 2.14.J). Thus, these data establish mEAK-7 as a novel effector of mTOR signaling that regulates both S6K2 activity and 4E-BP1 activity.

mEAK-7 supports cell proliferation and migration

After demonstrating that mEAK-7 supports mTOR signaling, we hypothesized that mEAK-7 was essential for critical cellular functions governed by mTOR. mTOR signaling is important for regulation of cell number (*1*). To elucidate the influence of mEAK-7 on proliferation, cells were treated with either control or mEAK-7 siRNA, and counted after 3 and 5 days. In H1975 (Figure 2.5.A), MDA-MB-231 (Figure 2.5.B), H1299 (Figure 2.5.C), and HEK-293T cells (Figure 2.5.D), treatment with mEAK-7 siRNA resulted in a significant reduction in cell proliferation. Further, annexin V staining or acridine orange-propridium iodide (AO-PI) staining demonstrated no difference in cell death after mEAK-7 knockdown (Figure 2.15, A-C). Previous reports corroborate the finding that the loss of TLD domain-containing proteins (*47*) or single knockdown of S6K2 without an apoptotic stimulator (*99*) does not result in significant levels of cell death. Due to the low expression of mEAK-7 in some human cells, we hypothesized that mEAK-7 overexpression would promote cell proliferation. Thus, to test the effect of

mEAK-7 overexpression on cell proliferation, we transduced H1975, MDA-MB-231, H1299, and HEK-293T cells with pLenti-GIII-CMV-Control-HA and pLenti-GIII-CMV-mEAK-7-HA. Overexpression of HA-mEAK-7 in H1975 (Figure 2.5.E), MDA-MB-231 (Figure 2.5.F), H1299 (Figure 2.5.G), and HEK-293T (Figure 2.5.H) significantly enhanced cell proliferation at day 3 and day 5. Thus, we concluded that mEAK-7 is vital for cell proliferation in mEAK-7^{+} cells.

mTORC1 signaling has substantial control over cell migration and metastasis, with the 4E-BP1-eIF4E axis regulating mTOR-sensitive migration and invasion genes (*38*). Given the role of mEAK-7 in mTOR signaling, we investigated the impact of mEAK-7 on cell migration. H1975, MDA-MB-231, and H1299 cells were treated with either control or mEAK-7 siRNA and seeded into CIM-plates, which use xCELLigence technology to quantify cell migration in real-time, collecting hundreds of data points through a dimensionless cell-index parameter. Cells must pass through a pore embedded in a gold-plated electric grid, creating electrical impedance and registering a signal for real-time, quantifiable cell migration. We proceeded to conduct statistical analyses at select time points of 12, 24, 36, and 48 hours. Treatment of H1975 (Figure 2.5.I), MDA-MB-231 (Figure 2.5.J), H1299 (Figure 2.5.K), and HEK-293T (Figure 2.5.L) cells with mEAK-7 siRNA resulted in statistically significant reductions of real-time cell migration at 24, 36, and 48 hours. In addition, scratch wound assay analysis of H1975 (Figure 2.5.M), MDA-MB-231 (Figure 2.5.N), H1299 (Figure 2.5.O), and HEK-293T (Figure 2.5.P) cells treated with mEAK-7 siRNA resulted in a dramatic defect of wound closure after two days demonstrating that mEAK-7 is essential for cell migration in these cells.

The S6 Kinases have differential functions mediated through mEAK-7

Data from several sources suggest that S6 kinases play redundant roles due to their high homology, but recent evidence reveals that independent role of S6K2 remains undetermined (*61*). Genome-wide assessment of S6K1 and S6K2 in human tumors and *in vitro* silencing of these kinases demonstrate that their targets are different from each other, and that S6K2 more closely mirrors eIF4E function (*100*). S6K2 has also been shown to be an essential regulator of cell proliferation, due to its involvement with Heterogeneous Ribonucleoprotein F (*101*). Previous reports demonstrate that S6 is essential for mammalian cell proliferation and that S6K1 controls eukaryotic size (*102*). Given that mEAK-7 regulates S6K2 function, we hypothesized that mEAK-7 also regulates S6K2-mediated cell proliferation.

To determine the extent to which S6K2 regulates cell proliferation and to compare its functional role in other mTOR targets, H1975 cells were treated with control, S6K1, S6K2, or eIF4E siRNA for 48 hours in $DMEM^{+serum}$ (Figure 2.6.A). Cells were then seeded into new tissue culture plates and were counted after 3 and 5 days. Treatment with S6K1, S6K2, and eIF4E siRNA resulted in a significant reduction of cell proliferation at day 3 and day 5 (Figure 2.6.B). Importantly, treatment with S6K2 or eIF4E siRNAs significantly reduced cell proliferation at day 5, compared to S6K1 siRNA. However, H1975 cells treated with S6K2 siRNA, compared to eIF4E siRNA, did not result in a statistically significant reduction, suggesting that S6K2 functions similarly to eIF4E with regards to cell proliferation, as the literature reports (*100*). These results demonstrate S6K2 is essential for cell proliferation under these conditions.

mTOR signaling also controls cell size in eukaryotes (*30*). Because we found that mEAK-7 is a positive activator of mTOR signaling, we sought to determine the role of mEAK-7 in regulating cell size. H1975, MDA-MB-231, and H1299 cells were treated with control or mEAK-7 siRNA for 48 h, seeded onto new tissue culture plates, and processed at day 3. Cells were analyzed on a Beckman-Coulter CyAn 5 flow cytometer for forward scatter. Interestingly, H1975 (Figure 2.15.D), MDA-MB-231 (Figure 2.15.E), and H1299 (Figure 2.15.F) cells treated with mEAK-7 siRNA resulted in an increase in cell size, suggesting that dysfunctional S6K1 activity results in aberrant cell size regulation after mEAK-7 knockdown. Under the same conditions, cell size was also assessed using the Logos Biosystems Luna Cell Counter. H1975 (Figure 2.6.C), MDA-MB-231 (Figure 2.6.D), and H1299 (Figure 2.6.E) cells treated with mEAK-7 siRNA resulted in a significant increase in cell size. These data demonstrate that while loss of mEAK-7 resulted in decreased downstream mTOR signaling, aberrant activation of S6K1 leads to dysregulation of cell size. Additionally, H1975 cells were treated with control, S6K1, or S6K2 siRNA and then analyzed via forward scatter in flow cytometry. S6K1 knockdown reduced cell size, while S6K2 knockdown demonstrated limited change in cell size (Figure 2.6.F).

Because overexpression of pcDNA3-HA-S6K2-WT or pRK7-HA-S6K1-WT was not sufficient to rescue mTOR signaling in H1299 cells treated with mEAK-7 siRNA (Figure 2.4, I-M), we posited that this obstacle could be overcome by transfecting cells with constitutively activated forms of S6K1 or S6K2. To determine whether this could rescue mEAK-7 knockdown effects, cells were treated with control siRNA, mEAK-7 siRNA, mEAK-7 siRNA + pRK7-HA-S6K1-F5A-E389-deltaCT (50 kDa – deletion that

results in a truncated kinase) (cS6K1) plasmid, or mEAK-7 siRNA + pcDNA3-HA-S6K2-E388-D3E (60 kDa) (cS6K2) plasmid. Concomitant knockdown of mEAK-7 and overexpression of cS6K1 and cS6K2 in H1299, H1975, and MDA-MB-231 cells resulted in rescue of ($Ser^{240/244}$) p-S6 levels (Figure 2.6.G). Knockdown of mEAK-7 and overexpression of cS6K1 or cS6K2 resulted in partial rescue of cell proliferation defects (Figure 2.6.H). Thus, we demonstrate that mEAK-7 functions upstream of S6K2 and promotes S6K2-mediated signaling and proliferation.

Discussion

In this study, we determined mEAK-7 is an important, evolutionarily-conserved, lysosomal protein that activates mTOR signaling in response to nutrient stimulation in many cell types (Figure 2.6.I). We provide mechanistic insight for a novel protein that is required for serum-, amino acid-, and insulin-mediated mTOR signaling in human cells. We also demonstrate mEAK-7 is necessary for S6K2 function by regulating S6K2-mTOR interaction, 4E-BP1-eIF4E interaction, and supporting cell proliferation and cell migration in mEAK-7^{+} cells. We identified mEAK-7 as an essential interacting protein of mTOR and mLST8, but not other mTORC1 components, raptor, DEPTOR, or PRAS40, and mTORC2 components, rictor, DEPTOR, or Sin1. mEAK-7 interacts with mTOR through the MTB domain (Figure 2.6.J). mEAK-7 regulates mTORC1 signaling at the lysosome and is a key player for mTOR recruitment to the lysosome. Thus, we determined that mEAK-7 functions as an essential component of mTOR signaling to regulate S6K2 and 4E-BP1, through a potentially alternative pathway to the canonical mTORC1 or mTORC2 models.

Since the discovery of rapamycin, decades of research have contributed to understanding the mechanism by which mTOR is regulated in response to nutrients and stress (*1*). The two best-known complexes that contain mTOR are mTOR complex 1 (mTORC1) and mTOR complex 2 (mTORC2). mTORC1 is comprised of regulatory-associated protein of mTOR (raptor), mammalian lethal with SEC13 protein 8 (mLST8) or GβL, Proline-rich AKT1 substrate 1 (PRAS40), and DEPTOR (*1*). mTORC2 is comprised of mLST8, rapamycin-insensitive companion of mTOR (rictor), mammalian stress-activated protein kinase interacting protein 1 (mSIN1), Protor, DEPTOR, and Tti1 & Tel2 (*1*).

With the finding that mEAK-7 is an interacting and functioning partner of mTOR and mLST8, we posited that mEAK-7 may form a novel complex to regulate the specificity of S6K2 interaction with mTOR. 4E-BP1 binding to eIF4E is also affected by the loss of mEAK-7, and data suggest a potential new complex may, in certain contexts, regulate this mTOR-mediated function as well. Our evidence suggests that mEAK-7 functions at the level of mTOR as a coordinator for S6K2 and 4E-BP1, but the downstream partners that mediate this process remain unknown.

It has been theorized that additional mTOR complexes may complement mTORC1 and mTORC2 in mammalians. Astrocytes of the central nervous system provide one such example of how mTOR may function in a cell-type dependent manner. In this context, GIT1 functions as an interacting partner of mTOR that does not associate with either raptor or rictor (*42*). This finding is intriguing because it demonstrates that cell-type specificity may dictate the molecular landscape that allows for full mTOR regulation and activation. mEAK-7 may have eluded previous mTOR

immunoprecipitation and mass spectrometry analyses because it is found to a limited extent in human cells (Figure 2.1.C, Figure 2.7.C, and Figure 2.10.C). It is also unknown where mEAK-7 is expressed during development. The interaction between mEAK-7 and mTOR, as well as the associated influence on S6K2 and 4E-BP1 functions, suggests there are more mTOR components yet to be identified that may interact in a cell-type, or context-dependent manner (Figure 2.6.I).

Because we did not screen mEAK-7 in all human cell types, further investigation of mEAK-7 in other physiological contexts is essential for understanding how mEAK-7 functions in human development or disease. We provide molecular insight demonstrating that mEAK-7 supports the interaction of S6K2 and mTOR, but the full complement of interacting partners is yet to be determined. In addition, evolutionary differences arose between mammalian EAK-7 and nematode EAK-7. Nematode EAK-7 functions in parallel to Akt signaling to regulate DAF-16 (human FoxO) during development and lifespan (*43*). We demonstrate that mEAK-7 is essential for mTOR signaling to regulate S6K2 and 4E-BP1, but nematodes only possess one S6 kinase, RSKS-1. Thus, it is unclear how, or if, EAK-7 regulates TOR signaling in nematodes.

One of the challenges in studying mTOR in mammalian systems is the difficulty in discerning tissue or organ-specific functions, as knockout of major components of mTORC1 or mTORC2 results in embryonic lethality (*53*). S6K1 is the best-studied target of mTOR in eukaryotes. In mice, loss of S6K1 reduces weight and improves insulin sensitivity with high-fat diets (HFD) (*54*), while mice with a standard diet (SD) are glucose-intolerant, hypoinsulinaemic, and have reduced β cell size (*55*). Intriguingly, loss of both S6K1 and S6K2 reverses the deleterious effects of S6K1 knockout mice,

restores glucose tolerance under a SD, and further improves glucose tolerance with a HFD (*56*).

Because S6K2 has been studied to a lesser extent in the scientific community, much less is known about the importance of S6K2 in development, metabolism, and disease. Compared to wild-type mice, S6K1 null mice are much smaller, S6K2 null mice are slightly larger, and double knockout animals result in perinatal lethality (*57*). Recent data suggest that S6K2 may not be a purely redundant kinase to S6K1 because S6K1 null mice demonstrate higher S6K2 expression in the liver, muscles, thymus, and brain, and because S6K2 remains responsive to rapamycin-mediated inhibition of S6 phosphorylation in S6K1 null mice (*58*). Thus, S6K2 was largely neglected and tissue-specific functions of S6K2 are now beginning to be understood. The loss of S6K2 resulted in higher basal levels of insulin in plasma, 2.5x more β cell mass with a SD, and improved glucose tolerance, as well as enhanced insulin sensitivity with a HFD (*59*). Additionally, single S6K2 knockout enhances ketone body production and increases peroxisome proliferator-activated receptor alpha activity in the liver, and S6K1 knockout mice are capable of maintaining ($Ser^{240/244}$) p-S6 levels, while S6K2 knockout mice are not, as we have demonstrated (*60*). Thus, elucidating the role of mEAK-7-mediated regulation of S6K2 and mTOR signaling in mammals will further our understanding of diseases where hyper-activation of mTOR signaling occurs through aberrant S6K2 activity.

Materials and Methods

Cell lines

H1299, H1975, MDA-MB-231, and HEK-293T cell lines were obtained from ATCC. Other cell lysates were donations and used as part of the initial cell screen. Figure 2.1.C and Figure 2.7.C lysates: the donor labs verified the cell lysates and hold the validation paperwork. Cell lysates derived from our lab: human embryonic stem cell line H1 undifferentiated, H1 endoderm (differentiated to pancreatic progenitors), H1 mesoderm (cardiac progenitors), H1 ectoderm (neuronal progenitors), H1 embryoid body, Human gingival fibroblasts (2 different patients). Dr. Tom Carey: UM-SCC-1, UM-SCC-10A, UM-SCC-11A, UM-SCC-14A, UM-SCC-17A, UM-SCC-17B, UM-SCC-74A, UM-SCC-74B, and UM-SCC-81B. Dr. Mark Cohen: H1975 and H1299. Dr. Shuichi Takayama: MDA-MB-231. Dr. Max S. Wicha: BT474, HCC1937, MDA-MB-436, SK-BR-3, SUM149, SUM159, T4D7, MDA-MB-468.

Cell culture

Cell culture: Cell lines were grown in Dulbecco's minimal essential medium (DMEM, Thermo Fisher Scientific (TFS): cat# 11995-073), without antibiotics/antimycotics and supplemented with a concentration of 10% fetal bovine serum (FBS, TFS: cat# 10437-036, Lot # 1399413) at 37°C in 5.0% CO_2 incubator. Cells were grown in Falcon™ Tissue Culture Treated Flasks T-75 (Fisher Scientific (FS): cat# 13-680-65) until 75% confluent, split with Trypsin-EDTA 0.25% (TFS: cat# 25200-056) for 5 min in the 37°C cell incubator. Cells were washed 1x with PBS and

resuspended in 10% FBS containing DMEM. Cells were counted with the LUNA™ Automated Cell Counter (Logos Biosystems (LB): cat# L10001) utilizing LUNA™ Cell Counting Slides (LB: cat# L12003) and AO-PI dye (LB: cat# F23001).

Starvation protocol: Cells were starved in DMEM lacking amino acids (DMEM^{-AAs}: TFS, cat# ME120086L1) for 50 minutes (min) or 2 hours, then stimulated with amino acids (normal DMEM), insulin (1 μM or 10 μM: Sigma-Aldrich; cat# I9278-5ML), or both for 30 or 60 min.

Small interfering RNA or plasmid transfection

Cells were seeded at a density of 500,000 cells per 60 mm TCP and grown for 24 hours. For siRNA transfection, we incubated Lipofectamine® RNAiMAX Transfection Reagent (TFS: cat# 13778-150) within Opti-MEM® I Reduced Serum Medium (TFS: cat# 31985-070) and 100 nM siRNA was incorporated before being introduced into cells at 100 nM concentration. For plasmid transfection, we utilized FuGENE® 6 Transfection Reagent (Promega: cat# E2691) into Opti-MEM I Reduced Serum Medium and 2 μg plasmid was incorporated before being introduced into cells. For dual transfection, we added both solutions. Mammalian EAK-7 (mEAK-7) siRNAs are identified as KIAA1609 or TLDC1: for siRNA mEAK-7 #1 (TFS: ID# s33640), #2 (TFS: ID# HSS126697), #3 (TFS: ID# HSS126699). We also utilized these siRNAs; mEAK-7 (TFS: ID# s33641, ID# s33642, and ID# HSS126698), S6K1 (TFS: ID# 1 - s12282, 2- s12283), S6K2 siRNA (TFS: ID# 1- s12286, 2-s12287), eIF4E (TFS: ID# s4578), control siRNA (TFS: cat# 4390843). Plasmids were purchased from Addgene. pRK7-HA-S6K1-WT was a gift from John Blenis (Addgene, # 8984). pcDNA3-S6K2-WT was a gift from John Blenis

(Addgene, # 17729). pRK7-HA-S6K1-F5A-E389-deltaCT was a gift from John Blenis (Addgene, # 8990). pcDNA3-S6K2-E388-D3E was a gift from John Blenis (Addgene, # 17731).

Immunoblot analysis

Cells were collected with a cell scraper and lysed in cold NP40 lysis buffer (50 mM Tris, 150 mM NaCl, and 1.0% NP-40 at pH 8.0). 50 µg of protein lysate was separated in Novex™ WedgeWell™ 4-20% Tris-Glycine Gels (TFS; cat# XP04205BOX) or 10% Tris-Glycine Gels (TFS; cat# XP00105BOX). Proteins were transferred to PVDF membranes, incubated with primary antibodies overnight at 4°C, and then incubated with secondary antibodies at room temperature for 1 hour. Membranes were incubated with SuperSignal™ West Pico Chemiluminescent Substrate (TFS; cat# 34078) or Femto (TFS; cat# 34095). Primary antibodies were as follows: mouse monoclonal antibody against mEAK-7 (KIAA1609) was obtained from Origene Technologies (clone OTI12B1, formerly 12B1: cat# TA501037). All antibodies from Cell Signaling Technologies (CST) were as follows: glyceraldehyde-3-phosphate dehydrogenase (cat# 2118S), (Ser240/244) phospho (p)-S6 ribosomal protein (2215S), S6 ribosomal protein (2217S), (Thr389) p-p70 S6 kinase (9234S), S6K1 (2708S), S6K2 (14130S), mTOR (2983S), HA-tag mouse (2367S), HA-tag rabbit (3724S), (Ser65) p-4E-BP1 (9451S), (Thr37/46) p-4E-BP1 (9459S), (Thr70) p-4E-BP1 (13396S), mLST8 (3274S), raptor (2280S), PRAS40 (2691S), DEPTOR/DEPDC6 (11816S), rictor (2114S), Sin1 (12860S), 4E-BP1 (9452S), and eIF4E (2067S). Antibodies p-S6, S6, and 4E-BP1 were used at 1:3,000 dilution and the remainder at 1:1,000 dilution in 5% BSA in 1X TBST buffer with 0.04%

sodium azide. Secondary antibodies for immunoblot analysis: 1:4,000 dilution for α-mouse IgG HRP Conjugate (Promega; cat# W4021) and 1:7,500 dilution for α-rabbit IgG HRP Conjugate (Promega; cat# W4011).

Molecular cloning of HA-mEAK-7^{WT} into mutants

Gibson Assembly Reaction (GAR) (New England Biolabs; cat# E2611S) was used to generate mutant constructs in accordance to manufacturer's instructions. In **table S1** we outline the list of primers used to produce the different mutant plasmids and extended materials and methods. pLenti-GIII-CMV-mEAK-7-HA (abm inc., cat# LV198982) was used as backbone. All mutants were confirmed by DNA sequencing. 10X lentiviral supernatant for wild type and mutant constructs was prepared by the Vector Core at the University of Michigan. H1299 cells were infected with 1X virus and selected with 1 μg/mL puromycin in 10% serum-containing DMEM medium. After two weeks, cells were used for immunoblot analysis and confocal microscopy.

Immunoprecipitation (IP) analysis

After siRNA and/or plasmid transfection, cells were harvested in 1% NP40 lysis buffer or CHAPs lysis buffer (FIVEphoton Biochemicals (FB): cat# CIB-1) supplemented with protease inhibitors (FB: cat# PI-1) and phosphatase inhibitors (FB: cat# PIC1). 250 μg proteins were used for immunoprecipitation reactions and 25 μg proteins were used for whole cell lysate (WCL) analysis. 2 μg antibodies and 40 μL of ImmunoCruz™ IP/WB Optima C agarose beads (Santa Crus Biotechnologies (SCB): Cat# sc-45040) were incubated in 1 mL PBS for 1 hour at 4°C. Separately, 250 μg proteins were

incubated with 50 µL Preclearing Matrix C (SCB: cat# sc-45054) in CHAPs buffer for 1 hour. After washing, the antibody-bead conjugate was incubated with pre-cleared protein lysate for 1.5 hours at 4°C and precipitated beads were washed 3 times with PBS. Antibodies for immunoprecipitation were as follows: Goat anti-HA epitope tag (Novus Biologicals: cat# NB600-362), goat IgG (SCB: cat# sc-2028), mTOR (CST: cat# 2983S), mEAK-7 (SCB: cat# sc-247321), and eIF4E (SCB: cat# sc-271480).

Cell immunofluorescence analysis

250,000 cells were seeded into Nunc™ Lab-Tek™ II Chamber Slide™ System 2-well (FS: cat# 12-565-5) for 24 hours. Cells were starved for 50 min in DMEM^{-AAs} and stimulated with amino acids or 1 µM insulin for 30 min. Then, cells were fixed with Z-Fix solution (Anatech LTD: cat# 170) for 10 min at RT, washed 3 times in PBS, incubated with the following: unmasking solution (PBS, 2N HCL, 0.5% TritonX) for 10 min, quenching solution (TBS, 0.1% Sodium Borohydride) for 10 min, permeabilization solution (PBS, 0.02% TritonX) for 10 min, and 5% BSA for 1 hour. Cells were incubated overnight at 4˚C with primary antibody. Next, slides were washed with PBS and incubated in secondary antibodies for 1 hour at room temperature. We used Nikon Ti Eclipse Confocal Microscope (100x magnification) to capture images. We captured images with or without 3x digital zoom, 1/32 frames per second, 1024x1024 image capture, 1.2 Airy Units, 2x line averaging, appropriate voltage and power settings optimized per antibody. No modification was done, except image sizing reduction for figure preparation. Quantitative analyses were completed via Imaris software for confocal images with calculation of co-localization as percentages. Identical threshold

settings captured images across three to five individual fields (10 to 15 cells) per condition, with the data representing at least three independent experiments. Primary antibodies for immunofluorescence were as follows: mouse HA-tag (CST: cat# 2367S), rabbit HA-tag (CST: cat# 3724S), LAMP1 (CST: cat# 9091S), LAMP2 (SCB: cat# sc-18822), mEAK-7 (SCB: cat# sc-247321), EEA1 endosome (CST: cat# 3288S), AIF mitochondria (CST: cat# 5318S), PDI endoplasmic reticulum (CST: cat# 3501S), RCAS-1 Golgi complex (CST: cat# 12290S), and mTOR [1:1,000] (CST: cat# 2983S). All antibodies were used at 1:1,500 with a working volume of 1.5 mL in 5% BSA in PBS, unless noted otherwise. Secondary antibodies for immunofluorescence were as follows: Donkey anti-Mouse IgG Alexa Fluor® 488 (TFS: cat# R37114). Donkey anti-Rabbit IgG Alexa Fluor® 594 (TFS: cat# A-21207). All antibodies were used at a concentration of 1:1,500 with a working volume of 1.5 mL in 5% BSA in PBS. DAPI stain was used for DNA.

Cell proliferation, size, migration, apoptosis, and scratch wound assay analysis

For cell proliferation and size assay, cells were processed with the LUNA™ Automated Cell Counter (Logos Biosystems (LB): cat# L10001) utilizing LUNA™ Cell Counting Slides (LB: cat# L12003) and AO-PI dye (LB: cat# F23001). After siRNA/plasmid transfection or lentiviral transduction, 200,000 cells were seeded in 100 mm TCPs for 3 and 5 day analysis. All cell size data was processed at day 3. Cell size was consistent across multiple platforms for analysis. For cell migration assay, cells were seeded at a density of 50,000 cells/well in CIM-plate 16 (ACEA BIO: cat# 05665817001). Real-time capture of cell migration was performed over 48 hours on the

xCELLigence System, RTCA DP Instrument (ACEA BIO: cat# 00380601050) and processed by RTCA Software 2.0. This technology is a widely utilized and validated tool, with over 1,200 publications (https://aceabio.com/publications/). Cells must pass through a pore embedded in a gold-plated electric grid, creating electrical impedance and registering a signal for real-time, quantifiable cell migration. As cells migrate through a small pore, they pass over a gold grid, which causes electrical impedance that is registered in real-time as cellular migration. In order to prepare the data, we plotted the Cell Index every 12 hours. . We can distribute all data points upon request. For scratch wound assays, cells were seeded at a density of 1,500,000 cells in 35 mm TCPs. After 24 hours, cell plates were linearly scratched with a pipet tip, and images representative of wound healing were captured after 48 hours. For cell size and death analysis via flow cytometry, cells were analyzed for forward scatter with the Beckman-Coulter CyAn flow cytometer at the University of Michigan Flow Cytometry Core. Cells were analyzed by Annexin V/PI staining with Annexin V (TFS: cat# A13199) and PI (Sigma-Aldrich: cat# 25535-16-4), according to manufacturer's protocols.

Statistical analysis and reproducibility

Cell proliferation, migration, and size were analyzed via paired student's t-test. Immunoblot and immunoprecipitation assays were repeated at least three times in all cell lines. All data needed to evaluate the conclusions in the paper are present in the paper and/or the Supplementary Materials. Additional data available from authors upon request.

Acknowledgements

We thank T. Carey, M. Cohen, S. Takayama, and M. Wicha for cell lysates and use of equipment. We thank E. Pedersen, A. Hawkins, and E. Lawlor's Lab for use of ACEA RCTA DP instrument. We thank F. Haidar and H. Amatullah for replicating key experiments. We thank F. Haidar for the artwork (Figure 2.6.I). We thank our funding sources: National Institute of Dental and Craniofacial Research (1F30DE026048-01, R01-DE016530, and T32-DE007057) and Stuart & Barbara Padnos Research Award from the Comprehensive Cancer Center at the University of Michigan.

Figures

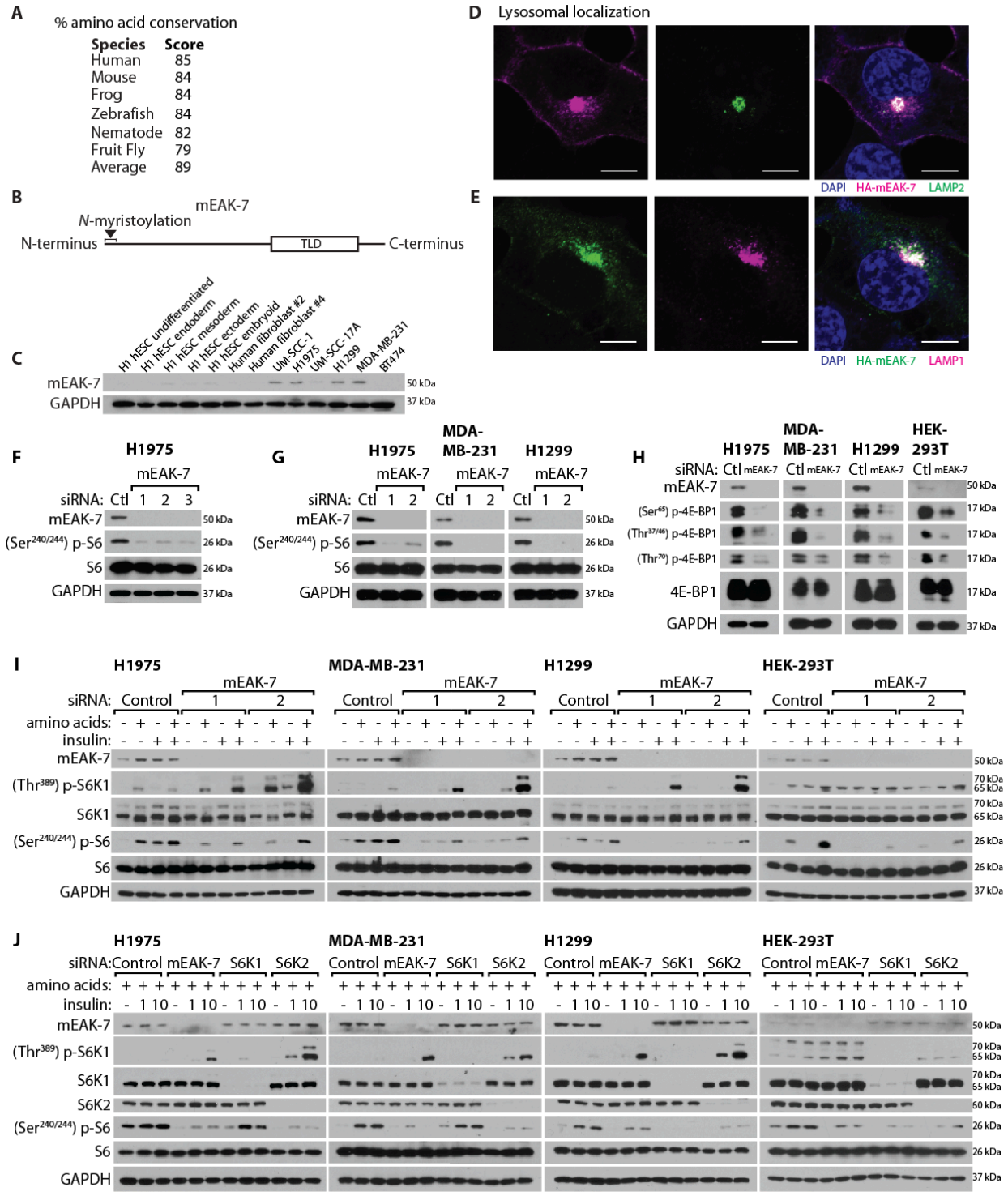
A
% amino acid conservation
Species Score
Human 85
Mouse 84
Frog 84
Zebrafish 84
Nematode 82
Fruit Fly 79
Average 89
B
mEAK-7
N-myristoylation
N-terminus
TLD
C-terminus
C
H1 hESC undifferentiated
H1 hESC endoderm
H1 hESC mesoderm
H1 hESC ectoderm
H1 hESC embryoid
Human fibroblast #2
Human fibroblast #4
UM-SCC-1
H1975
UM-SCC-17A
H1299
MDA-MB-231
BT474
mEAK-7
GAPDH
50 kDa
37 kDa
D
Lysosomal localization
DAPI HA-mEAK-7 LAMP2
E
DAPI HA-mEAK-7 LAMP1
F
H1975
mEAK-7
siRNA: Ctl 1 2 3
mEAK-7
(Ser240/244) p-S6
S6
GAPDH
50 kDa
26 kDa
26 kDa
37 kDa
G
H1975
MDA-MB-231
H1299
mEAK-7
siRNA: Ctl 1 2
mEAK-7
(Ser240/244) p-S6
S6
GAPDH
50 kDa
26 kDa
26 kDa
37 kDa
H
H1975
MDA-MB-231
H1299
HEK-293T
siRNA: Ctl mEAK-7
mEAK-7
(Ser65) p-4E-BP1
(Thr37/46) p-4E-BP1
(Thr70) p-4E-BP1
4E-BP1
GAPDH
50 kDa
17 kDa
17 kDa
17 kDa
17 kDa
37 kDa
I
H1975
MDA-MB-231
H1299
HEK-293T
mEAK-7
siRNA: Control 1 2
amino acids:
insulin:
mEAK-7
(Thr389) p-S6K1
S6K1
(Ser240/244) p-S6
S6
GAPDH
50 kDa
70 kDa
65 kDa
70 kDa
65 kDa
26 kDa
26 kDa
37 kDa
J
H1975
MDA-MB-231
H1299
HEK-293T
siRNA: Control mEAK-7 S6K1 S6K2
amino acids:
insulin: - 1 10
mEAK-7
(Thr389) p-S6K1
S6K1
S6K2
(Ser240/244) p-S6
S6
GAPDH
50 kDa
70 kDa
65 kDa
70 kDa
65 kDa
60 kDa
26 kDa
26 kDa
37 kDa

Figure 2.1. mEAK-7 is a lysosomal protein, conserved across eukaryotes, and is required for mTOR signaling in human cells. (**A**) Comparison of eukaryotic mEAK-7 orthologs. (**B**) Diagram depicting the mEAK-7 N-myristoylation motif and the TLD (TBC/LysM associated) domain. (**C**) Immunoblot screen of human cell lines to detect mEAK-7 protein. (**D, E**) Confocal microscopy analysis of H1299 cells stably expressing HA-mEAK-7WT for HA and LAMP2 (D) or LAMP1 (E). White bar denotes 10 μm. (**F**) H1975 cells were treated with control or 3 unique mEAK-7 siRNAs to assess S6 phosphorylation. (**G**) H1975, MDA-MB-231, and H1299 cells were treated with control or 2 unique mEAK-7 siRNAs to assess S6 phosphorylation. (**H**) Cells were treated with control or mEAK-7 #1 siRNA to assess 4E-BP1 phosphorylation. (**I**) Cells were treated with control or 2 unique mEAK-7 siRNAs. Next, cells were starved in DMEM-AAs for 2 hours and AAs, insulin, or both were reintroduced for 30 min. (**J**) Cells were treated with control, mEAK-7 #1, S6K1, and S6K2 siRNA. Next, cells were starved in DMEM+AAs for 2 hours and insulin (1μM and 10 μM) were reintroduced for 30 min. All experiments were repeated at least 3 times. GAPDH was used for loading controls.

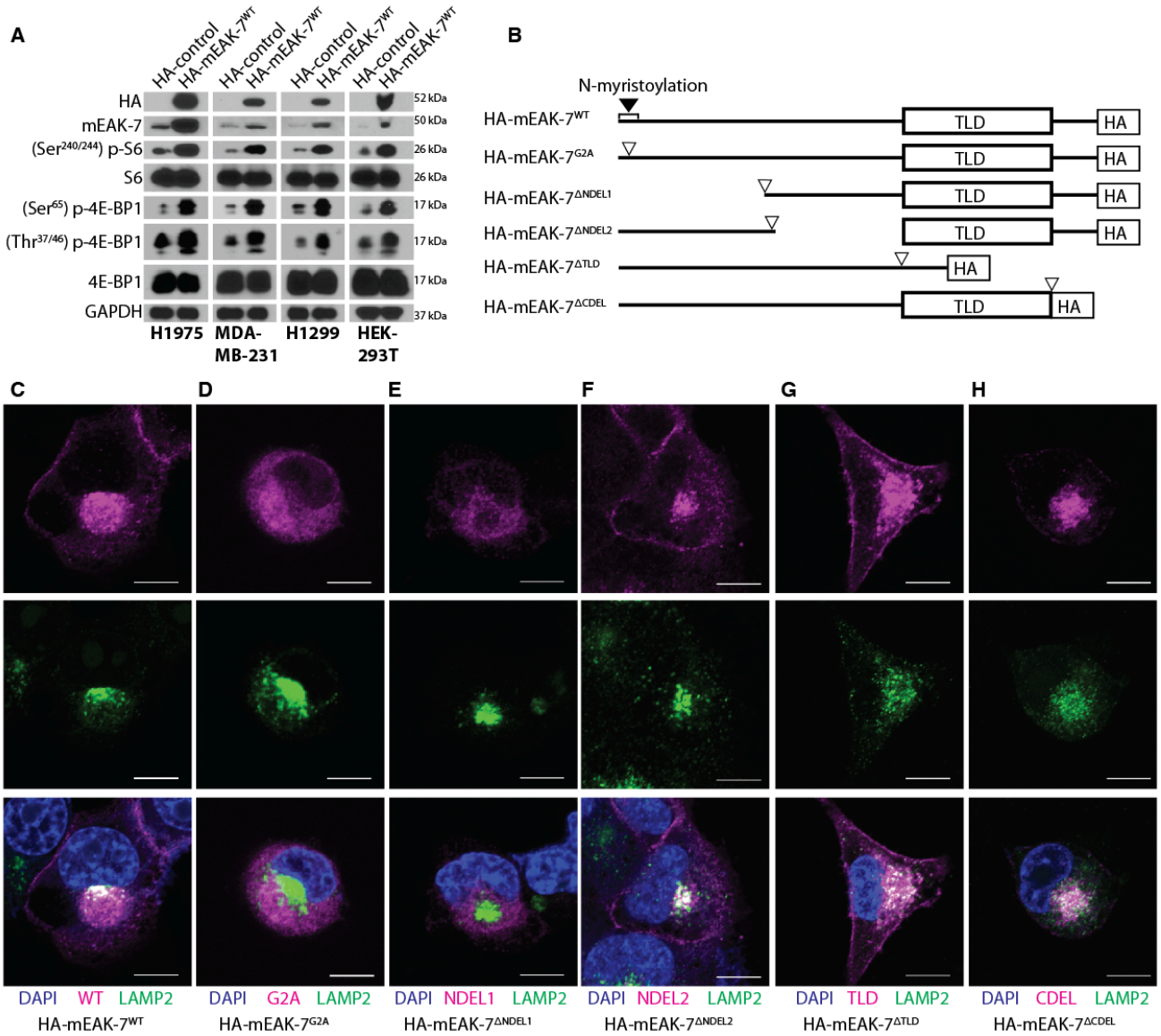
A
HA-control
HA-mEAK-7WT
HA
mEAK-7
(Ser240/244) p-S6
S6
(Ser65) p-4E-BP1
(Thr37/46) p-4E-BP1
4E-BP1
GAPDH
52 kDa
50 kDa
26 kDa
26 kDa
17 kDa
17 kDa
17 kDa
37 kDa
H1975
MDA-MB-231
H1299
HEK-293T
B
N-myristoylation
HA-mEAK-7WT
HA-mEAK-7G2A
HA-mEAK-7ΔNDEL1
HA-mEAK-7ΔNDEL2
HA-mEAK-7ΔTLD
HA-mEAK-7ΔCDEL
TLD
HA
C
D
E
F
G
H
DAPI WT LAMP2
DAPI G2A LAMP2
DAPI NDEL1 LAMP2
DAPI NDEL2 LAMP2
DAPI TLD LAMP2
DAPI CDEL LAMP2
HA-mEAK-7WT
HA-mEAK-7G2A
HA-mEAK-7ΔNDEL1
HA-mEAK-7ΔNDEL2
HA-mEAK-7ΔTLD
HA-mEAK-7ΔCDEL
I
H1299
NDEL
WT
G2A
1
2
TLD
CDEL
AAs & insulin:
HA
mEAK-7
(Ser240/244) p-S6
S6
GAPDH
52 kDa
37 kDa
50 kDa
26 kDa
26 kDa
37 kDa
J
H1299
WT
TLD
CDEL
AAs & insulin:
HA-mEAK-7
mEAK-7
(Thr389) p-S6K1
S6K1
(Ser240/244) p-S6
S6
GAPDH
52 kDa
37 kDa
50 kDa
65 kDa
65 kDa
26 kDa
26 kDa
37 kDa

Figure 2.2. Overexpression of mEAK-7 activates mTOR signaling and the TBC/LysM-Associated Domain and mTOR-binding (MTB) domain are necessary for mEAK-7 function. (**A**) H1975, MDA-MB-231, H1299, and HEK-293T cells were transduced with pLenti-III-HA-Control vector or pLenti-III-HA-mEAK-7-WT and selected with puromycin for 2 weeks. 1,000,000 cells were grown for 48 hours in 60 mm TCPs and collected for immunoblot analysis. (**B**) Design of the deletion mutants from HA-mEAK-7WT (wild-type); HA-mEAK-7G2A (G2A mutation), HA-mEAK-7ΔNDEL1 (Δ1-139 AAs), HA-mEAK-7ΔNDEL2 (Δ135-267 AAs), HA-mEAK-7ΔTLD (Δ243-412 AAs), and HA-mEAK-7ΔCDEL (Δ413-456 AAs). H1299 cells were transduced to stably express these mutant proteins. (**C—H**) Confocal microscopy analysis of H1299 cells stably expressing (C) HA-mEAK-7WT, (D) HA-mEAK-7G2A, (E) HA-mEAK-7ΔNDEL1, (F) HA-mEAK-7ΔNDEL2, (G) HA-mEAK-7ΔTLD, and (H) HA-mEAK-7ΔCDEL to stain for HA and LAMP2. White bar denotes 10 μm. (**I**) H1299 cells stably expressing HA-mEAK-7WT and mutants were starved in DMEM-AAs for 2 hours. Subsequently, amino acids and insulin were reintroduced for 30 min. (**J**) Under the same conditions in (I), HA-mEAK-7ΔTLD and HA-mEAK-7ΔCDEL cells were assessed for (Thr389) p-S6K1 levels. All experiments were replicated at least 3 times. GAPDH was used as a loading control.

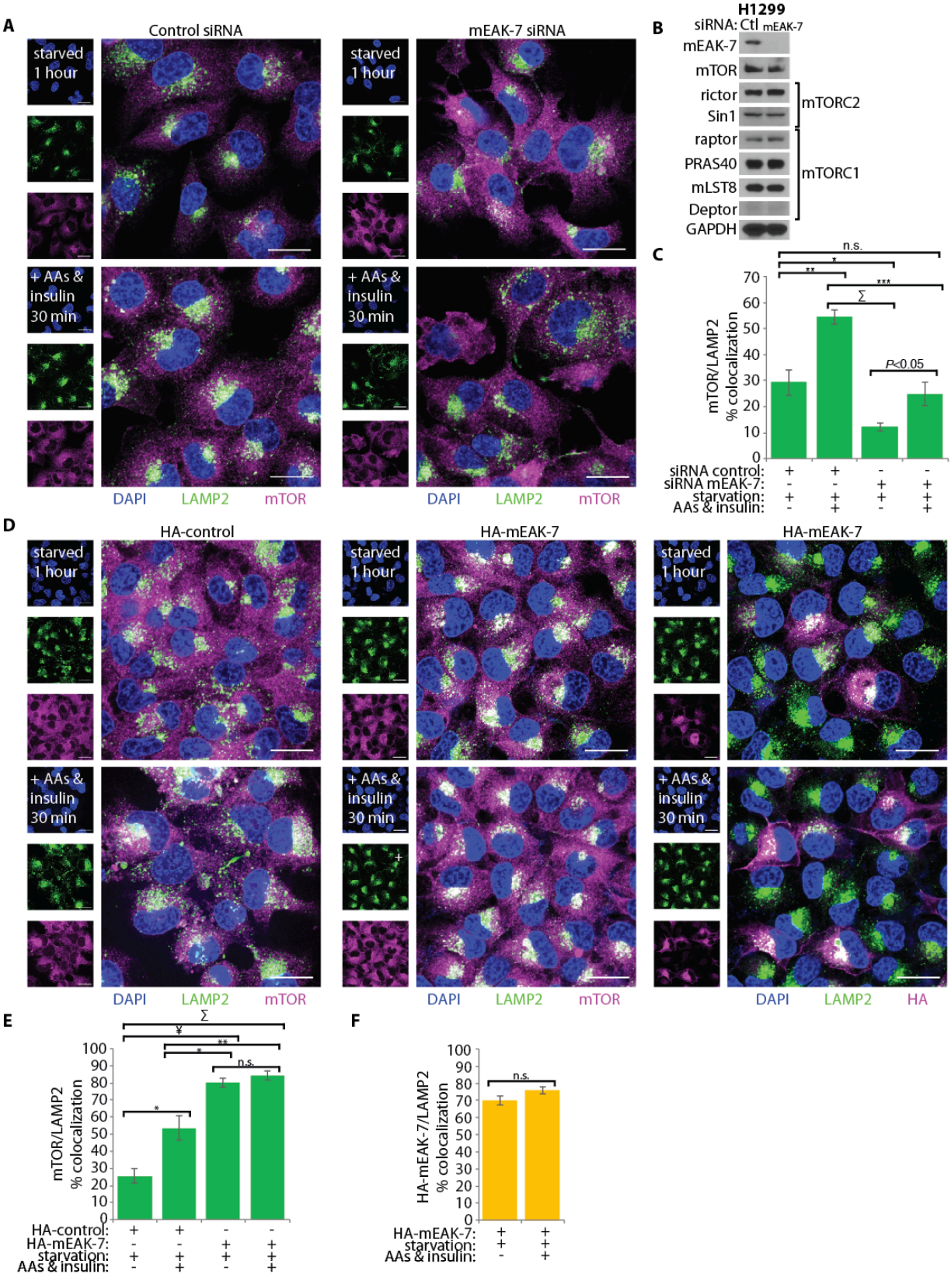
A
Control siRNA
mEAK-7 siRNA
starved 1 hour
+ AAs & insulin 30 min
DAPI
LAMP2
mTOR
B
H1299
siRNA: Ctl mEAK-7
mEAK-7
mTOR
rictor
Sin1
mTORC2
raptor
PRAS40
mLST8
Deptor
mTORC1
GAPDH
C
mTOR/LAMP2 % colocalization
n.s.
*
**
***
Σ
P<0.05
siRNA control:
siRNA mEAK-7:
starvation:
AAs & insulin:
D
HA-control
HA-mEAK-7
HA-mEAK-7
HA
E
mTOR/LAMP2 % colocalization
HA-control:
HA-mEAK-7:
starvation:
AAs & insulin:
F
HA-mEAK-7/LAMP2 % colocalization
HA-mEAK-7:
starvation:
AAs & insulin:

Figure 2.3. mEAK-7 is required for lysosomal localization of mTOR. (**A**) H1299 cells were treated with control or mEAK-7 siRNA for 48 hours in 10% serum-containing DMEM medium. Subsequently, 200,000 cells were transferred to 2-well glass chamber slides and allowed to settle for 24 hours. H1299 cells were then starved in DMEM-AAs for 1 hour and AAs and insulin were reintroduced for 30 min. (**B**) Immunoblot analysis of H1299 cells treated with control or mEAK-7 siRNA to assess the expression of mEAK-7 and mTOR complex proteins after mEAK-7 knockdown. (**C**) Statistical analysis of co-localization of mTOR and LAMP2 for Figure 2.3.A. (**D**) 200,000 normal H1299 cells or H1299 cells stably expressing HA-mEAK-7 were seeded to 2-well glass chamber slides and allowed to settle for 24 hours. Cells were then starved in DMEM-AAs for 1 hour and AAs and insulin were reintroduced for 30 min. (**E, F**) Statistical analysis of co-localization of mTOR and LAMP2 or HA-mEAK-7 and LAMP2 for Figure 2.3.D. 100x oil magnification. Cells were processed to detect DAPI (DNA), LAMP2 (lysosomal marker), mTOR, and HA (mEAK-7). *P<0.01, **P<0.001, ***P<0.0001, ‡P<0.00001, §P<0.000001, ΩP<0.0000001, ¥P<0.00000001, ∑P<0.000000001. White bar denotes 25 μm.

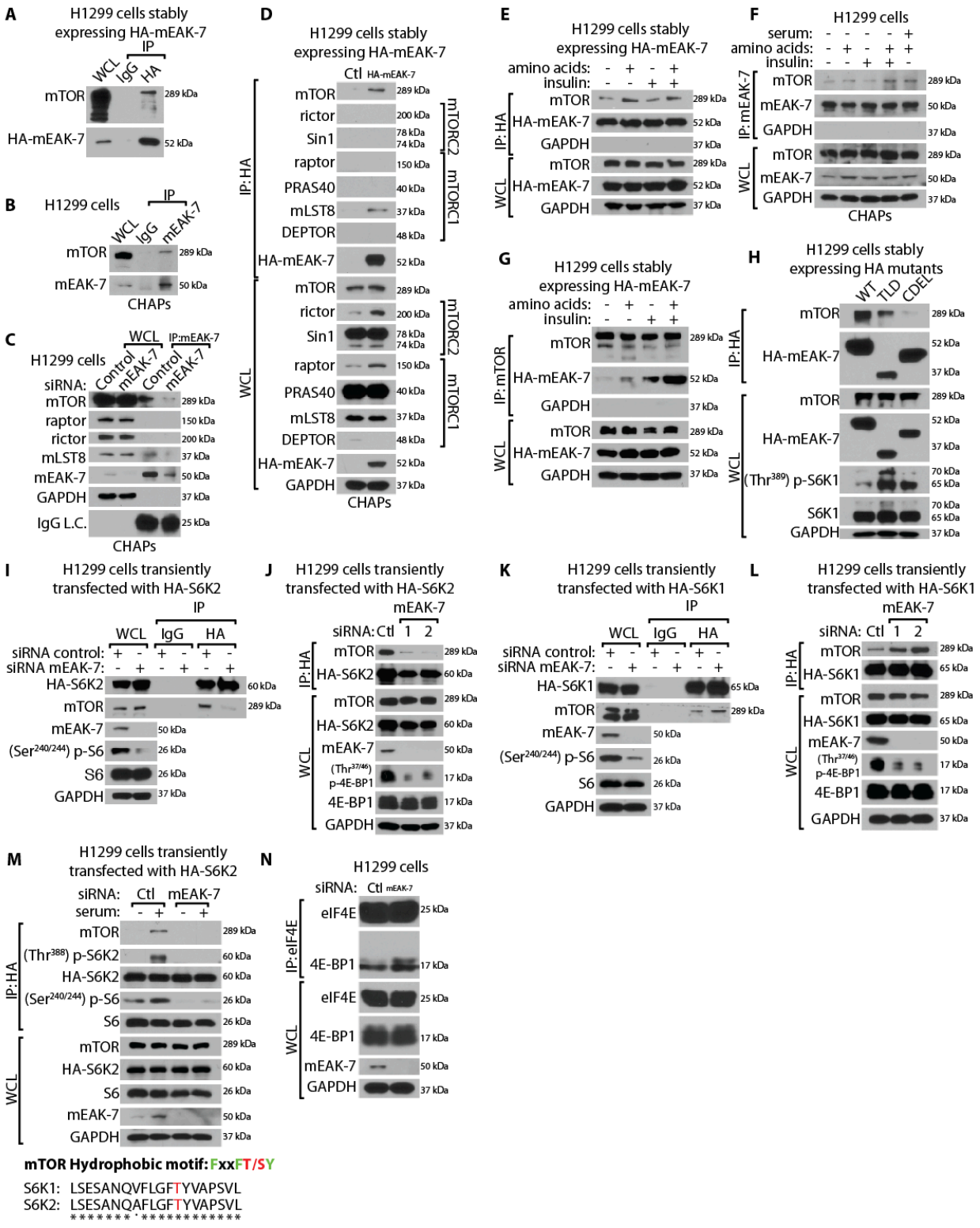
A
H1299 cells stably expressing HA-mEAK-7
IP
WCL
IgG
HA
mTOR
289 kDa
HA-mEAK-7
52 kDa
B
H1299 cells
IP
WCL
IgG
mEAK-7
mTOR
289 kDa
mEAK-7
50 kDa
CHAPs
C
H1299 cells
WCL
IP:mEAK-7
siRNA:
Control
mEAK-7
Control
mEAK-7
mTOR
289 kDa
raptor
150 kDa
rictor
200 kDa
mLST8
37 kDa
mEAK-7
50 kDa
GAPDH
37 kDa
IgG L.C.
25 kDa
CHAPs
D
H1299 cells stably expressing HA-mEAK-7
Ctl
HA-mEAK-7
IP:HA
WCL
mTOR
289 kDa
rictor
200 kDa
Sin1
78 kDa
74 kDa
raptor
150 kDa
PRAS40
40 kDa
mLST8
37 kDa
DEPTOR
48 kDa
HA-mEAK-7
52 kDa
GAPDH
37 kDa
mTORC2
mTORC1
CHAPs
E
H1299 cells stably expressing HA-mEAK-7
amino acids:
insulin:
IP:HA
WCL
mTOR
HA-mEAK-7
GAPDH
289 kDa
52 kDa
37 kDa
F
H1299 cells
serum:
amino acids:
insulin:
IP:mEAK-7
WCL
mTOR
mEAK-7
GAPDH
289 kDa
50 kDa
37 kDa
CHAPs
G
H1299 cells stably expressing HA-mEAK-7
amino acids:
insulin:
IP:mTOR
WCL
mTOR
HA-mEAK-7
GAPDH
289 kDa
52 kDa
37 kDa
H
H1299 cells stably expressing HA mutants
WT
TLD
CDEL
IP:HA
WCL
mTOR
HA-mEAK-7
(Thr389) p-S6K1
S6K1
GAPDH
289 kDa
52 kDa
37 kDa
70 kDa
65 kDa
I
H1299 cells transiently transfected with HA-S6K2
IP
WCL
IgG
HA
siRNA control:
siRNA mEAK-7:
HA-S6K2
mTOR
mEAK-7
(Ser240/244) p-S6
S6
GAPDH
60 kDa
289 kDa
50 kDa
26 kDa
37 kDa
J
H1299 cells transiently transfected with HA-S6K2
mEAK-7
siRNA: Ctl 1 2
IP:HA
WCL
mTOR
HA-S6K2
mEAK-7
(Thr37/46) p-4E-BP1
4E-BP1
GAPDH
289 kDa
60 kDa
50 kDa
17 kDa
37 kDa
K
H1299 cells transiently transfected with HA-S6K1
IP
WCL
IgG
HA
siRNA control:
siRNA mEAK-7:
HA-S6K1
mTOR
mEAK-7
(Ser240/244) p-S6
S6
GAPDH
65 kDa
289 kDa
50 kDa
26 kDa
37 kDa
L
H1299 cells transiently transfected with HA-S6K1
mEAK-7
siRNA: Ctl 1 2
IP:HA
WCL
mTOR
HA-S6K1
mEAK-7
(Thr37/46) p-4E-BP1
4E-BP1
GAPDH
289 kDa
65 kDa
50 kDa
17 kDa
37 kDa
M
H1299 cells transiently transfected with HA-S6K2
siRNA:
Ctl
mEAK-7
serum:
IP:HA
WCL
mTOR
(Thr388) p-S6K2
HA-S6K2
(Ser240/244) p-S6
S6
mEAK-7
GAPDH
289 kDa
60 kDa
26 kDa
50 kDa
37 kDa
mTOR Hydrophobic motif: FxxFT/SY
S6K1: LSESANQVFLGFTYVAPSVL
S6K2: LSESANQAFLGFTYVAPSVL
N
H1299 cells
siRNA:
Ctl
mEAK-7
IP:eIF4E
WCL
eIF4E
4E-BP1
mEAK-7
GAPDH
25 kDa
17 kDa
50 kDa
37 kDa

Figure 2.4. mEAK-7 interacts with mTOR through the MTB domain and is required for S6K2 activity. (**A**) HA-mEAK-7^{WT} cells immunoprecipitated with goat IgG or goat anti-HA. (**B**) H1299 cells, in CHAPs, immunoprecipitated with anti-mEAK-7. (**C**) H1299 cells transfected with control or mEAK-7 siRNA, in CHAPs, immunoprecipitated with anti-mEAK-7. (**D**) Normal H1299 or HA-mEAK-7^{WT} cells, in CHAPs, immunoprecipitated with anti-HA. (**E**) HA-mEAK-7^{WT} cells starved in DMEM^{-AAs} for 2 hours, nutrient stimulated for 30 min, immunoprecipitated with anti-HA. (**F**) H1299 cells starved in DMEM^{-AAs} for 2 hours, nutrient stimulated for 60 min, immunoprecipitated with anti-mEAK-7. **(G)** Conditions mimicked in (E), immunoprecipitated with anti-mTOR antibody. **(H)** HA-mEAK-7^{WT}, HA-mEAK-7$^{\Delta TLD}$, and HA-mEAK-7$^{\Delta CDEL}$ cells immunoprecipitated with anti-HA. (**I, J**) H1299 cells transfected with pcDNA3-HA-S6K2-WT and control, mEAK-7 #1, or mEAK-7 #2 siRNA, immunoprecipitated with anti-HA. (**K, L**) H1299 cells transfected with pRK7-HA-S6K1-WT and control, mEAK-7 #1, or mEAK-7 #2 siRNA, immunoprecipitated with anti-HA. (**M**) mTOR targeting hydrophobic motif. H1299 cells transfected with pcDNA3-HA-S6K2-WT and control or mEAK-7 #1 siRNA. Cells starved in DMEM^{-AAs} for 2 hours, 10% serum stimulated, immunoprecipitated with anti-HA. (**N**) H1299 cells transfected with control or mEAK-7 siRNA and immunoprecipitated with anti-eIF4E. Experiments repeated 3 times. GAPDH was a loading control.

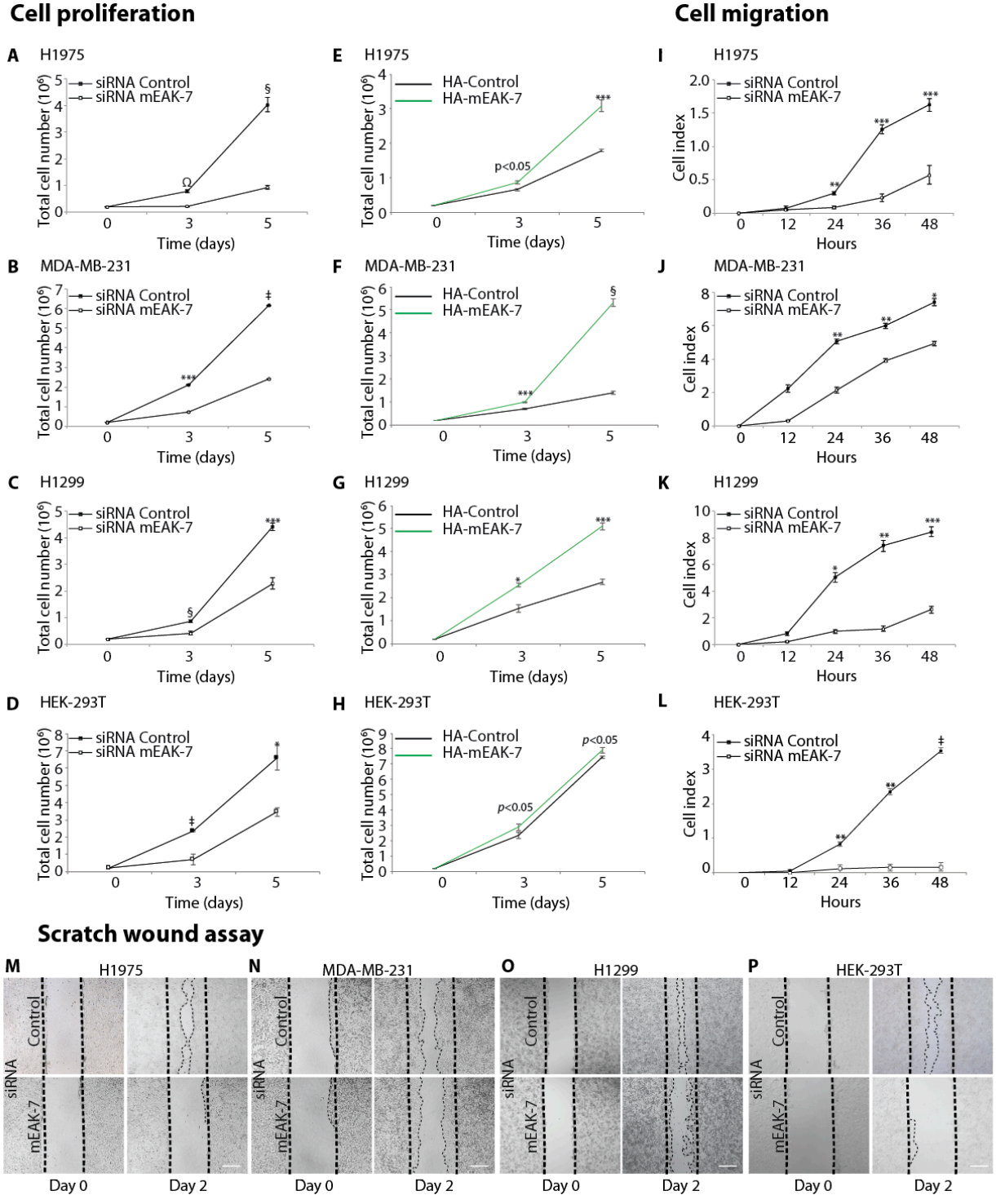
Cell proliferation
Cell migration
A H1975
B MDA-MB-231
C H1299
D HEK-293T
E H1975
F MDA-MB-231
G H1299
H HEK-293T
I H1975
J MDA-MB-231
K H1299
L HEK-293T
siRNA Control
siRNA mEAK-7
HA-Control
HA-mEAK-7
Total cell number (10^6)
Cell index
Time (days)
Hours
p<0.05
Scratch wound assay
M H1975
N MDA-MB-231
O H1299
P HEK-293T
Control siRNA
mEAK-7 siRNA
Day 0
Day 2

Figure 2.5. mEAK-7 is essential for cell proliferation and cell migration. (**A—D**) (A) H1975 (n=13), (B) MDA-MB-231 (n=9), (C) H1299 (n=8), and (D) HEK-293T (n=6) cells treated with control or mEAK-7 #1 siRNA. 200,000 cells transferred to 100 mm TCPs and counted at day 3 and 5. (**E—H**) (E) H1975 (n=6), (F) MDA-MB-231 (n=6), (G) H1299 (n=6), and (H) HEK-293T (n=6) cells were transduced with pLenti-III-HA-Control vector or pLenti-III-HA-mEAK-7-WT. 200,000 cells were transferred to 100 mm TCPs and counted at day 3 and 5. (**I—L**) (I) H1975 (n=6), (J) MDA-MB-231 (n=5), (K) H1299 (n=5), and (L) HEK-293T (n=6) cells were treated with control or mEAK-7 #1 siRNA. 50,000 cells were transferred to CIM 16-well plates and real-time analysis was performed for 48 hours using ACEA Bioscience's RCTA DP instrument. (**M—P**) (M) H1975, (N) MDA-MB-231, (O) H1299, (P) HEK-293T cells were treated with control or mEAK-7 siRNA. 1,500,000 cells were transferred into 35 mm TCPs. The following day, a scratch is created down the middle and pictures were taken at 0 and 48 hours. White bar denotes 125 μm. Data are represented as mean ± SEM. Statistical significance denoted: *P<0.01, **P<0.001, ***P<0.0001, ‡P<0.00001, §P<0.000001, ΩP<0.0000001, ¥P<0.00000001.

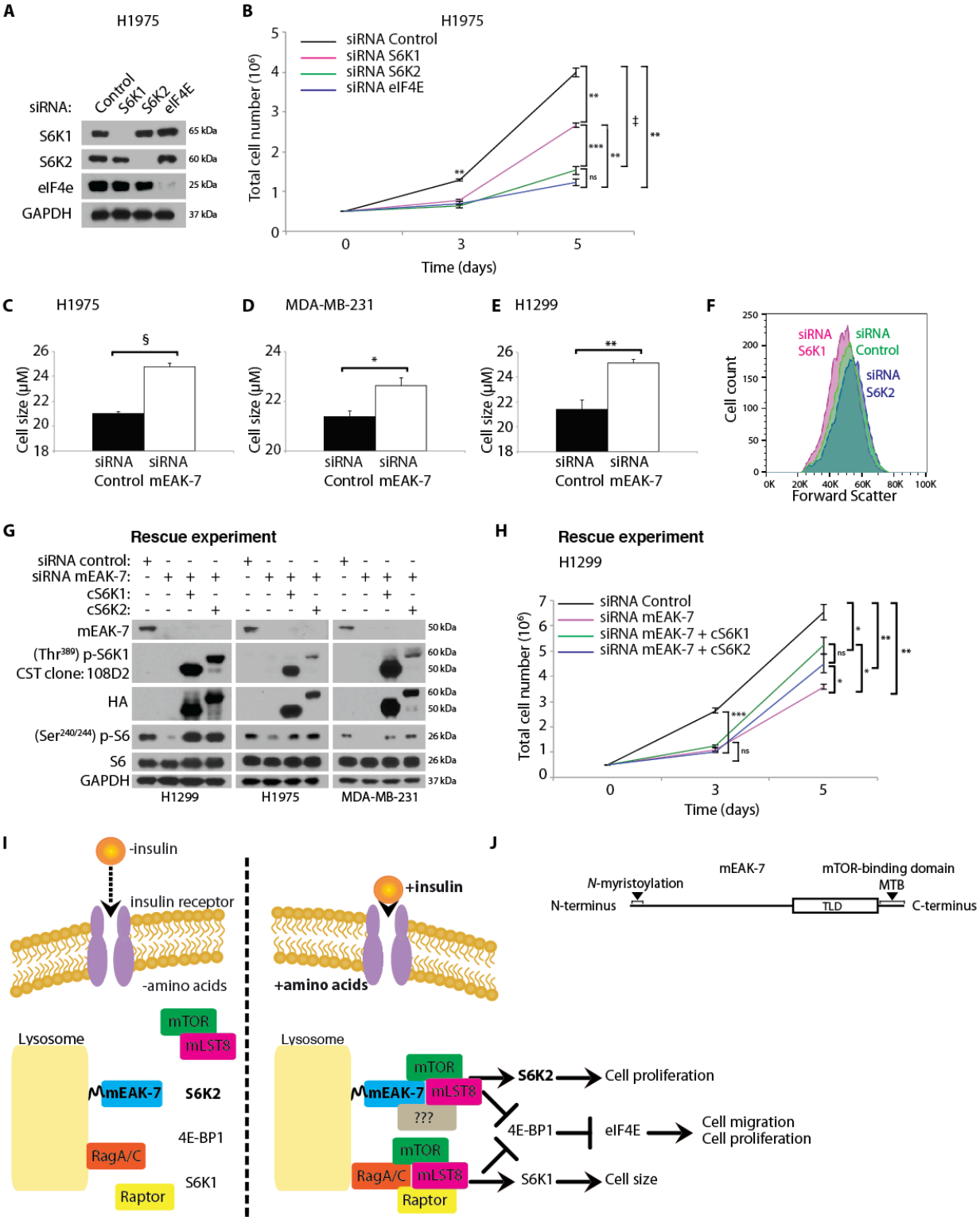
A
H1975
siRNA:
Control
S6K1
S6K2
eIF4E
S6K1
S6K2
eIF4e
GAPDH
65 kDa
60 kDa
25 kDa
37 kDa
B
H1975
siRNA Control
siRNA S6K1
siRNA S6K2
siRNA eIF4E
Total cell number (10⁶)
Time (days)
C
H1975
Cell size (μM)
siRNA Control
siRNA mEAK-7
D
MDA-MB-231
E
H1299
F
siRNA S6K1
siRNA Control
siRNA S6K2
Cell count
Forward Scatter
G
Rescue experiment
siRNA control:
siRNA mEAK-7:
cS6K1:
cS6K2:
mEAK-7
(Thr389) p-S6K1
CST clone: 108D2
HA
(Ser240/244) p-S6
S6
GAPDH
H1299
H1975
MDA-MB-231
H
Rescue experiment
H1299
siRNA Control
siRNA mEAK-7
siRNA mEAK-7 + cS6K1
siRNA mEAK-7 + cS6K2
Total cell number (10⁶)
Time (days)
I
-insulin
insulin receptor
-amino acids
+insulin
+amino acids
Lysosome
mTOR
mLST8
mEAK-7
S6K2
4E-BP1
RagA/C
S6K1
Raptor
???
Cell proliferation
eIF4E
Cell migration
Cell proliferation
Cell size
J
mEAK-7
mTOR-binding domain
MTB
N-myristoylation
N-terminus
TLD
C-terminus

Figure 2.6. Overexpression of constitutively activated S6K2 or S6K1 is capable of rescuing cell defects due to mEAK-7 knockdown. (**A**) H1975 cells were treated with control, S6K1, S6K2, or eIF4E siRNA. (**B**) From (A), 500,000 cells were transferred to 100 mm TCPs and counted at day 3 and 5. (**C—E**) (C) H1975 (n=13), (D) MDA-MB-231 (n=9), and (E) H1299 (n=8) cells were treated with control or mEAK-7 siRNA. 500,000 cells were transferred to 100 mm TCPs and cell size was analyzed at day 3 with AO-PI staining via Logos Biosystems. (**F**) H1975 cells were treated with control, S6K1, or S6K2 siRNA and analyzed for forward scatter via flow cytometry. (**G**) H1299, H1975, and MDA-MB-231 cells were transiently transfected with control siRNA, mEAK-7 siRNA, mEAK-7 siRNA + pRK7-HA-S6K1-F5A-E389-deltaCT plasmid, or mEAK-7 siRNA + pcDNA3-HA-S6K2-E388-DE plasmid. (**H**) 500,000 H1299 cells treated as described in (G) were transferred to 100 mm TCPs and counted at day 3 and 5 via Logos Biosystems. (**I**) Diagram depicting mEAK-7 function on mTOR complex formation for S6K2. (**J**) Summary of mEAK-7 domains: N-myristoylation motif, TLD domain, and mTOR-binding (MTB) domain. Data are represented as mean ± SEM. Statistical significance denoted: *P<0.01, **P<0.001, ***P<0.0001, ‡P<0.00001, §P<0.000001. GAPDH was used as a loading control.

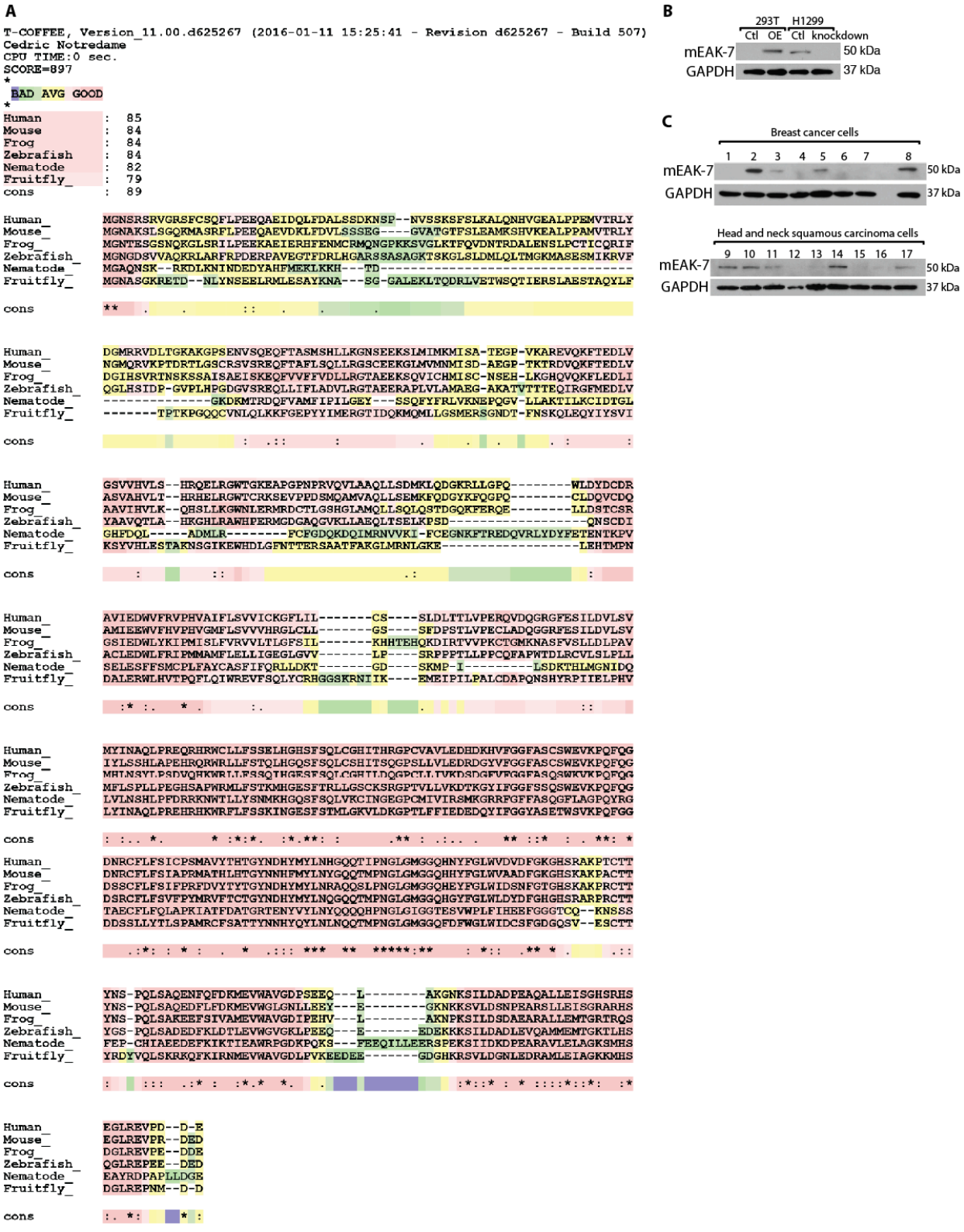
A
T-COFFEE, Version_11.00.d625267 (2016-01-11 15:25:41 - Revision d625267 - Build 507)
Cedric Notredame
CPU TIME:0 sec.
SCORE=897
BAD AVG GOOD
Human : 85
Mouse : 84
Frog : 84
Zebrafish : 84
Nematode : 82
Fruitfly : 79
cons : 89
B
293T H1299
Ctl OE Ctl knockdown
mEAK-7 50 kDa
GAPDH 37 kDa
C
Breast cancer cells
1 2 3 4 5 6 7 8
mEAK-7 50 kDa
GAPDH 37 kDa
Head and neck squamous carcinoma cells
9 10 11 12 13 14 15 16 17
mEAK-7 50 kDa
GAPDH 37 kDa

Figure 2.7. T-coffee analysis of mEAK-7 in eukaryotes, validation of human mEAK-7 antibody, and an expanded cell screen for mEAK-7 protein. (**A**) T-Coffee analysis of mEAK-7 primary protein structure across human, mouse, frog, zebrafish, nematode, and fruit fly. (**B**) Analysis of mouse monoclonal antibody clone 12B1 targeting mEAK-7. Normal HEK-293T or HEK-293T cells stably expressing exogenous mEAK-7 protein were probed with anti-mEAK-7 antibody. H1299 cells were treated with control or mEAK-7 siRNA and probed with anti-mEAK-7 antibody. (**C**) Cell screen of breast carcinoma and head & neck squamous cell carcinoma cell lines. (1) BT474, (2) HCC1937, (3) MDA-MB-436, (4) SK-BR-3, (5) SUM149, (6) SUM159, (7) T4D7, (8) MDA-MB-468, (9) UM-SCC-1, (10) UM-SCC-10A, (11) UM-SCC-11A, (12) UM-SCC-14A, (13) UM-SCC-17A, (14) UM-SCC-17B, (15) UM-SCC-74A, (16) UM-SCC-74B, and (17) UM-SCC-81B. GAPDH was used as a loading control.

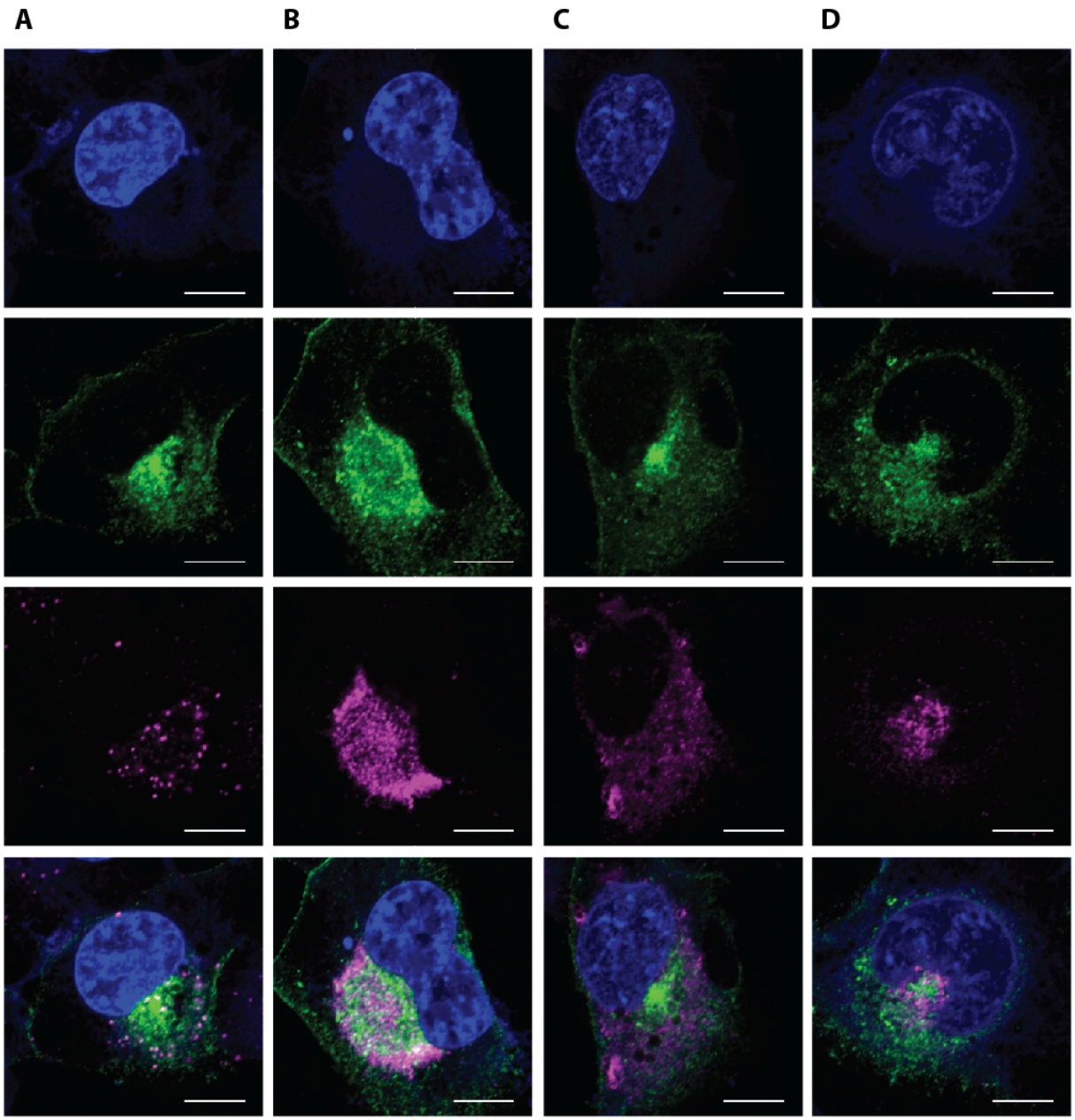
A
B
C
D
DAPI HA-mEAK-7 EEA1
Endosome
DAPI HA-mEAK-7 AIF
Mitochondria
DAPI HA-mEAK-7 PDI
Endoplasmic Reticulum
DAPI HA-mEAK-7 RCAS1
Golgi Complex

Figure 2.8. Extended immunofluorescence analysis of HA-mEAK-7WT in other cellular compartments. (**A**) H1299 cells stably expressing HA-mEAK-7WT were stained with HA antibody and early endosome antigen-1 (EEA1, endosome) antibody. (**B**) H1299 cells stably expressing HA-mEAK-7WT were stained with HA antibody and apoptosis inducing factor (AIF, mitochondria) antibody. (**C**) H1299 cells stably expressing HA-mEAK-7WT were stained with HA antibody and protein disulfide isomerase (PDI, endoplasmic reticulum) antibody. (**D**) H1299 cells stably expressing HA-mEAK-7WT were stained with HA antibody and receptor-binding cancer antigen expressed on SiSo cells (RCAS1, Golgi complex) antibody. Experiments were replicated at least three times. White bar denotes 10 μm.

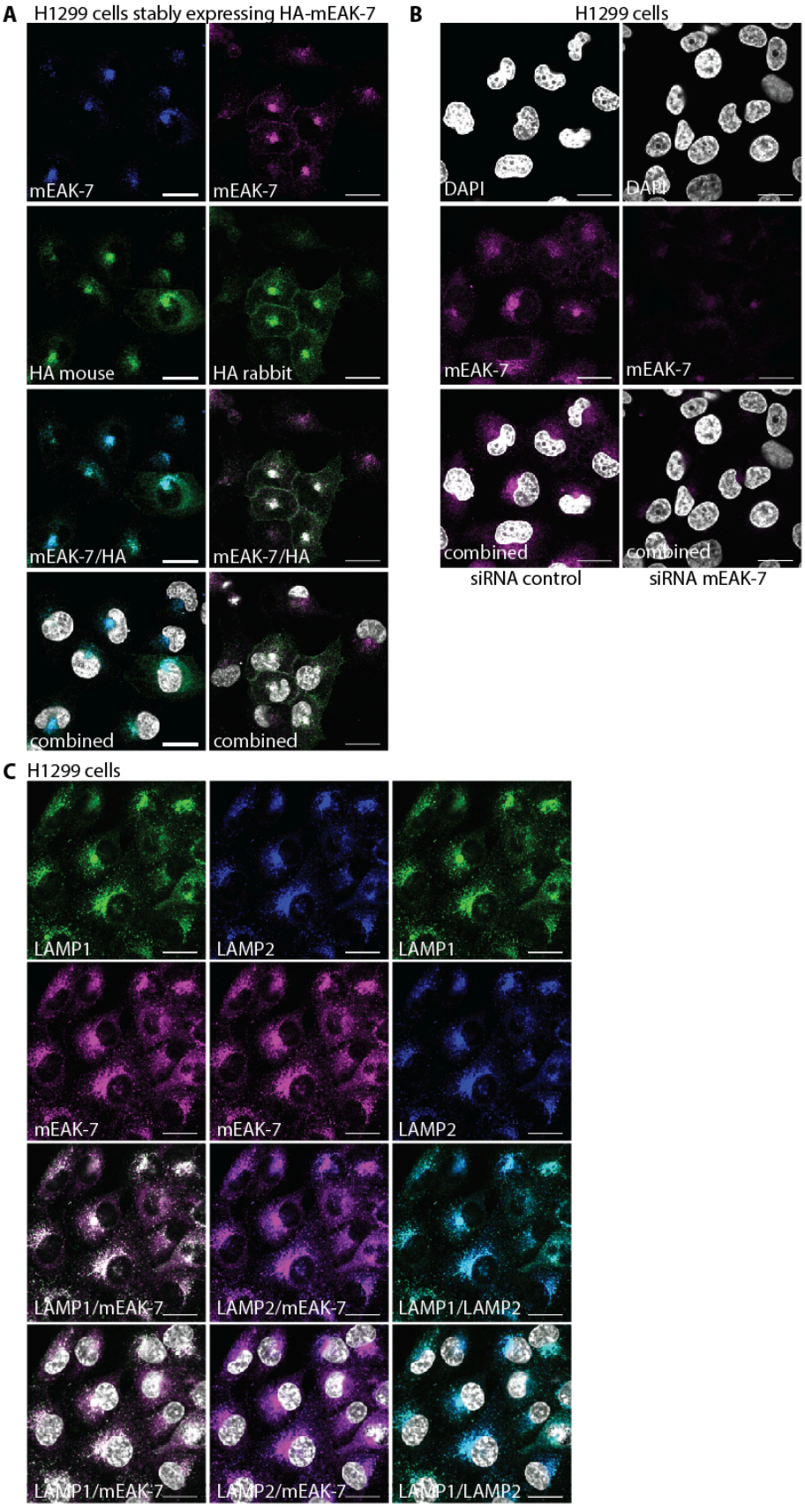
A
H1299 cells stably expressing HA-mEAK-7
mEAK-7
mEAK-7
HA mouse
HA rabbit
mEAK-7/HA
mEAK-7/HA
combined
combined
B
H1299 cells
DAPI
DAPI
mEAK-7
mEAK-7
combined
combined
siRNA control
siRNA mEAK-7
C
H1299 cells
LAMP1
LAMP2
LAMP1
mEAK-7
mEAK-7
LAMP2
LAMP1/mEAK-7
LAMP2/mEAK-7
LAMP1/LAMP2
LAMP1/mEAK-7
LAMP2/mEAK-7
LAMP1/LAMP2

Figure 2.9. Validation of mEAK-7 antibody for immunofluorescence analysis of endogenous mEAK-7 at the lysosome. Polyclonal goat antibody SCB cat# sc-247321 was utilized for anti-mEAK-7 immunofluorescence analysis. (**A**) H1299 cells stably expressing HA-mEAK-7WT were grown under 10% serum DMEM+AAs, fixed, and stained with (left panel) anti-mEAK-7, anti-HA mouse, and anti-LAMP1 or (right panel) anti-mEAK-7, anti-HA rabbit, and anti-LAMP2. (**B**) H1299 cells were treated with control or mEAK-7 siRNA for 48 hours under 10% serum DMEM+AAs and stained with anti-mEAK-7. (**C**) H1299 cells were cultured under 10% serum DMEM+AAs and stained with (left panel) anti-mEAK-7 and anti-LAMP1, (middle panel) anti-mEAK-7 and anti-LAMP2, or (right panel) anti-LAMP1 and anti-LAMP2. Experiments were replicated at least three times. Images were captured with 100x oil confocal microscopy. White bar denotes 25 μm.

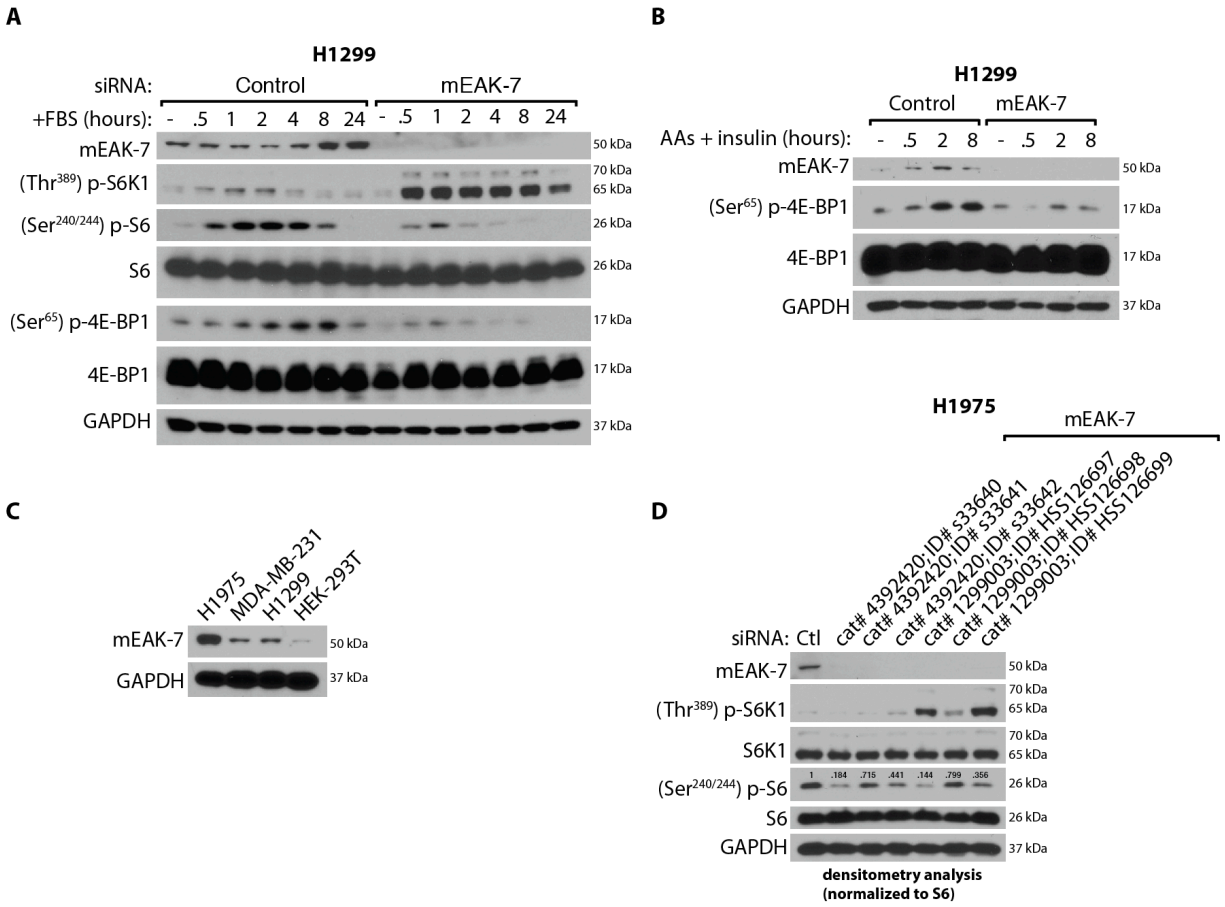

Figure 2.10. mEAK-7 regulates serum-mediated activation of mTORC1 signaling and knockdown of mEAK-7 results in increased (Thr389) p-S6K1 levels. (**A**) H1299 cells were treated with control or mEAK-7 siRNA for 48 hours in 10% serum-containing DMEM medium. Subsequently, cells were starved in DMEM+AAs for 2 hours and 20% serum-containing DMEM medium was reintroduced for up to 24 hours to assess S6 and 4E-BP1 activation status. (**B**) H1299 cells were treated with control or mEAK-7 #1 siRNA for 48 hours in 10% serum-containing DMEM medium. Subsequently, cells were starved in DMEM+AAs for 2 hours and AAs and insulin were reintroduced for the course of 8 hours to assess 4E-BP1 activation status. (**C**) H1975, MDA-MB-231, H1299, and HEK-293T cells were analyzed via immunoblot analysis for comparing relative protein levels of mEAK-7. (**D**) H1975 cells were treated with control or one of six unique mEAK-7 siRNAs for 48 hours in 10% serum-containing DMEM medium. Experiments were replicated at least three times. ImageStudioLite and Microsoft Excel software were utilized. GAPDH was used as a loading control.

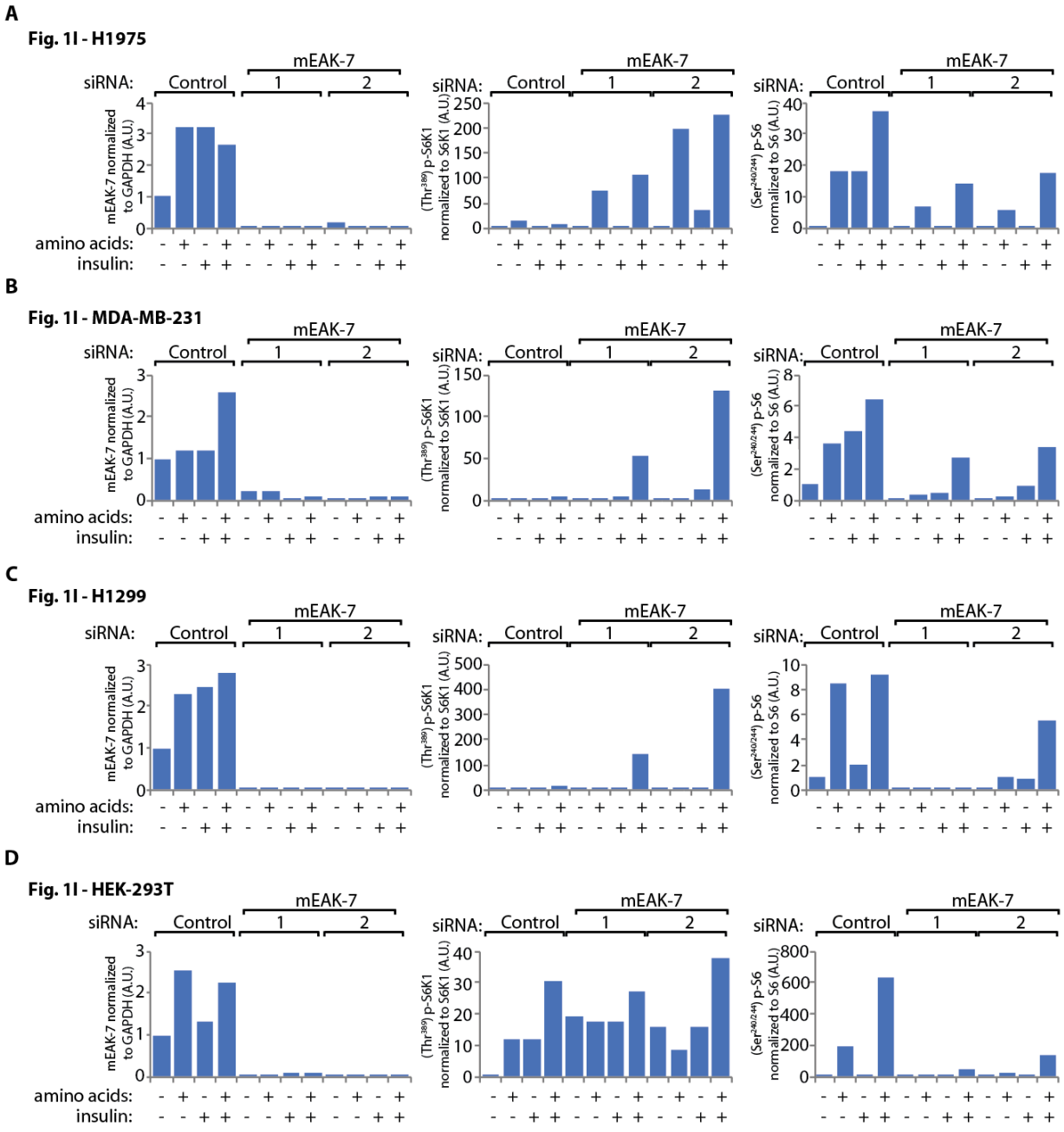

Figure 2.11. Densitometry analysis of Figure 2.1 (I). Densitometry analysis of Figure 2.1.I for (**A**) H1975 cells, (**B**) MDA-MB-231 cells, (**C**) H1299 cells, and (**D**) HEK-293T cells. A.U. represents arbitrary units. ImageStudioLite and Microsoft Excel software were utilized.

A

Fig. 1J - H1975

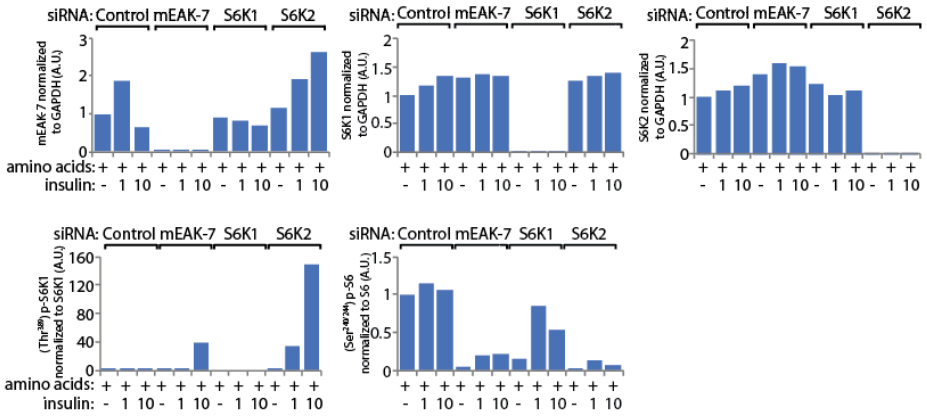

B

Fig. 1J - MDA-MB-231

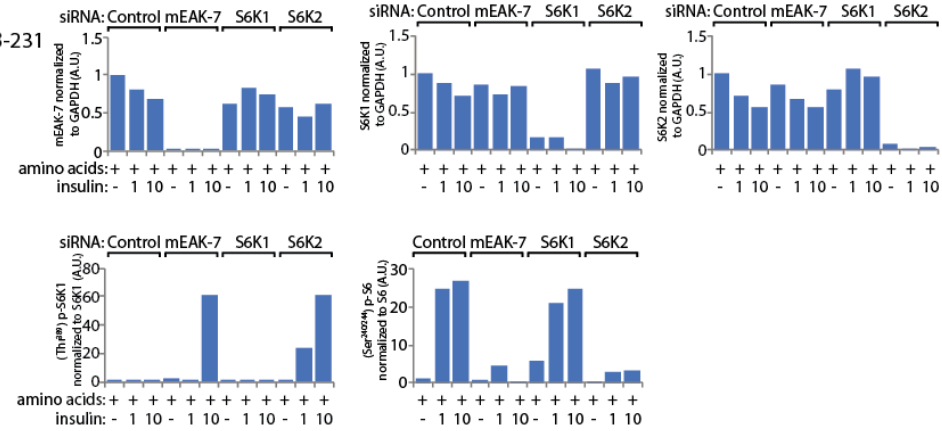

C

Fig. 1J - H1299

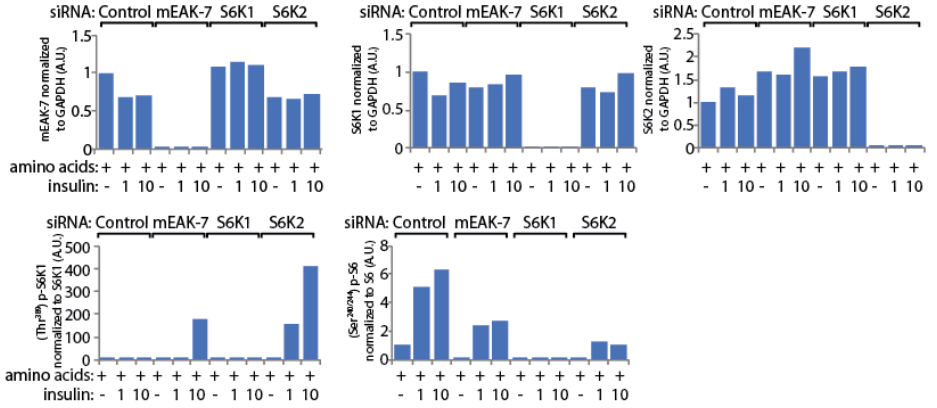

D

Fig. 1J - HEK-293T

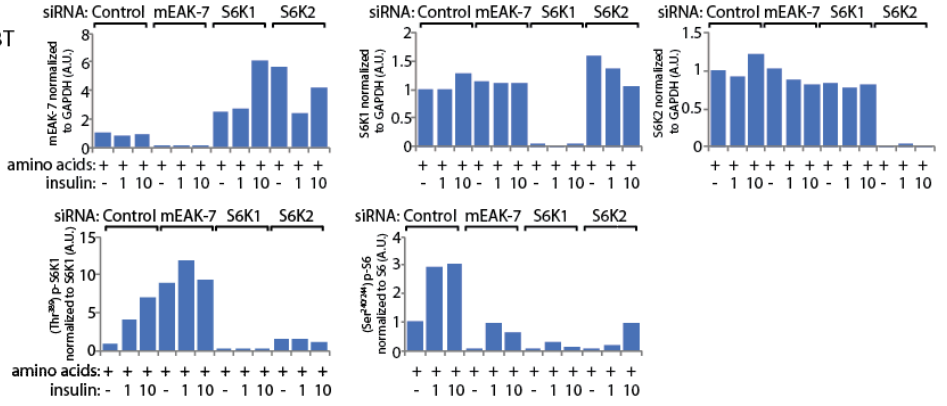

Figure 2.12. Densitometry analysis of Figure 2.1 (J). Densitometry analysis of Figure 2.1.wJ for (**A**) H1975 cells, (**B**) MDA-MB-231 cells. (**C**) H1299 cells, and (**D**) for HEK-293T cells. A.U. represents arbitrary units. ImageStudioLite and Microsoft Excel software were utilized.

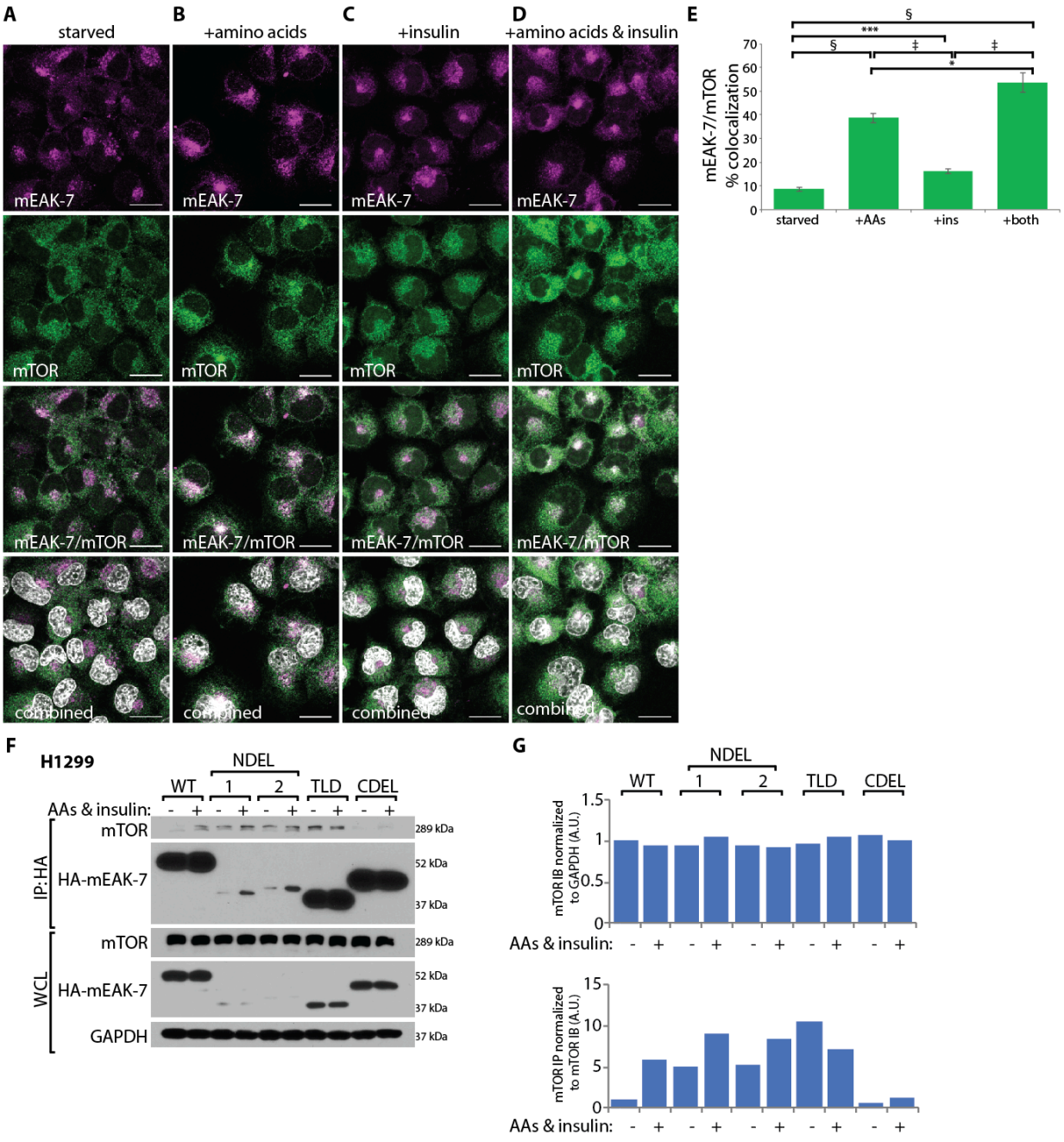
A
starved
B
+amino acids
C
+insulin
D
+amino acids & insulin
mEAK-7
mTOR
mEAK-7/mTOR
combined
E
mEAK-7/mTOR
% colocalization
starved
+AAs
+ins
+both
F
H1299
NDEL
WT
1
2
TLD
CDEL
AAs & insulin:
IP:HA
WCL
mTOR
HA-mEAK-7
GAPDH
289 kDa
52 kDa
37 kDa
G
mTOR IB normalized to GAPDH (A.U.)
mTOR IP normalized to mTOR IB (A.U.)

Figure 2.13. Immunofluorescence analysis of endogenous mEAK-7 co-localizing with endogenous mTOR in response to nutrients and immunoprecipitation analysis of HA-mEAK-7 mutants for mTOR interaction. (**A**) H1299 cells were starved in DMEM-AAs for 1 hour and stained with anti-mEAK-7 and anti-mTOR. (**B**) H1299 cells were starved in DMEM-AAs for 1 hour. After reintroducing AAs for 1 hour, cells were stained with anti-mEAK-7 and anti-mTOR. (**C**) H1299 cells were starved in DMEM-AAs for 1 hour. After reintroducing insulin for 1 hour, cells were stained with anti-mEAK-7 and anti-mTOR. (**D**) H1299 cells were starved in DMEM-AAs for 1 hour. After reintroducing AAs and insulin for 1 hour, cells were stained with anti-mEAK-7 and anti-mTOR. (**E**) Statistical analyses of A-D. Experiments were replicated at least three times. Images were captured with 100x oil confocal microscopy. Images were analyzed with Imaris Software. *P<0.01, **P<0.001, ***P<0.0001, ‡P<0.00001, §P<0.000001. White bar denotes 25 μm. (**F**) H1299 cells stably expressing HA-mEAK-7 WT or mutants were starved in DMEM-AAs. After reintroducing AAs and insulin for 1 hour, cells were immunoprecipitated with goat anti-HA antibody. (**G**) Densitometry analysis of Figure S 2.7.F. A.U. represents arbitrary units. ImageStudioLite and Microsoft Excel software were utilized.

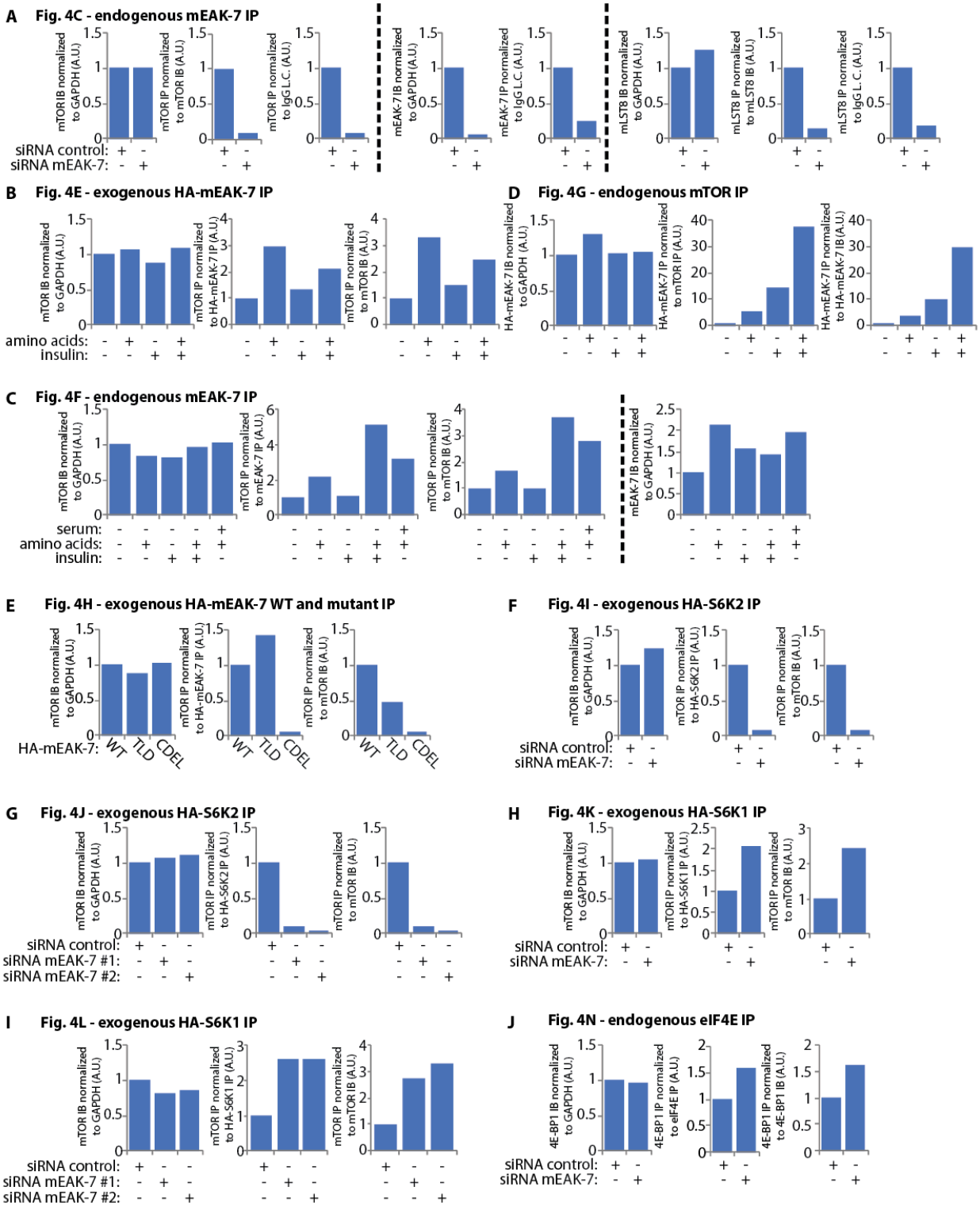
A
Fig. 4C - endogenous mEAK-7 IP
mTOR IB normalized to GAPDH (A.U.)
mTOR IP normalized to mTOR IB (A.U.)
mTOR IP normalized to IgG L.C. (A.U.)
mEAK-7 IB normalized to GAPDH (A.U.)
mEAK-7 IP normalized to IgG L.C. (A.U.)
mLST8 IB normalized to GAPDH (A.U.)
mLST8 IP normalized to mLST8 IB (A.U.)
mLST8 IP normalized to IgG L. C. (A.U.)
siRNA control:
siRNA mEAK-7:
B
Fig. 4E - exogenous HA-mEAK-7 IP
mTOR IB normalized to GAPDH (A.U.)
mTOR IP normalized to HA-mEAK-7 IP (A.U.)
mTOR IP normalized to mTOR IB (A.U.)
amino acids:
insulin:
D
Fig. 4G - endogenous mTOR IP
HA-mEAK-7 IB normalized to GAPDH (A.U.)
HA-mEAK-7 IP normalized to mTOR IP (A.U.)
HA-mEAK-7 IP normalized to HA-mEAK-7 IB (A.U.)
C
Fig. 4F - endogenous mEAK-7 IP
mTOR IB normalized to GAPDH (A.U.)
mTOR IP normalized to mEAK-7 IP (A.U.)
mTOR IP normalized to mTOR IB (A.U.)
mEAK-7 IB normalized to GAPDH (A.U.)
serum:
amino acids:
insulin:
E
Fig. 4H - exogenous HA-mEAK-7 WT and mutant IP
mTOR IB normalized to GAPDH (A.U.)
mTOR IP normalized to HA-mEAK-7 IP (A.U.)
mTOR IP normalized to mTOR IB (A.U.)
HA-mEAK-7:
WT
TLD
CDEL
F
Fig. 4I - exogenous HA-S6K2 IP
mTOR IB normalized to GAPDH (A.U.)
mTOR IP normalized to HA-S6K2 IP (A.U.)
mTOR IP normalized to mTOR IB (A.U.)
siRNA control:
siRNA mEAK-7:
G
Fig. 4J - exogenous HA-S6K2 IP
mTOR IB normalized to GAPDH (A.U.)
mTOR IP normalized to HA-S6K2 IP (A.U.)
mTOR IP normalized to mTOR IB (A.U.)
siRNA control:
siRNA mEAK-7 #1:
siRNA mEAK-7 #2:
H
Fig. 4K - exogenous HA-S6K1 IP
mTOR IB normalized to GAPDH (A.U.)
mTOR IP normalized to HA-S6K1 IP (A.U.)
mTOR IP normalized to mTOR IB (A.U.)
siRNA control:
siRNA mEAK-7:
I
Fig. 4L - exogenous HA-S6K1 IP
mTOR IB normalized to GAPDH (A.U.)
mTOR IP normalized to HA-S6K1 IP (A.U.)
mTOR IP normalized to mTOR IB (A.U.)
siRNA control:
siRNA mEAK-7 #1:
siRNA mEAK-7 #2:
J
Fig. 4N - endogenous eIF4E IP
4E-BP1 IB normalized to GAPDH (A.U.)
4E-BP1 IP normalized to eIF4E IP (A.U.)
4E-BP1 IP normalized to 4E-BP1 IB (A.U.)
siRNA control:
siRNA mEAK-7:

Figure 2.14. Densitometry analysis of Figure 4. Densitometry analysis of (**A**) Figure 2.4.C, (**B**) Figure 2.4.E, (**C**) Figure 2.4.F, (**D**) Figure 2.4.G, (**E**) Figure 2.4.H, (**F**) Figure 2.4.I, (**G**) Figure 2.4.J, (**H**) Figure 2.4.K, (**I**) Figure 2.4.L, and (**J**) Figure 2.4.N. A.U. represents arbitrary units. ImageStudioLite and Microsoft Excel software were utilized.

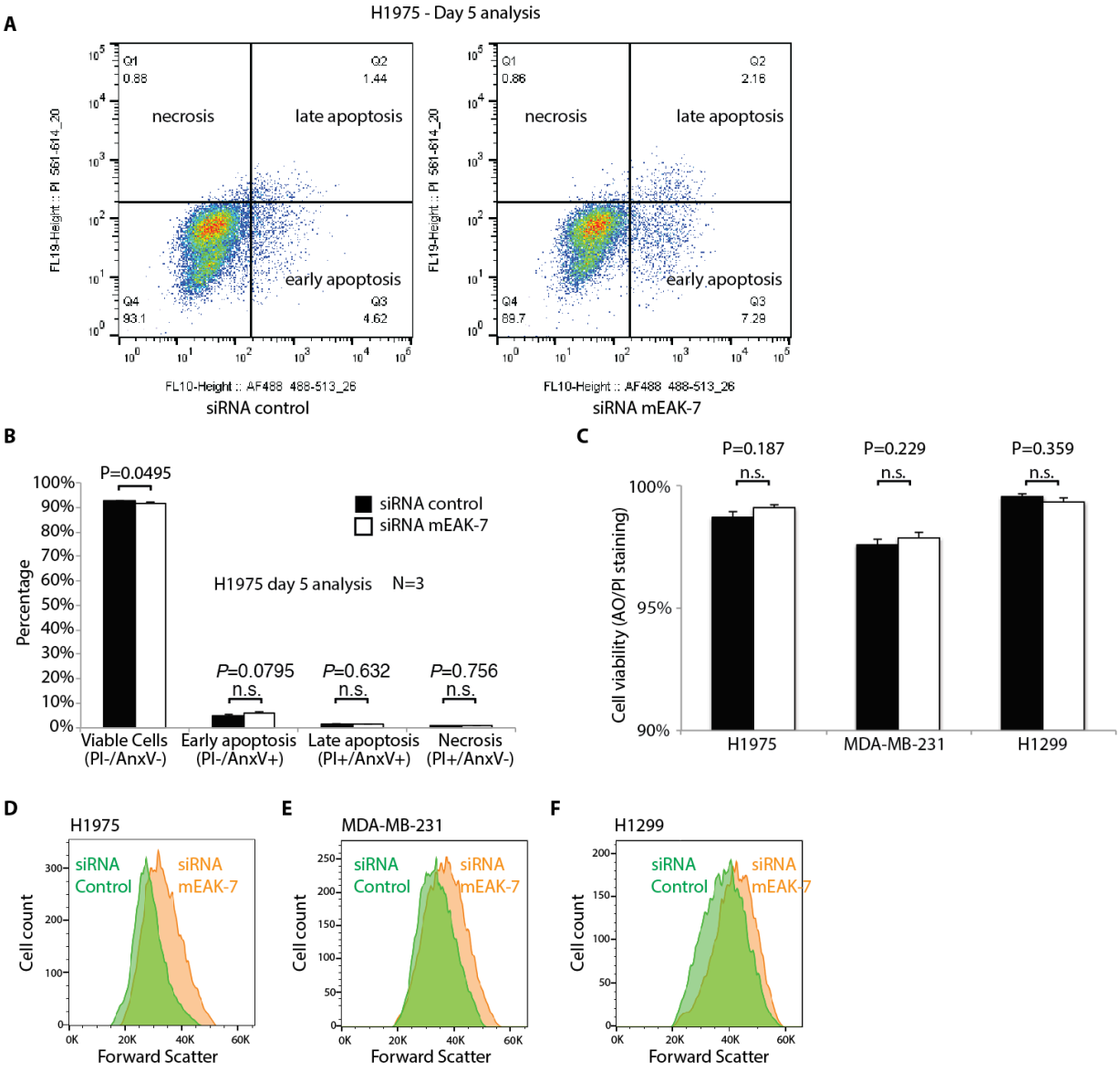

Figure 2.15. Knockdown of mEAK-7 does not result in enhanced cell apoptosis, but increases cell size. (**A**) 500,000 H1975 cells were seeded into 60 mm tissue culture plates (TCPs) and treated with 100 nM control or mEAK-7 siRNA for 48 hours. Subsequently, 500,000 siRNA treated cells were seeded into 100 mm TCPs and grown for 5 days. Next, 1,000,000 cells were processed for flow cytometric analysis and stained for PI and AnnexinV. (**B**) Percentages were mapped out according to PI-/AnxV-, PI-/AnxV+, PI+/AnxV+, and PI+/AnxV-. n=3 for H1975. (**C**) Cell viability assay of H1975, MDA-MB-231, and H1299 cells by AO/PI staining on the automated cell counter Logos Biosystems. Student's t-test was used for statistical analysis. (**D—F**) (D) H1975, (E) MDA-MB-231, and (F) H1299 cells were treated with control or mEAK-7 siRNA #1 for 48 hours in 10% serum-containing DMEM medium. Subsequently, 500,000 cells were transferred to 100 mm tissue culture plates and cell size was analyzed at day 3 via the Beckman-Coulter CyAn flow cytometer for forward scatter. Green = Control siRNA; Orange = mEAK-7 siRNA.

Table 2.1.Cloning primers.

HA Mutant name	**PCR primers**
HA-mEAK-7^{G2A}	PCR 1: NMYRF1 (Forward), Insert Reverse 1 (Reverse) NMYRF1: atatcaacaagtttgtacaaaaaagttggcatgGCAaacagcagaagccgtgtggggcgg Insert Reverse 1: ccggatcaagcgtatgcagccgccgcattgcatcagccatgatggatactttctcggcag PCR 2: Vector Forward 1 (Forward), NMYRF1 (Reverse) Vector Forward 1: ctgccgagaaagtatccatcatggctgatgcaatgcggcggctgcatacgcttgatccgg NMYRF1: ccgccccacacggcttctgctgttTGCcatgccaacttttttgtacaaacttgttgatat
HA-mEAK-7$^{\Delta NDEL1}$	PCR 3: NDEL1bF (Forward), Insert Reverse 1 (Reverse) NDEL1bF: tcaacaagtttgtacaaaaaagttggcatggtgctaagccacagacaggagctgagaggc Insert Reverse 1: ccggatcaagcgtatgcagccgccgcattgcatcagccatgatggatactttctcggcag PCR 4: Vector Forward 1 (Forward), NDEL1bR (Reverse) Vector Forward 1: ctgccgagaaagtatccatcatggctgatgcaatgcggcggctgcatacgcttgatccgg

	NDEL1bR: gcctctcagctcctgtctgtggcttagcaccatgccaacttttttgtacaaacttgttga
HA-mEAK-7$^{\Delta NDEL2}$	PCR 5: NDEL2F (Forward), Insert Reverse 1 (Reverse) NDEL2F: gaagtccaaaagtttacagaggatctggttctgctcttttcgtctgagctccatggacac Insert Reverse 1: ccggatcaagcgtatgcagccgccgcattgcatcagccatgatggatactttctcggcag PCR 6: Vector Forward 1 (Forward), NDEL2R (Reverse) Vector Forward 1: ctgccgagaaagtatccatcatggctgatgcaatgcggcggctgcatacgcttgatccgg NDEL2R: gtgtccatggagctcagacgaaaagagcagaaccagatcctctgtaaacttttggacttc
HA-mEAK-7$^{\Delta TLD}$	PCR 7: TLDF1 (Forward), Insert Reverse 1 (Reverse primer) TLDF1: ctgcctcgggagcagcggcaccgctggcgcgacccctcagaggagcagttggccaagggc Insert Reverse 1: ccggatcaagcgtatgcagccgccgcattgcatcagccatgatggatactttctcggcag PCR 8: Vector Forward 1 (Forward), NDEL2R (Reverse) Vector Forward 1: ctgccgagaaagtatccatcatggctgatgcaatgcggcggctgcatacgcttgatccgg TLDR2: gcccttggccaactgctcctctgaggggtcgcgccagcggtgccgctgctcccgaggcag

HA-mEAK-7$^{\Delta CDEL}$	PCR 9: CDEL1F: (Forward), Insert Reverse 1 (Reverse) CDEL1F: tttgataagatggaggtgtgggcggttggatgcccaactttcttgtacaaagtggttgat Insert Reverse 1: ccggatcaagcgtatgcagccgccgcattgcatcagccatgatggatactttctcggcag PCR 10: Vector Forward 1 (Forward), CDEL1R (Reverse) Vector Forward 1: ctgccgagaaagtatccatcatggctgatgcaatgcggcggctgcatacgcttgatccgg CDEL1R: atcaaccactttgtacaagaaagttgggcatccaaccgcccacacctccatcttatcaaa

Full Sequence of HA-mEAK-7^{WT} Plasmid Based off of NCBI Accession # BC060844.

Extended materials and methods for cloning:

Primers are 60 mers and have a melting temperature optimized for 72°C. All primers were purchased from Thermo Fisher Scientific. *PCR.* Q5® Hot Start High-Fidelity DNA Polymerase was used (NEB; cat# E0555L) in accordance to manufacturer specifications. *Gibson assembly reaction (GAR).* The PCR products were quantified to have the correct picomolar concentration and ratio necessary for an optimized GAR protocol. Please visit the New England Biolabs website to see their recommendation for concentration ratios. Optimized cloning efficiency is 50–100 ng of vectors (larger 6 kb PCR fragments) with 2–3 fold molar of excess inserts (smaller 4 kb PCR fragments). We incubated samples in a thermocycler at 50°C for 60 min and stored at -20°C to be

used for downstream bacterial transformation. *Bacterial transformation*. We utilized One Shot® MAX Efficiency® DH5α™-T1^{R} Competent Cells (TFS; cat # 12297-016), following their protocol for transformation. Thawing DH5α cells on ice, we placed 50 µL of bacteria, added 2 µL of diluted GAR product (diluted 1:4) in a 1.5 mL microfuge tube and placed the mixture on ice for 30 min. Next, we heat shocked the bacteria at 42°C for 30 seconds, placed the sample on ice for 2 min and added 950 µL Super Optimized Conditioned medium in a 37°C incubator, rotating at 250 rpm for 45 min. Next, we spread 50 µL of transformed bacteria onto LB plates with 50 µM kanamycin (FS: cat# 50-990-246); that was grown for 16 hours at 37°C. Afterwards, 5-7 clones were selected and grown in LB medium with 50 µM kanamycin grown overnight at 37°C and miniprepped (Qiagen) for DNA sequencing at the DNA Sequencing Core at the University of Michigan and lentiviral supernatant production. *Lentiviral production and stable transduction of cells.* We sent HA-mEAK-7 mutant constructs to the Vector Core at the University of Michigan to create 1X lentiviral supernatants to treat H1299 cells for stable expression. We infected 500,000 H1299 cells with 1X or 10X lentiviral supernatant for (HA-mEAK-7^{WT}, HA-mEAK-7$^{\Delta G2A}$, HA-mEAK-7$^{\Delta NDEL1}$, HA-mEAK-7$^{\Delta NDEL2}$, HA-mEAK-7$^{\Delta TLD}$, and HA-mEAK-7$^{\Delta CDEL}$) in a 60 mm TCP in 10% serum-containing DMEM medium. After 24 h, we split cells and placed all cells in a T-75 tissue culture flask with 1 µg/mL puromycin in 10% serum-containing DMEM medium. We replenished with puromycin containing medium every 24 hours. After two weeks, we confirmed mutants via immunoblot and confocal microscopy. HA-mEAK-7 plasmid is the KIAA1609 Lentiviral Vector (Human) (CMV) (pLenti-GIII-CMV-C-term-HA) and was created under the NCBI accession # BC060844 (abm; cat# LV198982).

References

1. H. Alam, T. W. Williams, K. J. Dumas, C. Guo, S. Yoshina, S. Mitani, P. J. Hu, EAK-7 controls development and life span by regulating nuclear DAF-16/FoxO activity. *Cell Metab* **12**, 30-41 (2010).
2. M. Shimobayashi, M. N. Hall, Making new contacts: the mTOR network in metabolism and signalling crosstalk. *Nat Rev Mol Cell Biol* **15**, 155-162 (2014).
3. R. A. Saxton, D. M. Sabatini, mTOR Signaling in Growth, Metabolism, and Disease. *Cell* **168**, 960-976 (2017).
4. J. Chung, C. J. Kuo, G. R. Crabtree, J. Blenis, Rapamycin-FKBP Specifically Blocks Growth-Dependent Activation of and Signaling by the 70 kd S6 Protein Kinases. *Cell* **69**, 1227-1236 (1992).
5. D. M. Sabatini, H. Erdjument-Bromage, M. Lui, P. Tempst, S. H. Snyder, RAFT1: a mammalian protein that binds to FKBP12 in a rapamycin-dependent fashion and is homologous to yeast TORs. *Cell* **78**, 35-43 (1992).
6. J. Huang, B. D. Manning, The TSC1-TSC2 complex: a molecular switchboard controlling cell growth. *Biochem J* **412**, 179-190 (2008).
7. Y. Sancak, T. R. Peterson, Y. D. Shaul, R. A. Lindquist, C. C. Thoreen, L. Bar-Peled, D. M. Sabatini, The Rag GTPases bind raptor and mediate amino acid signaling to mTORC1. *Science* **320**, 1496-1501 (2008).
8. Y. Sancak, L. Bar-Peled, R. Zoncu, A. L. Markhard, S. Nada, D. M. Sabatini, Ragulator-Rag complex targets mTORC1 to the lysosomal surface and is necessary for its activation by amino acids. *Cell* **141**, 290-303 (2010).

9. C. Betz, M. N. Hall, Where is mTOR and what is it doing there? *J Cell Biol* **203**, 563-574 (2013).

10. P. Riou, R. Saffroy, J. Comoy, M. Gross-Goupil, J.-P. Thiery, J.-F. Emile, D. Azoulay, D. Piatier-Tonneau, A. Lemoine, B. Debuire, Investigation in Liver Tissues and Cell Lines of the Transcription of 13 Genes Mapping to the 16q24 Region That Are Frequently Deleted in Hepatocellular Carcinoma. *Clinical Cancer Research* **8**, 3178-3186 (2002).

11. R. E. Ellsworth, L. A. Field, B. Love, J. L. Kane, J. A. Hooke, C. D. Shriver, Differential gene expression in primary breast tumors associated with lymph node metastasis. *Int J Breast Cancer* **2011**, 142763 (2011).

12. T. Nagase, R. Kikuno, M. Nakayama, M. Hirosawa, O. Ohara, Prediction of the Coding Sequences of Unidentified Human Genes. XVIII. The Complete Sequences of 100 New cDNA Clones from Brain Which Code for Large Proteins *in vitro*. *DNA Research* **7**, 273-281 (2000).

13. B. Schroder, C. Wrocklage, C. Pan, R. Jager, B. Kosters, H. Schafer, H. P. Elsasser, M. Mann, A. Hasilik, Integral and associated lysosomal membrane proteins. *Traffic* **8**, 1676-1686 (2007).

14. K. A. Gray, B. Yates, R. L. Seal, M. W. Wright, E. A. Bruford, Genenames.org: the HGNC resources in 2015. *Nucleic Acids Res* **43**, D1079-1085 (2015).

15. C. Notredame, D. G. Higgins, J. Heringa, T-Coffee: A novel method for fast and accurate multiple sequence alignment. *J Mol Biol* **302**, 205-217 (2000).

16. M. J. Finelli, L. Sanchez-Pulido, K. X. Liu, K. E. Davies, P. L. Oliver, The Evolutionarily Conserved Tre2/Bub2/Cdc16 (TBC), Lysin Motif (LysM), Domain

Catalytic (TLDc) Domain Is Neuroprotective against Oxidative Stress. *J Biol Chem* **291**, 2751-2763 (2016).

17. T. Doerks, R. R. Copley, J. Schultz, C. P. Ponting, P. Bork, Systematic identification of novel protein domain families associated with nuclear functions. *Genome Res* **12**, 47-56 (2002).
18. M. Blaise, H. M. Alsarraf, J. E. Wong, S. R. Midtgaard, F. Laroche, L. Schack, H. Spaink, J. Stougaard, S. Thirup, Crystal structure of the TLDc domain of oxidation resistance protein 2 from zebrafish. *Proteins* **80**, 1694-1698 (2012).
19. K. Moriya, K. Nagatoshi, Y. Noriyasu, T. Okamura, E. Takamitsu, T. Suzuki, T. Utsumi, Protein N-myristoylation plays a critical role in the endoplasmic reticulum morphological change induced by overexpression of protein Lunapark, an integral membrane protein of the endoplasmic reticulum. *PLoS One* **8**, e78235 (2013).
20. C. Settembre, A. Fraldi, D. L. Medina, A. Ballabio, Signals from the lysosome: a control centre for cellular clearance and energy metabolism. *Nat Rev Mol Cell Biol* **14**, 283-296 (2013).
21. P. P. Roux, D. Shahbazian, H. Vu, M. K. Holz, M. S. Cohen, J. Taunton, N. Sonenberg, J. Blenis, RAS/ERK signaling promotes site-specific ribosomal protein S6 phosphorylation via RSK and stimulates cap-dependent translation. *J Biol Chem* **282**, 14056-14064 (2007).
22. X. M. Ma, J. Blenis, Molecular mechanisms of mTOR-mediated translational control. *Nat Rev Mol Cell Biol* **10**, 307-318 (2009).

23. K. K. Lee-Fruman, C. J. Kuo, J. Lippincott, N. Terada, J. Blenis, Characterization of S6K2, a novel kinase homologous to S6K1. *Oncogene* **18**, 5108-5114 (1999).

24. M. Pende, S. H. Um, V. Mieulet, M. Sticker, V. L. Goss, J. Mestan, M. Mueller, S. Fumagalli, S. C. Kozma, G. Thomas, S6K1-/-/S6K2-/- Mice Exhibit Perinatal Lethality and Rapamycin-Sensitive 5'-Terminal Oligopyrimidine mRNA Translation and Reveal a Mitogen-Activated Protein Kinase-Dependent S6 Kinase Pathway. *Molecular and Cellular Biology* **24**, 3112-3124 (2004).

25. O. E. Pardo, M. J. Seckl, S6K2: The Neglected S6 Kinase Family Member. *Front Oncol* **3**, 191 (2013).

26. D.-H. Kim, D. D. Sarbassov, S. M. Al, J. E. King, R. R. Latek, H. Erdjument-Bromage, P. Tempst, D. M. Sabatini, mTOR interacts with raptor to form a nutrient-sensitive complex that signals to the cell growth machinery. *Cell* **110**, 163-175 (2002).

27. K. Kim, S. Pyo, S. H. Um, S6 kinase 2 deficiency enhances ketone body production and increases peroxisome proliferator-activated receptor alpha activity in the liver. *Hepatology* **55**, 1727-1737 (2012).

28. S. Sridharan, A. Basu, S6 kinase 2 promotes breast cancer cell survival via Akt. *Cancer Res* **71**, 2590-2599 (2011).

29. A. C. Hsieh, Y. Liu, M. P. Edlind, N. T. Ingolia, M. R. Janes, A. Sher, E. Y. Shi, C. R. Stumpf, C. Christensen, M. J. Bonham, S. Wang, P. Ren, M. Martin, K. Jessen, M. E. Feldman, J. S. Weissman, K. M. Shokat, C. Rommel, D. Ruggero, The translational landscape of mTOR signalling steers cancer initiation and metastasis. *Nature* **485**, 55-61 (2012).

30. E. Karlsson, I. Magic, J. Bostner, C. Dyrager, F. Lysholm, A. L. Hallbeck, O. Stal, P. Lundstrom, Revealing Different Roles of the mTOR-Targets S6K1 and S6K2 in Breast Cancer by Expression Profiling and Structural Analysis. *PLoS One* **10**, e0145013 (2015).

31. E. T. Goh, O. E. Pardo, N. Michael, A. Niewiarowski, N. Totty, D. Volkova, I. R. Tsaneva, M. J. Seckl, I. Gout, Involvement of heterogeneous ribonucleoprotein F in the regulation of cell proliferation via the mammalian target of rapamycin/S6 kinase 2 pathway. *J Biol Chem* **285**, 17065-17076 (2010).

32. R. J. Dowling, I. Topisirovic, T. Alain, M. Bidinosti, B. D. Fonseca, E. Petroulakis, X. Wang, O. Larsson, A. Selvaraj, Y. Liu, S. C. Kozma, G. Thomas, N. Sonenberg, mTORC1-mediated cell proliferation, but not cell growth, controlled by the 4E-BPs. *Science* **328**, 1172-1176 (2010).

33. D. C. Fingar, S. Salama, C. Tsou, E. Harlow, J. Blenis, Mammalian cell size is controlled by mTOR and its downstream targets S6K1 and 4EBP1/eIF4E. *Genes Dev* **16**, 1472-1487 (2002).

34. L. J. Smithson, D. H. Gutmann, Proteomic analysis reveals GIT1 as a novel mTOR complex component critical for mediating astrocyte survival. *Genes Dev.* **30**, 1383-1388 (2016).

35. D. A. Guertin, D. M. Stevens, C. C. Thoreen, A. A. Burds, N. Y. Kalaany, J. Moffat, M. Brown, K. J. Fitzgerald, D. M. Sabatini, Ablation in mice of the mTORC components raptor, rictor, or mLST8 reveals that mTORC2 is required for signaling to Akt-FOXO and PKCalpha, but not S6K1. *Dev Cell* **11**, 859-871 (2006).

36. S. H. Um, F. Frigerio, M. Watanabe, F. Picard, M. Joaquin, M. Sticker, S. Fumagalli, P. R. Allegrini, S. C. Kozma, J. Auwerx, G. Thomas, Absence of S6K1 protects against age- and diet-induced obesity while enhancing insulin sensitivity. *Nature* **431**, (2004).

37. M. Pende, S. C. Kozma, M. Jaquet, V. Oorschot, R. Burcelin, Y. K. Le Marchand-Brustel, Judith, B. Thorens, G. Thomas, Hypoinsulinaemia, glucose intolerance and diminished β-cell size in S6K1-deficient mice. *Nature* **408**, 994-997 (2000).

38. T. R. Castaneda, W. Abplanalp, S. H. Um, P. T. Pfluger, B. Schrott, K. Brown, E. Grant, L. Carnevalli, S. C. Benoit, D. A. Morgan, D. Gilham, D. Y. Hui, K. Rahmouni, G. Thomas, S. C. Kozma, D. J. Clegg, M. H. Tschop, Metabolic control by S6 kinases depends on dietary lipids. *PLoS One* **7**, e32631 (2012).

39. H. Shima, M. Pende, Y. Chen, S. Fumagalli, G. Thomas, S. C. Kozma, Disruption of the p70s6k:p85s6k gene reveals a small mouse phenotype and a new functional S6 kinase. *EMBO J* **17**, 6649-6659 (1998).

40. K. M. Taylor, J. Bajko, M. S. Cabrera, C. Kremer, B. Meyer-Puttlitz, A. M. Schulte, S. H. Cheng, R. K. Scheule, R. J. Moreland, S6 Kinase 2 Deficiency Improves Glucose Disposal in Mice Fed a High Fat Diet. *Journal of Diabetes & Metabolism* **05**, 1-7 (2014).

Chapter 3 – mEAK-7 forms an alternative mTOR complex with DNA-PK to promote radiation resistance in human cancer

Summary

Mammalian EAK-7, or MTOR associated protein, eak-7 homolog (mEAK-7), activates mTOR signaling in human cells. mEAK-7 forms an alternative mTOR complex to regulate S6K2 and 4E-BP1. However, the molecular roles of mEAK-7 in human cancer has not yet been identified. We demonstrate mEAK-7 and mTOR signaling were strongly elevated in lung tumor and metastatic lymph nodes of NSCLC patients compared to normal lung or lymph tissue. CD44+/CD90+ cancer stem cells showed more mEAK-7 and activated mTOR signaling. mEAK-7 was required for 2D clonogenic potential and 3D spheroid formation. mEAK-7 associated with DNA-PK and this interaction was increased in response to X-ray irradiation to regulate S6K2 signaling. DNA-PK inhibition reduced S6K2, mEAK-7, and mTOR binding with DNA-PK, resulting in loss of S6K2 activity and mTOR signaling. mEAK-7 is required for clonogenic potential, spheroid formation, and radiation resistance through an alternative mTOR signaling pathway involving DNA-PK and S6K2 in human cancer cells.

Introduction

In chapter 2, we describe the molecular determinants and mechanisms of mEAK-7 activity, but we did not demonstrate the extent to which it played a role in human

development or human disease. In chapter 3, we will begin to investigate the role for mEAK-7 in human disease. Aberrant mTOR signaling has been observed in many types of human cancer (*1*). Recently, mEAK-7 (Mammalian EAK-7 or MTOR associated protein, eak-7 homolog) was identified as a novel molecular activator of mTOR signaling in human cells (*12*). Interestingly, mEAK-7 exhibits a preferential expression pattern in human cancer cell lines (*12*). While EAK-7 regulates dauer formation and lifespan in *C. elegans* (*43*), it is unknown the extent to which EAK-7 functions similarly in nematodes and mammals in order to regulate TOR/mTOR function.

mEAK-7 uses the S6K2/4E-BP1 axis to regulate mTOR signaling (*12*). However, S6K2 signaling has not been adequately delineated from that of S6K1 signaling due to their assumed functional redundancies (*61*). Yet, in breast cancer cells, loss-of-function studies demonstrate that S6K1 and S6K2 have several different protein targets (*100*). Additionally, canonical models of mTOR complex 1 (mTORC1), the traditional S6K regulators, and mTORC2 may not exist similarly in all cell types. As examples of this phenomena, a novel mTOR complex that involves GIT1, which is distinct from mTORC1 and mTORC2 has been identified in astrocytes (*42*), and ETS Variant 7 is capable of binding to mTOR and sustaining mTOR signaling in the presence of rapamycin (*103*). These pivotal findings disrupt conventional ideas regarding the existence of only two mTOR complexes, and therefore suggest the possibility of unidentified mTOR complexes.

While it is largely believed that mTOR signaling is suppressed under genotoxic stress via AMPK regulation of TSC2 (*104*), studies have demonstrated aberrant activation of mTOR signaling in response to DNA damage. For example, mTORC1

signaling inhibits DNA damage response mechanisms *in vitro* and *in vivo* through RNF168 (*105*). S6K2 may also function in the DNA damage response, as S6K2 knockdown results in the strong reduction of mTOR signaling (*105*). Adding to the complexity of the role of mTOR signaling in DNA damage is the observation that CHK1 function requires mTORC1 signaling in response to DNA damage repair processes, suggesting that mTOR signaling supports DNA damage responses (*106*). Similarly, sustained radiation treatment to mice activates mTOR signaling and oxidative stress in the intestine (*107*) and normal tissues undergoing long-term radiation stress exhibited activated mTOR signaling in mini pigs (*85*). Thus, there is a rationale to treat patients with a combination of chemotherapeutics and rapamycin due to additive cytotoxic effects in breast carcinoma cell lines (*108*). These studies suggest that mTOR signaling and DNA damage repair processes may function synergistically in some biologic contexts. The proposed pathways include the downregulation of p53 via S6K-mediated activation of MDM2 (*109*), or 4E-BP1 phosphorylation in response to DNA damage (*110*). Thus, we posit a novel mechanism supporting sustained mTOR signaling after genotoxic stress, which may allow enhanced cell survival through radiation resistance.

Cancer stem cells (CSCs) are known to be radiation resistant and thrive under genotoxic stress, but the molecular mechanisms responsible for these observations remain unknown (*111, 112*). CSCs are a self-renewing population of cells within a tumor mass (*113*) and mTOR signaling has been implicated in regulating pancreatic CSC viability and self-renewal (*114*). This suggests that a population of cancer cells utilize mTOR signaling to contribute to the survival and pathogenicity of human cancers. Data from a medulloblastoma *in vivo* model of CSCs suggest that PI3K signaling is activated

in response to DNA damage, as indicated by S6 regulation, a crucial readout of mTOR signaling (*115*). This substantive evidence suggests that mTOR signaling plays an important role in CSC DNA damage response and self-renewal.

In light of reports that genotoxic stresses are capable of activating mTOR signaling, select CSCs were found to demonstrate radiation resistance, and because CSCs require mTOR signaling, we sought to determine the extent to which mEAK-7 contributes to radiation resistance and self-renewal in cancer cells through an alternative pathway involving mTOR.

Results

mEAK-7 protein levels are elevated in metastatic human NSCLC lymph nodes

Although mEAK-7 protein levels appear to be disproportionately high in human cancer cell lines (*12*), this limited observation does not exclude the possibility that mEAK-7 is present in healthy human tissues, since mTOR expression is found in many tissue types (*98*). To gain a better understanding of the expression pattern of mEAK-7 in healthy human tissues, we accessed the GTEx database and identified basal-level expression of *MEAK7* in many human tissues (Figure 3.1.A). The BioGPS database also confirmed that *MEAK7* is expressed in diverse tissue types (Figure 3.7.A) (*116-118*). Thus, future mEAK-7 analyses in healthy tissues are essential during mammalian development to understand its role in metabolism.

To identify *MEAK7* genomic alterations in human cancer patients, we accessed the cBioPortal database. Genetic modifications in *MEAK7* were found to be cancer type-

dependent and included deletions, copy number amplifications, and mutations (Figure 3.1.B and 3.1.C). For example, many prostate cancers exhibit *MEAK7* deletions, whereas breast cancers often sustain substantial *MEAK7* gene copy number amplification (Figure 3.1.B). Because of these different gene profiles, the search parameters were narrowed to include only gain-of-expression and copy number amplification. The percentage of patients who demonstrated either of these anomalies ranged between 5 and 50% (Figure 3.1.C) (*119, 120*), demonstrating that *MEAK7* genetic modifications are cancer-type specific and can be observed in several diverse human cancers.

The TCGA cBioPortal revealed high expression of *MEAK7* in NSCLC cell lines (*12*) and patients with NSCLC. The Oncomine database was accessed to analyze *MEAK7* expression patterns in lung carcinomas and were compared to healthy lung tissue. Through two different lung cancer studies, *MEAK7* was found to be highly expressed in many non-small cell lung carcinomas (NSCLC) and small cell lung carcinomas, compared to normal lung tissue, suggesting that *MEAK7* may play a role in lung tumorigenesis (Figure 3.1.D and 3.1.E) (*121*). Additionally, there was an association between *MEAK7* expression and cancer patient outcomes. Patients who had died from ductal breast carcinoma (P=2.72x10^{-6}, Fold Change: 2.136) and acute myeloid leukemia (P=7.99x10$^{-5,}$ Fold Change: 2.655) had enhanced *MEAK7* expression (Figure 3.7.B and 3.7.C) (24). Thus, the *MEAK7* expression profile in cancer patients may provide insight into predicting patient prognosis and survival.

In a screen of human squamous cell carcinomas, the UM-SCC-17A cell line (*122*), derived from the primary laryngeal cancer site of a 48-year-old female patient, did

not express detectable levels of mEAK-7 protein. Interestingly, the UM-SCC-17B cell line, derived from a metastatic site from the same patient, did express mEAK-7 (*12*). These findings suggest that increased expression of mEAK-7 may be associated with tumor metastasis. To test the hypothesis that elevated mEAK-7 protein levels are associated with metastasis, lymph nodes of cancer patients were compared to healthy lung tissues, healthy lymph tissues, or primary tumors of patients. A NSCLC tissue microarray containing thirty individual pathologist-graded, patient-matched sections of primary tumors, as well as their normal adjacent tissue, and metastatic lymph nodes were stained and analyzed. mEAK-7 and ($Ser^{240/244}$) p-S6 protein levels were significantly increased in the primary human tumor as opposed to normal adjacent tissue (Figure 3.2.A-3.2.C). Further, mEAK-7 and ($Ser^{240/244}$) p-S6 protein levels were significantly greater in the metastatic lymph nodes as compared to both primary tumor and normal adjacent tissue (Figure 3.2.A-3.2.C). In contrast, comparatively healthy adult lymph tissue did not yield substantial mEAK-7 or ($Ser^{240/244}$) p-S6 protein levels (Figure 3.8.A).

While Oncomine databases demonstrate that higher *MEAK7* expression is associated with poor patient prognoses (Figure 3.7.B and 3.7.C), direct evidence has not yet been procured. Therefore, to investigate the association of higher mEAK-7 protein levels with poor patient prognoses, a lung adenocarcinoma tissue microarray detailing patient survival data was stained with antibodies targeting endogenous mEAK-7 and ($Ser^{240/244}$) p-S6. A Kaplan-Meier Survival Curve analysis illustrated that mEAK-7 protein levels were strongly associated with poor patient prognosis, specifically in patients with relapse following surgical intervention (Figure 3.2.D).

Because mEAK-7 protein levels were highly expressed in metastasized lymph nodes, we tested the extent to which mEAK-7 is required for cell invasion *in vitro*. To test this, H1975 cells were treated with control or mEAK-7 siRNA for 48 hours and 50,000 cells were seeded into invasion chambers for 24 hours. Results showed a statistically significant reduction in cell invasion after 24 hours (Figure 3.2.E). Thus, mEAK-7 may be a clinically actionable biomarker for patients with metastatic NSCLC.

Cancer stem cells exhibit high protein levels of mEAK-7 and mTOR signaling

mEAK-7 is a strong, positive regulator of mTOR signaling (*12*) and several groups have demonstrated that mTOR signaling is essential for CSC self-renewal (*114*) and radiation resistance (*123*). Therefore, we hypothesized that mEAK-7 is differentially expressed in the CSC versus non-CSC populations. Because the majority of information on human mEAK-7 has been demonstrated in NSCLC cell lines H1975 and H1299, we sought to determine the expression profile of mEAK-7 and mTOR signaling in NSCLC CSCs. These cells are best identified as being CD44+ (*124*) and CD90+ (*125*); as a result, H1299 cells were subjected to fluorescence-activated cell sorting (FACS) for the aforementioned markers. CD44+/CD90+ cells, representing 1% of all cells sorted, were analyzed for mEAK-7 and mTOR signaling (Figure 3.3.A). Immunoblot analysis demonstrated that CD44+/CD90+ cells, when compared to CD44-/CD90-, yielded greater protein levels of mEAK-7 and S6K2, as well as mTOR signaling activation via p-S6 and p-4E-BP1 (Figure 3.3.B). The CD44+/CD90+ cell population expressed n-cadherin (Figure 3.3.B), which is known as an essential component of the epithelial-mesenchymal transition (EMT) state in CSCs (*126*). These results demonstrate that

there is a selective expression profile of mEAK-7 and S6K2 in human cancer, but more specifically in the self-renewing cancer cell population that display a CD44+/CD90+ phenotype.

mEAK-7 is necessary for clonogenic potential and spheroid formation in human cancer cells

To test the hypothesis that mEAK-7 impacts the survival of cells after X-ray irradiation damage, a 2D clonogenicity assay was used to assess the surviving fraction of cancer cells after radiation damage (*127, 128*). H1299 and H1975 cells were treated with control or mEAK-7 siRNA for 48 hours, then subjected to no treatment or X-irradiated with 2 gy or 6 gy, reseeded into new 60 mm tissue culture plates and allowed to grow for 10 days. Clonogenic potential was significantly decreased after mEAK-7 knockdown, and was further exacerbated after 2 gy and 6 gy X-ray irradiation in both H1299 and H1975 cells (Figure 3.3.C-3.3.H). Similar results were observed at higher cell seeding densities (Figure 3.8.B) demonstrating that mEAK-7 enhances the clonogenic potential of human cancer cells in response to DNA damage.

While 2D assays measuring clonogenic potential demonstrate the essential role of mEAK-7 in the DNA damage response, 3D assays better simulate *in vivo* conditions. The spheroid forming assay is a widely accepted experimental strategy to identify stem cell self-renewal in mammalian cell systems *in vitro* and *in vivo* (*129*). Specifically, CSCs are the principal cancer cell population responsible for spheroid formation (*130*). Thus, to test the effect of mEAK-7 on spheroid size and formation, H1975 cells were treated with control or mEAK-7 siRNA for 48 hours, subjected to no treatment or 2 gy

and 6 gy X-ray irradiation, and then seeded in ultra-low attachment dishes for 1 week. mEAK-7 knockdown resulted in a dramatic reduction of spheroid size with no treatment, 2 gy, and 6 gy treatment (Figure 3.4.A). Additionally, the gross number of spheroids formed was significantly reduced after mEAK-7 knockdown, and even further reduced following 2 gy or 6 gy X-ray irradiation treatment (Figure 3.4.B). Similar results were observed when H1975 cells were seeded at a lower density (Figure 3.9). These results collectively indicate that mEAK-7 plays a significant role in cancer cell spheroid formation.

mEAK-7 is necessary for chemo-resistance, radiation-resistance, and sustained DNA damage-mediated mTOR signaling in human cancer cells

While X-ray irradiation is a potent inducer of the DNA damage response pathway, we hypothesized that other forms of genotoxic stress may be capable of regulating mEAK-7. Cisplatin, a chemotherapeutic drug that which forms DNA adducts, is often used to treat patients with solid tumors. However, following initial tumor regression, a fraction of solid tumors become chemoresistant (*131*). mTOR signaling can be activated during cisplatin treatment of ovarian cancer cells over time, as measured by enhanced (Thr^{389}) p-S6K1 levels (*132*). Since mEAK-7 is required for mTOR signaling, we tested the hypothesis that mEAK-7 responds to cisplatin treatment as an essential modulator of mTOR signaling after genotoxic stress. To test the extent to which genotoxic stress modifies mEAK-7 activity, H1299 cells were treated with mEAK-7 siRNA for 48 hours. Next, these cells were treated with either DMSO or 10 μM cisplatin for 4 or 8 hours. Under these conditions, mEAK-7 protein levels were increased

in response DNA damage by cisplatin treatment and that mEAK-7 was required for regulation of (Ser^{65}) p-4E-BP1, an indicator of mTOR signaling (Figure 3.4.C). Therefore, cisplatin is capable of regulating mEAK-7-mediated mTOR signaling.

mEAK-7 knockdown impairs the DNA damage response and enhances noxa levels after X-ray irradiation

CSCs utilize many mechanisms to promote radioresistance in response to cancer therapies (*133*). To determine the role of X-ray irradiation on mEAK-7 and the DNA damage response, H1975 cells were treated with control or mEAK-7 siRNA, and X-irradiated with 20 gy for up to 2 hours. Subsequently, immunoblot analyses was performed. H1975 cells treated with mEAK-7 siRNA exhibited in a dramatic increase in noxa levels (Figure 3.4.D). Noxa is upregulated in response to DNA damage, which ultimately leads to cellular apoptosis (*134*) suggesting that mEAK-7 plays a role in the DNA damage response and cancer cell survival.

The comet assay is used to quantify intracellular DNA damage resulting from an insufficient DNA damage repair response in eukaryotic cells (*135*). H1299 and H1975 cells were independently embedded in an agarose gel and lysed, thereby releasing intracellular DNA. During gel electrophoresis, DNA fragments migrate towards the anode, resulting in a “comet” pattern with a trail of DNA fragments, such that a longer trail signifies more DNA damage (*136*). Due to the dramatic results from radiation treatment with mEAK-7 knockdown in the clonogenicity (Figure 3.3.C-3.3.H) and spheroid assays (Figure 3.4.A and 3.4.B), we hypothesized that mEAK-7 plays a crucial role in the DNA damage repair pathways. The visualization of DNA strand migration,

and subsequent quantification of that migration, allowed us to predict the relative levels of the DNA repair response. H1299 and H1975 cells were treated with control or mEAK-7 siRNA and subjected to no treatment, 2 gy, and 6 gy X-ray irradiation for 30 minutes. Comet pattern formations, quantified as tail DNA %, were enhanced in H1299 and H1975 cells treated with mEAK-7 siRNA and X-ray irradiation (Figure 3.4.E-H) suggesting mEAK-7 is necessary for the DNA repair response in these cancer cells.

mEAK-7 interacts with DNA-PK in response to X-ray irradiation damage

To determine the extent to which mEAK-7 regulates genotoxic activation of mTOR signaling, we sought to identify novel interacting partners of mEAK-7 by transducing H1299 cells with a lentivirus expressing pLenti-GIII-HA(c-term)mEAK-7. Through HA-mEAK-7 immunoprecipitation and mass spectrometry analysis, a list of proteins that potentially interact with exogenously expressed mEAK-7 was generated (Table S 3.1). DNA-dependent protein kinase catalytic subunit isoform 1 (DNA-PKcs) scored highest with 241 exclusive spectral counts and 36% protein coverage (Figure 3.5.A). Thus, we posited that mEAK-7 regulates mTOR signaling, in part, through the interaction with DNA-PK.

Protein lysates were harvested from H1299 cells stably transduced with HA-mEAK-7 and immunopreciptation experiments confirmed the IP-mass spectrometry results to demonstrate that exogenous mEAK-7 interacts with endogenous DNA-PK (w3.5.B). Under ultraviolet B irradiation, DNA-PK has been shown to interact with mTOR kinase and SIN1 to affect mTORC2 signaling in epithelial skin keratinocytes, but the molecular rationale for this interaction remains elusive (*137*). Furthermore, nuclear

DNA-PK transverses to the cytosol in response to DNA damage (*137*). This ability to travel to the cytoplasm and evidence that DNA-PK can activate metabolism-related genes, suggest a novel role for DNA-PK in metabolic signaling. Thus, knowing that DNA-PK is capable of interacting with mTOR after DNA damage and that mEAK-7 interacts with mTOR (*12*), we sought to determine if mEAK-7 forms a complex with DNA-PK. H1299 cells stably expressing HA-mEAK-7 were subjected to no treatment or X-irradiated with 10 gy for 30 and 60 minutes, and results revealed that mEAK-7 increasingly interacted with DNA-PK over time in response to DNA damage (Figure 3.5.C). These data suggest that mEAK-7 associates with DNA-PK in response to DNA damage.

Since mEAK-7 is required for the mTOR-S6K2 axis (*12*), potential interaction between DNA-PK and S6K2 was tested to determine if both mEAK-7 and DNA-PK are part of a complex that regulates mTOR signaling. H1299 cells were transiently transfected with pcDNA3-HA-S6K2-WT, then X-irradiated at 10 gy for 1 hour, and HA-S6K2 was immunoprecipitated. X-ray irradiation considerably increased the interaction between DNA-PK and HA-S6K2, but had little-to-no influence on mTOR and HA-S6K2 interaction (Figure 3.5.D). Thus, DNA-PK is capable of interacting with S6K2 to regulate its function in response to DNA damage. To determine if S6K2 is required for mTOR signaling under X-ray irradiation, H1975 cells were treated with controls or two unique S6K1, or S6K2 siRNAs. Under these conditions, ($Ser^{240/244}$) p-S6 levels were abrogated after S6K2 knockdown (Figure 3.10) suggesting that S6K2 is necessary for sustained S6 phosphorylation in response to DNA damage.

To determine if mTOR is required for mEAK-7-mediated DNA-PK function and interaction, mTOR was knocked down with two different mTOR siRNAs, which resulted in a dramatic reduction of DNA-PK interaction with endogenous mEAK-7 (Figure 3.5.E). This collective evidence links mEAK-7 to the major metabolic sensor, mTOR, and the crucial DNA-damage repair regulator, DNA-PK.

While we established the function of mEAK-7 in mTOR signaling under nutrient conditions (*12*), the role of mEAK-7 in mTOR signaling under genotoxic stresses is unknown. To test the hypothesis that mEAK-7 is required for mTOR activation after DNA damage, H1299 and H1975 cells were treated with control or mEAK-7 siRNA for 48 hours in DMEM with 10% FBS. Two different conditions were compared: 1 hour nutrient starvation with 30 minute nutrient replenishment was compared to X-ray irradiation at 10 gy for 30 minutes. Under these conditions, mEAK-7 was also capable of regulating X-ray irradiation induced activation of mTOR signaling in NSCLC (Figure 3.5.F). Next, we posited that mEAK-7 was required for S6K2 phosphorylation and activation after X-ray irradiation. H1975 cells were treated with control or mEAK-7 siRNA for 48 hours and treated with 10 gy X-ray irradiation for 1 hour. IP of endogenous S6K2 demonstrated that mEAK-7 knockdown resulted in a dramatic decrease in X-ray irradiation-mediated S6K2 phosphorylation (Figure 3.5.G).

Finally, to test the extent to which DNA-PK activity is required for S6K2 function, H1299 and H1975 cells were treated with either DMSO or NU7441, a highly specific chemical inhibitor of DNA-PK, at 5 μM for 2 hours under freshly stimulated 10% FBS medium. NU7441 is 1000x more specific for DNA-PK than PI3K and 200x more specific for DNA-PK than mTOR. DNA-PK inhibition resulted in a substantial decrease in

S6K2/mTOR/DNA-PK binding, S6K2 functional activity, and a reduced ability to phosphorylate ($Ser^{240/244}$) p-S6 (Figure 3.5.H). These results suggest that mEAK-7 physically links DNA-PK and S6K2 to mTOR signaling.

mEAK-7 is required for sustained IR-mediated mTOR signaling in human cancer cells and loss of mEAK-7 results in enhanced PARP cleavage

There are some examples that describe sustained mTOR signaling through DNA damage as a modulator of self-renewal and radiation resistance (*138*). To test the hypothesis that mEAK-7 is necessary for sustained X-ray irradiation-mediated mTOR signaling, H1299 and H1975 cells were treated with control or mEAK-7 siRNA for 48 hours in DMEM with 10% FBS, then X-irradiated at 10 gy for 30 minutes, 2 hours, and 8 hours. H1299 and H1975 cells treated with mEAK-7 siRNA exhibited abrogated mTOR signaling over time (Figure 3.6.A). These results were also confirmed in MDA-MB-231 cells, a triple-negative breast carcinoma cell line (Figure 3.11). Additionally, H1299 cells treated with mEAK-7 siRNA demonstrated enhanced cleavage of PARP (*139*), an important regulator of cell death (Figure 3.6.B). These results provide further evidence that mEAK-7 is required for radiation resistance, and that the loss of mEAK-7 results in severe reduction of mTOR signaling and enhanced PARP cleavage.

Both S6K1 and S6K2 are essential components of mTOR signaling that are described to have similar, but distinct cellular roles in human development and disease (*61*). To elucidate the roles of S6K1 and S6K2 under X-ray irradiation damage, ($Ser^{240/244}$) p-S6 levels were measured in response to siRNA-mediated knockdown of mEAK-7, S6K1, or S6K2 and subsequent X-ray irradiation at 10 gy. H1975 cells were

treated with control, mEAK-7, S6K1, or S6K2 siRNA for 48 hours in DMEM with 10% FBS, then X-irradiated at 10 gy for 30 minutes and 1 hour. mEAK-7 and S6K2 knockdown each markedly reduced ($Ser^{240/244}$) p-S6 levels, but S6K1 knockdown did not have a substantial effect on ($Ser^{240/244}$) p-S6 levels (Figure 3.6.C). These results mirrored the nutrient conditions, as previously published (*12*). Furthermore, mEAK-7 or S6K2 knockdown dramatically increased (Thr^{389}) p-S6K1 levels after X-ray irradiation-induced damage, suggesting a specific role for S6K2 and mEAK-7 during X-ray irradiation-mediated mTOR signaling (Figure 3.6.C).

While some reports suggest a possible intersection of DNA-PK and mTOR signaling, these ideas have not been fully validated. In an effort to test the hypothesis that DNA-PK and mTOR signaling depend on mEAK-7 to carry out a shared function, we treated H1299 and H1975 cells with NU7441. NU7441 treatment significantly reduced IR-mediated mTOR signaling in a dose-dependent manner, but had little effect on (Ser^{2448}) p-mTOR levels (Figure 3.12.A). To determine whether NU7441 significantly inhibits IR-induced activation of mTOR signaling compared to other mTOR inhibitors, we used specific inhibitors of DNA-PK (NU7441), mTOR (Rapamycin), and PI3K (LY249002). Inhibition of DNA-PK, mTOR, or PI3K significantly decreased mTOR signaling in H1975 cells (Figure 3.6.D). These results were also consistent in H1299 cells (Figure 3.12.B).

Discussion

Surgical intervention and radiation therapy are common treatment modalities for patients with solid tumors. However, many patients relapse as tumors acquire

resistance through intratumoral evolution (*140*). CD44+/CD90+ cells have been identified as a unique population of cancer cells that may be required for the regulation of chemo- and radio-resistance through PI3K and mTOR signaling (*141*). Furthermore, the literature demonstrates that S6K2 inhibits apoptosis in lung cancer (*142*), and that S6K2 amplification is associated with more aggressive forms of breast cancer (*143*). Similarly, a retrospective study conducted on breast cancer patients demonstrated that 4E-BP1 and S6K2 were correlated with poor prognosis and endocrine resistance (*144*). This evidence, combined with our findings that mTOR signaling, mEAK-7, and S6K2 are upregulated in CD44+/CD90+ cancer cell populations, suggests that mEAK-7 is involved in radiation resistance.

Although CD44+/CD90+ cells demonstrate radiation resistance and self-renewal capacity in association with mEAK-7 protein levels, loss of mEAK-7 alone does not result in enhanced cell apoptosis in human cancer cells (*12*). However, this is likely due to the fact that the mechanisms that support cell survival and self-renewal are different. PI3K and mTOR signaling are crucial regulators of radiation resistance and self-renewal in many epithelial-based cancers, including cervical cancer (*145*), head and neck squamous cell carcinoma (*146*), and breast carcinoma (*147*). Specifically, CSCs have been identified as a cell population that modulates radiation resistance and self-renewal in solid tumors (*148*).

Alternative mTOR signaling appears to be upregulated in human cancer patients, specifically in patients with metastatic disease (Figure 3.2.A-3.2.C). Here, DNA-PK was identified as a new interacting partner of mEAK-7 (Figure 3.5.A-3.5.H) and may participate in the regulation of this alternative mTOR signaling. DNA-PK is a member of

the phosphatidylinositol 3-kinase-related kinases (PIKKs) family that includes mechanistic target of rapamycin (mTOR), ataxia-telangiectasia mutated (ATM), ataxia- and Rad3- related (ATR), suppressor of morphogenesis in genitalia (SMG1), and transformation/transcription domain-associated protein (TRRAP) (*149*). DNA-PK has been extensively studied in the context of non-homologous end joining and homologous recombination, both of which are DNA damage repair pathways (*150*). PIKKs typically have redundant cellular roles, depending on their cellular localization and biologic context. For example, DNA-PK, ATM, and ATR all have similar cellular targets in response to DNA damage (*151*). Intriguingly, DNA-PK was found to play a critical role in metabolic gene regulation in response to insulin (*52*). However, DNA-PK predominantly resides in the nucleus, so it was initially unclear how DNA-PK could exit the nucleus to affect nutrient metabolism. The literature supports the observation that pockets of DNA-PK exists in lipid rafts outside of the nucleus, suggesting the existence of a novel role for DNA-PK in cytoplasmic cellular signaling (*152*). In support of these diverse findings, we demonstrate that DNA-PK interacts with mEAK-7 to regulate mTOR signaling, predominantly through S6K2.

In mini pigs, mTOR signaling is enhanced in salivary glands after 5 days of X-ray irradiation (*85*). In addition, PI3K and mTOR are essential regulators of radiation resistance in prostate cancer cells (*153*) as dual PI3K-mTOR inhibitors re-sensitize cancer cells to radiation treatment (*154*). Here, we demonstrate that mEAK-7 is required for the sustained activity of mTOR signaling under X-ray irradiation damage. Continued investigation of mEAK-7 and other molecular machinery that regulates IR damage-

mediated activation of mTOR signaling will allow for the creation of novel inhibitors promoting radiation re-sensitization.

As the role of mEAK-7 is further studied in the context of human disease, its unique role in nutrient-sensing mechanisms and the DNA damage response (Figure 3.6.E) will likely expand. S6K2 is a crucial component of mTOR signaling that has been widely overlooked (*61*). Many studies demonstrate that S6K2 is associated with a human diseases, including non-small cell lung cancer (*142*) and late stage breast cancer (*100*). We determined that there are high mEAK-7 protein levels in the tumors and lymph nodes of metastatic cancer patients, mEAK-7^{high} patients have poor prognoses, and that mEAK-7 is essential for self-renewal and radio-resistance. To determine the evolutionary benefit that cancer cells gain from upregulating mEAK-7, future research should be focused on elucidating the mechanisms allowing tumorigenesis in a broader range of cancers. Likewise, development of mEAK-7 inhibitors may benefit patients with metastatic cancers that demonstrate aberrant mTOR signaling associated with high levels of mEAK-7.

Limitations of the Study

Here, we report the novel binding partners of the mEAK-7-mTOR complex, namely DNA-PK. Some pitfalls of these studies are namely that we lack animal models that could recapitulate human disease. Since most of our work is to identify novel binding partners and the detailed mechanism by which they interact, future studies will be required to examine the role of mEAK-7 *in vivo.* Also, our inhibitor studies against DNA-PK, though several fold more specific to DNA-PK versus mTOR, could still yield

some off-target effects, suggesting genetic approaches are required to understand the role of DNA-PK binding to mTOR. Thus, the role of this alternative complex to canonical mTOR signaling requires further study in animal models where mTOR signaling is required for eukaryotic development and disease progression.

Methods and Materials

Cell lines

H1299 and H1975 are non-small cell lung carcinoma cell lines obtained from ATCC. MDA-MB-231 is a triple negative breast carcinoma cell line obtained from ATCC.

Cell culture

Cell culture: Cell lines were grown in Dulbecco's minimal essential medium (DMEM, Thermo Fisher Scientific (TFS): cat# 11995-073), without antibiotics/antimycotics and supplemented with a concentration of 10% fetal bovine serum (FBS, TFS: cat# 10437-036, Lot # 1399413) at 37°C in 5.0% CO_2 incubator. Cells were grown in Falcon™ Tissue Culture Treated Flasks T-75 (Fisher Scientific (FS): cat# 13-680-65) until 75% confluent and split with Trypsin-EDTA 0.25% (TFS: cat# 25200-056) for 5 min in the 37°C cell incubator. Cells were washed 1x with PBS and resuspended in 10% FBS containing DMEM. Cells were counted with the LUNA™ Automated Cell Counter (Logos Biosystems (LB): cat# L10001) utilizing LUNA™ Cell Counting Slides (LB: cat# L12003) and AO-PI dye (LB: cat# F23001).

Small interfering RNA or plasmid transfection

Cells were seeded at a density of 500,000 cells per 60 mm TCP and grown for 24 hours. For siRNA transfection, Lipofectamine® RNAiMAX Transfection Reagent (TFS: cat# 13778-150) was incubated with Opti-MEM® I Reduced Serum Medium (TFS: cat# 31985-070) and 100 nM siRNA was incorporated before introduction to cells at 100 nM concentration. For plasmid transfection, FuGENE® 6 Transfection Reagent (Promega: cat# E2691) was incubated with Opti-MEM I Reduced Serum Medium and 2 µg plasmids were incorporated before introduction into cells. For dual transfection, we added both solutions. siRNAs used were as follows: siRNA mEAK-7 #1 (TFS: ID# s33640). S6K1 #1 siRNA (TFS: ID# s12282). S6K1 #2 siRNA (TFS: ID# s12283). S6K2 #1 siRNA (TFS: ID # s12287). S6K2 #2 siRNA (TFS: ID # s12286). Control siRNA (TFS: cat# 4390843). Plasmids were purchased from Addgene. HA-S6K2 plasmid: pcDNA3-S6K2-WT was a gift from John Blenis (Addgene plasmid # 17729).

Immunofluorescence

Deparaffinization and rehydration steps were as follows: xylene for 10 minutes, 100% ethanol for 5 minutes , 95% ethanol for 5 minutes, 70% ethanol for 5 minutes, Milli Q water for 10 minutes, and 1x PBST for 10 minutes. Antigen retrieval steps were as follows: slides were placed in the slide holder to pressure cooker immersed in 10 mM citric acid (pH 6.0). Then, slides were placed in the microwave and cooked at full power for 12.5 minutes, finishing when pressure valve has been up for 1 min. Pressurized steam was exhausted from the pressure cooker. The pressure cooker and slides were cooled under running water for 15 minutes. Slides were washed with 1x PBS for 10

minutes. Slides were permeabilized for 10 minutes with 1x PBS with 0.4%Triton-X. Slides were blocked with 2.5% bovine serum albumin and 1% Tween20 in 1x TBS. Slides were incubated overnight at 4˚C with primary antibody. Next, slides were washed with PBS and incubated in secondary antibodies for 1 hour at room temperature. Slides were washed with PBS with DAPI for 10 minutes. Prolong Gold Antifade with DAPI was used to mount slides (Fisher cat# P36935). Nikon Ti Eclipse Confocal Microscope (60x with oil magnification) was used to capture images. Images were captured with or without 3x digital zoom, 1/32 frames per second, 1024x1024 image capture, 1.2 Airy Units, 2x line averaging, appropriate voltage and power settings optimized per antibody. No image modification was performed, except image sizing reduction for figure preparation. Quantitative analyses were completed via Nikon Analysis Software, with the data analysis and images representing the average of 3 fields of view and more than 50% of the tissue core. NSCLC tissue microarray used for protein level detection of mEAK-7 and p-S6 was purchased from US Biomax (cat# HLug-Squ090Lym-01). Healthy lymph tissue microarray used for protein level detection of mEAK-7 and p-S6 was purchased from US Biomax (cat# LN802A). NSCLC tissue microarray used for patient survival was purchased from US Biomax (cat# HLug-Squ150Sur-02). Primary antibodies for immunofluorescence were as follows: mEAK-7 (Santa Cruz Biotechnology (SCB) cat# sc-247321) and ($Ser^{240/244}$) p-S6 ribosomal protein (D68F8) XP® (Cell Signaling Technologies (CST): cat#5364S). All antibodies were used at 1:1,000 with a working volume of 1.5 mL in 5% BSA in PBS, unless noted otherwise. Secondary antibodies for immunofluorescence were as follows: Donkey anti-Goat IgG Alexa Fluor® 647 (TFS: cat# A-21447), Anti-rabbit IgG (H+L), and F(ab')2 Fragment

Alexa Fluor® 488 Conjugate (CST: cat# 4412S). All antibodies were used at a concentration of 1:1,000, with a working volume of 1.5 mL in 5% BSA in PBS. DAPI stain was used for DNA staining.

Immunoblot analysis

Cells were lysed in cold NP40 lysis buffer (50 mM Tris, 150 mM NaCl, and 1.0% NP-40 at pH 8.0). 50 µg of protein lysate was separated with Novex® Tris-Glycine SDS Running Buffer 10X (TFS: cat# LC2675-4) and Novex™ WedgeWell™ 4-20% Tris-Glycine Gels (TFS; cat# XP04205BOX), NuPAGE™ 3-8% Tris-Acetate Protein Gels (TFS; cat# EA03785BOX). Proteins were transferred to PVDF membranes. 4-20% gels were used for proteins 100 kDa and below, while 3-8% gels were used for proteins 100 kDa and above. Primary antibodies were incubated with membranes overnight at 4°C, and secondary antibodies were incubated with membranes at room temperature for 1 hour. Membranes were incubated with SuperSignal™ West Pico Chemiluminescent Substrate (TFS; cat# 34078) or Femto (TFS; cat# 34095) for film capture on HyBlot CL autoradiography film (Denville Scientific: cat# e3018). Primary antibodies were as follows: α-mEAK-7 (KIAA1609) mouse monoclonal antibody clone OTI12B1 (formerly 12B1) was obtained from Origene Technologies (OT; cat# TA501037, lot A01). All antibodies from Cell Signaling Technologies (CST) are rabbit: α-glyceraldehyde-3-phosphate dehydrogenase (CST: cat# 2118S), α-phospho-S6 ribosomal protein ($Ser^{240/244}$) (CST: cat# 2215S), α-phospho-S6 ribosomal protein ($Ser^{235/236}$) (CST: cat# 2211S), α-S6 ribosomal protein (CST: cat# 2217S), α-phospho-p70 S6 kinase (Thr^{389}) (CST: cat# 9234S), α-S6K1 (CST: cat# 2708S), α-S6K2 (CST: cat# 14130S), α-mTOR

(CST: cat# 2983S), α-HA-tag mouse (CST: cat# 2367S), α-HA-tag rabbit (CST: cat# 3724S), α-(Ser^{65}) p-4E-BP1 (CST: cat# 9451S), α-(Thr$^{37/46}$) p-4E-BP1 (CST: cat# 9459S), α-(Thr^{70}) p-4E-BP1 (CST: cat# 13396S), α-4E-BP1 (CST: cat# 9452S), α-N-cadherin (CST: cat# 13116S), α-noxa (CST: cat# 14766S), α-Cleaved PARP (CST: 5625S), α-(Thr^{68}) p-Chk2 (CST: cat# 2197S), α-Chk2 (CST: cat# 3440S), α-(Ser^{2448}) p-mTOR (CST: cat# 2971S). Concentration of antibodies: p-S6, S6, and 4E-BP1 used at 1:3,000 dilution and remainder at 1:1,000 dilution in 5% BSA in 1X TBST buffer with 0.04% sodium azide. Secondary antibodies for immunoblot analysis: 1:4,000 dilution for α-mouse IgG (Promega; cat# W4021). 1:7,500 dilution for α-rabbit (Promega; cat# W4011), and 1:2,000 dilution for α-rabbit light chain specific antibody (Abcam: cat# ab99697) only for S6K2 IP experiments.

Chemical Inhibitors

All chemical were resuspended in DMSO, according to manufacturer recommendations. Rapamycin (CST; cat# 9904S), LY293002 (CST; cat# 9901S), NU7441 (Tocris Biotechne; cat# 3712). All inhibitors were applied to cells for at least 2 hours, unless stated otherwise in the manuscript.

Immunoprecipitation (IP) analysis and mass spectrometry

After siRNA and/or plasmid transfection, cells were harvested in 1% NP40 lysis buffer or CHAPS lysis buffer (FIVEphoton Biochemicals (FB): cat# CIB-1) supplemented with protease inhibitors (FB: cat# PI-1) and phosphatase inhibitors (FB: cat# PIC1). For antibody-bead conjugation, 1 to 2 µg of antibodies and 50 µL of mixed Protein A/G

PLUS-Agarose (SCB; Cat # sc-2003) were incubated for 1 hour on vertical shaker at 4°C. Afterwards, the antibody-bead mix was washed 3 times with 1x PBS. Next, 250 µg of protein in CHAPS buffer were incubated with the antibody-bead mix for 1.5 hours on vertical shaker at 4°C. After incubation, the antibody-bead conjugates were washed 3 times with 1x PBS. Beads were washed 3 times with 1x PBS, and 3x loading buffer with SDS was added to the bead mix, boiled, spun down, and utilized for immunoblot analysis. Immunoprecipitation-mass spectrometry: Samples were processed by the University of Michigan Proteomics core for IP/MS analysis and protocols can be found on their webpage. Samples submitted to the core were pooled from 3x reactions of HA-mEAK-7 in H1299 cells, as described above. Full excel sheet supplied as Table S1. Antibodies used for immunoprecipitation reactions were as follows: Anti-HA epitope tag polyclonal goat IgG Antibody (Novus Biologicals: cat# NB600-362), polyclonal goat IgG antibody (SCB: cat# sc-2028), α-S6K2 (CST: cat# 14130S), α-mTOR (CST: cat# 2983S), mEAK-7 (SCB, cat# sc-247321).

Cell Invasion assay

After siRNA transfection and X-ray irradiation, cells were trypsinized and 50,000 cells were seeded onto Corning® Matrigel® Invasion Chamber 24-Well Plate 8.0 Micron (Corning: cat# 354480), with 1 mL of DMEM^{-AAs} without FBS within the top chamber, and 1 mL of 10% FBS-containing DMEM medium on the bottom of the plate. After 24 hours, we processed the samples with Hema 3™Stat Pack (Fisher: cat# 123-869), according to manufacturer specifications. Images were captured with a stereoscope, attached to a digital camera. Brightness and contrast were adjusted, as needed.

Analysis was conducted via student's t-test. % invasion was counted on 6 individual experiments per condition as: # cells adhered to the bottom chamber divided by # cells seeded total.

Comet Assay

Lysis Buffer, Alkaline Solution, and Eletrophoresis Running Solution were prepared according to manufacturer's instructions. Solutions were stored at 4°C. Oxiselect Comet Agarose (Cell Bio Labs (CBL): #235002) was heated to 95°C for 20 minutes, then placed in 37°C water bath until use. Cells were grown according to experimental procedures for siRNA treatment. Two days post siRNA treatment, cells were subjected to no treatment, 2 gy, and 6 gy X-ray irradiation. Cells were trypsinized and resuspended at a concentration of $1x10^5$ cells/mL in cold PBS. Then, 10 µL of cell suspension was mixed with 90 µL of comet agarose. After mixing thoroughly, 75 µL of this mixture was transferred to the OxiSelect Comet Slide (CBL: #STA-352). Slides were placed in the dark at 4°C for 15 minutes. Slides were transferred to a small basin containing pre-chilled Lysis buffer and placed at 4°C for 60 minutes in the dark. Lysis solution was aspirated from the basin, replaced with pre-chilled Alkaline solution, and placed at 4°C in the dark for 30 minutes. Then, Alkaline solution was aspirated and replaced with pre-chilled TBE Electrophoresis solution. After 5 minutes, TBE Electrophoresis solution was aspirated and replaced with new TBE Electrophoresis solution. Slides were transferred to a horizontal electrophoresis chamber and the well was filled with enough TBE Electrophoresis solution to fully cover the slides. Voltage was applied for 45 minutes at 20 volts. After electrophoresis, slides were transferred to

a small basin containing pre-chilled DI H2O, and the slides were fully immersed. After 2 minutes, the DI H2O was aspirated and replaced. This rinse was repeated twice. After the third rinse, slides were immersed in cold 70% ethanol for 5 minutes, then removed from the basin and allowed to air dry. Once the agarose was dried fully, 100 µL of diluted Vista Green DNA dye (CBL: cat# 235003, diluted 1:10,000 in TE buffer) was added to each well and allowed to incubate at room temperature for 15 minutes. Slides were imaged with Nikon Ti Eclipse Confocal Microscope at 10x magnification lens to capture images. Images were captured at 1/8 frames per second, 1024x1024 image capture, 1.2 Airy Units, 2x line averaging, appropriate voltage and power settings for FITC (488 nm). No image modification was performed, except image sizing reduction for figure preparation.

Cancer Stem Cell sorting

Cells were trypsinized and resuspended in DMEM medium with 10% FBS and counted on Luna cell counter (Logos Biosystems (LB): cat# L10001) using Acridine Orange/Propidium Iodide dye (LB: cat# F23001) for viability. $1x10^7$ cells were filtered into each of 5 labeled 50 mL falcon tubes, through a 40 µm filter. $1x10^7$ cells were filtered into each of 5 labeled 5 mL round bottom tubes (Falcon: cat# 352235) to be used as single-color controls. Tubes were centrifuged at 1,000 rpm for 4 minutes at 4°C and supernatant was discarded. One 5 mL single color control tube was resuspended with 200 µL PBS with 10% FBS to be used as a negative control. Three of the other single-color control tubes were resuspended with 200 µL PBS with 10% FBS, and single color dyes were added as detailed: 2 µL DAPI (Thermo Fisher: cat# D1306), 25 µL

CD90 (Biolegend: cat# 328107), and 10 µL CD44 (BD Biosciences: cat# 559942). The final single-color tube was used for Isotype control. This pellet was resuspended with 191 µL PBS with 10% FBS and 2 µL DAPI, 2 µL APC Isotype (BD Biosciences: cat# 340442), and 5 µL FITC Isotype (BD Bioscience: cat# 555909) were added. Cells in the 50 mL tubes were resuspended with 10 mL PBS with 10% FBS. The stain master mix was added to each tube to be sorted. Tubes were placed on a rack and incubated at 37°C for 30 minutes. Cells were rinsed with 1x PBS and resuspended 1x PBS containing 3% FBS. Place all tubes on ice until samples will be run on Flow Cytometer (Sony: Cat# SH800).

Clonogenicity Assay

Cells were grown according to experimental procedures for siRNA treatment. Two days post siRNA treatment, cells were subjected to no treatment, 2 gy, and 6 gy X-ray irradiation. 10,000 H1975 cells or 2,500 H1299 cells were plated into 60 mm dishes with 2 mL DMEM with 10% FBS. Cells were cultured in the incubator for 10 days (until control colonies contained >50 cells), and new media and new siRNA were added every 4 days. Cells were fixed with 2 mL of fixation mix (glacial acetic acid (Sigma-Aldrich 537020) and methanol (Sigma-Aldrich 67-56-1), at a 1:7 ratio) for 2-3 minutes at room temperature and incubated with 2 mL Crystal Violet (Sigma-Aldrich C6158-50G, diluted to 0.5% in Milli-Q water) for 2 hours at room temperature. After 2 hours, the Crystal Violet was removed and the dishes were rinsed with 2 mL of media (no FBS added), pipetting vigorously to dislodge cells. Dishes were rinsed carefully in DI water and

placed on paper towel to dry for 2-3 days. Once plates were dry, colonies were counted and recorded.

Spheroid Formation Assay

Cells were grown according to normal experimental procedures for siRNA treatment (n=6). Two days post siRNA treatment, cells were subjected to no treatment, 2 gy and 6 gy X-ray irradiation. 10,000 H1975 cells or 5,000 H1299 cells were plated into ultralow attachment plates (Costar: cat# 3471). 2 mL of Serum Free Medium (435 mL MEBM Medium (Lonza: cat# CC-3151), 10 mL B27 (Gibco: cat# 17504-044), 5 mL Pen/Strep (Gibco: cat# 15070), 5 mL Lipid Concentrate (Gibco: cat# 11905-031), 2.5 mL Insulin (Sigma-Aldrich: cat# I6634), 10 µg EGF (BD Biosciences: cat# 354052), 10 µg bFGF (BD Bioscience: cat# 354060), 500 µg Hydrocortisone (Sigma-Aldrich: cat# H4001), 500 µL 100 mM ß-mercaptoethanol (Sigma-Aldrich: cat# M3148), 2 mg Cholesterol (Sigma-Aldrich: cat# C4951)) were added to each well. Cells were grown for 2 weeks, adding 500 µL of Serum Free Medium every 4 days to ensure cells have adequate nutrients. After 2 weeks, the number of spheres growing in each well (spheres must have defined, circular edges and be made of at least 10 cells) was counted, and representative images of spheres from each treatment group were taken.

Statistical analysis and reproducibility

GTEx data acquisition, processing, and statistical analysis information can be found on “gtexportal.org”. cBioportal was accessed by searching for “*MEAK7*” or “*MEAK7*: gain amp”. Patient derived data from Oncomine were analyzed via unpaired

student's t-test. Patient derived tissue microarray data were analyzed via paired Mann-Whitney's U-test. 2D/3D clonogenicity assay, comet assay, cell proliferation, cell migration, and cell size were analyzed via paired student's t-test. Immunoblot and immunoprecipitation assays were repeated at least thrice in all cell lines.

Acknowledgements

We thank M. Wicha for expertise and use of equipment. We thank F. Haidar and H. Amatullah for replicating key experiments. The Genotype-Tissue Expression (GTEx) Project was supported by the Common Fund of the Office of the Director of the National Institutes of Health, and by NCI, NHGRI, NHLBI, NIDA, NIMH, and NINDS. The data used for the analyses described in this manuscript were obtained from: the GTEx Portal on 04/08/18 using term "*MEAK7*". Figure 3.6.E was "Created with BioRender". We thank our funding sources: National Institute of Dental and Craniofacial Research (1F30DE026048-01, R01-DE016530, and T32-DE007057) and Stuart & Barbara Padnos Research Award from the Comprehensive Cancer Center at the University of Michigan.

Figures

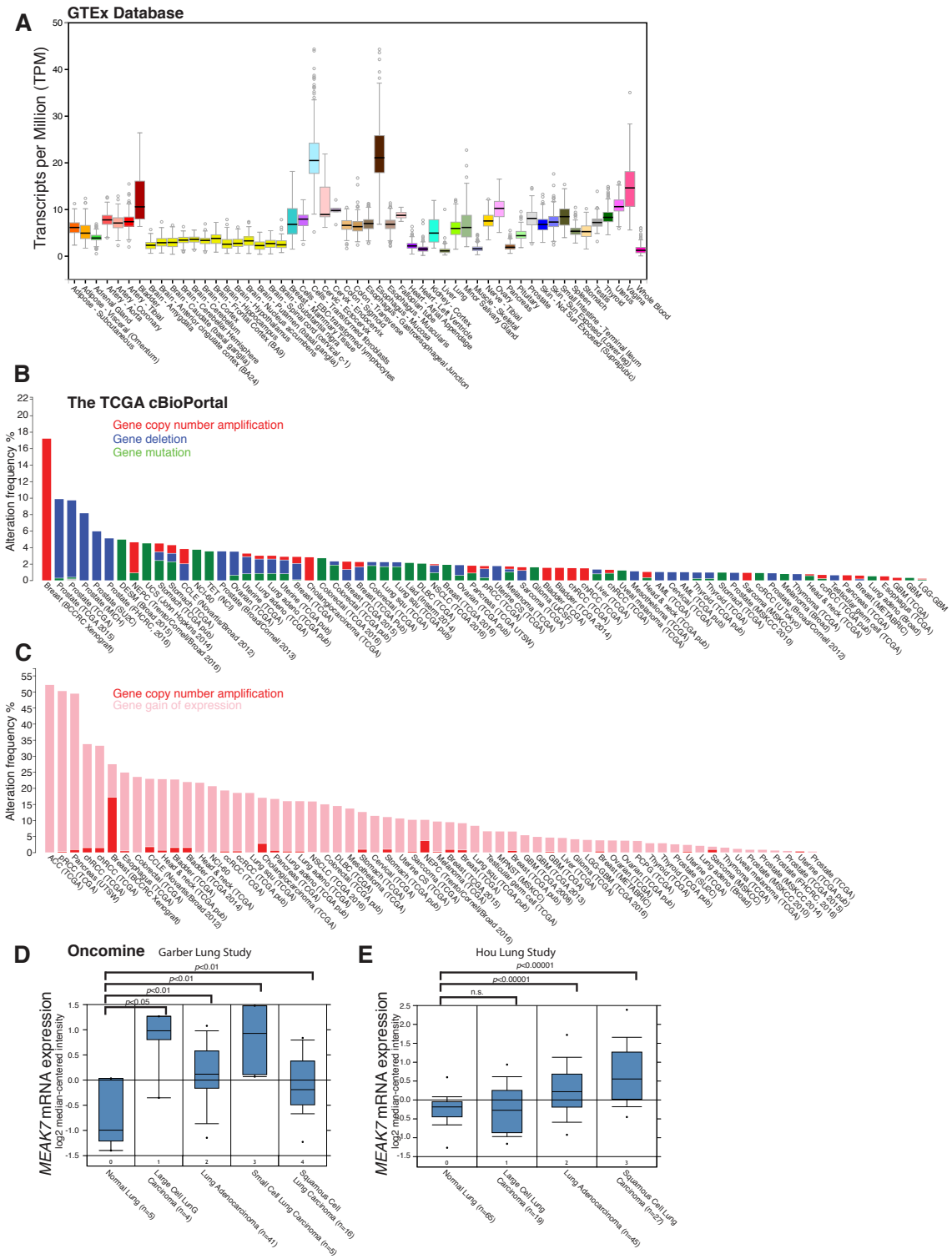
A
GTEx Database
Transcripts per Million (TPM)
B
The TCGA cBioPortal
Gene copy number amplification
Gene deletion
Gene mutation
Alteration frequency %
C
Gene copy number amplification
Gene gain of expression
Alteration frequency %
D
Oncomine
Garber Lung Study
MEAK7 mRNA expression
log2 median-centered intensity
Normal Lung (n=9)
Large Cell Lung Carcinoma (n=4)
Lung Adenocarcinoma (n=41)
Small Cell Lung Carcinoma (n=6)
Squamous Cell Lung Carcinoma (n=16)
E
Hou Lung Study
MEAK7 mRNA expression
log2 median-centered intensity
Normal Lung (n=65)
Large Cell Lung Carcinoma (n=19)
Lung Adenocarcinoma (n=45)
Squamous Cell Lung Carcinoma (n=27)

Figure 3.1. MEAK7 gene expression is detected in normal human cells and upregulated in select human cancer types. (**A**) Genotype-Tissue Expression (GTEx) database analysis of MEAK7 expression in normal human tissues. (**B**) The Cancer Genome Atlas cBioPortal analysis MEAK7 for all genomic alterations or (**C**) for only gain of mRNA expression or amplification of gene copy number. The results shown here are based upon data generated by TCGA Research Network: http://cancergenome.nih.gov/. (**D, E**) Oncomine analysis of MEAK7 gene expression of patients with normal lung and lung cancer via two different studies: (D) Garber Lung Study analysis by student's t-test 2-sample equal variance, (E) Hou Lung Study analysis by Mann Whitney U-test, $P<0.01$, 2 tailed.

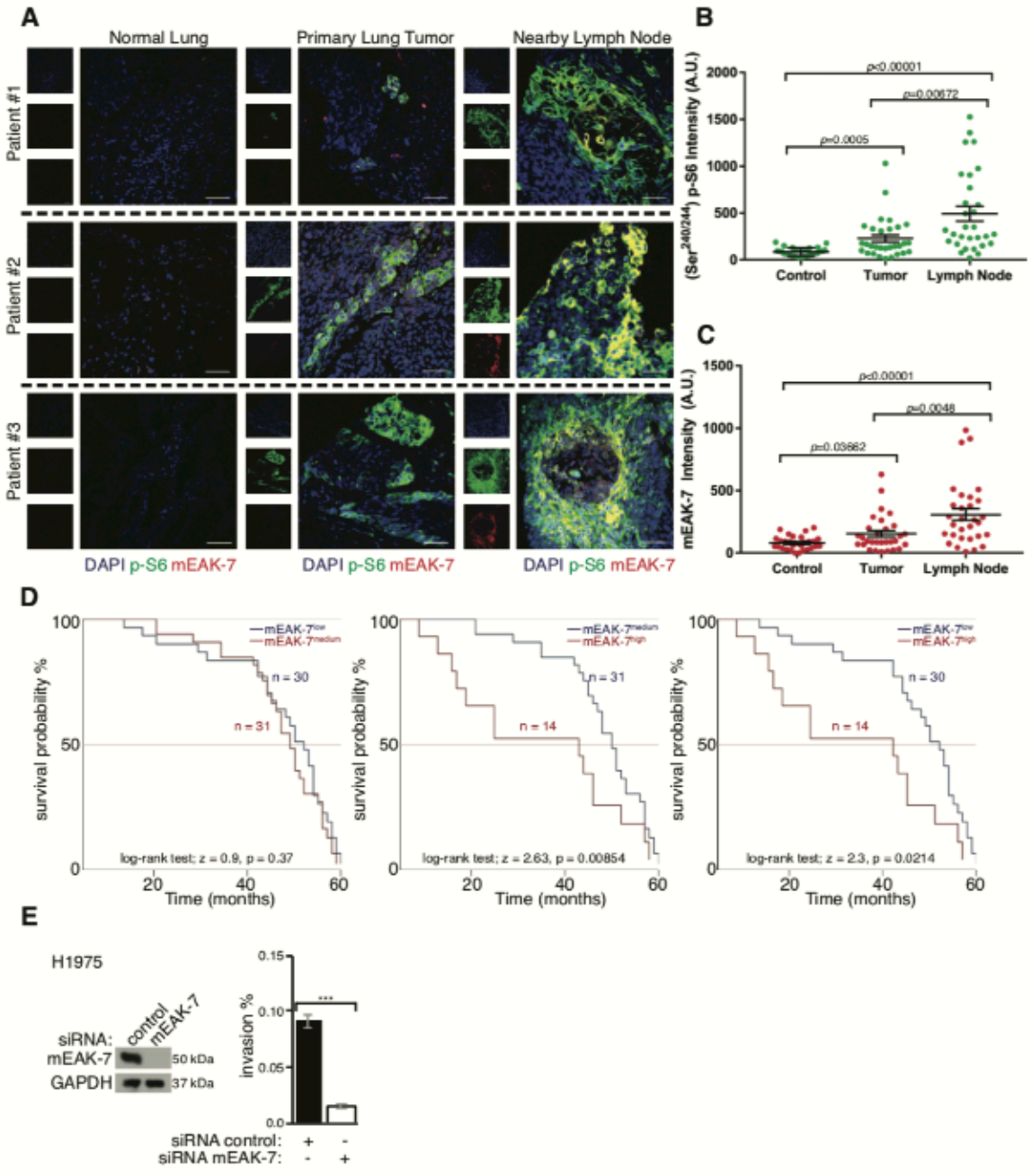
A
Normal Lung
Primary Lung Tumor
Nearby Lymph Node
Patient #1
Patient #2
Patient #3
DAPI p-S6 mEAK-7
DAPI p-S6 mEAK-7
DAPI p-S6 mEAK-7
B
p<0.00001
p=0.00672
p=0.0005
(Ser240/244) p-S6 Intensity (A.U.)
Control
Tumor
Lymph Node
C
p<0.00001
p=0.0048
p=0.03862
mEAK-7 Intensity (A.U.)
Control
Tumor
Lymph Node
D
survival probability %
n = 30
n = 31
log-rank test; z = 0.9, p = 0.37
Time (months)
survival probability %
n = 31
n = 14
log-rank test; z = 2.63, p = 0.00854
Time (months)
survival probability %
n = 30
n = 14
log-rank test; z = 2.3, p = 0.0214
Time (months)
E
H1975
siRNA:
control
mEAK-7
mEAK-7
50 kDa
GAPDH
37 kDa
invasion %
***
siRNA control:
siRNA mEAK-7:

Figure 3.2. mEAK-7 protein levels are highly detected in nearby lymph nodes of the tumor mass in NSCLC patients. (**A**) 3 representative human patient tissue sections stained for (Ser240/244) p-S6 and mEAK-7. White bar denotes 250 μm. (**B**) Statistical analysis of 30 paired NSCLC patients with the normal lung, primary tumor, and metastasized lymph node for (Ser240/244) p-S6 staining. Mann-Whitney U-test was utilized. (**C**) Statistical analysis of 30 paired NSCLC patients with the normal lung, primary tumor, and metastasized lymph node for mEAK-7 staining. Mann-Whitney U-test was utilized. (**D**) NSCLC tissue microarray analysis of Kaplan-Meier survival curve. Log rank test was utilized. (**E**) H1975 cells were treated with control or mEAK-7 siRNA for 48 hours. 50,000 cells were seeded into *in vitro* matrigel-based invasion chambers and allowed to grow for 24 hours. Analyzed by student's t-test (n=6). *P<0.01, **P<0.001, ***P<0.0001. Experiments were repeated at least 6 times.

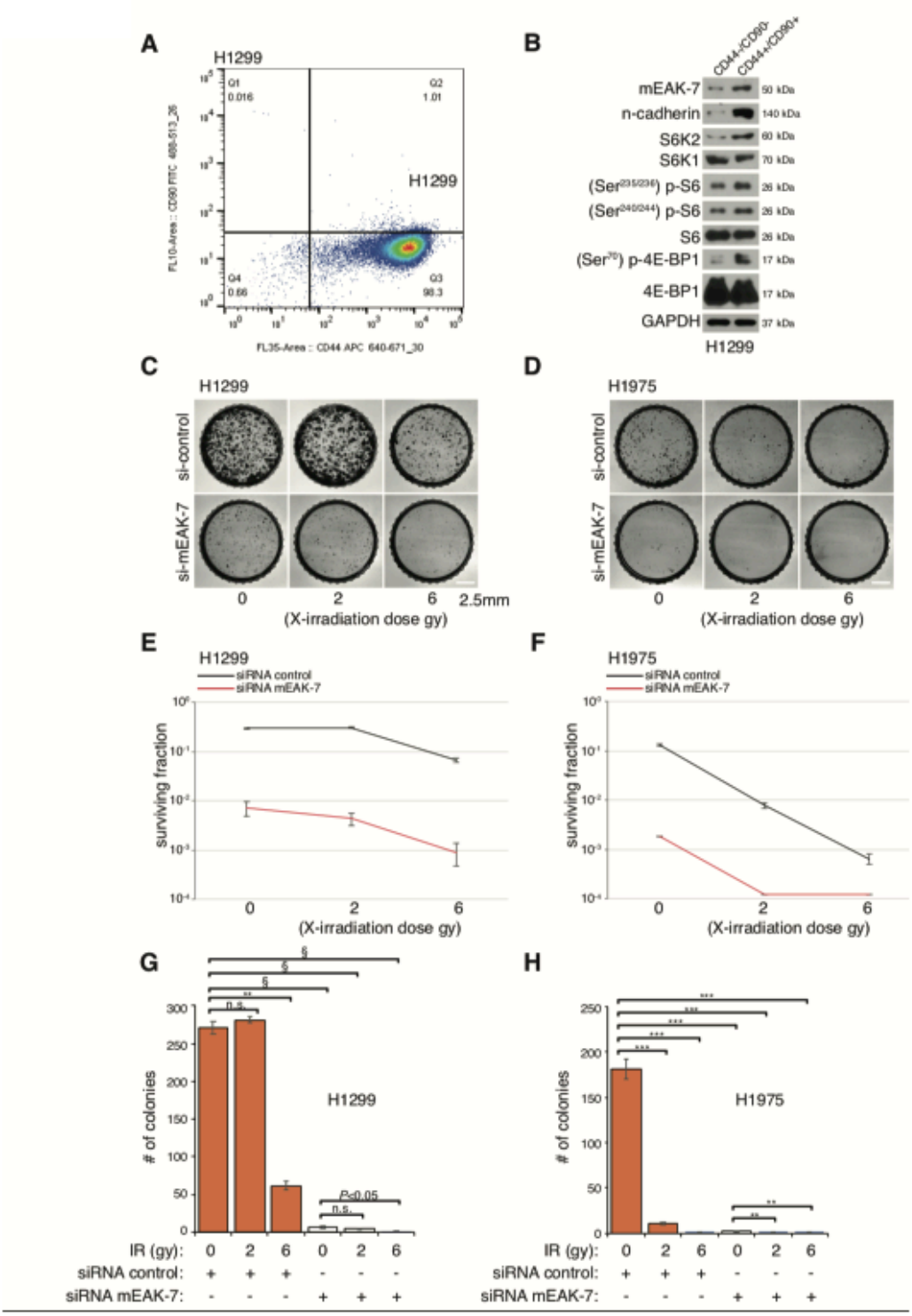
A
H1299
Q1
0.016
Q2
1.01
H1299
Q4
0.66
Q3
98.3
FL10-Area :: CD90 FITC 488-513_26
FL35-Area :: CD44 APC 640-671_30
B
CD44+/CD90-
CD44+/CD90+
mEAK-7
n-cadherin
S6K2
S6K1
(Ser235/236) p-S6
(Ser240/244) p-S6
S6
(Ser70) p-4E-BP1
4E-BP1
GAPDH
90 kDa
140 kDa
60 kDa
70 kDa
26 kDa
26 kDa
26 kDa
17 kDa
17 kDa
37 kDa
H1299
C
H1299
si-control
si-mEAK-7
0
2
6
2.5mm
(X-irradiation dose gy)
D
H1975
si-control
si-mEAK-7
0
2
6
(X-irradiation dose gy)
E
H1299
siRNA control
siRNA mEAK-7
surviving fraction
0
2
6
(X-irradiation dose gy)
F
H1975
siRNA control
siRNA mEAK-7
surviving fraction
0
2
6
(X-irradiation dose gy)
G
§
§
§
**
n.s.
# of colonies
H1299
P<0.05
n.s.
IR (gy): 0 2 6 0 2 6
siRNA control: + + + - - -
siRNA mEAK-7: - - - + + +
H
***
***
***
***
***
# of colonies
H1975
**
**
IR (gy): 0 2 6 0 2 6
siRNA control: + + + - - -
siRNA mEAK-7: - - - + + +

Figure 3.3. mEAK-7 is found in CD44+/CD90+ group and required for clonogenic potential and radiation resistance. (**A**) Flow sort diagram depicting the CD44+/CD90+ cell population in H1299 cells. (**B**) Immunoblot analysis of CD44-/CD90- and CD44+/CD90+ H1299 cells for mEAK-7 and mTOR signaling. (**C**) H1299 cells were treated with control or mEAK-7 siRNA for 48 hours, X-irradiated at 2 or 6 gy, and 2,500 cells were seeded into 60 mm TCPs and grown for 10 days. (**D**) H1975 cells were treated with control or mEAK-7 siRNA for 48 hours, subjected to no treatment, 2 gy, and 6 gy X-ray irradiation, and 5,000 cells were seeded into 60 mm TCPs and grown for 10 days. White bars denote 2.5 mm. (**E**) H1299 surviving fraction analysis for (C). (**F**) H1975 surviving fraction analysis for (D). (**G**) H1299 colony number graphs for (C). (**H**) H1975 colony number graphs for (D). Analysis of clonogenic analysis via student's t-test. *P<0.01, **P<0.001, ***P<0.0001, ‡P<0.00001, §P<0.000001. All experiments were repeated at least 3 times, and (C-H) was repeated 6 times.

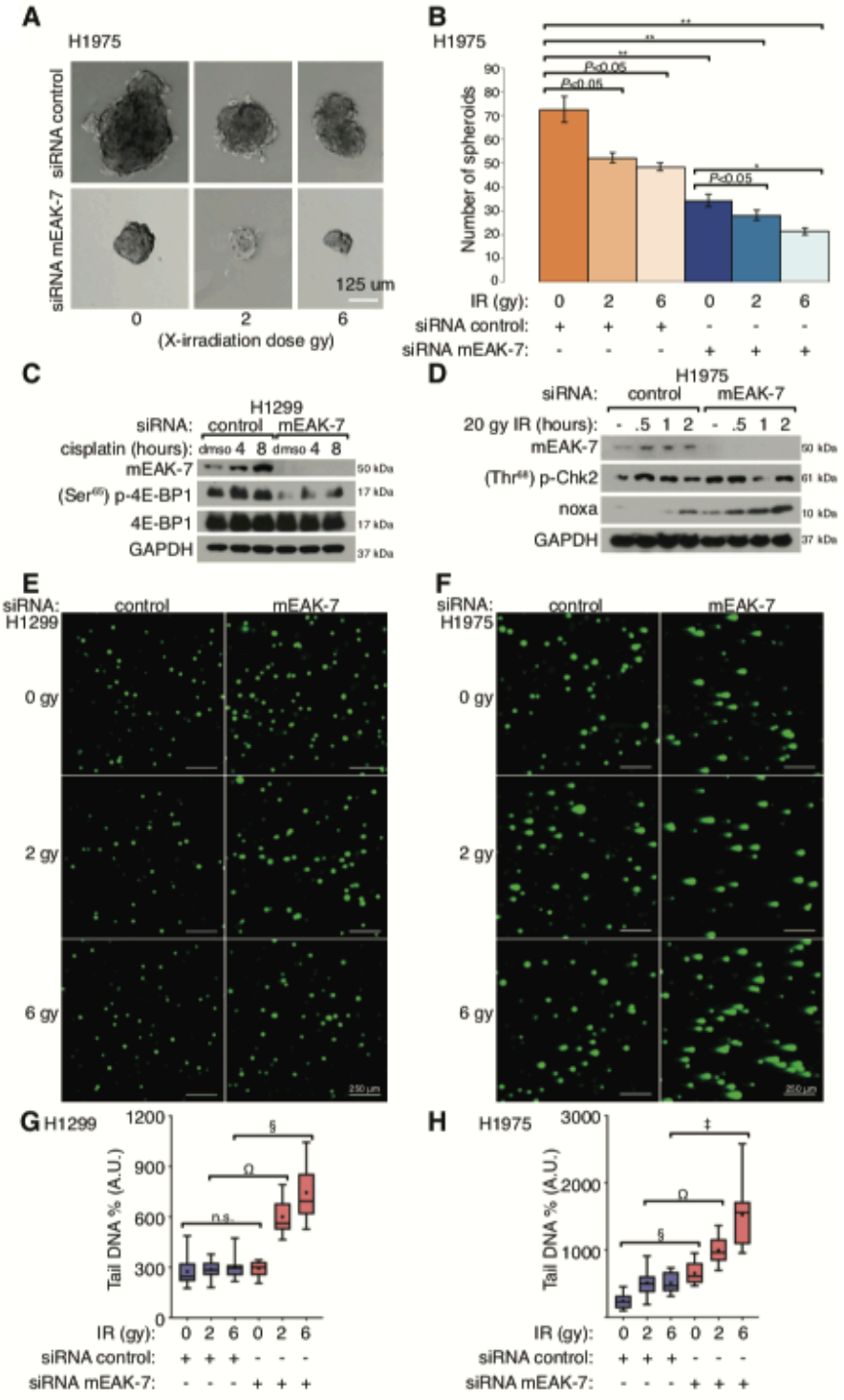
A
H1975
siRNA control
siRNA mEAK-7
125 um
0
2
6
(X-irradiation dose gy)
B
H1975
Number of spheroids
P<0.05
P<0.05
P<0.05
IR (gy): 0 2 6 0 2 6
siRNA control: + + + - - -
siRNA mEAK-7: - - - + + +
C
H1299
siRNA: control mEAK-7
cisplatin (hours): dmso 4 8 dmso 4 8
mEAK-7
(Ser65) p-4E-BP1
4E-BP1
GAPDH
50 kDa
17 kDa
17 kDa
37 kDa
D
H1975
siRNA: control mEAK-7
20 gy IR (hours): - .5 1 2 - .5 1 2
mEAK-7
(Thr68) p-Chk2
noxa
GAPDH
50 kDa
61 kDa
10 kDa
37 kDa
E
siRNA: control mEAK-7
H1299
0 gy
2 gy
6 gy
F
siRNA: control mEAK-7
H1975
0 gy
2 gy
6 gy
G H1299
Tail DNA % (A.U.)
n.s.
IR (gy): 0 2 6 0 2 6
siRNA control: + + + - - -
siRNA mEAK-7: - - - + + +
H H1975
Tail DNA % (A.U.)
IR (gy): 0 2 6 0 2 6
siRNA control: + + + - - -
siRNA mEAK-7: - - - + + +

Figure 3.4. mEAK-7 is required for spheroid formation and is necessary for an effective DNA damage response. (**A**) Images of spheroid. H1975 cells were treated with control or mEAK-7 siRNA, X-irradiated at 2 gy or 6 gy, and 10,000 cells were seeded into 60 mm ultra-low attachment plates and grown for 10 days. White bar denotes 125 μm. (**B**) Quantification of spheroid formation and analysis via student's t-test (n=6) of (a). *P<0.01, **P<0.001. (**C**) H1299 cells were treated with control or mEAK-7 siRNA, and treated with DMSO or 10 μM cisplatin for 4 or 8 hours and mTOR signaling was analyzed. (**D**) H1975 cells were treated with control or mEAK-7 siRNA and X-irradiated at 20 gy for 30 minutes, 1 hour, or 2 hours and analyzed for noxa expression by DNA damage response. (**E, F**) H1299 and H1975 cells were treated with control or mEAK-7 siRNA and X-irradiated at 2 or 6 gy for 30 minutes and assessed via the comet assay to detect damaged DNA. (**G, H**) Statistical analysis via student's t-test (n=15) of (e,f) represented as box plots. White bar denotes 250 μm. *P<0.01, **P<0.001, ***P<0.0001, ‡P<0.00001, §P<0.000001, ΩP<0.0000001. All experiments were repeated at least 3 times.

A

#	Identified human proteins	M.W. (kDa)	% coverage	Exclusive counts
1	DNA-dependent protein kinase catalytic subunit isoform 1	469	36.10	241
2	filamin-A isoform 1	280	51.90	164
3	60 kDa heat shock protein, mitochondrial	61	66.70	113
4	fatty acid synthase	273	30.00	101
5	filamin-C isoform a	291	32.00	83
6	glyceraldehyde-3-phosphate dehydrogenase	36	68.10	70
7	keratin 1	66	46.30	66
8	dynein, cytoplasmic, heavy chain 1, isoform CRA_b	525	15.80	59
9	general transcription factor II-I isoform 1	112	43.30	55
10	vimentin	54	57.30	40

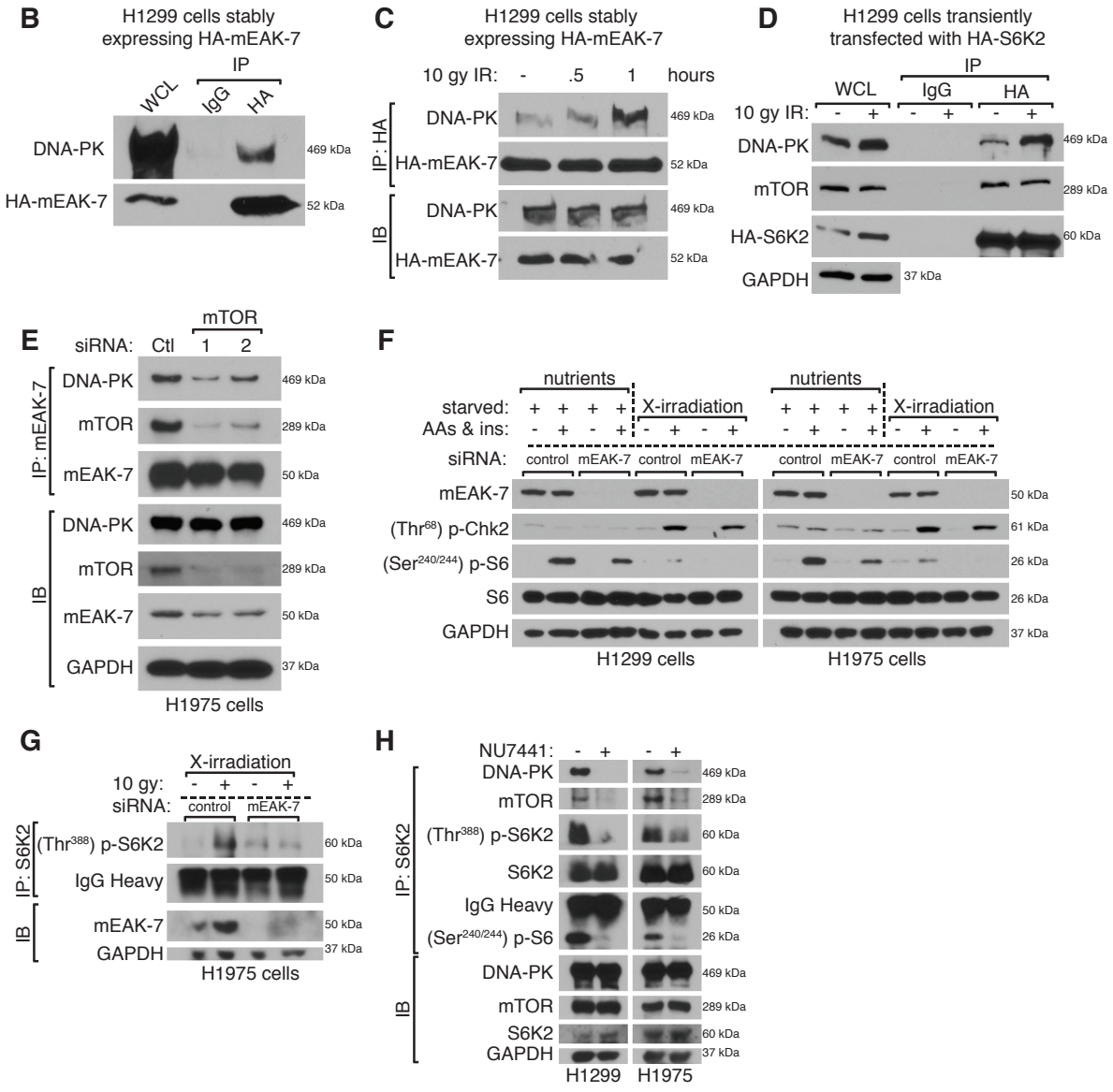

Figure 3.5. mEAK-7 interacts with DNA-PK in response to X-ray irradiation to activate S6K2. (**A**) H1299 cells stably expressing HA-mEAK-7 were lysed in CHAPS buffer and HA-mEAK-7 was immunoprecipitated and co-immunoprecipitated proteins were analyzed for mass spectrometry quantitative profiling. This figure only contains the top 10 proteins listed. (**B**) H1299 cells stably expressing HA-mEAK-7 were lysed in NP40 lysis buffer and HA-mEAK-7 was immunoprecipitated to check DNA-PK interaction. (**C**) H1299 cells stably expressing HA-mEAK-7 were X-irradiated at 10 gy for 30 minutes and 1 hour and lysed in NP40 lysis buffer. HA-mEAK-7 was immunoprecipitated to check DNA-PK interaction. (**D**) H1299 cells were transiently transfected with pcDNA3-HA-S6K2, then X-irradiated at 10 gy for 1 hour. HA-S6K2 was immunoprecipitated to check DNA-PK or mTOR interaction. (**E**) H1975 cells were transiently transfected with control or mTOR #1 or mTOR #2 siRNA for 48 hours. Cells were collected in CHAPS and endogenous mEAK-7 was immunoprecipitated to check DNA-PK interaction. (**F**) H1299 and H1975 cells were transiently transfected with control or mEAK-7 siRNA for 48 hours. Cells were subsequently starved of nutrients for 1 hour and replenished with DMEM+AAs and 10 μM insulin for 30 minutes or cultured normally and treated with 10 gy X-ray irradiation for 30 minutes. Immunoblot analysis was conducted on mTOR signaling. (**G**) H1975 cells were transiently transfected with control or mEAK-7 siRNA for 48 hours. Next, cells were treated with 10 gy X-ray irradiation, followed by IP of endogenous S6K2. (**H**) H1299 and H1975 cells were treated with either DMSO or NU7441 (DNA-PK inhibitor) at 5 μM for 2 hours. Cells were collected in CHAPS and S6K2 was immunoprecipitated and immunoblots were utilized to assess mTOR signaling. GAPDH was used for loading controls. All experiments were repeated at least 3 times.

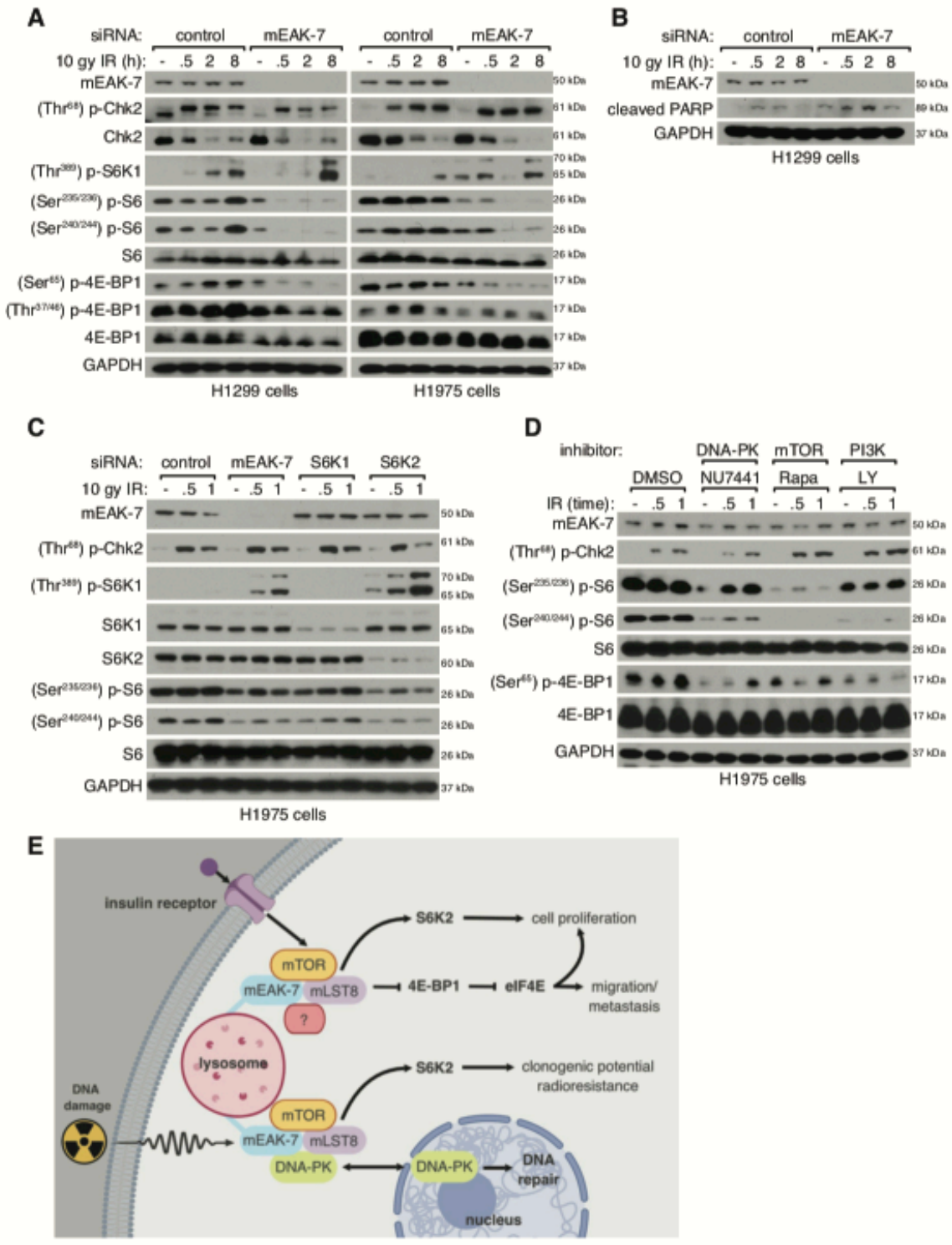
A
siRNA:
control
mEAK-7
control
mEAK-7
10 gy IR (h):
- .5 2 8 - .5 2 8 - .5 2 8 - .5 2 8
mEAK-7
(Thr68) p-Chk2
Chk2
(Thr389) p-S6K1
(Ser235/236) p-S6
(Ser240/244) p-S6
S6
(Ser65) p-4E-BP1
(Thr37/46) p-4E-BP1
4E-BP1
GAPDH
50 kDa
61 kDa
61 kDa
70 kDa
65 kDa
26 kDa
26 kDa
26 kDa
17 kDa
17 kDa
17 kDa
37 kDa
H1299 cells
H1975 cells
B
siRNA:
control
mEAK-7
10 gy IR (h):
- .5 2 8 - .5 2 8
mEAK-7
cleaved PARP
GAPDH
50 kDa
89 kDa
37 kDa
H1299 cells
C
siRNA:
control
mEAK-7
S6K1
S6K2
10 gy IR:
- .5 1 - .5 1 - .5 1 - .5 1
mEAK-7
(Thr68) p-Chk2
(Thr389) p-S6K1
S6K1
S6K2
(Ser235/236) p-S6
(Ser240/244) p-S6
S6
GAPDH
50 kDa
61 kDa
70 kDa
65 kDa
65 kDa
60 kDa
26 kDa
26 kDa
26 kDa
37 kDa
H1975 cells
D
inhibitor:
DMSO
DNA-PK
NU7441
mTOR
Rapa
PI3K
LY
IR (time):
- .5 1 - .5 1 - .5 1 - .5 1
mEAK-7
(Thr68) p-Chk2
(Ser235/236) p-S6
(Ser240/244) p-S6
S6
(Ser65) p-4E-BP1
4E-BP1
GAPDH
50 kDa
61 kDa
26 kDa
26 kDa
26 kDa
17 kDa
17 kDa
37 kDa
H1975 cells
E
insulin receptor
mTOR
mEAK-7
mLST8
?
S6K2
cell proliferation
4E-BP1
eIF4E
migration/
metastasis
lysosome
DNA
damage
S6K2
clonogenic potential
radioresistance
mTOR
mEAK-7
mLST8
DNA-PK
DNA-PK
DNA
repair
nucleus

Figure 3.6. mEAK-7 and DNA-PK are required for X-ray irradiation-mediated mTOR signaling. (**A**) H1299 and H1975 cells were treated with control or mEAK-7 siRNA for 48 hours, X-irradiated at 10 gy for 30 minutes, 2 hours, and 8 hours, and analyzed for mTOR signaling. (**B**) H1299 cells were subjected to the same protocol in (a) and analyzed for PARP cleavage. (**C**) H1975 cells were treated with control, mEAK-7, S6K1, and S6K2 siRNA for 48 hours and X-irradiated at 10 gy for 30 minutes and 1 hour, and analyzed for mTOR signaling. (**D**) H1975 cells were treated with DMSO, DNA-PK inhibitor (5 μM NU7441 IC50 = 14 nM), mTOR inhibitor (100 nM rapamycin, IC50 = 1 nM), and PI3K inhibitor (50 μM LY249002, IC50 = 2.3 μM) for 1 hour before treated with X-ray irradiation at 10 gy for 30 minutes and 1 hour, and analyzed for mTOR signaling. (**E**) Working model for a mEAK-7-mTOR-DNA-PK complex. All experiments were repeated at least 3 times. GAPDH was used for loading controls.

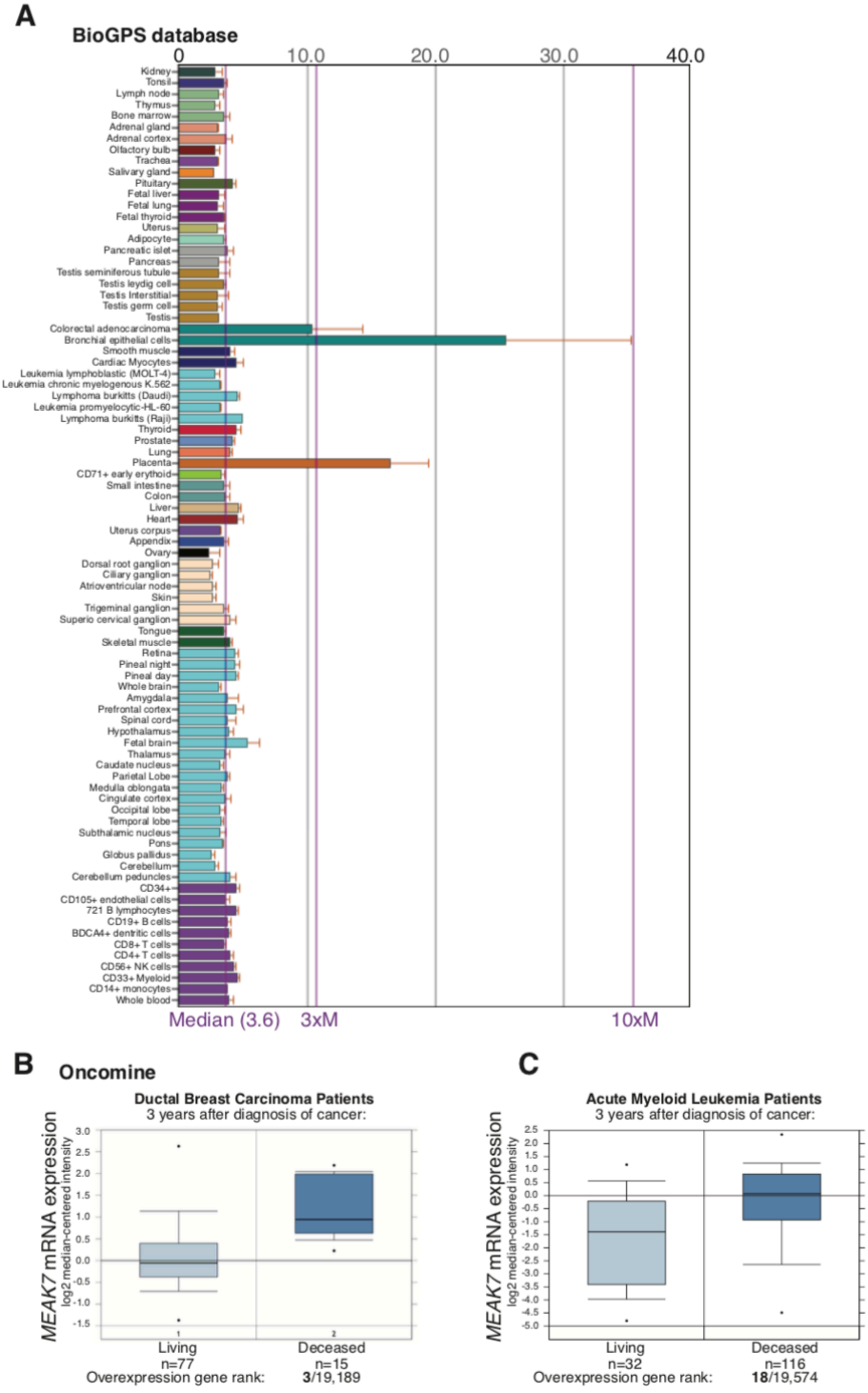
A
BioGPS database
0
10.0
20.0
30.0
40.0
Kidney
Tonsil
Lymph node
Thymus
Bone marrow
Adrenal gland
Adrenal cortex
Olfactory bulb
Trachea
Salivary gland
Pituitary
Fetal liver
Fetal lung
Fetal thyroid
Uterus
Adipocyte
Pancreatic islet
Pancreas
Testis seminiferous tubule
Testis leydig cell
Testis interstitial
Testis germ cell
Testis
Colorectal adenocarcinoma
Bronchial epithelial cells
Smooth muscle
Cardiac Myocytes
Leukemia lymphoblastic (MOLT-4)
Leukemia chronic myelogenous K.562
Lymphoma burkitts (Daudi)
Leukemia promyelocytic-HL-60
Lymphoma burkitts (Raji)
Thyroid
Prostate
Lung
Placenta
CD71+ early erythroid
Small intestine
Colon
Liver
Heart
Uterus corpus
Appendix
Ovary
Dorsal root ganglion
Ciliary ganglion
Atrioventricular node
Skin
Trigeminal ganglion
Superio cervical ganglion
Tongue
Skeletal muscle
Retina
Pineal night
Pineal day
Whole brain
Amygdala
Prefrontal cortex
Spinal cord
Hypothalamus
Fetal brain
Thalamus
Caudate nucleus
Parietal Lobe
Medulla oblongata
Cingulate cortex
Occipital lobe
Temporal lobe
Subthalamic nucleus
Pons
Globus pallidus
Cerebellum
Cerebellum peduncles
CD34+
CD105+ endothelial cells
721 B lymphocytes
CD19+ B cells
BDCA4+ dentritic cells
CD8+ T cells
CD4+ T cells
CD56+ NK cells
CD33+ Myeloid
CD14+ monocytes
Whole blood
Median (3.6)
3xM
10xM
B
Oncomine
Ductal Breast Carcinoma Patients
3 years after diagnosis of cancer:
MEAK7 mRNA expression
log2 median-centered intensity
3.0
2.5
2.0
1.5
1.0
0.5
0.0
-0.5
-1.0
-1.5
1
2
Living
n=77
Deceased
n=15
Overexpression gene rank:
3/19,189
C
Acute Myeloid Leukemia Patients
3 years after diagnosis of cancer:
MEAK7 mRNA expression
log2 median-centered intensity
2.5
2.0
1.5
1.0
0.5
0.0
-0.5
-1.0
-1.5
-2.0
-2.5
-3.0
-3.5
-4.0
-4.5
-5.0
Living
n=32
Deceased
n=116
Overexpression gene rank:
18/19,574

Figure 3.7. *MEAK7* is expressed at basal levels in many normal human tissues, but significantly overexpressed in human cancer patients with mortality. (**A**) BioGPS analysis of MEAK7 in human tissues and cells. (**B, C**) Oncomine analysis of MEAK7 gene expression of patients with (B) ductal breast carcinoma (P=2.72x10-6, Fold Change: 2.136) and (C) acute myeloid leukemia (P=7.99x10-6, Fold Change: 2.655).

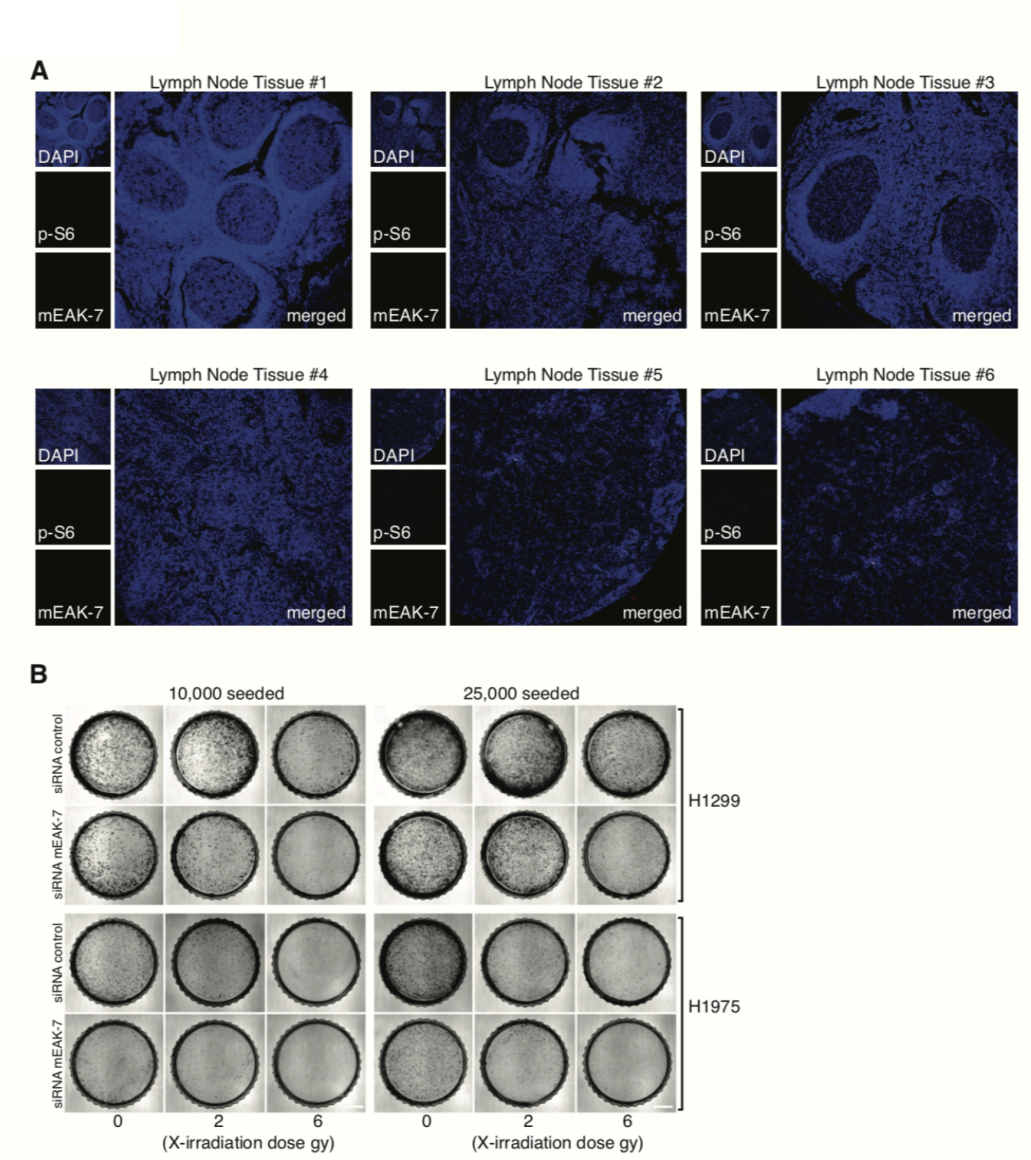

Figure 3.8. Normal lymph tissue analysis of mEAK-7 and p-S6 and clonogenicity assay in H1299 and H1975 cells at differing cell densities after X-ray irradiation. (**A**) 6 representative sections of US Biomax tissue microarray LN802a was analyzed using the antibodies against mEAK-7 and p-S6. (**B**) H1299 and H1975 cells were treated with control or mEAK-7 siRNA, X-irradiated at 2 or 6 gy, and 10,000 or 25,000 cells were seeded into 60 mm TCPs and grown for 10 days. White bars denote 2.5 mm. This experiment was repeated at least 6 times.

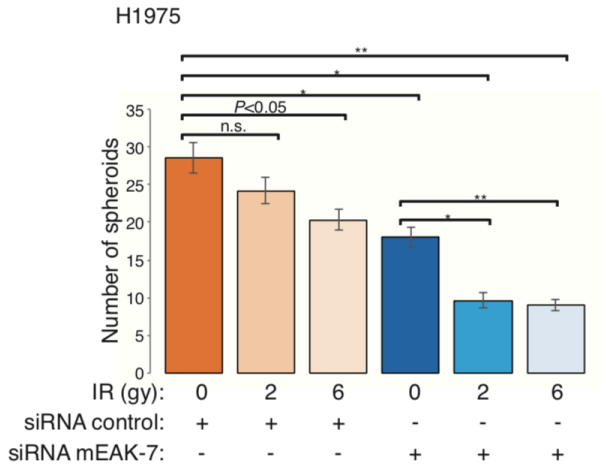

Figure 3.9. Spheroid assay at a lower cell density. H1975 cells were treated with control or mEAK-7 siRNA, X-irradiated at 2 or 6 gy, and 5,000 cells were seeded into 60 mm ultra-low attachment plates and grown for 10 days. *P<0.01, **P<0.001. This experiment was repeated at least 6 times.

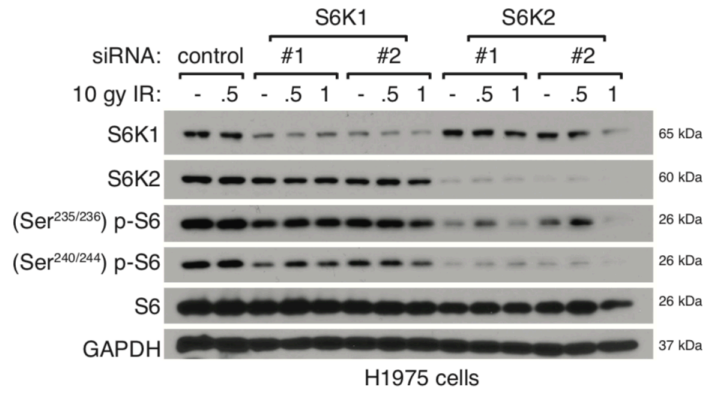

Figure 3.10. Analysis of S6K1 and S6K2 on IR-mediated mTOR signaling. H1975 cells were treated with control, 2 unique S6K1, or 2 unique S6K2 siRNAs, then treated with 10 gy IR for 30 minutes or 1 hour. Immunoblot analysis on mTOR signaling. This experiment was completed at least 3 times.

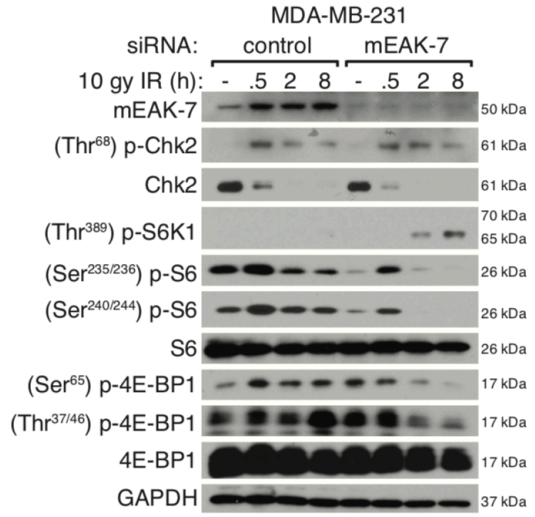

Figure 3.11. mEAK-7 is required for X-ray irradiation-mediated mTOR signaling in MDA-MB-231 cells. MDA-MB-231 cells were treated with control or mEAK-7 siRNA for 48 hours, X-irradiated at 10 gy for 30 minutes, 2 hours, and 8 hours and processed for mTOR signaling. This experiment was completed at least 3 times.

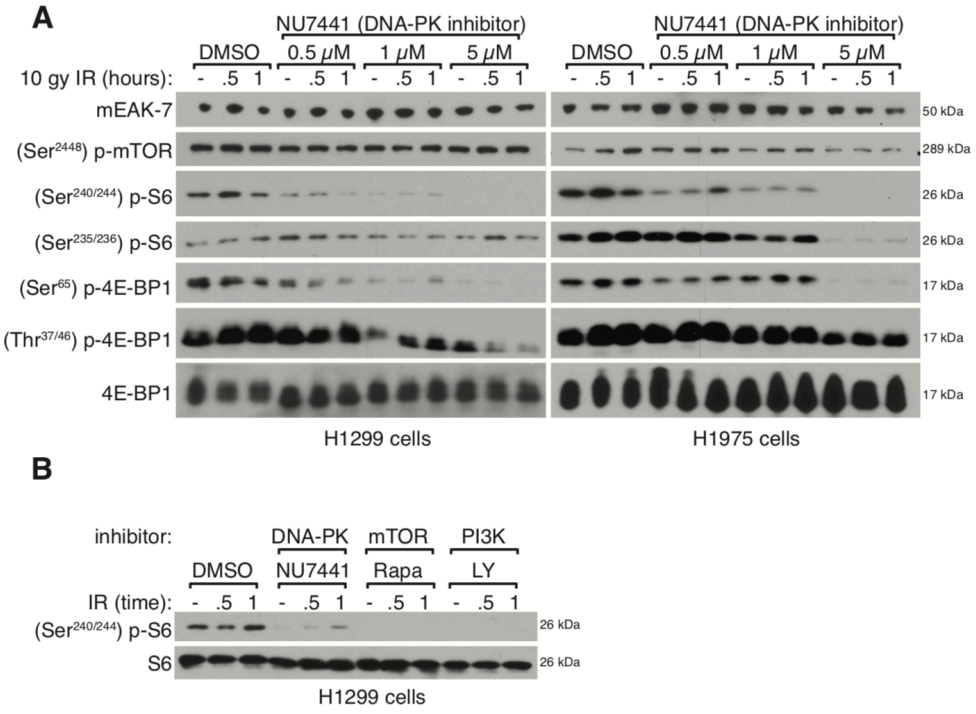

Figure 3.12. Dose-dependent analysis of NU7441 on IR-mediated mTOR signaling and inhibition of DNA-PK, mTOR, and PI3K significantly decreased IR-mediated mTOR signaling in H1299 cells. (**A**) H1299 and H1975 cells were treated with DMSO or 0.5 μM, 1 μM, 5 μM NU7441 for 2 hours before treated with X-ray irradiation at 10 gy for 30 minutes and 1 hour. Immunoblot analysis on mTOR signaling. All experiments were repeated at least 3 times. 4E-BP1 was utilized as a loading control. (**B**) H1299 cells were treated with inhibitors of DNA-PK (5 μM NU7441, IC50 = 14 nM), mTOR (100 nM rapamycin, IC50 = 1 nM), and PI3K (50 μM LY249002, IC50 = 2.3 μM) for 1 hour before treated with X-ray irradiation at 10 gy for 30 minutes and 1 hour. Immunoblot analysis on mTOR signaling. We observed that inhibition of DNA-PK, mTOR, or PI3K significantly decreased IR-mediated mTOR signaling. All experiments were repeated at least 3 times. S6 was utilized as a loading control.

References

1. R. A. Saxton, D. M. Sabatini, mTOR Signaling in Growth, Metabolism, and Disease. *Cell* **168**, 960-976 (2017).
2. J. T. Nguyen *et al.*, Mammalian EAK-7 activates alternative mTOR signaling to regulate cell proliferation and migration. *Science Advances* **4**, 1-15 (2018).
3. H. Alam *et al.*, EAK-7 controls development and life span by regulating nuclear DAF-16/FoxO activity. *Cell Metab* **12**, 30-41 (2010).
4. O. E. Pardo, M. J. Seckl, S6K2: The Neglected S6 Kinase Family Member. *Front Oncol* **3**, 191 (2013).
5. E. Karlsson *et al.*, Revealing Different Roles of the mTOR-Targets S6K1 and S6K2 in Breast Cancer by Expression Profiling and Structural Analysis. *PLoS One* **10**, e0145013 (2015).
6. L. J. Smithson, D. H. Gutmann, Proteomic analysis reveals GIT1 as a novel mTOR complex component critical for mediating astrocyte survival. *Genes Dev.* **30**, 1383-1388 (2016).
7. F. C. Harwood *et al.*, ETV7 is an essential component of a rapamycin-insensitive mTOR complex in cancer. *Science Advances* **4**, 1-18 (2018).
8. Z. Feng *et al.*, The regulation of AMPK beta1, TSC2, and PTEN expression by p53: stress, cell and tissue specificity, and the role of these gene products in modulating the IGF-1-AKT-mTOR pathways. *Cancer Res* **67**, 3043-3053 (2007).
9. X. Xie *et al.*, The mTOR-S6K pathway links growth signalling to DNA damage response by targeting RNF168. *Nat Cell Biol* **20**, 320-331 (2018).

10. X. Zhou *et al.*, Regulation of CHK1 by mTOR contributes to the evasion of DNA damage barrier of cancer cells. *Sci Rep* **7**, 1535 (2017).
11. K. Datta, S. Suman, A. J. Fornace, Jr., Radiation persistently promoted oxidative stress, activated mTOR via PI3K/Akt, and downregulated autophagy pathway in mouse intestine. *Int J Biochem Cell Biol* **57**, 167-176 (2014).
12. Z. Zhu *et al.*, Prevention of irradiation-induced salivary hypofunction by rapamycin in swine parotid glands. *Oncotarget* **7**, 20271-20281 (2016).
13. W. H. Mondesire *et al.*, Targeting Mammalian Target of Rapamycin Synergistically Enhances Chemotherapy-Induced Cytotoxicity in Breast Cancer Cells. *Clinical Cancer Research* **10**, 7031-7042 (2004).
14. K. P. Lai *et al.*, S6K1 is a multifaceted regulator of Mdm2 that connects nutrient status and DNA damage response. *EMBO J* **29**, 2994-3006 (2010).
15. S. Braunstein, M. L. Badura, Q. Xi, S. C. Formenti, R. J. Schneider, Regulation of protein synthesis by ionizing radiation. *Mol Cell Biol* **29**, 5645-5656 (2009).
16. M. Diehn *et al.*, Association of reactive oxygen species levels and radioresistance in cancer stem cells. *Nature* **458**, 780-783 (2009).
17. S. Bao *et al.*, Glioma stem cells promote radioresistance by preferential activation of the DNA damage response. *Nature* **444**, 756-760 (2006).
18. M. Al-Hajj, M. S. Wicha, A. Benito-Hernandez, S. J. Morrison, M. F. Clarke, Prospective identification of tumorigenic breast cancer cells. *Proc Natl Acad Sci U S A* **100**, 3983-3988 (2003).
19. S. Matsubara *et al.*, mTOR plays critical roles in pancreatic cancer stem cells through specific and stemness-related functions. *Sci Rep* **3**, 3230 (2013).

20. D. Hambardzumyan *et al.*, PI3K pathway regulates survival of cancer stem cells residing in the perivascular niche following radiation in medulloblastoma *in vivo*. *Genes Dev* **22**, 436-448 (2008).

21. D.-H. Kim *et al.*, mTOR interacts with raptor to form a nutrient-sensitive complex that signals to the cell growth machinery. *Cell* **110**, 163-175 (2002).

22. C. Wu *et al.*, BioGPS: an extensible and customizable portal for querying and organizing gene annotation resources. *Genome Biol* **10**, R130 (2009).

23. C. Wu, I. Macleod, A. I. Su, BioGPS and MyGene.info: organizing online, gene-centric information. *Nucleic Acids Res* **41**, D561-565 (2013).

24. C. Wu, X. Jin, G. Tsueng, C. Afrasiabi, A. I. Su, BioGPS: building your own mash-up of gene annotations and expression profiles. *Nucleic Acids Res* **44**, D313-316 (2016).

25. E. Cerami *et al.*, The cBio cancer genomics portal: an open platform for exploring multidimensional cancer genomics data. *Cancer Discov* **2**, 401-404 (2012).

26. J. Gao *et al.*, Integrative Analysis of Complex Cancer Genomics and Clinical Profiles Using the cBioPortal. *Sci. Signal.* **6**, (2013).

27. D. R. Rhodes *et al.*, ONCOMINE: A Cancer Microarray Database and Integrated Data-Mining Platform. *Neoplasia* **6**, 1-6 (2004).

28. J. C. Brenner *et al.*, Genotyping of 73 UM-SCC head and neck squamous cell carcinoma cell lines. *Head Neck* **32**, 417-426 (2010).

29. D. D. Fang *et al.*, Antitumor Efficacy of the Dual PI3K/mTOR Inhibitor PF-04691502 in a Human Xenograft Tumor Model Derived from Colorectal Cancer Stem Cells Harboring a PIK3CA Mutation. *PLoS One* **8**, e67258 (2013).

30. E. L. Leung *et al.*, Non-small cell lung cancer cells expressing CD44 are enriched for stem cell-like properties. *PLoS One* **5**, e14062 (2010).

31. P. Wang *et al.*, Identification and characterization of cells with cancer stem cell properties in human primary lung cancer cell lines. *PLoS One* **8**, e57020 (2013).

32. S. Liu *et al.*, Breast cancer stem cells transition between epithelial and mesenchymal states reflective of their normal counterparts. *Stem Cell Reports* **2**, 78-91 (2014).

33. T. T. Puck, P. L. Marcus, Action of X-rays on mammalian cells. *J Exp Med.* **103**, 653-666 (1956).

34. N. A. Franken, H. M. Rodermond, J. Stap, J. Haveman, C. van Bree, Clonogenic assay of cells *in vitro*. *Nat Protoc* **1**, 2315-2319 (2006).

35. E. Pastrana, V. Silva-Vargas, F. Doetsch, Eyes wide open: a critical review of sphere-formation as an assay for stem cells. *Cell Stem Cell* **8**, 486-498 (2011).

36. L. B. Weiswald, D. Bellet, V. Dangles-Marie, Spherical cancer models in tumor biology. *Neoplasia* **17**, 1-15 (2015).

37. L. Galluzzi *et al.*, Molecular mechanisms of cisplatin resistance. *Oncogene* **31**, 1869-1883 (2012).

38. D. J. Peng, J. Wang, J. Y. Zhou, G. S. Wu, Role of the Akt/mTOR survival pathway in cisplatin resistance in ovarian cancer cells. *Biochem Biophys Res Commun* **394**, 600-605 (2010).

39. Y. Kim, K. M. Joo, J. Jin, D.-H. Nam, Cancer Stem Cells and Their Mechanism of Chemo-Radiation Resistance. *International Journal of Stem Cells* **2**, 109-114 (2009).

40. C. Ploner, R. Kofler, A. Villunger, Noxa: at the tip of the balance between life and death. *Oncogene* **27 Suppl 1**, S84-92 (2008).

41. A. R. Collins, The Comet Assay for DNA Damage and Repair: Principles, Applications, and Limitations. *Molecular Biotechnology* **26**, 249-261 (2004).

42. O. Ostling, K. J. Johanson, Microelectrophoretic study of radiation-induced DNA damages in individual mammalian cells. *Biochem Biophys Res Commun* **123**, 291-298 (1984).

43. Y. Tu *et al.*, DNA-dependent protein kinase catalytic subunit (DNA-PKcs)-SIN1 association mediates ultraviolet B (UVB)-induced Akt Ser-473 phosphorylation and skin cell survival. *Molecular Cancer* **12**, 1-12 (2013).

44. D. Silvera *et al.*, mTORC1 and -2 Coordinate Transcriptional and Translational Reprogramming in Resistance to DNA Damage and Replicative Stress in Breast Cancer Cells. *Mol Cell Biol* **37**, (2017).

45. J. C. Morales *et al.*, Review of Poly (ADP-ribose) Polymerase (PARP) Mechanisms of Action and Rationale for Targeting in Cancer and Other Diseases. *Crit Rev Eukaryot Gene Expr* **24**, 15–28 (2014).

46. N. McGranahan, C. Swanton, Clonal Heterogeneity and Tumor Evolution: Past, Present, and the Future. *Cell* **168**, 613-628 (2017).

47. L. Chang *et al.*, Acquisition of epithelial-mesenchymal transition and cancer stem cell phenotypes is associated with activation of the PI3K/Akt/mTOR pathway in prostate cancer radioresistance. *Cell Death Dis* **4**, e875 (2013).

48. O. E. Pardo *et al.*, FGF-2 protects small cell lung cancer cells from apoptosis through a complex involving PKCepsilon, B-Raf and S6K2. *EMBO J* **25**, 3078-3088 (2006).

49. G. Pérez-Tenorio *et al.*, Clinical potential of the mTOR targets S6K1 and S6K2 in breast cancer. *Breast Cancer Res Treat* **128**, 713-723 (2011).

50. E. Karlsson *et al.*, The mTOR effectors 4EBP1 and S6K2 are frequently coexpressed, and associated with a poor prognosis and endocrine resistance in breast cancer- a retrospective study including patients from the randomised Stockholm tamoxifen trials. *Breast Cancer Research* **15**, 1-12 (2013).

51. M. K. Kim *et al.*, High expression of mTOR is associated with radiation resistance in cervical cancer. *J Gynecol Oncol* **21**, 181-185 (2010).

52. A. J. Leiker *et al.*, Radiation Enhancement of Head and Neck Squamous Cell Carcinoma by the Dual PI3K/mTOR Inhibitor PF-05212384. *Clin Cancer Res* **21**, 2792-2801 (2015).

53. L. S. Steelman *et al.*, Involvement of Akt and mTOR in chemotherapeutic- and hormonal-based drug resistance and response to radiation in breast cancer cells. *Cell Cycle* **10**, 3003-3015 (2011).

54. F. Pajonk, E. Vlashi, W. H. McBride, Radiation resistance of cancer stem cells: the 4 R's of radiobiology revisited. *Stem Cells* **28**, 639-648 (2010).

55. C. A. Lovejoy, D. Cortez, Common mechanisms of PIKK regulation. *DNA Repair (Amst)* **8**, 1004-1008 (2009).

56. G. C. M. Smith, S. P. Jackson, The DNA-dependent protein kinase. *Genes Dev* **13**, 916-934 (1999).

57. A. Ciccia, S. J. Elledge, The DNA damage response: making it safe to play with knives. *Mol Cell* **40**, 179-204 (2010).

58. R. H. Wong *et al.*, A role of DNA-PK for the metabolic gene regulation in response to insulin. *Cell* **136**, 1056-1072 (2009).

59. H. Lucero, D. Gae, G. E. Taccioli, Novel localization of the DNA-PK complex in lipid rafts: a putative role in the signal transduction pathway of the ionizing radiation response. *J Biol Chem* **278**, 22136-22143 (2003).

60. L. Chang *et al.*, PI3K/Akt/mTOR pathway inhibitors enhance radiosensitivity in radioresistant prostate cancer cells through inducing apoptosis, reducing autophagy, suppressing NHEJ and HR repair pathways. *Cell Death Dis* **5**, e1437 (2014).

61. B. Mukherjee *et al.*, The Dual PI3K/mTOR Inhibitor NVP-BEZ235 Is a Potent Inhibitor of ATM- and DNA-PKCs-Mediated DNA Damage Responses. *Neoplasia* **14**, 34-IN38 (2012).

Chapter 4 – Conclusions and future directions

A third mTOR complex 3 (mTORC3)?

Strong evidence supports a role for mTOR in the regulation of essential cell processes and its dysregulation is involved in the pathogenesis of several human diseases. Aberrant activation of mTOR signaling contributes to malignant behavior of cancer cells by controlling proliferation, invasion, and metastasis. In Chapter 1, we provide an overview of mTOR signaling in relation to development and disease. This is not an exhaustive review as mTOR signaling research has influenced many facets of biology. Thus, we chose to focus on relevant growth processes of interest and human cancers that upregulate mTOR signaling. In Chapter 2, we demonstrate the function a novel regulator of mTOR signaling in human cells, which we have named mammalian EAK-7 (MTOR associated protein eak-7 homolog, mEAK-7). Preliminary data suggests that mEAK-7 forms a novel mTOR complex, independent of mTORC1/2, to regulate cell invasion *in vitro* and correlates to high levels of mEAK-7 protein detected in the metastasized lymph nodes of patients. This finding was most intriguing because this new signaling complex regulated S6K2 signaling rather than S6K1. In canonical mTORC1 signaling, conventional targeting was done via S6K1 phosphorylation. Thus, identifying molecules that suppressed S6K1 phosphorylation was not sufficient to specify the downstream targets specific to S6K2. This leads us and others (*1, 2*) to

reveal that novel mTOR complexes could exist. In Chapter 3, immunoprecipitation (IP)/mass spectrometry (MS) experiments provide evidence to suggest that DNA-PK can bind mEAK-7 and that this binding is increased with DNA damage induced by X-ray irradiation. This is intriguing because DNA-PK has been primarily demonstrated as a protein kinase essential for DNA damage repair by non-homologous end joining (NHEJ). Based on these data, we hypothesize that a new mTOR complex, mTORC3, composed minimally of mTOR, mLST8, mEAK-7 and DNA-PK may be more abundant in response to stress/DNA damage in certain cancer cells. In our final chapter, we will outline the lingering controversies, how our work will impact the mTOR community as a whole, and the research that will likely impact the future of mTOR signaling, in relation to mEAK-7.

Lingering controversies and poor efficacy of mTOR inhibitors in clinical settings

The findings outlined in this thesis will advance the field of mTOR signaling because it brings about a novel way to think about mTOR complexes in health and disease. Many rapamycin analogues or mTOR kinase catalytic site inhibitors demonstrate little efficacy for patients, suggesting that alternative mTOR signaling may be occurring in select patients. Additionally, the reason that patients who fail standard therapy of surgery, chemotherapeutics, or radiation therapy, is likely due to mechanisms that can alter cancer-specific signaling. Investigating the role of mTOR signaling in response to DNA damage will elucidate the nature by which chemo- or radio- resistant tumor cells alter mTOR signaling. mEAK-7 was never identified as a component of mTOR complexes in the past, likely due to the limited cell types, e.g. HEK293T or Hela,

that were used in the experiments. Since we have demonstrated that mEAK-7 is a bona fide interacting molecule of mTOR in human cancer cells, we posit that a third mTOR complex containing mEAK-7 plays an important role in cancer biology.

While numerous research groups around the world demonstrate that inhibition of mTOR signaling can lead to significant reductions in tumor size and progression, this is not the case for mTOR inhibitors in the clinic. Since the discovery of rapamycin on Easter Island, scientists discovered the valuable role of rapamycin as an immunosuppressant (*3, 4*). Years after this discovery, mTOR inhibitors were reverse engineered and the first class of drugs created included rapamycin analogs or "rapalogs". The first rapalog known as Temsirolimus was developed by Pfizer and was used for the treatment of renal cell carcinoma in 2007 (*5*). Patients who received temsirolimus alone had longer overall survival and progression-free survival than patients who received interferon alone (*5*). This was the first proof-of-principal study that demonstrated the effectiveness of mTOR inhibition of cancer. These findings were quickly followed by another rapalog, Everolimus, developed by Novartis in 2009 (*6*). Everolimus demonstrated encouraging antitumor activity against metastatic renal cell carcinoma (*6*). Curiously, mTOR signaling has been implicated in numerous cancer types in patients, but rapamycin analogs that target mTORC1 are not sufficient to induce cytotoxic effects, and rather yield cytostatic results. While there have been a small number of extraordinary responders when given mTOR inhibitors, predictive modeling to specify which patients would be required to yield the best results. This is a significant issue for patients on mTOR inhibitors since the majority of mTOR inhibitors in clinical trials have not fared well. One possible strategy is to pair genomic analyses with

different disease states to confirm that patients have upregulated mTOR signaling within key pathways. These ideas have been around for decades, as we have built a massive amount of data from -omics approaches. Thus, pharmacogenomics will allow us to investigate drug targets against specific scenarios based on a whole systems approach and the patients genome (*7*).

With the amount of big data being generated for patient responses, health records, and genetic information, the most rational path forward is to incorporate advanced artificial intelligence paired with deep learning and machine learning to enable novel therapeutics to be developed (*8*). This will enable clinicians to determine which patients would benefit from specific mTORC1, mTORC2, or mTORC3 inhibitors. One issue with rapalogs is that, while *in vitro* and *in vivo* pre-clinical models demonstrate large efficacy, rapalogs do not fully suppress the downstream signaling and targets of other mTORC1 substrates (*4, 9-11*). Additionally, it is known that as mTORC1 inhibition releases the negative feedback on insulin/PI3K/Akt signaling, patients taking rapalogs have resulted in upregulated Akt signaling, leading to cancer cell survival (*12*). Therefore, one strategy that has been deployed is the use of second generation mTOR inhibitors that target the ATP-competitive catalytic site of mTOR. By targeting mTOR itself, we are able to block the downstream substrate specificities of mTORC1, mTORC2, and likely, mTORC3 and undiscovered mTOR complexes can be blocked. However, even with these advances in second generation mTOR inhibitors, their ability to block Akt signaling is transient and Insulin/PI3K is capable of overcoming the negative feedback loop with long-term treatment of mTOR specific inhibitors. Curiously, mTORC3 also involves another PIKK family member, DNA-PK. DNA-PK is also known

to be the physiological kinase that targets Akt under specific requirements, in conjunction with mTORC2 (*13*). Since mEAK-7 is required for DNA-PK/mTOR/S6K2 signaling, it is likely that an alternative mTOR pathway functions in some biologic contexts. Finally, newly described “third-generation” mTOR inhibitors called “RapaLink” blocks ATP sites as well as mTORC1 via rapamycin, suggesting that prohibiting the binding of other substrates to mTOR substantially decreases both Akt and 4E-BP1 (*14*). Thus, developing novel ways to block mTOR binding to downstream substrate targets is the most effective way to inhibit aberrant mTOR signaling in human cancer and other diseases.

There are three long-term goals of understanding mEAK-7 in the context of cancer in this thesis. First, is identifying mTORC3 downstream targets by phosphoproteomics before/after DNA damage. Second, is defining mTORC3 binding partners before and after DNA damage as these protein-protein interactors will provide insight to radioresistance mechanisms. Third, is determining the topographical structure of novel mTOR complexes, like mTORC3, and identifying essential protein-partner binding sites. Thus, while the field of mEAK-7 and its role in mTOR signaling is nascent, much work needs to be done before we can understand and assess the role of mTORC3 in response to DNA damage. These findings will be pivotal in creating create tools to study mTORC3 as a therapeutic target in human cancer.

Unexplored mTOR complexes in human cancer

The mTOR signaling field made dramatic advances when raptor (mTORC1) and rictor (mTORC2) were identified. After these initial discoveries, more proteins that are essential components of mTORC1 and mTORC2 have been identified. Within the field of mTOR signaling, there is a growing awareness of cell-type or tissue-type specific mTOR complexes that are essential for regulation of metabolism. Although complex, the molecular constituents of novel mTOR complexes will continue to be discovered as new technologies are introduced and developed in protein biology. Since mTOR is the major component of a larger multimeric protein complex, it's still unclear how all of the proteins interact and in what contexts. A single point mutation, R628C, is sufficient to change the binding affinity and kinase activity of mTOR (*15*), suggesting a decrease in binding of essential interacting proteins. Since aberrant mTOR signaling contributes to human cancer, many groups hoped to treat mTOR related cancers with mTOR direct or indirect inhibitors (*16*). However, widespread expression of mTOR kinase in normal human tissues has limited the effectiveness of single agent use of mTOR inhibitors for mTOR-related malignancies (*17*). An alternative strategy for treatment of mTOR malignancies is to pair it with other inhibitors, since those protein targets may be required for residual mTOR activity. mEAK-7 would be one such protein target which could yield positive benefits for patents,

Aberrant mTOR signaling has been observed in many types of cancers (*16*). Interestingly, mEAK-7 exhibits a preferential expression pattern in human cancer cell lines (*18*). However, prior to our manuscript, no other group has rigorously identified the molecular role for mEAK-7 in human cells. While EAK regulates dauer formation and

lifespan in nematodes (*19*), the molecular mechanism remains unknown and unexplored in mammals. S6K2 signaling has not been adequately distinguished from that of S6K1 due to their perceived redundancies (*20*), but the realization that mEAK-7 utilizes the S6K2/4E-BP1 axis to regulate mTOR signaling (*18*) had challenged those notions. However, in breast cancer cells, loss-of-function studies demonstrate that S6K1 and S6K2 have several different protein targets (*21*). Additionally, canonical models of mTORC1 and mTORC2, the traditional S6K regulators, may not exist in all cells, or function similarly in them. Expanding our knowledge of mTOR complexes in human disease may allow for the development of novel therapeutic agents to target aberrant mTOR signaling. Recently, a novel mTOR complex—other than mTORC1 and mTORC2—involving GIT1 in astrocytes was identified (*2*). Additionally, another mTOR complex was discovered, where a novel rapamycin insensitive molecule, ETV7, binds to mTOR in B cell neoplasms to regulate its kinase activity, even in the presence of rapamycin (*1*). Most recently, research labs around the world have identified novel mTOR complexes in different tissue types and disease states. These findings have modified how we think about mTOR and have led us to hypothesize the possibility of a new set of mTOR complexes forming under different tissue types or disease states.

While it is largely believed that mTOR signaling is suppressed under genotoxic stress via AMPK regulation of TSC2 (*22*), some studies have demonstrated aberrant activation of mTOR signaling in response to these same conditions. For example, mTORC1 signaling can inhibit DNA damage response mechanisms *in vitro* and *in vivo* through RNF168 (*23*). S6K2 knockdown induces a strong reduction of mTOR signaling and leads to chemoresistance in cancer cells (*24*). CHK1 function requires mTORC1

signaling in response to DNA damage, providing further evidence in support of a role for mTOR signaling in DNA damage responses (*25*). Sustained radiation treatment of mice activates mTOR signaling and oxidative stress in the intestine (*26*). There is a rationale to treat patients with chemotherapeutics and rapamycin since the combination results in an additive cytotoxic effect in breast carcinoma cell lines (*27*). Normal tissues undergoing radiation stress exhibit activated mTOR signaling, suggesting a role for DNA damage responses (*28*). These studies suggest that mTOR signaling and DNA damage responses are intertwined, but complex, and therefore require further study. Proposed mechanisms include the downregulation of p53 via S6K-mediated activation of MDM2 (*29*), and/or 4E-BP1 phosphorylation in response to DNA damage (*30*).

Given reports that genotoxic stress is capable of regulating mTOR signaling, we propose that mEAK-7 may contribute to these stress responses through an mTORC1/2 independent mechanism. Future directions or study of mEAK-7 could include: (1) to identify mTORC3 downstream targets before and after DNA damage, (2) to identify proteins that form a complex with mEAK-7, but not Raptor or Rictor, and (3) to determine how they bind.

The role for mEAK-7 and mTORC3 in human cancers

mTOR signaling has been demonstrated to be an essential controller of metastasis-related genes in prostate cancer (*31*). In a screen of human squamous cell carcinomas, we found that the UM-SCC-17A cell line, derived from a primary laryngeal cancer, did not express detectable levels of mEAK-7 protein. Interestingly, the UM-SCC-17B cell line, derived from a metastatic site in the same patient, did express

mEAK-7 (*18*). These findings suggest that the increased expression of mEAK-7 may be associated with tumor metastasis (*32*). To test this hypothesis in patients with cancer, we utilized mEAK-7 and activated mTOR specific antibodies against a patient tissue microarray that pairs normal tissue, primary lung cancer, and metastasized lymph node tissues. In our analyses, we determined that mEAK-7 and activated mTOR signaling were significantly increased in primary tumors and more so in the metastasized lymph nodes (Figure 3.2.,A-C). Thus, mEAK-7 protein is highly expressed in metastatic cancer, implying that it might be a new target for intervention (Figure 3.2). Furthermore, it could also be utilized as an essential marker for metastatic tumors, since normal lymph nodes do not express mEAK-7 or activated mTOR signaling.

Several research labs have demonstrated that novel mTOR complexes exist in the absence of raptor (mTORC1) or rictor (mTORC2). We hypothesized that mEAK-7 may be part of a novel mTOR complex and we sought to identify additional interacting partners of mEAK-7 (Figure 4.2). We determined by immunoprecipitation (IP) and mass spectrometry analyses that DNA-dependent protein kinase catalytic subunit isoform 1 (DNA-PKcs) was significantly pulled down with HA-mEAK-7 (Figure 3.5.A), suggesting a role for regulation of mTOR signaling. To validate the IP-mass spectrometry results, we demonstrated that exogenous mEAK-7 interacts with endogenous DNA-PK (Figure 3.5.B). Additionally, mEAK-7 increased its interaction with DNA-PK over time in response to DNA damage (Figure 3.5.C). These data suggest that mEAK-7 associates with DNA-PK in response to DNA damage. Other groups have demonstrated that mTOR and DNA-PK may interact after DNA damage, and that interaction regulates mTORC2 signaling in epithelial skin keratinocytes (*33*). Furthermore, nuclear DNA-PK

has been found to localize to the cytosol in response to DNA damage (*33*). These findings are intriguing because proteins with canonical roles in the nucleus may well be essential for other signaling pathways or cell processes in the cytosol. One example of this is NUF1P1, which has conserved nuclear functions to regulate snoRNPs, but in response to nutrient starvation it acts as a ribosome receptor for ribophagy (*34*).

We demonstrated that mEAK-7 regulates mTOR signaling through an alternative mTOR complex (*18*). To determine if both mEAK-7 and DNA-PK are part of a complex that helps regulate mTOR signaling, we hypothesized that DNA-PK was capable of interacting with S6K2, as mEAK-7 is required for the mTOR-S6K2 axis (*18*). We discovered that HA-S6K2 is capable of binding to DNA-PK, and that interaction strongly increased after DNA damage, but mTOR and HA-S6K2 interaction did not increase (Figure 3.5.D). Thus, DNA-PK is capable of interacting with S6K2 to regulate its function in response to DNA damage.

In conclusion, there is substantive evidence that a third mTOR complex exists in human cancer cells. In addition, it is plausible that cell-type and tissue-type and disease-specific mTOR complexes exist. The findings outlined in this thesis will be the catalyst for research groups to explore novel ideas with regard to mTOR signaling.

Phosphoproteomics of mTORC3 downstream targets by DNA damage

Transgenic mice with constitutive reductions of mTOR lose feedback inhibition of Akt signaling (*35*), thereby activating Akt; this phenotype also suggests that an alternative complex may regulate mTOR signaling. One of the challenges of mTOR signaling research is the lack of tissue-specific tools, since mTOR null mice are

embryonic lethal (*36*). Future work will require better tools to investigate novel mTOR complexes in different tissue types to specify the role of mTOR signaling in different cells. To understand the role of mTORC3 in human cancers, novel technologies such as clustered, regularly interspaced, short palindromic repeat (CRISPR) loci along with CRISPR-associated (cas) genes can create specific genetic lesions to delete mEAK-7. CRISPR knockout cells targeting Raptor (mTORC1), Rictor (mTORC2), and mEAK-7 (mTORC3) would enable us to determine the essential effects of different mTOR complexes on mTOR signaling. Additionally, pursuing comparative phosphoproteomic analyses before/after DNA damage or differing nutrient conditions by stable isotope labeling with amino acids in cell culture (SILAC), would further support the likelihood of novel mTORC3 downstream targets. This will allow us to determine the extent to which mTORC3 downstream targets are similar to mTORC1/2 before/after DNA damage.

mTOR is a promiscuous kinase and targets several proteins depending on the nature of the stimuli, cell type, and environment (*16*). One single amino acid change (R628C) is sufficient to reduce mTOR kinase activity (*15*). These results suggest that an alternative mTOR complex may take the reins of mTOR signaling when canonical signaling is diminished. While there have been many approaches to understanding the phosphoproteome, there is still much that we do not know when it comes to novel mTOR complexes. The mTOR phosphoproteome has revealed novel downstream targets, such as Grb10 (*37, 38*). Thus, proteomics analysis is capable of revealing new signaling networks originally hidden from view. Preliminary mass-spec data reveals that mEAK-7 interacts with mTOR and DNA-PK (Figure 3.5.A). These findings are surprising, given that DNA-PK functions primarily in the DNA damage repair response,

via non-homologous end joining. There is evidence that DNA-PK is essential for regulating animal metabolism and insulin signaling, but the rationale or mechanism remains unknown (*39, 40*). Thus, understanding the role of mEAK-7 and DNA-PK in alternative mTOR signaling will be an essential quest for the future.

mTORC3 phosphoproteome overlap between mTORC1 and mTORC2.

There are likely to be common and unique protein targets of mTORC1/2/3 before/after DNA damage. To tease these out, CRISPR-Cas9 knockout (Rictor, Raptor or mEAK-7) constructs against cancer and normal cell lines may allow us to identify the key targets lost as a result of sequential knockout of mTORC1, mTORC2, or mTORC3. One strategy is to evaluate the phosphoproteomes of control versus knock-out using stable isotope labeling with amino acids in cell culture (SILAC), an approach for *in vivo* incorporation of a label into proteins for mass spectrometry-based quantitative proteomics. Thus, in the future we hope to identify shared and unique targets of mTORC1/2/3 to identify and validate the signaling networks associated with DNA damage responses. We hypothesize that there will be differential utilization of mTORC3 during DNA damage by the allelic variants of mTOR.

Novel mTORC3 binding partners before/after DNA damage

Immunoprecipitation (IP) and mass spectrometry (MS) analysis of mEAK-7 demonstrated that DNA-PK, a DNA damage sensor, is an interacting molecule and its binding increases after DNA damage (Figure 3.5.A). Further, the mEAK-7/DNA-PK

interaction required mTOR to promote the DNA damage response. Point mutations in the mTOR (R628C) HEAT domain are sufficient to reduce mTOR kinase activity (*15*) and may be involved in regulating the sensitivity to total body radiation (data not shown); preliminary IP-MS data indicates that DNA-PK binds to WT and mutant alleles of mTOR, with differential affinity. Therefore, it is essential to identify the novel binding partners of mTORC3 before/after DNA damage via quantitative mass spectrometry, and map the mEAK-7, mTOR, and DNA-PK domains required for mTORC3 formation.

DNA-PK co-localizes and interacts with mEAK-7 and mTOR.

Since the discovery that mEAK-7 regulates an alternative mTOR signaling pathway, we have placed a great deal of effort to identify the novel complex that governs this signaling complex. mEAK-7 interacts with mTOR (*18*) and DNA-PK (Figure 3.5). DNA-PK and mEAK-7 interact strongly and their interaction increases in the presence of DNA damage (Figure 3.5., B and C). To link S6K2 to mEAK-7 and mTOR, we demonstrated that DNA-PK interacts with S6K2 in response to DNA damage, suggesting cross-talk signaling with mTOR. DNA-PK is capable of localizing to the cytoplasm in response to DNA damage (*41*), but the extent to which it may co-localize with mTOR at the lysosome is unknown. To test this hypothesis, it will be essential to apply DNA damage to cancer cells and determine the extent to which DNA-PK colocalizes with mTOR and mEAK-7 at the lysosome. Additionally, examining this binding under different modalities of DNA damage, like chemotherapeutics or gamma ray irradiation will be helpful to undertand this phenomenon. Given that mEAK-7 and DNA-PK interact with mTOR to form a novel complex in the absence of Raptor or

Rictor, it will be essential to determine which domains of mEAK-7, mTOR, and DNA-PK are required for mTORC3 formation at the lysosome.

Topographical structure of mTORC3

Advances in Cryo-EM technologies, computational power, and direct-electron-detectors (DEDs) have revolutionized our ability to obtain structural information of lipid-bound proteins and large multimeric complexes. Additionally, Cryo-EM technologies have enhanced our capacity to obtain 3D structural information of the most difficult multimeric complexes. Therefore, Cryo-EM is rapidly becoming the powerful tool of choice to study atomic resolution protein-protein, DNA-protein, and RNA-protein interactions to further the goals of basic research and drug discovery (*42*). One challenge of traditional structural biology studies, e.g. X-ray crystallography, has been the limitation of growing well-diffracting crystals of large and multimeric complexes. The main advantage of Cryo-EM being that single molecules in solution are used rather than crystals. The mTOR community has been stymied without the ability to visualize how the mTOR complexes are formed. Now, we have high-quality resolution structures available for mTORC1 (*43*) and mTORC2 (*44*), and we can visualize how all of the components interact (Figure 4.1). These structural insights are essential for understanding the basic mechanics of the protein-protein interactions. Based on our preliminary data, we hypothesize that mTORC3 comprises mEAK-7, mTOR, mLST8, and DNA-PK and we will be interested in elucidating the structure of this complex to determine how these proposed subunits interact and how they function as a complex to target other proteins.

mTORC3 protein interactors on lipid membranes

One crucial challenge towards our efforts in understanding lipid-bound protein complexes is the lack of lipid-membranes and their interactions to activate mTOR complexes. Numerous strategies have been employed to do so, one being the generation of lipid nanodiscs and the incorporation of proteins that are known to be lipid bound membrane proteins, as their folding integrity is dictated by their interaction with lipid membrane proteins (*45*). This method was recently employed to understand the mechanistic action of TRPV1, an ion channel embedded in plasma membranes, to reveal the specific mechanism of action and ligand binding through recreated movies (*46*). However, we recognize that a method that works for one particular protein may not be suitable for another, since stabilization of any membrane protein is purely an empirical trial-and-error process. Since mEAK-7 is a lipid-bound protein, we hypothesize that it will require lipid nanodiscs to demonstrate proper structural expression. Thus, it will be essential to test this purification strategy to exogenously tagged mEAK-7, mTOR, mLST8, and DNA-PK to test their binding. Additionally, we will determine the extent to which mEAK-7 binds to mTORC3 after treatment with rapamycin in a dose-dependent and time-dependent fashion.

A curious and broad role for mEAK-7 in early mammalian development

Throughout the development of this thesis project, it has been challenging to develop the necessary tools to observe mEAK-7 in relevant *in vivo*. After screening 10

commercially available antibodies, we identified a human mEAK-7 specific antibody capable of IF staining. Thus, we were interested in investigating the potential role of mEAK-7 during development, since we saw minimal mEAK-7 staining in adult tissues, when compared to metastatic tissues. Another challenge is that the antibodies we have screened to date do not work across species, limiting the utility of these tools. In collaboration with Dr. Isabelle Lombaert, we obtained human fetal tissues to determine the extent that mEAK-7 was expressed during early development. We discovered that mEAK-7 and activated mTOR signaling was strongly expressed in human fetal eyes (Figure 4.3.A). mTOR has been demonstrated as an essential metabolic program for the development of mammalian eyes. mTORC1 inhibition via rapamycin inhibits retinal progenitor cell cycle and retinal development (*47*). Finally, other eukaryotes, such as *Drosophila* or zebrafish require functional mTOR signaling for proper retinal development (*48, 49*). mEAK-7 is expressed in the epithelial layer, where retinal progenitor cells are located, in human fetal eye tissues, which is overlapped with activated mTOR signaling. This suggests that mEAK-7 could play an important role in eye development.

In addition, we discovered that mEAK-7 and activated mTOR signaling was strongly expressed human fetal salivary glands (Figure 4.3.B). Curiously, PI3K signaling was implicated in the development of salivary glands, where EGF-stimulation is necessary for branching morphogenesis in fetal mouse submandibular glands (SMG) (*50*). Additionally, another group demonstrated via a genetic mouse model approach that SMG and SLG development was delayed in mTOR conditional KO (*Wnt1*-cre: NCC specific) mice, where the SMG and SLG were smaller in size and resulted in fewer

epithelial branching of the SMG and SLG (*51*). Surprisingly, mTORC1 disruption through Raptor conditional KO mice (*Wnt1*-cre: NCC specific) mirrored similar results to mTOR conditional KO mice, but Rictor conditional KO mice (*Wnt1*-cre: NCC specific) only resulted in a mild defect (*51*). Since this group only focused on mTORC1 and mTORC2, it will be essential to identify the role of mTORC3 (mEAK-7 specific) in these organ systems and the extent to which mEAK-7 is required for embryonic development of craniofacial organs and structures.

Another important organ, as a dentist-scientist, is the human tongue. We identified mEAK-7 to be robustly found at the basilar epithelium and suprabasal epithelium of the human fetal tongue, as marked by K19 staining (Figure 4.3.C) Interestingly, it is also located in the developing taste bud, suggesting that mEAK-7 could play a role in taste sensation or noxious stimuli (Figure 4.3.C). PI3K inhibition resulted in a decrease of cell proliferation of *ex vivo* culture of tongue organs (*52*). The tongue epithelium of newborn mice with mTOR conditional KO (epithelium) resulted in a lack of cell stratification when compared to wild-type mice (*53*). Further investigation of mEAK-7 in the human tongue is important in understanding its role in epithelial development of the tongue and how aberrant mEAK-7/mTOR signaling can result in cancer.

Our understanding of mEAK-7 during organismal development and disease is at its earliest stages and much more work will be required to understand mEAK-7 function. We have demonstrated mEAK-7 is a crucial regulator of mTOR signaling in humans, but there is a high likelihood that mEAK-7 will play an essential role in other eukaryotes.

Conclusions and future directions

mTOR's classical role in metabolism ranges from controlling protein synthesis, nucleotide synthesis, lipid synthesis, and autophagy (*54*). Aberrant mTOR signaling is found in most cancers since mTOR signaling is a critical regulator of cancer initiation and metastasis (*31*). These processes require eukaryotic translation initiation factor 4E-binding protein 1 (4E-BP1), a critical downstream target of mTORC1, for the specific expression of invasion sensitive genes (*31*). mTORC1 controls cell proliferation, but not cell size, through 4E-BP1 in mammalian cells (*55*). Furthermore, double-knockout mouse models of 4E-BP1 and 4E-BP2 result in increases tumorigenesis and causes tumor progression to occur significantly faster in p53 loss-of-function mice. This suggests that without the endogenous function of 4E-BP1 to inhibit eukaryotic translation initiation factor 4E (eIF4E), rampant tumor formation ensues. While loss-of-function 4E-BPs contribute to tumorigenesis, overexpression of a gain-of-function 4E-BP1 significantly reduces the tumor formation in PI3K and KRAS overexpressed mice. Thus, mTOR signaling plays a significant role in tumorigenesis.

The long-term goal of this thesis is to further our understanding of the mechanisms that regulate mEAK-7 and, in turn, the mechanisms that are regulated by mEAK-7. In this context, we discovered a role for mEAK-7 as a key component of mTORC3, and understanding how mTORC3 behaves in human cancer will yield novel insights into mTOR signaling and cancer biology. Rapamycin analogues or mTOR kinase catalytic site inhibitors demonstrate limited efficacy for patients, suggesting that alternative mTOR signaling is occurring. Patients who fail standard therapies (e.g. surgery, chemotherapeutics, radiation therapy), may do so through mechanisms that

commandeer cancer specific signaling. Investigating the role of novel mTOR complexes in response to DNA damage will provide insights into how chemo- or radio-resistant tumor cells hijack mTOR signaling. This will give us insight to develop targeted therapeutics against mEAK-7 for the specific treatment of cancer. Developing therapeutics will depend on demonstrating that mTORC3 has a critical, positive biological role in cancer. Further, since mEAK-7 is required for sustained mTOR signaling in response to IR, we hypothesize that mEAK-7 may promote radioresistance in cancer. However, the elucidation of all complex binding partners of mTORC3 or if mTORC3 plays a role in other human diseases will take more time to investigate. These studies will set the stage to identify new mTOR complexes which may form under different conditions and which may be cell-type specific (Figure 4.2).

Acknowledgements

We sincerely thank Dr. Isabelle Lombaert for providing us with the samples for (Figure 4.3. A-C). Human fetal tissue was obtained via the University of Washington, and shipped to the University of Michigan, all under approved IRB's. The 'Laboratory of Developmental Biology' at the University of Washington was supported by NIH Award Number 5R24HD000836 from the Eunice Kennedy Shriver National Institute of Child Health & Human Development. We also thank Dr. Charlotte Mistretta for gifting us the K19 antibody utilized in tongue epithelium staining in Figure 4.3.

Figures

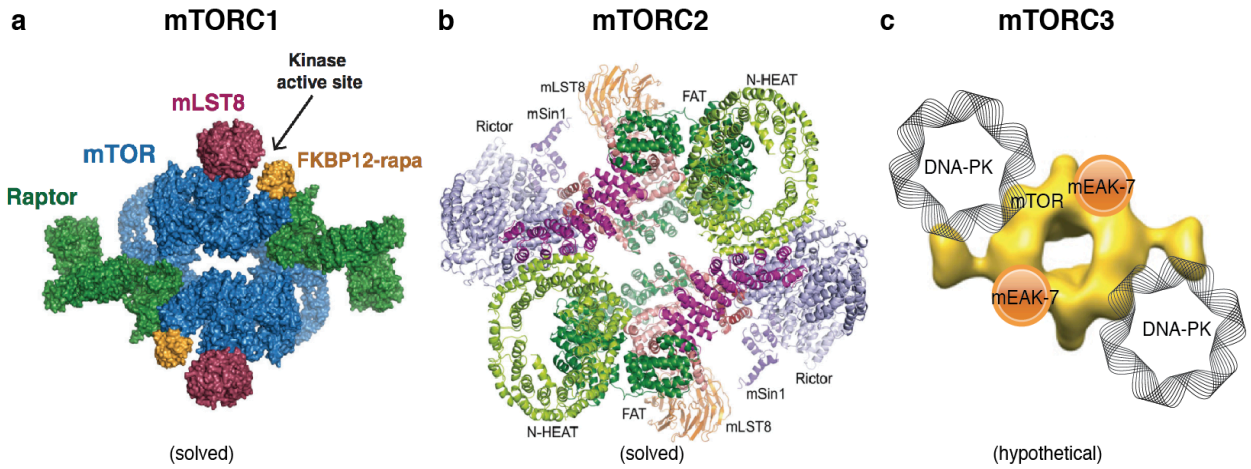

Figure 4.1. Experimental plan for investigating novel mTOR complexes in human cells. (**A**) mTORC1 structure: mTOR, mLST8, and Raptor (*1*) (reproduced with permission from Elsevier). (**B**) mTORC2 structure: mTOR, mLST8, mSin1, Rictor (*187*) (reproduced with permission from Springer Nature). (**C**) hypothetical mTORC3 structure: mEAK-7, DNA-PK, mTOR, mLST8.

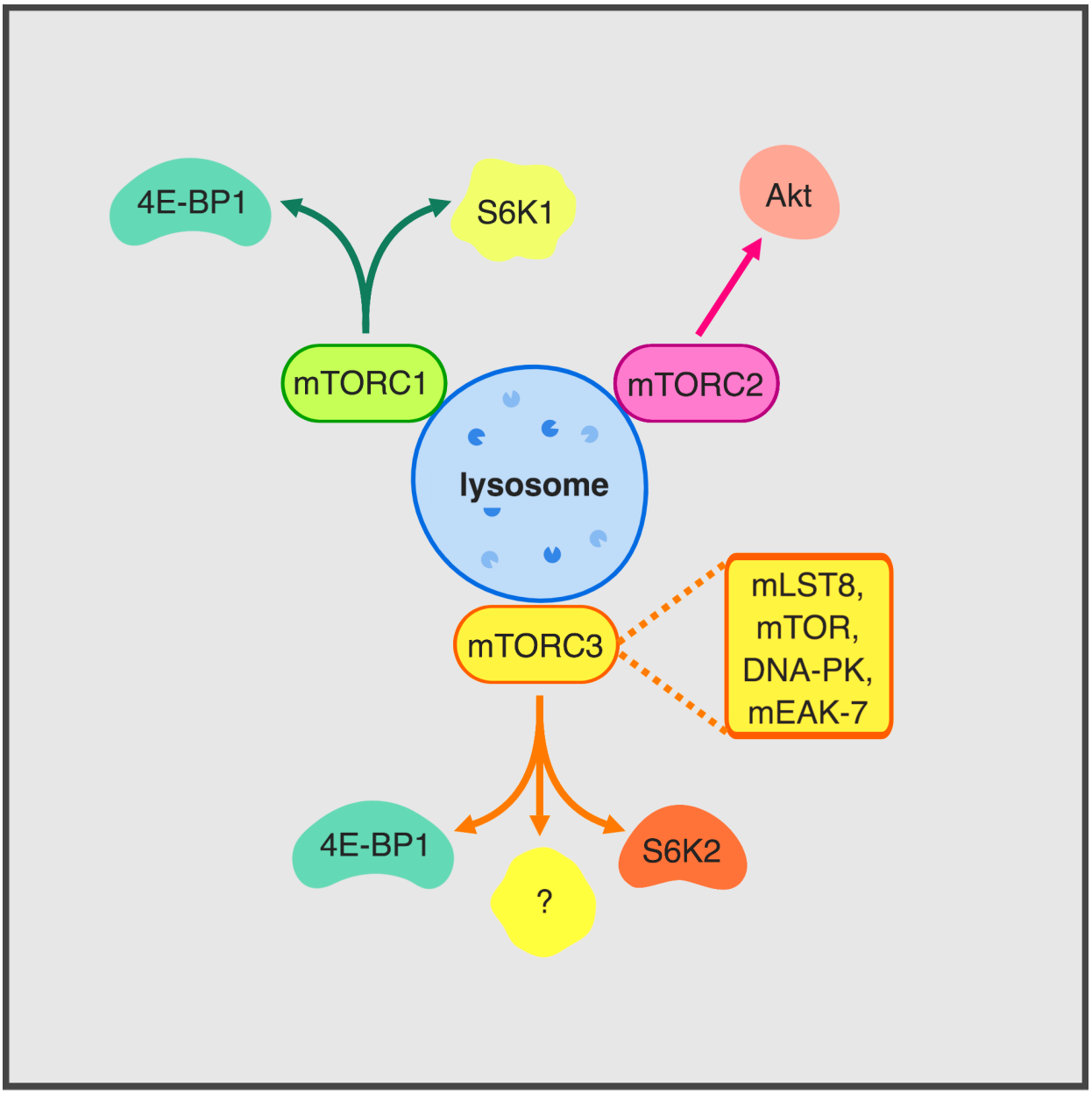

Figure 4.2. Diagram of mTOR signaling. The classical mTORC1 and mTORC2 signaling pathways have well established protein targets. mTORC1 targets S6K1 and 4E-BP1, while mTORC2 targets Akt. However, the newest member, mTORC3, which is comprised of mLST8, mEAK-7, mTOR and DNA-PK, which targets Akt and 4E-BP1.

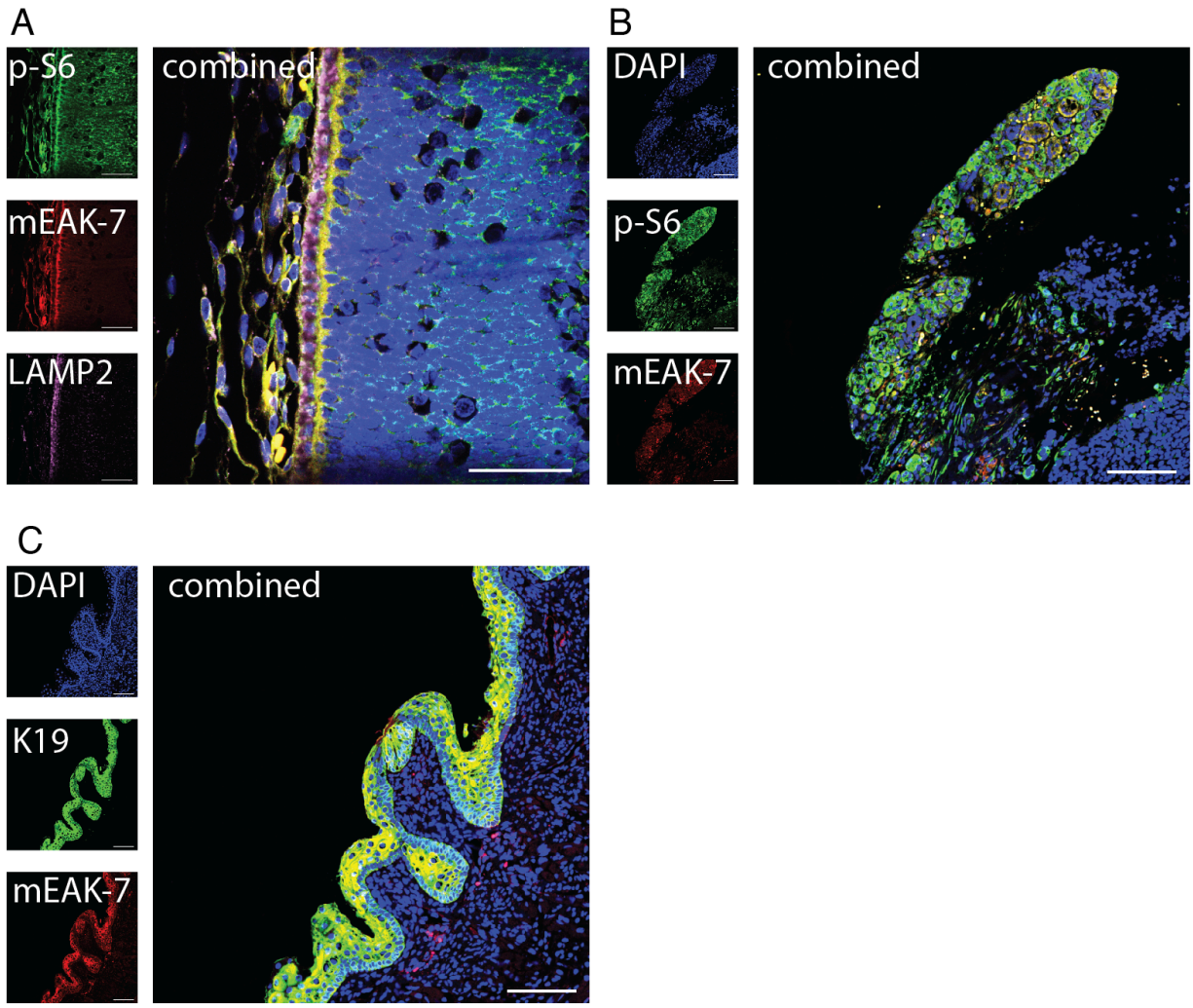

Figure 4.3. Human fetal tissue staining of mEAK-7 and activated mTOR signaling. (**A**) Section of epithelial layer of human fetal eye. (Ser240/244) p-S6 (Cell Signaling Technologies # 5364), mEAK-7 (Santa Cruz Biotechnology (SCB) # sc-18822), Cell Signaling Technologies # (**B**) Section of human fetal salivary gland. (Ser240/244) p-S6 (Cell Signaling Technologies # 5364), mEAK-7 (Santa Cruz Biotechnology # sc-247321). (**C**) Section of human fetal tongue (Ser240/244) p-S6 (Cell Signaling Technologies # 5364), (Santa Cruz Biotechnology # sc-247321). K19 (Cell Signaling Technologies # 12434). DAPI for nuclear stain. Tissues were a gift from Dr. Isabelle Lombaert's Lab. Scale bars represent 250 um.

References

1. F. C. Harwood, R. I. K. Geltink, B. P. O'Hara, M. Cardone, L. Janke, D. Finkelstein, I. Entin, L. Paul, P. J. Houghton, G. C. Grosveld, ETV7 is an essential component of a rapamycin-insensitive mTOR complex in cancer. *Science Advances* **4**, 1-18 (2018).
2. L. J. Smithson, D. H. Gutmann, Proteomic analysis reveals GIT1 as a novel mTOR complex component critical for mediating astrocyte survival. *Genes Dev.* **30**, 1383-1388 (2016).
3. D. F.J., S. Q., Mechanism of action of the immunosuppressant rapamycin. *Life Sci.* **58**, 373-395 (1996).
4. A. Y. Choo, S. O. Yoon, S. G. Kim, P. P. Roux, J. Blenis, Rapamycin differentially inhibits S6Ks and 4E-BP1 to mediate cell-type-specific repression of mRNA translation. *Proc Natl Acad Sci U S A* **105**, 17414-17419 (2008).
5. G. Hudes, M. Carducci, P. Tomczak, J. Dutcher, R. Figlin, A. Kapoor, E. Staroslawska, J. Sosman, D. McDermott, I. Bodrogi, Z. Kovacevic, V. Lesovoy, I. G. H. Schmidt-Wolf, O. Barbarash, E. Gokmen, T. O'Toole, S. Lustgarten, L. Moore, R. J. Motzer, Temsirolimus, Interferon Alfa, or Both for Advanced Renal-Cell Carcinoma. *The New England Journal of Medicine* **356**, 2271-2281 (2007).
6. R. J. Amato, J. Jac, S. Giessinger, S. Saxena, J. P. Willis, A phase 2 study with a daily regimen of the oral mTOR inhibitor RAD001 (everolimus) in patients with metastatic clear cell renal cell cancer. *Cancer* **115**, 2438-2446 (2009).
7. W. E. Evans, M. V. Relling, Pharmacogenomics- Translating Functional Genomics into Rational Therapeutics. *Science* **286**, 487-491 (1999).

8. H. Chen, O. Engkvist, Y. Wang, M. Olivecrona, T. Blaschke, The rise of deep learning in drug discovery. *Drug Discov Today* **23**, 1241-1250 (2018).

9. M. E. Feldman, B. Apsel, A. Uotila, R. Loewith, Z. A. Knight, D. Ruggero, K. M. Shokat, Active-site inhibitors of mTOR target rapamycin-resistant outputs of mTORC1 and mTORC2. *PLoS Biol* **7**, e38 (2009).

10. S. A. Kang, M. E. Pacold, C. L. Cervantes, D. Lim, H. J. Lou, K. Ottina, N. S. Gray, B. E. Turk, M. B. Yaffe, D. M. Sabatini, mTORC1 phosphorylation sites encode their sensitivity to starvation and rapamycin. *Science* **341**, 1236566 (2013).

11. C. C. Thoreen, S. A. Kang, J. W. Chang, Q. Liu, J. Zhang, Y. Gao, L. J. Reichling, T. Sim, D. M. Sabatini, N. S. Gray, An ATP-competitive mammalian target of rapamycin inhibitor reveals rapamycin-resistant functions of mTORC1. *J Biol Chem* **284**, 8023-8032 (2009).

12. J. Tabernero, F. Rojo, E. Calvo, H. Burris, I. Judson, K. Hazell, E. Martinelli, S. Ramon y Cajal, S. Jones, L. Vidal, N. Shand, T. Macarulla, F. J. Ramos, S. Dimitrijevic, U. Zoellner, P. Tang, M. Stumm, H. A. Lane, D. Lebwohl, J. Baselga, Dose- and schedule-dependent inhibition of the mammalian target of rapamycin pathway with everolimus: a phase I tumor pharmacodynamic study in patients with advanced solid tumors. *J Clin Oncol* **26**, 1603-1610 (2008).

13. B. Surucu, L. Bozulic, D. Hynx, A. Parcellier, B. A. Hemmings, In vivo analysis of protein kinase B (PKB)/Akt regulation in DNA-PKcs-null mice reveals a role for PKB/Akt in DNA damage response and tumorigenesis. *J Biol Chem* **283**, 30025-30033 (2008).

14. V. S. Rodrik-Outmezguine, M. Okaniwa, Z. Yao, C. J. Novotny, C. McWhirter, A. Banaji, H. Won, W. Wong, M. Berger, E. de Stanchina, D. G. Barratt, S. Cosulich, T. Klinowska, N. Rosen, K. M. Shokat, Overcoming mTOR resistance mutations with a new-generation mTOR inhibitor. *Nature* **534**, 272-276 (2016).

15. V. Bliskovsky, E. S. Ramsay, J. Scott, W. DuBois, W. Shi, S. Zhang, X. Qian, D. R. Lowy, B. A. Mock, Frap, FKBP12 rapamycin-associated protein, is a candidate gene for the plasmacytoma resistance locus Pctr2 and can act as a tumor suppressor gene. *Proc Natl Acad Sci U S A* **100**, 14982-14987 (2003).

16. R. A. Saxton, D. M. Sabatini, mTOR Signaling in Growth, Metabolism, and Disease. *Cell* **168**, 960-976 (2017).

17. A. M. Eiden, S. Zhang, J. M. Gary, J. K. Simmons, B. A. Mock, Molecular Pathways: Increased Susceptibility to Infection Is a Complication of mTOR Inhibitor Use in Cancer Therapy. *Clin Cancer Res* **22**, 277-283 (2016).

18. J. T. Nguyen, C. Ray, A. L. Fox, D. B. Mendonça, J. K. Kim, P. H. Krebsbach, Mammalian EAK-7 activates alternative mTOR signaling to regulate cell proliferation and migration. *Science Advances* **4**, 1-15 (2018).

19. H. Alam, T. W. Williams, K. J. Dumas, C. Guo, S. Yoshina, S. Mitani, P. J. Hu, EAK-7 controls development and life span by regulating nuclear DAF-16/FoxO activity. *Cell Metab* **12**, 30-41 (2010).

20. O. E. Pardo, M. J. Seckl, S6K2: The Neglected S6 Kinase Family Member. *Front Oncol* **3**, 191 (2013).

21. E. Karlsson, I. Magic, J. Bostner, C. Dyrager, F. Lysholm, A. L. Hallbeck, O. Stal, P. Lundstrom, Revealing Different Roles of the mTOR-Targets S6K1 and S6K2

in Breast Cancer by Expression Profiling and Structural Analysis. *PLoS One* **10**, e0145013 (2015).

22. Z. Feng, W. Hu, E. de Stanchina, A. K. Teresky, S. Jin, S. Lowe, A. J. Levine, The regulation of AMPK beta1, TSC2, and PTEN expression by p53: stress, cell and tissue specificity, and the role of these gene products in modulating the IGF-1-AKT-mTOR pathways. *Cancer Res* **67**, 3043-3053 (2007).

23. X. Xie, H. Hu, X. Tong, L. Li, X. Liu, M. Chen, H. Yuan, X. Xie, Q. Li, Y. Zhang, H. Ouyang, M. Wei, J. Huang, P. Liu, W. Gan, Y. Liu, A. Xie, X. Kuai, G. W. Chirn, H. Zhou, R. Zeng, R. Hu, J. Qin, F. L. Meng, W. Wei, H. Ji, D. Gao, The mTOR-S6K pathway links growth signalling to DNA damage response by targeting RNF168. *Nat Cell Biol* **20**, 320-331 (2018).

24. C. L. Amaral, L. B. Freitas, R. E. Tamura, M. R. Tavares, I. C. Pavan, M. C. Bajgelman, F. M. Simabuco, S6Ks isoforms contribute to viability, migration, docetaxel resistance and tumor formation of prostate cancer cells. *BMC Cancer* **16**, 602 (2016).

25. X. Zhou, W. Liu, X. Hu, A. Dorrance, R. Garzon, P. J. Houghton, C. Shen, Regulation of CHK1 by mTOR contributes to the evasion of DNA damage barrier of cancer cells. *Sci Rep* **7**, 1535 (2017).

26. K. Datta, S. Suman, A. J. Fornace, Jr., Radiation persistently promoted oxidative stress, activated mTOR via PI3K/Akt, and downregulated autophagy pathway in mouse intestine. *Int J Biochem Cell Biol* **57**, 167-176 (2014).

27. W. H. Mondesire, W. Jian, H. Zhang, J. Ensor, M.-C. Hung, G. B. Mills, F. Meric-Bernstam, Targeting Mammalian Target of Rapamycin Synergistically Enhances

Chemotherapy-Induced Cytotoxicity in Breast Cancer Cells. *Clinical Cancer Research* **10**, 7031-7042 (2004).

28. Z. Zhu, B. Pang, R. Iglesias-Bartolome, X. Wu, L. Hu, C. Zhang, J. Wang, J. S. Gutkind, S. Wang, Prevention of irradiation-induced salivary hypofunction by rapamycin in swine parotid glands. *Oncotarget* **7**, 20271-20281 (2016).

29. K. P. Lai, W. F. Leong, J. F. Chau, D. Jia, L. Zeng, H. Liu, L. He, A. Hao, H. Zhang, D. Meek, C. Velagapudi, S. L. Habib, B. Li, S6K1 is a multifaceted regulator of Mdm2 that connects nutrient status and DNA damage response. *EMBO J* **29**, 2994-3006 (2010).

30. S. Braunstein, M. L. Badura, Q. Xi, S. C. Formenti, R. J. Schneider, Regulation of protein synthesis by ionizing radiation. *Mol Cell Biol* **29**, 5645-5656 (2009).

31. A. C. Hsieh, Y. Liu, M. P. Edlind, N. T. Ingolia, M. R. Janes, A. Sher, E. Y. Shi, C. R. Stumpf, C. Christensen, M. J. Bonham, S. Wang, P. Ren, M. Martin, K. Jessen, M. E. Feldman, J. S. Weissman, K. M. Shokat, C. Rommel, D. Ruggero, The translational landscape of mTOR signalling steers cancer initiation and metastasis. *Nature* **485**, 55-61 (2012).

32. J. C. Brenner, M. P. Graham, B. Kumar, L. M. Saunders, R. Kupfer, R. H. Lyons, C. R. Bradford, T. E. Carey, Genotyping of 73 UM-SCC head and neck squamous cell carcinoma cell lines. *Head Neck* **32**, 417-426 (2010).

33. Y. Tu, C. Ji, B. Yang, Z. Yang, H. Gu, C.-C. Lu, R. Wang, Z.-L. Su, B. Chen, W.-L. Sun, J.-P. Xia, Z.-G. Bi, L. He, DNA-dependent protein kinase catalytic subunit (DNA-PKcs)-SIN1 association mediates ultraviolet B (UVB)-induced Akt Ser-473 phosphorylation and skin cell survival. *Molecular Cancer* **12**, 1-12 (2013).

34. G. A. Wyant, M. Abu-Remaileh, E. M. Frenkel, N. N. Laqtom, V. Dharamdasani, C. A. Lewis, S. H. Chan, I. Heinze, A. Ori, D. M. Sabatini, NUFIP1 is a ribosome receptor for starvation-induced ribophagy. *Science*, (2018).

35. S. Zhang, J. A. Readinger, W. DuBois, M. Janka-Junttila, R. Robinson, M. Pruitt, V. Bliskovsky, J. Z. Wu, K. Sakakibara, J. Patel, C. A. Parent, L. Tessarollo, P. L. Schwartzberg, B. A. Mock, Constitutive reductions in mTOR alter cell size, immune cell development, and antibody production. *Blood* **117**, 1228-1238 (2011).

36. M. Murakami, T. Ichisaka, M. Maeda, N. Oshiro, K. Hara, F. Edenhofer, H. Kiyama, K. Yonezawa, S. Yamanaka, mTOR Is Essential for Growth and Proliferation in Early Mouse Embryos and Embryonic Stem Cells. *Molecular and Cellular Biology* **24**, 6710-6718 (2004).

37. Y. Yu, S.-O. Yoon, G. Poulogiannis, Q. Yang, X. M. Ma, J. Villén, N. Kubica, G. R. Hoffman, L. C. Cantley, S. P. Gygi, J. Blenis, Phosphoproteomic analysis identifies Grb10 as an mTORC1 substrate that negatively regulates insulin signaling. *Science* **332**, 1322-1326 (2011).

38. P. P. Hsu, S. A. Kang, J. Rameseder, Y. Zhang, K. A. Ottina, D. Lim, T. R. Peterson, Y. Choi, N. S. Gray, M. B. Yaffe, J. A. Marto, D. M. Sabatini, The mTOR-Regulated Phosphoproteome Reveals a Mechanism of mTORC1-Mediated Inhibition of Growth Factor Signaling. *Science* **332**, 1317-1322 (2011).

39. S. J. Park, O. Gavrilova, A. L. Brown, J. E. Soto, S. Bremner, J. Kim, X. Xu, S. Yang, J. H. Um, L. G. Koch, S. L. Britton, R. L. Lieber, A. Philp, K. Baar, S. G. Kohama, E. D. Abel, M. K. Kim, J. H. Chung, DNA-PK Promotes the

Mitochondrial, Metabolic, and Physical Decline that Occurs During Aging. *Cell Metab* **25**, 1135-1146 e1137 (2017).

40. R. H. Wong, I. Chang, C. S. Hudak, S. Hyun, H. Y. Kwan, H. S. Sul, A role of DNA-PK for the metabolic gene regulation in response to insulin. *Cell* **136**, 1056-1072 (2009).

41. Q. Deng, C. J. Holler, G. Taylor, K. F. Hudson, W. Watkins, M. Gearing, D. Ito, M. E. Murray, D. W. Dickson, N. T. Seyfried, T. Kukar, FUS is phosphorylated by DNA-PK and accumulates in the cytoplasm after DNA damage. *J Neurosci* **34**, 7802-7813 (2014).

42. J. P. Renaud, A. Chari, C. Ciferri, W. T. Liu, H. W. Remigy, H. Stark, C. Wiesmann, Cryo-EM in drug discovery: achievements, limitations and prospects. *Nat Rev Drug Discov* **17**, 471-492 (2018).

43. H. Yang, J. Wang, M. Liu, X. Chen, M. Huang, D. Tan, M. Q. Dong, C. C. Wong, J. Wang, Y. Xu, H. W. Wang, 4.4 A Resolution Cryo-EM structure of human mTOR Complex 1. *Protein Cell* **7**, 878-887 (2016).

44. M. Karuppasamy, B. Kusmider, T. M. Oliveira, C. Gaubitz, M. Prouteau, R. Loewith, C. Schaffitzel, Cryo-EM structure of Saccharomyces cerevisiae target of rapamycin complex 2. *Nat Commun* **8**, 1729 (2017).

45. J. Frauenfeld, R. Löving, J. Armache, A. Sonnen, F. Guettou, P. Moberg, L. Zhu, C. Jegerschöld, A. Flayhan, J. Briggs, H. Garoff, C. Löw, Y. Cheng, P. Nordlund, A saposin-lipoprotein nanoparticle system for membrane proteins. *Nat Methods* **13**, 345-351 (2016).

46. Y. Gao, E. Cao, D. Julius, Y. Cheng, TRPV1 structures in nanodiscs reveal mechanisms of ligand and lipid action. *Nature* **534**, 347-351 (2016).

47. J. H. Choi, H. S. Jo, S. Lim, H. T. Kim, K. W. Lee, K. H. Moon, T. Ha, S. S. Kwak, Y. Kim, E. J. Lee, C. O. Joe, J. W. Kim, mTORC1 accelerates retinal development via the immunoproteasome. *Nat Commun* **9**, 2502 (2018).

48. J. M. Bateman, H. McNeill, Temporal control of differentiation by the insulin receptor/tor pathway in Drosophila. *Cell* **119**, 87-96 (2004).

49. N. K. Love, N. Keshavan, R. Lewis, W. A. Harris, M. Agathocleous, A nutrient-sensitive restriction point is active during retinal progenitor cell differentiation. *Development* **141**, 697-706 (2014).

50. N. Koyama, M. Kashimata, H. Sakashita, H. Sakagami, E. W. Gresik, EGF-stimulated signaling by means of PI3K, PLCgamma1, and PKC isozymes regulates branching morphogenesis of the fetal mouse submandibular gland. *Dev Dyn* **227**, 216-226 (2003).

51. X. Nie, J. Zheng, C. L. Ricupero, L. He, K. Jiao, J. J. Mao, mTOR acts as a pivotal signaling hub for neural crest cells during craniofacial development. *PLoS Genet* **14**, e1007491 (2018).

52. J.-K. Jung, H.-I. Jung, S. Neupane, K.-R. Kim, J.-Y. Kim, H. Yamamoto, S.-W. Cho, Y. Lee, H.-I. Shin, W.-J. Sohn, J.-Y. Kim, Involvement of PI3K and PKA pathways in mouse tongue epithelial differentiation. *Acta Histochemica* **119**, 92-98 (2017).

53. X. Ding, W. Bloch, S. Iden, M. A. Ruegg, M. N. Hall, M. Leptin, L. Partridge, S. A. Eming, mTORC1 and mTORC2 regulate skin morphogenesis and epidermal barrier formation. *Nat Commun* **7**, 13226 (2016).

54. M. Shimobayashi, M. N. Hall, Making new contacts: the mTOR network in metabolism and signalling crosstalk. *Nat Rev Mol Cell Biol* **15**, 155-162 (2014).

55. R. J. Dowling, I. Topisirovic, T. Alain, M. Bidinosti, B. D. Fonseca, E. Petroulakis, X. Wang, O. Larsson, A. Selvaraj, Y. Liu, S. C. Kozma, G. Thomas, N. Sonenberg, mTORC1-mediated cell proliferation, but not cell growth, controlled by the 4E-BPs. *Science* **328**, 1172-1176 (2010).

56. X. Chen, M. Liu, Y. Tian, J. Li, Y. Qi, D. Zhao, Z. Wu, M. Huang, C. C. L. Wong, H. W. Wang, J. Wang, H. Yang, Y. Xu, Cryo-EM structure of human mTOR complex 2. *Cell Res* **28**, 518-528 (2018).